

Novel Biocidal Formulation

A thesis submitted to The University of Manchester for the degree of a Doctor of Philosophy in the Faculty of Engineering and Physical Sciences.

2013

By

Peter William Wills

School of Chemistry

Contents

| | |
|---|-----------|
| Abbreviations | 7 |
| List of Figures | 8 |
| List of Tables | 11 |
| Abstract | 14 |
| Declaration | 15 |
| Copyright and ownership of intellectual rights | 16 |
| Acknowledgements | 17 |
| | |
| Chapter 1 – Introduction | 18 |
| 1.1 Opening Statement | 19 |
| 1.2 Bacteria | 20 |
| 1.3 Biocide Types | 22 |
| 1.3.1 Phenolic Compounds | 23 |
| 1.3.2 Silver | 23 |
| 1.3.3 Cationically Charged Biocides | 24 |
| 1.3.4 N-Halamines | 31 |
| 1.3.5 Summary | 32 |
| 1.4 Antimicrobial Surfaces | 32 |
| 1.4.1 Contact Kill | 33 |
| 1.4.2 Polyelectrolytes Multilayers (PEMs) | 35 |
| 1.4.3 Adhesion Resistance | 36 |
| 1.5 Solution Interactions | 37 |
| 1.5.1 Surfactants | 37 |
| 1.5.2 Polyelectrolytes | 46 |
| 1.5.3 Low Concentration Surfactant / Polymer Mixtures | 49 |
| 1.5.4 Concentrated Surfactant / Polymer Mixtures – Phase Separation | 51 |
| 1.6 Aims of the Project | 53 |
| 1.7 References | 54 |

| | |
|---|---------------|
| Chapter 2 – Experimental | 59 |
| 2.1 Reagents | 60 |
| 2.2 Standard Procedures | 62 |
| 2.2.1 Formulating | 62 |
| 2.2.2 Observations of Sample Phase Separation | 62 |
| 2.2.3 Analysis of Sample Phases | 63 |
| 2.2.4 Determination of Critical Phase Separating Concentration | 63 |
| 2.2.5 Substrate Cleaning | 64 |
| 2.2.6 Surface Treatment | 64 |
| 2.3 Techniques | 65 |
| 2.3.1 Size Exclusion Chromatography (SEC) | 65 |
| 2.3.2 NMR | 66 |
| 2.3.3 IR | 66 |
| 2.3.4 SI-MS | 66 |
| 2.3.5 Viscometry | 66 |
| 2.3.6 Tensiometry | 67 |
| 2.3.6 Conductivity | 67 |
| 2.3.7 Isothermal Titration Calorimetry (ITC) | 68 |
| 2.3.9 Photo-Luminescence | 68 |
| 2.3.10 Photon Correlation Spectroscopy | 68 |
| 2.3.11 Equilibrium Contact Angle Measurement | 69 |
| 2.3.12 Drying Drop Contact Angle Measurement | 69 |
| 2.3.13 Optical Microscopy | 70 |
| 2.3.14 Non-Contact Atomic Force Microscopy (NC-AFM) | 70 |
| 2.3.15 Time of Flight Secondary Ion Mass Spectrometry (ToFSIMS) | 71 |
| 2.3.16 Inkjet Printing | 71 |
| 2.4 Microbiology Procedures | 72 |
| 2.4.1 MIC Testing of Polyelectrolytes | 72 |
| 2.4.2 Surface Testing | 74 |
| 2.5 References | 76 |
| Chapter 3 – Characterisation of Principal Materials | 77 |

| | |
|--|----|
| 3.1 Polyelectrolytes | 78 |
| 3.1.1 Poly(diallyl dimethyl ammonium chloride) (pDADMAC) | 78 |
| 3.1.2 Poly(hexamethylene biguanide) chloride (PHMB) | 80 |
| 3.1.3 Poly(2-dimethylamino)ethyl methacrylate) methyl chloride Quaternary salt (PDMC) | 81 |
| 3.2 Polyelectrolyte Molecular Weight Determination | 82 |
| 3.2.1 Viscometry | 83 |
| 3.2.2 Size Exclusion Chromatography (SEC) | 86 |
| 3.3.3 End Group Analysis | 88 |
| 3.3.4 Summary of Determined Molecular Weights | 90 |
| 3.3 Surfactants | 91 |
| 3.3.1 Alkyl (C ₁₂ 70%; C ₁₄ 30%) dimethyl benzyl ammonium chloride (BAC) | 91 |
| 3.3.2 Didecyl dimethyl ammonium chloride (DDQ) | 92 |
| 3.4 References | 93 |

Chapter 4 – Polyelectrolytes in Solution 94

| | |
|--|-----|
| 4.1 Polyelectrolytes | 95 |
| 4.2 Solution Properties | 96 |
| 4.2.1 Manning Parameter | 96 |
| 4.2.2 Surface Activity | 100 |
| 4.2.3 Relating Surface Activity / Image Charge / Manning Parameter | 102 |
| 4.2.4 Concentration Regimes | 103 |
| 4.3 Minimum Inhibitory Concentration (MIC) | 106 |
| 4.4 Discussion of MIC | 108 |
| 4.4.1 Polyelectrolyte Type | 108 |
| 4.4.2 Molecular Weight | 109 |
| 4.5 Conclusion | 110 |
| 4.6 References | 110 |

Chapter 5 – Polyelectrolyte/Surfactant Mixtures of Similar Charge 113

| | |
|--------------------------|-----|
| 5.1 Cationic Surfactants | 114 |
|--------------------------|-----|

| | |
|--|---------|
| 5.1.1 Surface Tensiometry | 115 |
| 5.1.2 Conductivity | 116 |
| 5.1.3 Pyrene | 118 |
| 5.1.4 Isothermal Titration Calorimetry (ITC) | 120 |
| 5.1.5 Photon Correlation Spectroscopy (PCS) | 122 |
| 5.1.6 Discussion of Micelle Characteristics | 127 |
| 5.2 Concentrated Polyelectrolyte/Surfactant Mixtures | 131 |
| 5.2.1 pDADMAC Systems | 133 |
| 5.2.2 PHMB Systems | 142 |
| 5.3 Conclusion | 144 |
| 5.4 References | 144 |
| Chapter 6 – Surface Patterning | 147 |
| 6.1 Introduction | 148 |
| 6.1.1 Evaporation of a Sessile Drop | 149 |
| 6.1.2 Coffee Staining | 150 |
| 6.2 Dilute Polymer/Surfactant/Water Sessile Drops | 152 |
| 6.2.1 Drying Drop Studies | 153 |
| 6.2.2 Direct Visualisation of Phase Separation | 157 |
| 6.2.3 Calculation of the Critical Phase Separation Concentration | 162 |
| 6.2.4 Summary | 163 |
| 6.3 Film Structures of pDADMAC/Surfactant/Water Systems | 164 |
| 6.3.1 Controls | 164 |
| 6.3.2 pDADMAC (21 kDa)/Surfactant/Water System | 166 |
| 6.3.3 Film Analysis (ToF-SIMS) | 171 |
| 6.3.4 Overview | 174 |
| 6.3.5 Effect of pDADMAC Molecular Weight | 175 |
| 6.3.6 Inkjet Printing | 176 |
| 6.4 PHMB /Surfactant/Water Systems | 181 |
| 6.4.1 Direct Visualisation of Phase Separation | 182 |
| 6.4.2 Film Structure | 183 |
| 6.5 Potential Antimicrobial Surface Application | 186 |

| | |
|---|---------|
| 6.6 Conclusions | 188 |
| 6.7 References | 189 |
| Chapter 7 – Conclusions and Further Work | 190 |
| 7.1 Conclusion | 191 |
| 7.1.1 Polyelectrolytes in Solution | 191 |
| 7.2.2 Polyelectrolyte/Surfactant Mixtures of Similar Charge | 192 |
| 7.1.3 Surface Patterning | 192 |
| 7.2 Further Work | 193 |
| 7.2.1 Phase Separation Mechanism | 193 |
| 7.2.2 Inkjet Printing | 194 |
| 7.2.3 Film Analysis | 195 |
| Chapter 8 – Instrumentation | 196 |
| 8.1 Surface Tensiometry | 197 |
| 8.2 Isothermal Titration Calorimetry (ITC) | 197 |
| 8.3 Photon Correlation Spectroscopy (PCS) | 200 |
| 8.4 Size Exclusion Chromatography (SEC) | 202 |
| 8.5 Anton Paar Viscometer | 204 |
| 8.6 Ubbelohde Viscometer | 204 |
| 8.7 Non-Contact Atomic Force Microscopy (NC-AFM) | 205 |
| 8.8 Time of Flight Secondary Ion Mass Spectrometry (ToF-SIMS) | 207 |
| 8.9 Diamatrix Printer | 208 |
| 8.10 References | 208 |
| Appendices | 210 |

Word Count Main Text = 35,408

Abbreviations

| | |
|----------|---|
| BAC | Alkyl (C ₁₂ 70%; C ₁₄ 30%) dimethyl benzyl ammonium chloride. |
| DDQ | Didecyldimethylammonium chloride |
| pDADMAC | Poly(diallyldimethylammonium) chloride |
| PHMB | Poly(hexamethylene biguanide) chloride |
| PDMC | Poly(2-dimethylamino)ethyl methacrylate) methylchloride quaternary salt |
| QAC | Quaternary Ammonium Compound |
| NC-AFM | Non-Contact Atomic Force Microscopy |
| ToF-SIMS | Time of Flight Secondary Ion Mass Spectroscopy |
| ITC | Isothermal Titration Calorimetry |
| PCS | Photon Correlation Spectroscopy |
| SEC | Size Exclusion Chromatography |
| NMR | Nuclear Magnetic Resonance |
| IR | Infrared Spectroscopy |
| SI-MS | Electrospray Ionisation Mass Spectroscopy |
| MIC | Minimum Inhibitory Concentration |
| PEMs | Polyelectrolyte Multilayers |

List of Figures

| | | |
|------|---|----|
| 1.1 | Chemical structure of crystal violet and a schematic diagram of gram-positive and gram-negative cell walls. | 20 |
| 1.2 | Chemical structures of surfactant. | 25 |
| 1.3 | Chemical structures of Homo-Quaternary ammonium polymers. | 27 |
| 1.4 | Chemical structure of Hydroxyethylcellulose ethoxylate, quaternised. | 27 |
| 1.5 | Chemical structure of Chlorhexidine gluconate salt. | 28 |
| 1.6 | Chemical structure of Polyhexamethylene biguanide chloride (PHMB). | 29 |
| 1.7 | Schematic illustration of the antimicrobial activity as a function of molecular weight. | 30 |
| 1.8 | An example of a polymeric N-Halamine. | 31 |
| 1.9 | Different strategies for creating antimicrobial surfaces. | 32 |
| 1.10 | Schematic illustration of the PEMs coating procedure. | 36 |
| 1.11 | Schematic diagram of a surfactant molecule. | 37 |
| 1.12 | Diagram illustrating Gibbs dividing surface. | 40 |
| 1.13 | Schematic illustration of different micellar structures. | 45 |
| 1.14 | Schematic diagram of polyelectrolyte conformations as a function of concentration / ionic strength. | 47 |
| 1.15 | Computer simulation of hydrogen bonded kinked globular structures of PHMB in water at 300K. | 48 |
| 1.16 | Schematic diagram of the Pearl-Necklace Model. | 49 |
| 3.1 | ^{13}C NMR Spectra of Poly(diallyl dimethyl ammonium chloride) 140 kDa (pDADMAC). | 79 |
| 3.2 | ^1H NMR Spectra of Poly(hexamethylene biguanide) chloride (PHMB). | 80 |
| 3.3 | ^1H NMR Spectra of Poly(2-dimethylamino)ethyl methacrylate) methyl chloride quaternary salt (PDMC). | 81 |
| 3.4 | Example of a Huggins/Kraemer plot for a pDADMAC sample with extrapolation to $c = 0$ used to determine intrinsic viscosity $[\eta]$. | 85 |
| 3.5 | GPC trace of pDADMAC polyelectrolytes in the high column SEC system. M= Molecular mass, W = Weight fraction. | 87 |
| 3.6 | Chemical structures of the three possible PHMB end groups. Left to Right; Amine, Guanide, Cyanoguanide. | 88 |

| | | |
|------|---|-----|
| 3.7 | Magnified ^1H NMR spectra of Poly(hexamethylene biguanide) chloride (PHMB) required for end group analysis. | 89 |
| 3.8 | ^1H NMR Spectra of Alkyl (C_{12} 70%; C_{14} 30%) dimethyl benzyl ammonium chloride (BAC). | 91 |
| 3.9 | ^1H NMR Spectra of Didecyl dimethyl ammonium chloride (DDQ). | 92 |
| 4.1 | Schematic diagrams of polyelectrolytes relating chemical structures to assumptions required for Manning parameter calculation. | 98 |
| 4.2 | Surface tension profile in DI water at 25°C of a) pDADMAC 8.5 kDa, PHMB and PDMC. b) pDADMAC 8.5 kDa, 21 kDa, 140 kDa. | 100 |
| 4.3 | Isothermal Titration (ITC) profile of PHMB at 25°C . | 101 |
| 4.4 | a) MICs for different polyelectrolyte types. b) MICs for a range of different molecular weight pDADMAC sample. | 107 |
| 5.1 | Surface tension profiles in water at 25°C of BAC, DDQ, and BAC/DDQ (2:3 mol:mol). | 115 |
| 5.2 | Conductivity profiles in water at 25°C of BAC, DDQ, and BAC/DDQ (2:3 mol:mol). | 117 |
| 5.3 | Pyrene monomer fluorescence in aqueous BAC solutions, at BAC concentration a) below CMC, b) above CMC. | 119 |
| 5.4 | Variation in the ratio of peaks III and I as a function of surfactant concentration BAC, DDQ, and BAC/DDQ (2:3 mol:mol). | 119 |
| 5.5 | ITC Thermodynamic profile of aqueous surfactant solutions as a function of concentration BAC, DDQ, and BAC/DDQ (2:3 mol:mol) at 25°C . | 121 |
| 5.6 | Schematic diagram illustrating the determination of the micellar diffusion coefficient at infinite dilution. | 123 |
| 5.7 | PCS intensity profiles at 25°C as a function of concentration of (a) BAC (b) BAC/DDQ (2:3 mol:mol) and (c) DDQ. | 125 |
| 5.8 | Schematic diagram of the proposed micellar headgroup structure of BAC with the phenyl group close to the quaternary ammonium headgroup. | 129 |
| 5.9 | a) Phase Separation boundary for pDADMAC (8.5 kDa)/DDQ/water at 25°C (b) Phase separation image for sample pDADMAC (3 wt%)/DDQ (3 wt%)/water. | 133 |
| 5.10 | ^1H NMR of the top phase and the bottom phase for the sample pDADMAC 8.5 kDa (3 wt%)/DDQ (3 wt%)/water sample. | 134 |
| 5.11 | Phase separation boundary (a) pDADMAC/DDQ/water as a function of pDADMAC molecular weight (b) Phase boundary for pDADMAC (21 kDa)/surfactant/water. | 136 |
| 5.12 | Critical phase separation concentration as a function of BAC/DDQ mass ratio. | 137 |

| | | |
|------|--|-----|
| 5.13 | Number of chloride ions from electrolyte to induce phase separation ($N_{CL-Phase\ Separation}$) as a function of BAC/DDQ ratio. | 138 |
| 5.14 | Schematic diagram illustrating entropic depletion flocculation. | 141 |
| 6.1 | Phase boundary between one and two phase solutions, pDADMAC (21 kDa)/Surfactant/water. | 148 |
| 6.2 | Schematic diagram of a Sessile drop. | 150 |
| 6.3 | Coffee stain effect - Spheres within an evaporating drop. | 151 |
| 6.4 | Schematic Diagram of a pinned sessile drying drop. | 151 |
| 6.5 | Contact angle and diameter of a drying drop as a function of time. | 154 |
| 6.6 | Volume of a drying drop as a function of time. | 155 |
| 6.7 | Optical micrographs of a drying sessile drop (20 μ L) on a glass substrate, 0.1 wt% BAC only. | 158 |
| 6.8 | Optical micrographs of a drying sessile drop (20 μ L) on a glass substrate, 0.1 wt% pDADMAC (21 kDa) only. | 158 |
| 6.9 | Optical micrographs of a drying sessile drop (20 μ L) on a glass substrate, 0.1 wt% BAC + 0.1 wt% pDADMAC (21 kDa). | 160 |
| 6.10 | Optical micrographs of a drying sessile drop (20 μ L) on a glass substrate, 0.1 wt% BAC/DDQ (2:3) + 0.1 wt% pDADMAC (21 kDa). | 161 |
| 6.11 | Optical micrographs of a drying sessile drop (20 μ L) on a glass substrate, 0.1 wt% DDQ + 0.1 wt% pDADMAC (21 kDa). | 162 |
| 6.12 | Optical micrographs of glass substrates treated with 20 μ L of 0.1 wt% surfactant or pDADMAC (21 kDa) solution. | 165 |
| 6.13 | Optical micrographs of glass substrates treated with 20 μ L of 0.1 wt% surfactant + 0.1 wt% pDADMAC (21 kDa) solutions. | 166 |
| 6.14 | (Top) Optical micrographs of glass substrates treated with 20 μ L of 0.1 wt% BAC/DDQ + 0.1 wt% pDADMAC (21 kDa) formulations. (Bottom) Average Nodule diameter, nodule size plotted as a function of DDQ mass fraction. | 168 |
| 6.15 | NC-AFM of glass substrates treated with a 20 μ L 0.1 wt% surfactant + 0.1 wt% pDADMAC (21 kDa) formulation. | 169 |
| 6.16 | Height profile from NC-AFM topography images (Figure 6.15). | 170 |
| 6.17 | ToF-SIMS Ion mapping. | 172 |
| 6.18 | Possible surface structures in respect of surfactant and polymer location. | 173 |
| 6.19 | Combined analysis a) Optical micrograph of drying drop, b) i) optical micrograph ii) NC-AFM Topography and phase images. | 174 |

| | | |
|------|---|-----|
| 6.20 | Optical micrographs of glass substrates treated with 20 μ L of 0.1 wt% BAC/DDQ (2:3) + 0.1 wt% pDADMAC. | 175 |
| 6.21 | Optical micrographs of a drying sessile drop (20 μ L) on a glass substrate. 0.1 wt% DDQ + 0.1 wt% PHMB. | 183 |
| 6.22 | NC-AFM of glass substrates treated with 20 μ L of 0.1 wt% surfactant + 0.1 wt%. | 185 |
| | Height profile from NC-AFM topography images (Figure 6.22). | |
| 6.23 | Dashed line within topography images indicates where profile was taken. | 185 |
| 8.1 | Schematic diagram of the Isothermal Titration Calorimetry equipment. | 198 |
| 8.2 | ITC thermodynamic profile. | 199 |
| 8.3 | Data from a Malvern Zetasizer Nanoseries. | 201 |
| 8.4 | Schematic diagram of a SEC column illustrating the separation process. | 203 |
| 8.5 | Schematic Diagram of a Ubbelohde Viscometer. | 205 |
| 8.6 | Schematic diagram of a Park XE-100-AFM Setup. | 206 |
| 8.7 | Schematic diagram illustrating the ToF-SIMS process. | 207 |

List of Tables

| | | |
|-----|--|----|
| 1.1 | Examples of gram-positive and gram-negative bacteria. | 21 |
| 1.2 | Examples of different biocide types. | 22 |
| 1.3 | Strategies for designing antimicrobial abiotic surfaces. | 33 |
| 1.4 | Phase separation types in different surfactant-polymer mixtures. | 52 |
| 2.1 | Chemical structures of the principle polyelectrolytes and surfactants. | 61 |
| 2.2 | Electrolyte increments for the different surfactant BAC/DDQ series. | 64 |
| 2.3 | Summary of columns used for SEC. | 65 |

| | | |
|------|--|-----|
| 2.4 | Details of Luria-Bertani (LB) broth and agar formulations. | 73 |
| 3.1 | Intrinsic Viscosity of Polyelectrolytes in a 1M NaCl solvent at 25 °C and Molecular weight (M_v). | 86 |
| 3.2 | M_w , M_n and PDI determined by SEC, Systems calibrated against Poly(ethylene) oxide. | 87 |
| 3.3 | Summary of the different determined molecular weights of the studied polyelectrolytes and the methodology used for their determination. | 90 |
| 4.1 | Manning parameter calculations for PHMB, pDADMAC and PDMC at 20 °C in water. | 99 |
| 4.2 | Definition of the Odijk polyelectrolyte concentration regimes. | 104 |
| 4.3 | Tabulated C_R^* , C_b^* and C_m^* data for the studied polyelectrolytes. | 105 |
| 4.4 | Tabulated Minimum Inhibitory Concentration (MIC) of studied polyelectrolytes. | 106 |
| 5.1 | Tabulated CMC and area of surfactant headgroup values. Results obtained by surface tensiometry. | 116 |
| 5.2 | Determination of CMC and dissociation constant using Frahm's model. Results obtained via conductivity at 25 °C. | 118 |
| 5.3 | Surfactant CMCs determined via pyrene method. | 120 |
| 5.4 | Surfactant CMCs determined via ITC. | 121 |
| 5.5 | Cloud points of surfactants (100 mM) upon addition of NaCl. | 124 |
| 5.6 | Tabulated PCS hydrodynamic diameter values of the respective surfactants. | 126 |
| 5.7 | Summary of determined CMCs. | 127 |
| 5.8 | Comparison of Experimental CMC to Literature values. | 129 |
| 5.9 | Gravimetric analysis of top and bottom layer of pDADMAC 8.5 kDa (3 wt%)/DDQ (3 wt%)/water. | 135 |
| 5.10 | The number of chloride ions (N_{Cl^-}) added into the mixtures from the electrolyte to induce phase separation. | 140 |
| 5.11 | Tabulated results showing the number of chloride ions (N_{Cl^-}) added into the (PHMB) mixtures by the electrolyte to induce phase separation. | 143 |

| | | |
|------|---|-----|
| 6.1 | Concentration and surface tension of formulations. | 152 |
| 6.2 | CMC determination in the presence of 0.1 wt% pDADMAC (21 kDa) via surface tensiometry. | 153 |
| 6.3 | Rate of evaporation of a 20 μ L drop of 0.1 wt% surfactant + 0.1 wt% pDADMAC (21 kDa) formulation. | 156 |
| 6.4 | Phase separation concentration within a evaporating drop. | 163 |
| 6.5 | Solution properties of control formulations. | 165 |
| 6.6 | Solution properties of 0.1 wt% BAC/DDQ + 0.1 wt% pDADMAC (21 kDa) formulations. | 167 |
| 6.7 | Principle Positive Secondary Ions Species within controls. | 171 |
| 6.8 | Average nodule size of glass substrates treated with 20 μ L of 0.1 wt% BAC/DDQ (2:3) + 0.1 wt% pDADMAC. | 176 |
| 6.9 | Optical micrographs – Inkjet drops of \approx 10 pL printed onto a glass substrate. Formulation of 0.1 wt% Surfactant only | 177 |
| 6.10 | Optical micrographs - Inkjet drops of \approx 10 pL printed onto a glass substrate. Formulations of 0.1 wt% surfactant and 0.1 wt% pDADMAC (21 kDa). | 178 |
| 6.11 | Optical micrographs - Inkjet drops of \approx 10 pL printed onto a glass substrate. Comparison of 0.1 wt% surfactant + 0.1 wt% pDADMAC (21 kDa) formulations and 0.1 wt% surfactant only solutions. | 179 |
| 6.12 | Optical micrographs / NC-AFM Phase and Topography - Inkjet drops of \approx 10 pL printed onto a glass substrate. | 180 |
| 6.13 | Solution properties for 0.1 wt% surfactant + 0.1 wt% PHMB mixtures. | 182 |
| 6.14 | CMC determination in the presence of 0.1 wt% PHMB via surface tensiometry. | 182 |
| 6.15 | Optical micrographs of glass substrates treated with 20 μ L of 0.1 wt% surfactant + 0.1 wt% PHMB solution. | 184 |
| 6.16 | Residual antibacterial efficacy of formulations against <i>P. aeruginosa</i> on a stainless steel surface following 3 abrasive wear cycles. | 187 |

Abstract

The University of Manchester Faculty of Engineering and Physical Sciences

P W. Wills

A thesis submitted for the degree of Doctor of Philosophy

Novel Biocidal Formulation

28th March 2013

In this modern age, society has become much more aware of the danger bacteria can have on people's health. Personal and household antimicrobial formulations are commonly used within the home to lower the levels of harmful bacteria such as *E. Coli*, *Salmonella* and *Pseudomonas*. The active which kills the bacteria within the formulation is described as a biocide. This research looks at the often neglected potential of cationic polyelectrolyte as a biocide, firstly within solution and secondly in creating an antimicrobial surface. The solution properties and antimicrobial activity for a range of commercially available cationic polyelectrolytes (polymeric quaternary ammonium compounds (QAC) and biguanides) of differing molecular weights were investigated. All polyelectrolytes were observed to have some level of antimicrobial activity.

The second phase of this research investigated polyelectrolyte/surfactant/water mixture of similar charge (cationic). Two QAC surfactants were investigated: Alkyl (C_{12} 70%; C_{14} 30%) dimethyl benzyl ammonium chloride (BAC) and Didecyldimethylammonium chloride (DDQ). At a critical concentration, these mixtures segregatively phase separate into a surfactant rich upper phase and polyelectrolyte rich lower phase. This phase separation phenomenon was investigated in respect of surfactant and polyelectrolyte type as well as polyelectrolyte molecular weight. Surfactant type was observed to be the dominant factor in determining the onset of phase separation and by mixing different ratios of surfactants the ability to tune this phase separation concentration was shown.

Dilute solutions of these mixtures well below their respective phase separation concentration were then deposited onto glass substrates via a drop cast or inkjet printer method. The surfactant/polyelectrolyte film composites left after drop evaporation ranged from an amorphous film to nodular like structures. The ability to order/structure actives onto a surface could alter active adhesion and surface roughness properties of the film. This change in surface property could consequently affect antimicrobial performance.

Declaration

No portion of the work referred to in this thesis has been submitted in support of an application for another degree or qualification of The University of Manchester or any other university or any other institute of learning.

Peter William Wills 28/03/13

Copyright Statement

- i. The author of this thesis (including any appendices and/or schedules to this thesis) owns certain copyright or related rights in it (the “Copyright”) and s/he has given The University of Manchester (the “University”) certain rights to use such Copyright, including for administrative purposes.
- ii. Copies of this thesis, either in full or in extracts and whether in hard or electronic copy, may be made only in accordance with the Copyright, Designs and Patents Act 1988 (as amended) and regulations issued under it or, where appropriate, in accordance with licensing agreements which the University has from time to time. This page must form part of any such copies made.
- iii. The ownership of certain Copyright, patents, designs, trademarks and other intellectual property (the “Intellectual Property”) and any reproductions of copyright works in the thesis, for example graphs and tables (“Reproductions”), which may be described in this thesis, may not be owned by the author and may be owned by third parties. Such Intellectual Property and Reproductions cannot and must not be made available for use without the prior written permission of the owner(s) of the relevant Intellectual Property and/or Reproductions.
- iv. Further information on the conditions under which disclosure, publication and commercialisation of this thesis, the Copyright and any Intellectual Property and/or Reproductions described in it may take place is available in the University IP Policy (see <http://www.campus.manchester.ac.uk/medialibrary/policies/intellectual-property.pdf>), in any relevant Thesis restriction declarations deposited in the University Library, The University Library’s regulations (see <http://www.manchester.ac.uk/library/aboutus/regulations>) and in The University’s policy on presentation of Thesis.

Acknowledgements

I would first like to express my appreciation and thanks to my PhD supervisor Professor Stephen Yeates for helping and guiding me through my PhD research. The opportunity to study within his research group has been challenging but one which I have enjoyed immensely.

I would like to give a special mention to Miss Nishal Govindji who conducted the solution microbiology testing for me. I wish her luck in the completion of her PhD and subsequent Viva.

Thanks to my industrial sponsors Byotrol Plc for their useful and thought provoking discussions with special mention to Dr Trevor Francis, Dr Rachel Hirst, Dr Timothy Mills and Dr Christopher Plummer. A special thanks to Chris for conducting the surface microbiology testing for me.

For the help with the Ink Jet Printing studies I would like to thank Mr Joseph Wheeler and Dr Verónica Sánchez-Romaguera. I would also like to thank Dr Andromachi Malandraki and Dr Maria-Beatrice Madec for the training they provided on numerous analytical instruments.

There are many great people past and present who worked in the Organic Materials Innovation Centre (OMIC) I am yet to mention but have given me advice and moral support during the course of my research. These include: Mr Sean Butterworth, Mr Reiner Sprick, Dr Jonathan Behrendt, Mr Ian Ingram and Dr David Crouch.

I would like to thank my parents for supporting me and encouraging me to pursue a career in science, with a special mention to my Dad who passed away during the course of this research; I hope this thesis does his memory justice.

Finally and most importantly I would like to thank my beautiful wife (Mrs Michelle Wills) for supporting me when things got difficult and lately proof reading my thesis. I could not have done this without you.

Chapter 1 – Introduction

Introduction

1.1 Opening Statement

In this modern age, society has become much more aware of the danger bacteria can have on people's health. Personal and household antimicrobial formulations are commonly used within the home to lower the levels of harmful bacteria such as *E. Coli*, *Salmonella* and *Pseudomonas*. These antimicrobial formulations are particularly helpful in hospitals, nursing homes and nurseries where a high proportion of people within these institutions are more susceptible to bacterial induced infections. An antimicrobial formulation contains a chemical active which suppresses and kills living organisms, in this case harmful bacteria. The active agent is often referred to as a biocide. Many types of biocides are used commercially including silver, triclosan, chloroxynol, quaternary ammonium (QAC) based surfactants and polymeric biguanides. However the overuse of these antimicrobial formulations can be counterproductive in trying to control bacterial numbers as resistant strains can develop. The future challenges for antimicrobial formulation is to reduce the amount of biocide used within the formulation while maintaining its effectiveness and making the formulation last longer.

This research is funded via an EPSRC PhD case award Studentship and was a collaboration between The University of Manchester's Organic Materials Innovation Centre and the AIM listed biocide company Byotrol. Byotrol is interested in biocidal formulations, specifically formulations containing cationic polyelectrolytes and surfactants. Surfactant/Polymeric QACs and biguanides are of particular interest to the company and the focus of this work. The following introduction will describe the different types of biocides and associated mechanism of actions. Particular attention will be paid to cationic polyelectrolyte and surfactant biocides and how these are currently used to create antimicrobial surfaces. The interactions between polyelectrolyte-surfactant formulations at low and high concentrations will also be discussed.

1.2 Bacteria

Bacteria are one domain single cell prokaryotes. Prokaryotes lack a cell nucleus. Bacteria are commonly divided into two categories based on their differing cell wall structures and associated gram staining behaviour. The gram staining technique dyes the bacteria with crystal violet and then an alcohol extraction is taken place. If the bacteria cell retains the dye it is termed gram-positive and if the dye has been removed by the alcohol extraction it is termed gram-negative. Crystal violet binds electrostatically to the bacteria's negatively charged polysaccharides, proteins and nucleic acids.^{1, 2}

To illustrate the structural differences of gram-positive and gram-negative bacteria the differing cell structures are schematically illustrated in Figure 1.1

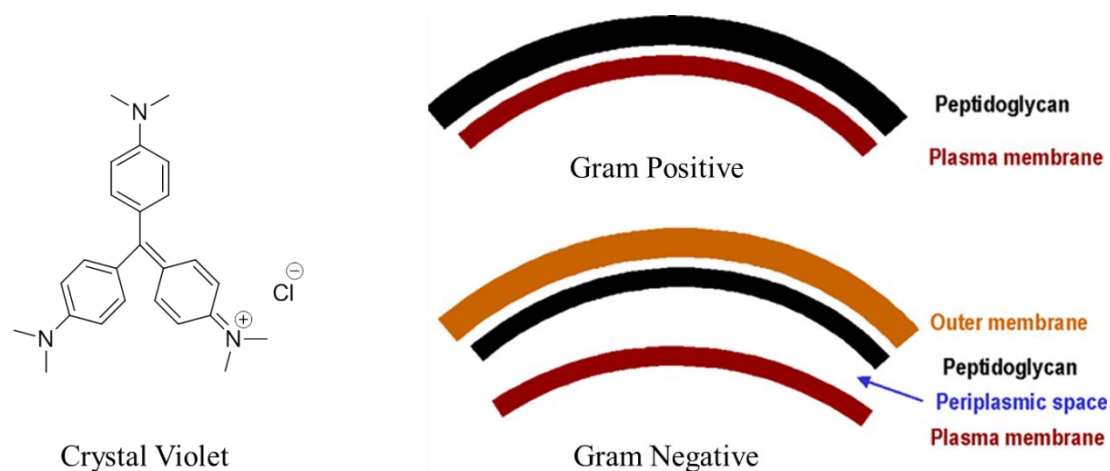


Figure 1.1 Chemical structure of crystal violet and a schematic diagram of gram-positive and gram-negative cell walls.³

The cell wall of gram-positive bacteria is ≈ 30 nm thick and located outside the plasma membrane. The main component of the cell wall is a polysaccharide-peptide complex called peptidoglycan. Also contained within the peptidoglycan layer are polysaccharides, polypeptides and teichoic acids. Teichoic acids are anionic polymers containing glycerol or ribitol derivatives which are attached into chains via

phosphodiester bridges. All these molecules are covalently linked to the peptidoglycan skeleton network. It is believed that these molecules have an important function in the regulation of some enzymes and the binding of specific cations required for plasma membrane stability and function.^{1, 2}

The cell structure of gram-negative bacteria differs in several ways to gram-positive bacteria. Firstly the cell wall or peptidoglycan layer is only 3-8 nm thick and less cross-linked compared to the gram-positive peptidoglycan layer. The other main difference of gram-negative bacteria is the presence of an extra structure outside the peptidoglycan layer. This layer is termed the outer membrane. The protein and lipid composition is completely different from the plasma membrane and contains lipopolysaccharides. Lipopolysaccharides consist of sugar chains to which fatty acid residues are attached to one end thus these are amphiphilic molecules. Within this outer membrane, the fatty acid residues are contained in the lipid layer interior while the polysaccharide is exposed at the membrane surface. These differences are believed to be the reason why the dye staining reacts in a different way.^{1, 2}

Bacteria also come in different shapes with spherical (cocci), egg (coccobacillus) and rod (bacillus) a few well know geometries. Examples of common gram-positive and gram-negative bacteria are listed in Table 1.1.^{1, 2}

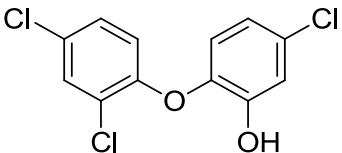
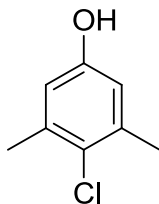
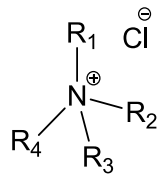
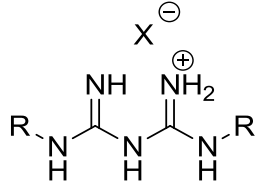
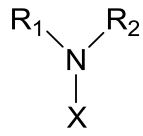
Table 1.1 Examples of gram-positive and gram-negative bacteria.^{1, 2}

| Gram-positive | Gram-negative |
|-----------------------------------|--------------------------------|
| <i>Staphylococcus aureus</i> | <i>Escherichia coli</i> |
| <i>Staphylococcus epidermidis</i> | <i>Pseudomonas aeruginosa.</i> |
| <i>Bacillus subtilis</i> | <i>Aerobacter aerogenes</i> |

1.3 Biocide Types

In general, a biocide is a substance with a broad range of activity to inhibit/kill microorganisms in or on living tissue. In comparison an antibiotic is an organic substance which inhibits/kills selective bacteria at very low concentrations.⁴ A range of different biocides are summarised in Table 1.2.

Table 1.2 Examples of different biocide types.

| Biocide Type | Description | Chemical Structure |
|--------------|-------------------------------|--|
| Phenolic | Small molecule –Triclosan |  |
| Phenolic | Small molecule –Chloroxylenol |  |
| Inorganic | Ionised Silver | Ag^{+1} |
| QACs | Surfactants/Polymeric |  |
| Biguanide | Small molecule/Polymeric |  |
| N-Halamine | Small molecule/Polymeric |  X = Halogen |

1.3.1 Phenolic Compounds

Triclosan and chloroxylenol are the most commonly used phenolic compounds and have a broad range of antimicrobial activity against both gram-positive and negative bacteria.⁴

Although within the same phenolic sub-category, they differ in mechanism of action. Triclosan is a phenyl ether and works by blocking the active site of the enoyl-acyl carrier protein reductase enzyme responsible for fatty acid synthesis. The fatty acid is required to build the cell membrane and reproduce hence the bacteria eventually dies. The drawback of Triclosan is its overuse has led to resistant bacterial strains.⁵

Chloroxylenols mechanism of action has surprisingly not been studied in great detail but is believed to involve the disruption of the cell membrane inducing cell lysis.^{4, 6 7}

1.3.2 Silver

The antimicrobial property of silver has been known for centuries. Silver gets its antimicrobial property when in its ionised form Ag^{+1} . The mechanism of action for silver is not fully understood but it is thought that the silver ions interact with the thiol groups of enzymes and proteins within the bacteria leading to bacteria inactivation.⁸

The drawback of silver is its overuse which is responsible for the emergence of silver resistant strains of bacteria.^{9, 10}

1.3.3 Cationically Charged Biocides

In this section, molecules contain a positively charged nitrogen and have similar mechanisms of action against bacteria. The better antimicrobial molecules have some degree of amphiphilicity in them hence distinct hydrophilic-hydrophobic regions. This amphiphilic property appears to be beneficial in the molecules ability to adsorb onto the bacteria.¹¹

1.3.3.1 *Mechanism of Action*

Although only studied in depth for a couple of specific molecules, the general mechanism of action is believed to be as follows:

The molecules adsorb and penetrate into the cell wall. The cationic molecules interact with the phospholipids contained within the membrane causing membrane reorganisation and the release of cations (K^+) resulting in destabilisation of the plasma membrane inducing cell lysis.¹²⁻¹⁷

1.3.3.2 *QAC Surfactants*

Quaternary ammonium compounds (QACs) contain a nitrogen with four alkyl or aryl groups giving the nitrogen a positive charge; while to maintain electrostatic neutrality a negatively charged chloride is also present. The positive charge on the nitrogen is independent of pH.¹⁸

QACs are used commercially as antimicrobials but more specifically QAC surfactants are used.¹⁸ Surfactants are amphiphilic molecules which contain a hydrophilic headgroup and a hydrophobic tail. In this case the quaternary ammonium nitrogen is the hydrophilic head group while the alkyl/aryl groups form the hydrophobic tail. This amphiphilic structure makes surfactants highly surface active hence an increased preference to absorb onto the negatively charged bacteria. A wide

range of different surfactant structures are used as antimicrobials. The most common include; alkyl trimethyl ammonium chloride, dialkyl dimethyl ammonium chloride and alkyldimethylbenzyl ammonium chloride.¹⁸

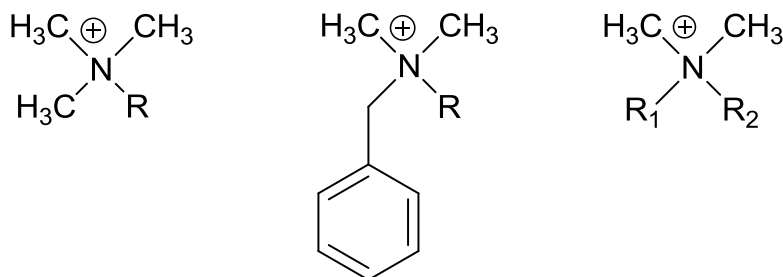


Figure 1.2. Chemical structures, (left) Alkyltrimethyl ammonium, (centre) Alkyldimethylbenzyl ammonium and (right) Dialkyldimethyl ammonium. R = Alkyl group.

Different R group lengths have been tested against a range of gram-positive and gram-negative bacteria to establish the chain length with the optimal antimicrobial activity, although the optimal antimicrobial activity varies from organism to organism due to the different structural differences between the respective bacteria.

For alkyldimethylbenzyl ammonium chlorides (BAC) an alkyl chain of C₁₄ was found to have the best all round antimicrobial activity. Although C₁₀₋₁₂ were more active against yeasts and fungi, C_{14-C16} were most susceptible to gram-negative bacteria. Due to these different activities, commercially they are sold as mixtures with a range of different R group lengths (C₁₂₋₁₈). These mixtures give BAC a broader range of antimicrobial activity.^{18, 19}

Different length R groups of various dialkyldimethyl ammonium chlorides (DMAC) have also been investigated for their antimicrobial activity against *Pseudomonas*. The minimum bactericidal concentration was determined. The C₁₀/C₁₀, C₈/C₁₂ and C₉/C₁₁ all gave comparable results of 500 ppm while the C₉/C₁₂ and C₁₀/C₁₁ gave a slightly

increased 550 ppm. Similarly to BAC, mixtures of different R group lengths are available commercially for DMACs.¹⁸

Building on the idea that synergistic mixtures of QAC surfactants gives a broader and improved level of antimicrobial activity Schaeufele *et al.*²⁰ observed that a 3/2 blend of DMAC (C₈/C₈ 25%, C₁₀/C₁₀ 25%, C₁₈/C₁₈ 50%) / BAC (C₁₂ 40%, C₁₄ %50, C₁₆ 10%) gave superior results compared to the individual components of the mixture.

1.3.3.3 Polymeric QACs

Polymeric or polymer molecules are compounds consisting of repeating monomeric units which form a macromolecule after a process known as polymerisation. Polymeric QACs are within a class of polymers referred to as polyelectrolytes. Polyelectrolytes are polymers which have ionisable groups within the repeat unit and when placed into a polar solvent (water) these groups dissociate. In this case the ionisable group is the quaternary ammonium nitrogen with a corresponding chloride counter ion.²¹

Homo-polymeric QACs have been reported to show some low level antimicrobial activity however none are used commercially as antimicrobials as other biocide types have superior antimicrobial activity. Instead they are used as conditioning actives in shampoo formulations with molecular weights > 100 kDa.¹⁸ Two common homo-polymeric QACs are Polydiallyldimethyl ammonium chloride (pDADMAC) and Poly(2-dimethylamino)ethyl methacrylate) methyl chloride quaternary salt (PDMC).

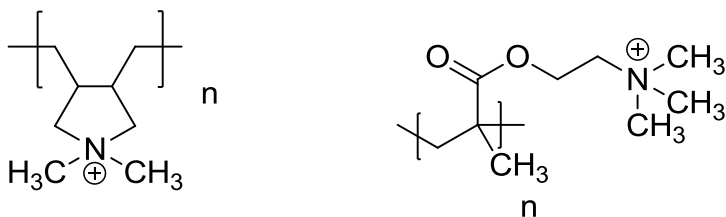


Figure 1.3. Chemical structures of Homo-Quaternary ammonium polymers, (Left) Polydiallyldimethyl ammonium, (Right) Poly(2-dimethylamino)ethyl methacrylate) methyl chloride quaternary salt. (Chloride counter ion omitted for clarity).

Co-polymers of acrylamide and diallyldimethylammonium chloride and vinylpyrrolidone and methacrylamidopropyl trimethylammonium have been observed to have low level antimicrobial activity, however these were inferior to alternative commercially available QACs.²²

Additionally a quaternised hydroxyethylcellulose ethoxylate was studied with a similar level of antimicrobial performance to the *co*-polymers.²²

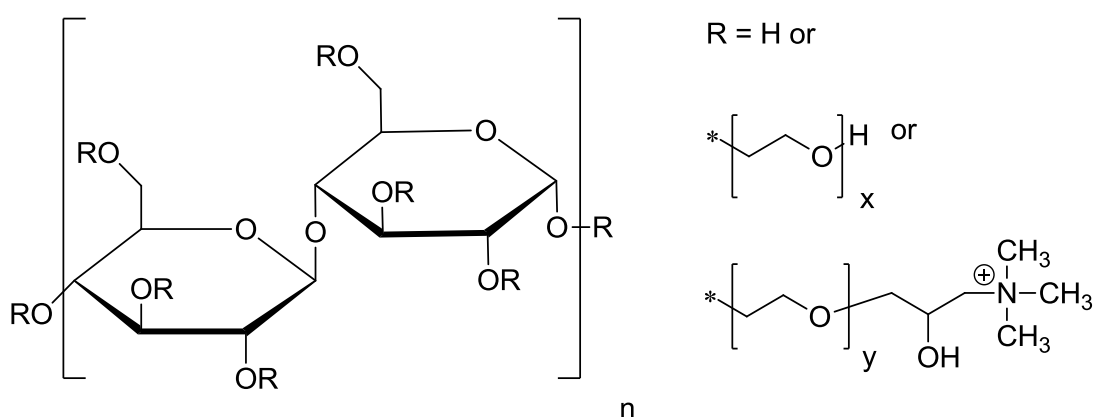


Figure 1.4. Chemical structure of Hydroxyethylcellulose ethoxylate, quaternised.

1.3.3.4 *Biguanides*

Biguanides consist of a combination of three secondary amines and two imines groups. Chlorhexidine is a biguanide based biocide which can come as a free base or in a salt form. Chlorohexidine gluconate is the most commonly used salt. At pH 7 gluconic acid forms the gluconate ion.

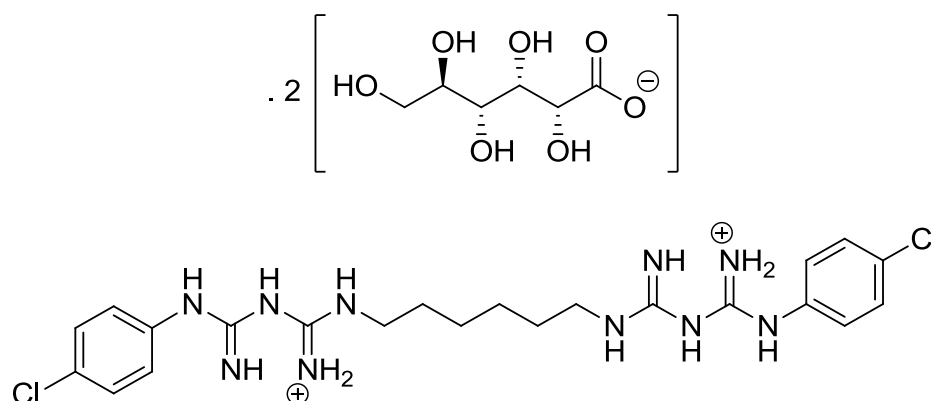


Figure 1.5. Chemical structure of Chlorhexidine gluconate salt.

Chlorohexidine has a broad range of antimicrobial activity against gram-positive and gram-negative bacteria. Chlorhexidine is commonly used in handwashes and oral products. The mechanism of action although initially believed to be due to the inhibition of the enzyme adenosine triphosphate (ATP) is now thought to be primarily a membrane disruption based mechanism.^{4, 23}

Polyhexamethylenebiguanide chloride (PHMB) is a polymeric biguanide and the only commercially available polymer currently used as an antimicrobial. PHMB is sold commercially (Arch Chemicals) with degree of polymerisation (n) of ≈ 12 . The +1 ionised species was determined as the most likely to exist with positive charge thought to be delocalised over the whole biguanide group. The favoured tautomeric form of PHMB is shown in Figure 1.6. The pK_a of PHMB is 13.8.²⁴

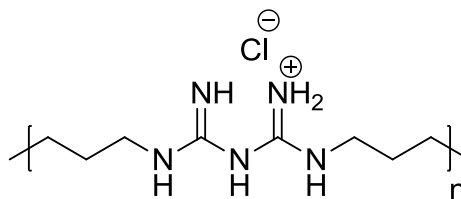


Figure 1.6. Chemical structure of Polyhexamethylene biguanide chloride (PHMB).

The antimicrobial activity of PHMB has been tested against a wide range of bacteria in terms of its ability to kill or inhibit, with results confirming its usefulness as an antimicrobial agent.¹⁴⁻¹⁶ Whilst within most polymeric molecules the bioactive groups lose activity when incorporated into a polymeric structure, this is not the case for PHMB. The separation of the biguanides by a hexamethylene group gives PHMB a degree of amphipilicity compared to the polymeric QACs mention previously and is a likely factor in PHMBs superior antimicrobial activity.

A paper from Broxton *et al.*¹⁴ studied an amine ended dimer ($n = 2$), (PHMB $n = 5.5$) and a higher molecular weight (PHMB $n > 10$). The higher the molecular weight of PHMB the better antibacterial activity observed against *E. coli*.

1.3.3.5 Non-Commercially available Polymeric Biocides

Numerous studies have looked at the effects of molecular weight, differing polymer structures, hydrophilic/lipophilic balance (HLB) and linker spacing on antimicrobial activity.

The dependence on antimicrobial activity for polyacrylates with side chain biguanide groups and polytributyl 4-vinyl benzyl phosphonium chloride on M_w was observed to be bell shaped. A critical region of optimal performance was identified, $M_w \approx 14$ -100 kDa.²⁵ These studies looked at the gram-positive bacteria *S. aureus*. While Chen *et*

*al.*²⁶ observed a parabolic dependence on molecular weight for a range of quaternary ammonium functionalized poly(propyleneimine) dendrimers. This study looked at the gram-positive *s. aureus* and the gram-negative *E. coli*.

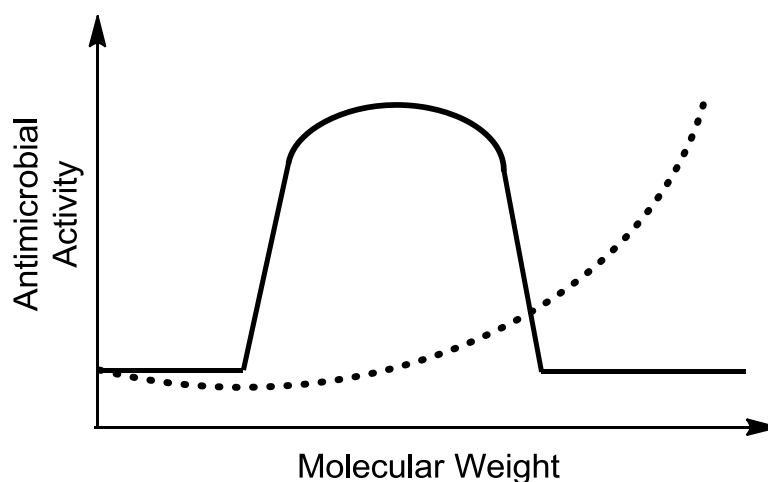


Figure 1.7 Schematic illustration of the antimicrobial activity as a function of molecular weight relationships observed within the literature. Solid line = Optimal region, Dotted line = Parabolic dependence.

A number of studies have altered the HLB of the polymer by changing alkyl chain lengths within the polymer structure. Panarin *et al.*²⁷ studied a range of quaternised polymeric vinylamine and aminoalkyl methacrylates which showed no difference in antimicrobial activity. This study looked at the gram-positive *s. aureus* and the gram-negative *E. coli*. While Ikeda *et al.*²⁸ studied a range of poly(trialkylvinylbenzylammonium chloride) with the C₁₂ chain observed to have the highest antimicrobial activity.

Additionally Ikeda *et al.*²⁹ look at the effect of altering the spacer distance between the cationic moieties for a range of polymeric pyridinium salts. A range of gram-positive and gram-negative bacteria were tested but no conclusive relationship was observed.

1.3.3.6 Limitations

The disadvantage of these cationically charged molecular biocides is that their antimicrobial performance is strongly inhibited by hardwater (CaCO_3 , MgCO_3), which can be problematic.¹⁸ The increased ion content with the water causes the chloride counter ion to be held more tightly to the nitrogen quenching the positive charge.^{30, 31}

1.3.4 N-Halamines

N-Halamines are defined as compounds containing one or more nitrogen-halogen covalent bonds. The monomeric form has been used for decades and is commonly used as a water disinfectant. Recently these compounds have been incorporated into polymeric materials, with these materials showing good antimicrobial activity.^{32, 33}

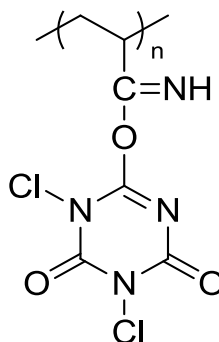


Figure 1.8. An example of a polymeric N-Halamine.

The mechanism of action is believed to be from the direct transfer of positively charged halogens (Cl^+ or Br^+) from the N-Halamine to a biological receptor on the bacteria leading to cell inhibition and deactivation. So far there has been no known documented cases of resistant microbes towards N-halamines.³⁴

1.3.5 Summary

A review of different biocide types was undertaken which looked at their different structural properties as well as their associated mechanism of action. Any trends in antimicrobial activity due to differing structural properties were discussed. Particular attention was given to cationic surfactants and polymer as this research project will be concentrating on formulations containing these biocides.

1.4 Antimicrobial Surfaces

This research project will be looking at creating antimicrobial surfaces with the potential to be used in hard surfaces and skin cleaning. Within the literature a large number of papers have been published in a similar field looking at bacterial resistant abiotic surfaces primarily for medical devices in the hope of preventing human infections when these devices are placed within the body. An abiotic surface is simply a non-living surface which is placed inside a biological system (the body). A number of different strategies have been suggested to create these antimicrobial surfaces and are summarised in Figure 1.9.

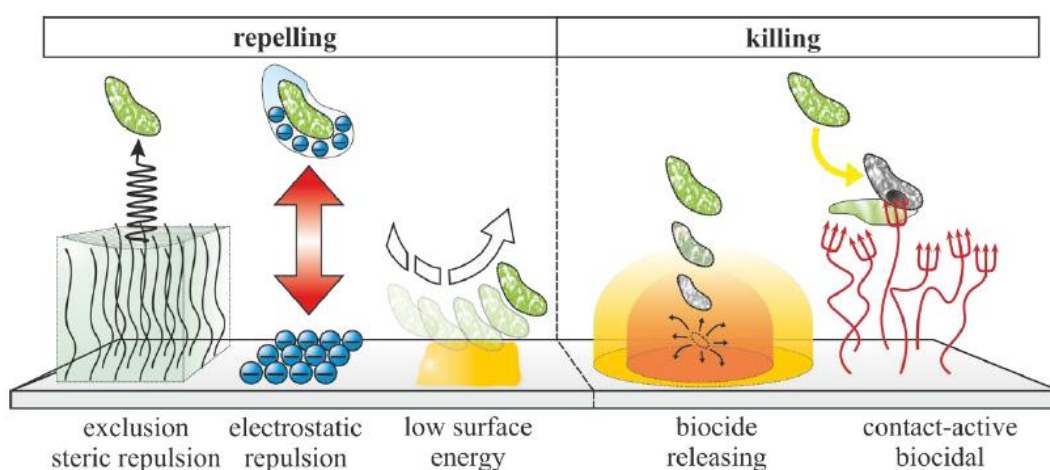


Figure 1.9 Different strategies for creating antimicrobial surfaces.³⁵

The three specific strategies for the development of these antimicrobial surfaces and the biocides used are summarised in Table 1.3.

Table 1.3. Strategies for designing antimicrobial abiotic surfaces.

| Strategies | Examples |
|------------------------------------|---|
| Contact kill | Covalently and hydrophobically attached cationic polymers. ^{26, 36-49} |
| Polyelectrolyte multilayers (PEMs) | Immobilised- QACs ⁵⁰ , guanidines. ⁵¹ and Chitosan ⁵² Leaching- silver ^{50, 53, 54} or antimicrobial peptides. ^{55, 56} |
| Adhesion resistance | Pegylated Surfaces. ⁵⁷⁻⁵⁹ |

1.4.1 Contact Kill

By far the most popular strategy is contact kill. These surfaces are permanently modified via the attachment of a biocide to the substrate. The biocides are permanently attached by chemisorption (covalent attachment). Various cationic polymers have been used including QACs, alkyl pyridiniums and quaternary phosphoniums. Different polymer architectures have also been studied including polymer brushes (polyDMAEMA) and hyper-branched dendrimers (quaternary ammonium functionalised poly(eneimine)).^{26, 36-48}

The advantage of attaching a biocide to a substrate is that the biocide is never released into the environment so it is seen as an environmentally friendly method of preventing bacterial growth. The disadvantage is that it is very expensive to create.

An alternative strategy to covalently attaching a biocide to a substrate is to hydrophobically anchor the biocide to the surface. This was demonstrated by Park *et al.*⁴⁹ who looked at a comparative study of N-dodecyl, N-Methyl-PEI and N-hexyl, N- methyl polyethylene imine. This has the advantage that it can be painted or potentially sprayed onto a surface instead of the expense of covalently attaching the biocide to the surface.

1.4.1.1 Hole-Poking Mechanism

It has been reported in the literature that surfaces with covalently attached quaternary ammonium compounds induce cell lysis via a “hole-poking” mechanism.⁴³⁻⁴⁸ The cationic moieties of quaternary ammonium compounds (QACs) are known to interact mainly with the bacterial plasma membrane. This accumulation of cationic charge next to the cell membranes causes the membrane to lose integrity leading to cell death via cell lysis.¹²

Lin *et al.*⁴⁸ looked at varying the molecular weight of covalently attached N-alkylated poly(ethyleneimine). It was found that molecular weights of 0.8 and 2 kDa had no antimicrobial activity response but molecular weights of 25 and 750 kDa had a very good antimicrobial activity. This result suggests the polymer chain length has to be of sufficient length to induce cell lysis. It was established that the cell envelope of a bacterial cell is ≈ 30 nm thus the polymer chain must be longer than this length to be able to fully transverse into the cell envelope and disrupt the cell membrane.⁴⁷

1.4.1.2 Critical Charge Density

In 2005 Kugler *et al.*⁴¹ grafted quantised poly(vinylpyridine) onto glass and varied the charge density of the surface with in these organic layers. This study illustrated that the charge density of a surface has a dramatic effect on the surfaces antimicrobial performance. An optimal charge density was observed where antimicrobial activity was improved. The gram-negative *E. coli* and gram-positive *S. Epidermidis* bacteria were studied. Subsequent studies by Murata *et al.*⁴² who grafted

poly(DMAEMA) onto glass and Lichter *et al.*⁶⁰ who used a polyelectrolyte multilayer (PEMs) strategy (Section 1.4.2), all observed an optimal charge density threshold.

The charge density threshold for the systems described above for both gram-positive and gram-negative bacteria was found to be between $10^{13-15} \text{ N}^+/\text{cm}^2$. It is worth noting that it has been observed that a higher charge density is needed for gram-positive bacteria compared to gram-negative which is likely due to the differing cell structures.

Based on this observed optimal density observation an ion exchange mechanism has been proposed. This involves the positively charged moieties on the polyelectrolyte absorbing to the bacteria and inducing the release of divalent cations from the bacteria. These cations are needed for membrane stability and their absence induces cell lysis and subsequent cell death.⁴¹

1.4.2 Polyelectrolyte Multilayers (PEMs)

Recently a Polyelectrolyte Multi-layers (PEMs) coating approach has been developed which can incorporate either a contact killing or biocide leaching strategy. Leaching involves the biocide being only physisorbed to the surface via a combination of electrostatic, hydrophobic and Van der Waals forces. The biocide then slowly dissociates off the surface into the solvent and subsequently kills the bacteria within the solution not at the surface.

PEMs involve coating a substrate with a cationic polyelectrolyte followed by an anionic polyelectrolyte, with this layering process continuing a number of times.⁶¹

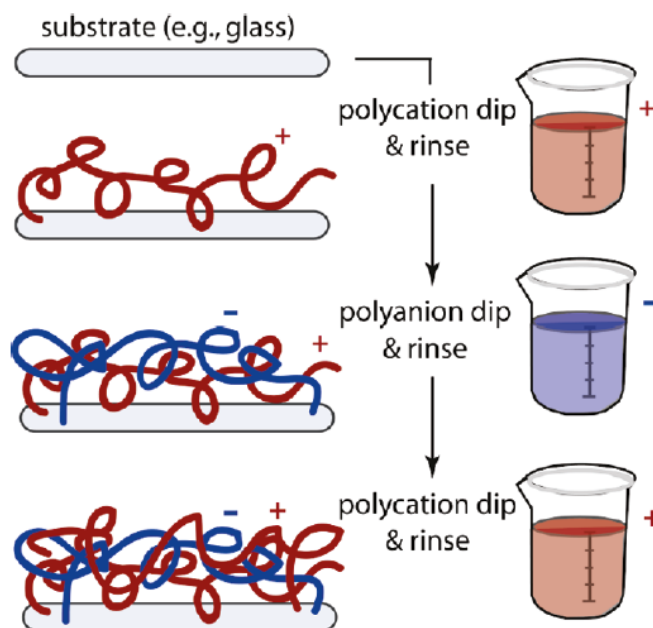


Figure 1.10 Schematic illustration of the PEMs coating procedure.⁶¹

Within these polyelectrolyte layers a biocide is placed. Biocides used within a PEMs system include QACs, guanidines, silver, peptides and chitosan^{50-56, 60-62}. These biocide actives are either immobilised within these layers or leach out from the layers.

1.4.3 Adhesion Resistance

The mechanism of bacterial attachment has not been fully established but it is widely believed to be a combination of specific and non-specific interactions which include surface charge, hydrophobicities, Van der Waals and specific receptor interactions.

A number of papers have looked at grafting polyethylene oxide (PEO) to surfaces which create a hydrophilic hydrated polymer layer. This polyethylene layer has been shown to be quite effective at preventing bacterial adhesion to the surface.⁵⁷⁻⁵⁹

1.5 Solution Interactions

This project will look at aqueous mixtures of QAC surfactants in combination with polymeric QACs and biguanides. The underlying principles of how these actives would be expected to behave in isolation and within a mixture will be discussed.

1.5.1 Surfactants

1.5.1.1 Surfactant Type

The surfactant-polyelectrolyte mixtures to be studied all contain one or a mixture of two cationic surfactants. Surfactants are amphiphilic molecules. Amphiphilic molecules contain a hydrophilic (water-loving) head group and a hydrophobic (oil-loving) tail.

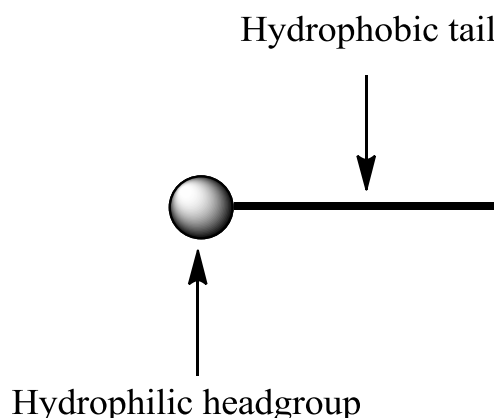


Figure 1.11 Schematic diagram of a surfactant molecule.

Surfactants are commonly classified via their head group. The three most common surfactant types are non-ionic, ionic and zwitterionic surfactants. Nonionic surfactants have head groups which do not contain electrostatic charge while ionic surfactants are split into two groups depending on the charge of the head group. Anionic surfactants have a negatively charged headgroup while cationic surfactants have a positively charged head group. Zwitterionic contain both a cationic and anionic moiety within the headgroup.^{31, 63, 64}

Cationic surfactants didecyldimethyl ammonium chloride (DDQ) and Alkyl (C_{12} 70%; C_{14} 30%) Dimethyl benzyl ammonium chloride (BAC) will be studied within the report.

1.5.1.2 Surface Activity

When a surfactant is placed in an aqueous environment the surfactant adsorbs onto the air-water interface. The hydrophobic tail is oriented towards the surface while the polar head group is exposed to the water interior. The driving force causing a surfactant to adsorb to the air-water interface is its desire to lower the interfacial energy (surface tension). The interfacial tension is caused by an imbalance of the attractive forces on a molecule at the interface compared to the bulk solution. In the case of water, when a molecule is at the interface it has less opportunities to hydrogen bond with neighbouring water molecules thus the molecule is in a higher energy state. This large imbalance in energy between the bulk water molecules and water molecules at the interface is why water has a high surface tension of 72-73 mN/m.

When a surfactant is placed into the water a distortion of the hydrogen bonding interaction takes place within the bulk solution. The presence of the hydrocarbon chain of a surfactant causes a solvent cage to form around the hydrophobe. This solvent cage causes a decrease in entropy within the bulk solution thus an increase in the systems free energy. Less work is required to bring the surfactant to the interface compared to a water molecule so the process of surfactant adsorption onto the air-water interface is spontaneous. The water molecule previously on the interface returns to the bulk thus reducing the interfacial tension of the air-water interface.^{31, 63,}

64

The interfacial energy (surface tension) is defined as the amount of work required to expand the surface area.

$$W = \gamma \cdot \Delta A \quad (1.1)$$

where W = Work (kJ), γ . = Surface tension (N/m), ΔA = Change in area (m^2).

The more densely packed the surfactant is at the interface the lower the interfacial (surface tension) will become. The concentration of surfactant absorbed at the air-water interface depends on the packing number of the surfactant. This is determined by a number of factors. Firstly the surface area of the surfactant head group on the water-air interface and secondly the intensity of any electrostatic charge on the head group (only for ionic surfactants).

1.5.1.3 Gibbs Adsorption Isotherm

Within surfactant chemistry an important concept is calculating the concentration of a surfactant absorbed at the interfacial region; the so called surface excess concentration. The surface excess is the concentration of a solute in a surface plane relative to a similar plane in the bulk solution. This is experimentally very difficult to determine so Gibbs developed an indirect method to estimate this concentration based on the Gibbs dividing surface.^{31, 64}

The Gibbs dividing surface is a mathematical two dimensional dividing plane used to describe this interfacial region. Figure 1.12 schematically describes this region.

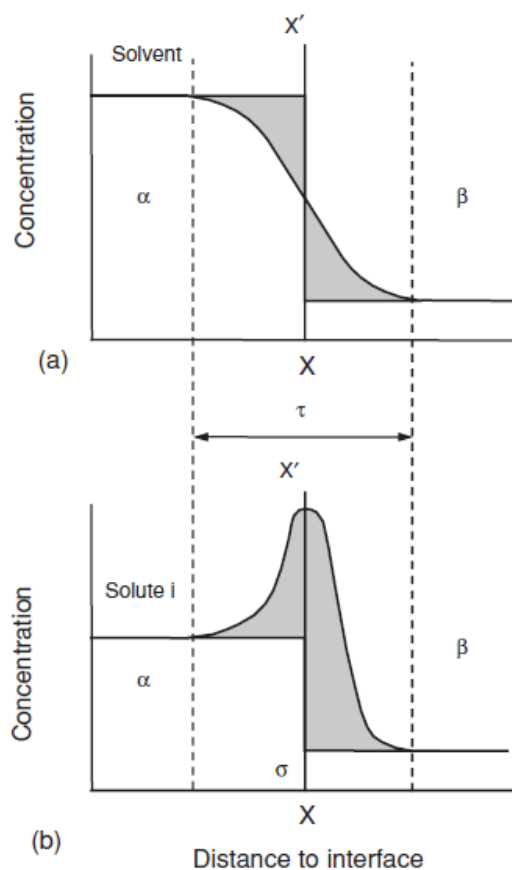


Figure 1.12 Diagram illustrating Gibbs dividing surface. α = Solvent Phase, β = Gas Phase, τ = Interfacial Region, X' = Gibbs dividing surface. Shaded area = concentration of component either side of plane.⁶⁴

The Gibbs dividing surface is the plane where the solvent excess concentration is defined as zero. The surface excess of the solute is then the difference in its concentration either side of the plane.

A surface tensiometry plot as a function of surfactant (log) concentration can be used to calculate the surfactants CMC but also can be used to calculate the surface excess concentration via the Gibbs adsorption isotherm.^{31, 64}

The most general formula for the Gibbs Adsorption isotherm is

$$d\sigma = -\Gamma_2 d\mu_2 \quad (1.2)$$

where $d\sigma$ = change in surface tension (N/m), Γ_2 = the surface excess concentration (mol/m²) and μ = Chemical potential of component.

When related to concentration

$$d\sigma = -RT\Gamma_2 d\ln x_2 \gamma_2 \quad (1.3)$$

where x = Mole fraction and γ = Activity coefficient of component.

At low concentration the activity coefficient can be assumed to be unity so;

$$d\sigma = -RT\Gamma_2 d\ln C_2 \quad (1.4)$$

where C_2 = Solute concentration (mol/L). For ionic surfactants the situation is more complicated due to the presence of the counter ion and the need to maintain electronic neutrality and as a consequence the Debye Huckel theory is needed to calculate the activity coefficient.

The Gibbs adsorption isotherm for a 1:1 fully dissociated ionic surfactant at a concentration $< 10^{-2}$ M is as follows;

$$d\sigma = -2RT\Gamma_2 d \ln C_2 \quad (1.5)$$

Once the surface excess concentration has been calculated it is possible to calculate the area per surfactant molecule at the air-water interface via Equation 1.6.³¹

$$A_2 = \frac{1}{N\Gamma_2} \quad (1.6)$$

where A_2 = Area per molecule at the interface, N = Avogadro's number (mol^{-1}).

1.5.1.4 Micellisation

At a critical concentration it becomes more thermodynamically favourable for the surfactant unimers to form dynamic aggregates within solution called micelles. Micelle formation or micellisation is a process which enables the hydrophobic tail of the surfactant to be removed from the water thus reducing the free energy of the system. The concentration which micelles begin to form is referred to as the critical micelle concentration (CMC).^{31, 63, 64}

As explained above the hydrophobic chain of the surfactant unimers within solution are surrounded by water which forms a cage like structure around the hydrophobe. The removal of the hydrophobe from an aqueous environment is driven via the so called hydrophobic effect which causes apolar species (surfactant tail) to aggregate together. The hydrophobic effect is driven by the free energy of cohesion of water or more specifically the hydrogen bonding between the water molecules.

The micellisation of the surfactant causes the water cages previously formed around the hydrophobe tails to disperse causing an increase in entropy within the bulk system. The decrease in entropy caused by micelle formation is minor compared to the increase in entropy due to the dispersing of these water cages. Micellisation is thus an entropically driven process. Micelles are dynamic aggregates and are in

dynamic equilibrium between the air-water interface, bulk solution and micelle form.^{31, 63, 64}

It should be noted that for micelles to form within solution the systems temperature must be above the Krafft point. The Krafft point is the critical temperature above which the surfactant is soluble. If the temperature is below the Krafft point the surfactant unimers precipitate out of solution and form crystalline structures. Thermodynamically at the Krafft point entropic forces become more dominant over enthalpic forces thus entropy induces the breakup of these surfactant crystalline structures.³¹

1.5.1.5 Factors affecting the Critical Micelle Concentration (CMC)

The CMC of the surfactant depends on the structural make-up of the molecule and the solvent properties. Given below are the different factors which affect the CMC.⁶³

- The larger the hydrophobe the lower the CMC of the surfactant. The formation of micelles is driven by the need of the hydrophobe to limit the surface area which is in contact with water (hydrophobic effect).
- Within the hydrophobe if there is branching, double bonds, aromatics or other polar character this can increase the CMC of the surfactant.
- The CMCs of non-ionic surfactants are significantly lower than ionic surfactants due to the strong electrostatic repulsion between the ionic head groups.
- For ionic surfactants the counter ion can affect the CMC. The CMC increases depending of the following counter ion types $F^- > Cl^- > Br^-$. This is due to differences in counter ion binding and subsequent quenching of the electrostatic charge.

- The addition of salt within the system can dramatically reduce the CMC of ionic surfactants as the salt shields the electrostatic repulsion between the ionic head groups thus making it more favourable for micelles to form. An increase in micelle aggregation number is also expected.

1.5.1.6 Surfactant Mixtures

This project will be looking at QAC surfactant mixtures of varying nomenclatures and alkyl/aryl chain lengths. In 1975 Clint developed a mixed micelle theory based on this type of micellisation.⁶⁵ The Clint equation enabled the prediction of the CMC of a surfactant mixture which contained similar headgroups. The Clint equation was originally used for non-ionic surfactants but has been successfully proven to be viable for ionic surfactants. It is important to note that deviations from the value obtained from the Clint equation (Equation 1.7) for a surfactant mixture is due to interactions between the surfactant pairs. There can be antagonist interactions which are unfavourable interactions between the surfactant pairs or synergistic interactions which are favourable interactions.

$$x_1 = \frac{C_1}{C_1 + C_2} \quad (1.7)$$

$$\frac{1}{CMC} = \frac{X_1}{CMC_1} + \frac{1 - X_1}{CMC_2} \quad (1.8)$$

where CMC = CMC of surfactant mixture, CMC_1 = CMC of Species 1, CMC_2 = CMC of Species 2, X_1 = Mole fraction of surfactant 1, C_1 = Molar surfactant concentration of species 1, C_2 = Molar surfactant concentration of species 2.

1.5.1.7 Micelle Structures

Amphiphilic molecules can aggregate into various structures when above its respective CMC with the hydrophobic tail directed towards the micelle interior (oil-loving) and the hydrophilic head group directed towards the aqueous medium.^{31, 63, 64} Some potential micellar structures are illustrated in Figure 1.13.

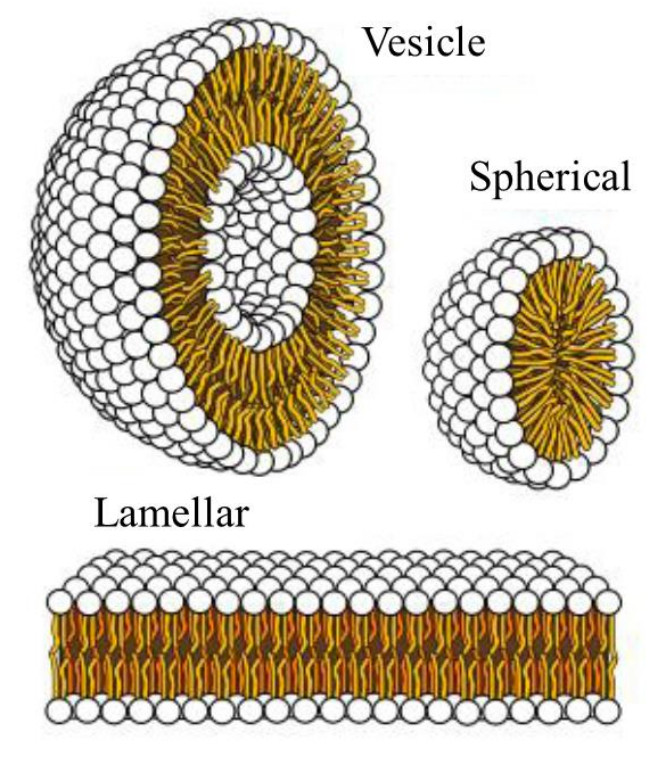


Figure 1.13. Schematic illustration of different micellar structures.⁶⁶

The number of surfactant unimers contained within the micelles is referred to as its aggregation number. Spherical micelles have a low surfactant number and the hydrocarbons core radius is approximately the length of the extended hydrocarbon tail. At higher surfactant aggregation numbers worm like micelles, vesicles and lamellar structures can form. Worm like micelles have a similar cross section to a spherical micelles but the length of the micelle can vary greater. Vesicles (unimellar or multimellar) contain at least two water compartments one forming the core and

one the external medium. Finally a lamellar phase contains surfactant bilayers.^{31, 63, 64}

What particular micelle structures form within solution depends on a number of factors including structural architecture, concentration and solvent salinity.³¹

1.5.2 Polyelectrolytes

1.5.2.1 Polyelectrolyte Type

Polyelectrolytes are polymers which have ionisable groups within their repeat unit and when placed into a polar solvent (water) these groups dissociate. Upon counter ion dissociation charge is left on the polymer while the corresponding counter ion is released into the solution.^{21, 30} This discussion will concentrate on cationic polyelectrolytes.

Polyelectrolytes are normally categorised into two types; weak or strong. Weak polyelectrolytes have a pK_a (Acid dissociation constant) between ≈ -2 -12 hence the polyelectrolyte will only partially dissociate at reasonable pHs (2-10). The alteration of the pH modifies the fraction of dissociation within the molecule significantly. An example of a weak polyelectrolyte is Poly(allylamine) hydrochloride.⁶⁷

The ionisable groups of a strong polyelectrolyte fully dissociate at all reasonable pHs (2-10) with the charge normally described as independent of pH. An example of a strong polyelectrolyte is poly(diallyldimethylammonium) chloride a polymeric QAC.⁶⁷

1.5.2.2 Chain Conformation

The chain conformation of a polyelectrolyte changes as a function of concentration and ionic strength. At low concentrations (dilute regime), the charged moieties repel

each other intramolecularly stretching the polyelectrolyte chain out. As the concentration increases and/or a low molecular weight electrolyte is added (NaCl) the polyelectrolyte changes geometrically from a rod like to a more spherical/gaussian coil like conformation.⁶⁷

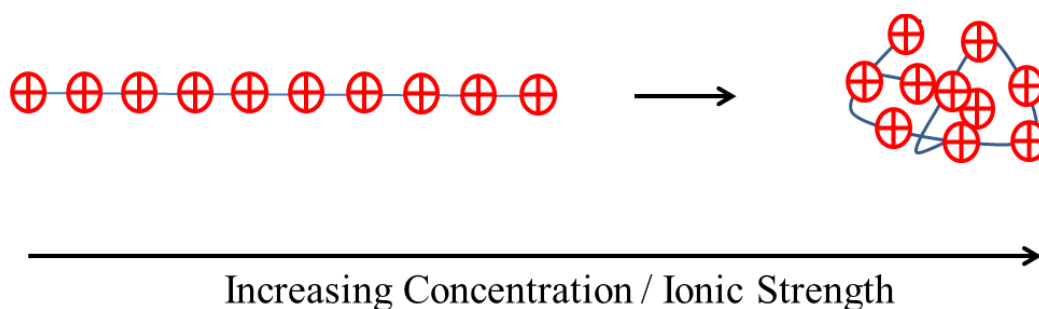


Figure 1.14. Schematic diagram of polyelectrolyte conformations as a function of concentration / ionic strength. Counter ion omitted for clarity.

The ionic atmosphere around these ionisable moieties is screened by the increasing ionic strength condensing the counter ion to the charged moiety. The condensing of the counter ion leads to a quenching of the residual charge on the polyelectrolyte. With the intramolecular repulsion reduced the polyelectrolyte becomes more flexible and starts to behave more like a neutral polymer forming a spherical/gaussian coil like conformation.⁶⁷

The chain conformation of salt free polyelectrolyte solution is very complex and the previously described model is a very simplistic view of this. A more complex model was proposed by T. Odijk⁶⁸ who suggested four distinct concentration regimes dilute rods, rigid rods, flexible rods and a gaussian coil like conformation. Polyelectrolyte conformations as a function of concentration will be explained in greater depth within Chapter 4 – Polyelectrolytes in Solution.

1.4.1.3 Poly(hexamethylene biguanide) Chloride (PHMB)

The polymeric biguanide PHMB differs from most polyelectrolytes because the distance between the ionisable groups along the contour length of the chain is greater than the Bjerrum length of the solvent (water, 20 °C = 0.712 nm). The Bjerrum length is defined as the characteristic distance that a stable dissociative state can form between a singly charged ion pair.⁶⁹

As far as we are aware no one has experimentally studied the solution behaviour of PHMB however a computer simulation was conducted by Blackburn *et al.*²⁴ It was shown that PHMB does not follow the conventional micelle model. It was instead observed that PHMB has a high potential for H-bonding within the water and the computational study suggests that the conformational structure of PHMB within solution is a kinked globular structure which they suggest is to do with intramolecular H-bonding taking places between the biguanide groups. Figure 1.15 illustrates this kinked globular structure.

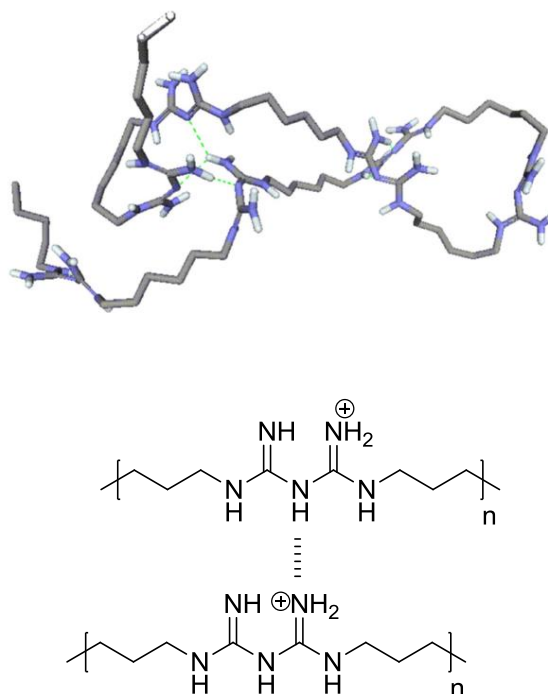


Figure 1.15. Computer simulation of hydrogen bonded kinked globular structures of PHMB in water at 300 K.²⁴

It was also suggested that at high concentrations the biguanides groups could begin forming intermolecular H-bonds thus producing an H-bonding network of PHMB within solution.²⁴

1.5.3 Low Concentration Surfactant/Polymer Mixtures

In recent years many investigations have been conducted looking at water soluble polymer-surfactant mixtures. A large number of these papers have looked at the interactions between neutral polymer-ionic surfactants and polyelectrolyte-ionic surfactants of opposite charge and been comprehensively reviewed by E. D. Goddard.^{70, 71} Particular attention has been given towards mixed aggregate formation within the bulk solution. The concentration at which mixed aggregate formation has been identified is termed the critical aggregation concentration (CAC).

In the literature there is a widely accepted view that in a weakly interacting surfactant-polymer system a pearl-necklace structure forms within solution when a synergistic interaction occurs between the surfactant and polymer. The interaction can either be driven by a hydrophobic interaction or a stronger electrostatic interaction. The pearl-necklace aggregates form by surfactants associating or binding onto the polymer by forming discrete micellar clusters along the polymer chain.

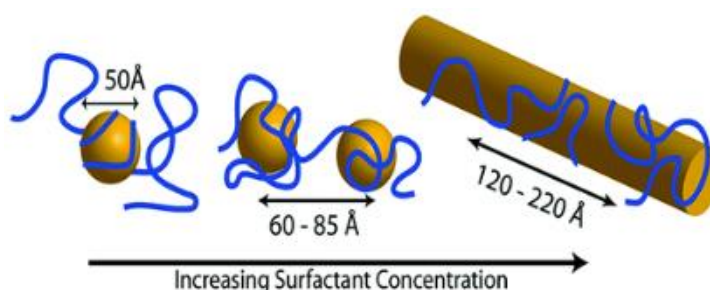


Figure 1.16. Schematic diagram of the Pearl-Necklace Model. Sphere/cylinder = micelles, Thread = Polymer.⁷²

Within the literature Sodium dodecyl sulphate (SDS)-polymer interactions have been widely studied. These studies report this pearl necklace model within the system.⁷³⁻⁷⁵ Although not as common a number of studies have looked at cationic surfactants and neutral polymer, again the pearl necklace based model was reported but the interaction appears to be weaker than with anionic surfactants. This weaker interaction was attributed to the fact the cationic surfactants have larger head group which cause a steric hinderance against association/binding with the polymer.⁷⁶

It is worth noting that that in the case of ionic surfactant-polyelectrolyte mixtures of opposite charge mixed aggregate formation can result in the complex precipitating out of solution as the charge of both the ionic surfactant and polyelectrolyte is neutralised.

One area of interest that has not been extensively reviewed and of important interest within this study is the interactions between polyelectrolytes-surfactants of similar charge. Within the literature, there as far as we have been aware no reports of mixed aggregate formation except in the cases where the polyelectrolyte has been hydrophobically modified so that the hydrophobic interactions of the polyelectrolyte can overcome the electrostatic repulsion of the surfactant head group. A mixed micellisation process was observed.^{77, 78}

Polyelectrolytes and surfactants of similar charge which have not been hydrophobically modified have only been scantily reviewed. A recent study by H. Comas-Rojas *et al.*⁷⁹ on this area reported a reduction in the CMC of Cetyltrimethylammonium bromide (CTAB) when in the presence of polyethyleneimine. This was determined to be due to an electrolyte effect.

Polyelectrolyte and ionic surfactants are electrolyte type additives. The addition of an electrolyte into aqueous mixtures screens/suppresses electrostatic charge. For the

case of ionic surfactants, a reduction in the critical micelle concentration (CMC) would be expected. The electrostatic repulsion between the charged headgroups will reduce due to the suppression of the ionic atmosphere causing the counter ions to be held more tightly. An increase in micelle aggregation number would also be expected.⁷⁹

1.5.4 Concentrated Surfactant/Polymer Mixtures - Phase Separation

As well as being interested with the interactions taking place at low concentration there are a number of studies looking at the phase separation of polymer-surfactant mixtures. The phase separation of polymer-surfactant mixtures have been comprehensively reviewed by L. Piculell and B. Lindman.⁸⁰

Phase separation can be categorised into two general types; segregative and associative. Segregative phase separation is when the solute composition is extremely asymmetric between the two phases. In the case when two polymers are present within the solution it is referred to as polymer incompatibility. This type of phase separation is driven when the interactions between the two solutes are repulsive and/or the solutes differ in solubility towards the solvent. The second type of phase separation is referred to as associative phase separation and is when one phase is concentrated in both solutes/polymers while the other phase essentially contains only solvent. For the case of polymer mixtures this is referred to as complex coacervation.⁸⁰

Different types of surfactant-polymer mixtures have been studied previously with the following phase separation type reported (Table 1.4).⁸⁰⁻⁸⁷

Table 1.4. Phase separation types in different surfactant-polymer mixtures.

| Mixtures | Phase Separation Type |
|---|------------------------|
| Nonionic Surfactant – Polymer | Both – System Specific |
| Ionic Surfactant – Nonionic Polymer | Segregative |
| Ionic Surfactant- Polymer Opposite charge | Associative* |
| Ionic Surfactant – Polymer of Similar Charge | Segregative |

*The addition of a critical concentration of salt has been observed to change the phase separation mechanism from associative to segregative.⁸⁵

Nonionic surfactant - polymers mixtures have been observed to phase separate via a segregative and associative mechanism depending on polymer hydrophilic-lipophilic balance (HLB). The HLB characteristics determines if the interactions between the polymer-surfactant are repulsive or attractive.⁸⁰ Ionic surfactant-polymer mixtures of opposite charge have been observed to phase separate via an associative mechanism. Complex formation between the surfactant-polymer is believed to be the driving force for the associative mechanism however the addition of a critical concentration of salt leads to the mechanism changing to a segregative mechanism.⁸⁵

The ionic surfactant – nonionic polymer mixtures and ionic surfactant - polymer of similar charge mixtures have a strong dependence on salt. With the addition of salt reported to reduce the critical phase separation concentration quite dramatically.^{80, 82, 88} Additionally in ionic surfactant – polymer mixtures of similar charge Nilsson *et al.*^{83, 84} illustrated that the addition of a hydrophobic cosolute can affect the

polyelectrolyte/surfactant compatibility hence the critical phase separation concentration. The addition of octane was observed to increase compatibility while the addition of octanol decreased the compatibility. These observations were justified in terms of micelle aggregation number changes.

1.6 Aims of the Project

To investigate dilute aqueous mixtures of cationically charged surfactant - polyelectrolytes and the resulting antimicrobial film left after drop evaporation. QAC surfactants are widely used as a biocide whereas polyelectrolytes (QACs) have often been ignored due to their lower antimicrobial activity. However the advantage of polyelectrolytes is their ability to adsorb strongly to oppositely charged surfaces.

The research is split into a number of sections;

- The antimicrobial activity for a range of homo-polymeric QACs within solution will be determined and compared against the only commercially available polymeric biocide PHMB. An attempt will be made to relate their antimicrobial activity to their structural/solution properties.
- The solution behaviour of like-charge polyelectrolyte/surfactant/water mixtures will be investigated with particular interest in their phase separating behaviour at high concentration.
- The drop drying characteristic of dilute like-charged polyelectrolyte/surfactant/water mixtures will be studied. An attempt will be made to alter the film structures left after drying. The ability to order/structure biocidal actives onto a substrate could have potential benefits such as improved active adhesion and better bio-availability.

1.7 References

1. J. Lewis, Valeria M. Kish, *Principles of Cell Biology*, Harpers and Rose, New York, 1988.
2. S. A. Wood, *Cell Biology*, 2nd Edition, Chapman & Hall, London, 1996.
3. <http://pathmicro.med.sc.edu/fox/bact-mem.jpg>, Accessed 22/6/2011.
4. G. McDonnell and A. D. Russell, *Clin. Microbiol Rev.*, 1999, **12**, 147-179.
5. C. W. Levy, A. Roujeinikova, S. Sedelnikova, P. J. Baker, A. R. Stuitje, A. R. Slabas, D. W. Rice and J. B. Rafferty, *Nature*, 1999, **398**, 383-384.
6. Bruch and Mary, *Handbook of Disinfectants and antispectics*, CRC Press, 1996.
7. J. C. Lear, J. Y. Maillard, P. W. Dettmar, P. A. Goddard and A. D. Russell, *J. Ind. Microbiol. Biot*, 2002, **29**, 238-242.
8. S. Y. Liao, D. C. Read, W. J. Pugh, J. R. Furr and A. D. Russell, *Lett. Appl. Microbiol.*, 1997, **25**, 279-283.
9. S. Silver, L. T. Phung and G. Silver, *J. Ind. Microbiol. Biot*, 2006, **33**, 627-634.
10. S. L. Percival, P. G. Bowler and D. Russell, *J. Hosp Infect.*, 2005, **60**, 1-7.
11. L. Timofeeva and N. Kleshcheva, *Appl. Microbiol. Biotechnol.*, 2011, **89**, 475-492.
12. M. R. Salton, *J. Gen. Physiol.*, 1968, **52**, 227-252.
13. J. P. S. Cabral, *Can. J. Microbiol.*, 1992, **38**, 115-123.
14. P. Broxton, P. M. Woodcock and P. Gilbert, *J. Appl. Bacteriol*, 1983, **54**, 345-353.
15. P. Broxton, P. M. Woodcock, F. Heatley and P. Gilbert, *J. Appl. Bacteriol*, 1984, **57**, 115-124.
16. T. Ikeda, A. Ledwith, C. H. Bamford and R. A. Hann, *Biochim Biophys Acta*, 1984, **769**, 57-66.
17. T. Ikeda, S. Tazuke and M. Watanabe, *Biochim Biophys Acta*, 1983, **735**, 380-386.
18. J. J. Merianos, *Block, S. S. Disinfection, Sterilization, and Preservation, Fourth Edition.*, Williams and Wilkins: York, Pennsylvania, USA; Lea and Febiger: Malvern, Pennsylvania, USA; London, England, Uk. Illus, 1991.
19. N. N. Daoud, N. A. Dickinson and P. Gilbert, *Microbios*, 1983, **37**, 73-85.

20. P. J. Schaeufele, *J Am Oil Chem Soc.*, 1984, **61**, 387-389.
21. H. Morawetz, *Macromolecules in Solution*, 2nd Edition., Robert E. Krieger Publishing Company, 1975.
22. N. Govindji, 'Inhibiting biofilms formed by Gram negative uropathogenic bacteria', PhD Thesis, The University of Manchester, 2013.
23. K. Barrettbee, L. Newbould and S. Edwards, *FEMS Microbiol. Lett.*, 1994, **119**, 249-253.
24. R. S. Blackburn, A. Harvey, L. L. Kettle, J. D. Payne and S. J. Russell, *Langmuir*, 2006, **22**, 5636-5644.
25. T. Ikeda, H. Yamaguchi and S. Tazuke, *J. Antimicrob. Chemother.*, 1984, **26**, 139-144.
26. C. Z. S. Chen, N. C. Beck-Tan, P. Dhurjati, T. K. van Dyk, R. A. LaRossa and S. L. Cooper, *Biomacromolecules*, 2000, **1**, 473-480.
27. E. F. Panarin, G. E. Afinogenov, M. V. S o l o v s k i i, N. A. Zaikina and G. E. Afinogenov, *Makromol. Chem., Suppl.*, 1985, **9**, 25-33.
28. T. Ikeda, S. Tazuke and Y. Suzuki, *Macromol. Chem. Physic*, 1984, **185**, 869-876.
29. T. Ikeda, H. Hirayama, K. Suzuki, H. Yamaguchi and S. Tazuke, *Macromol. Chem. Physic*, 1986, **187**, 333-340.
30. P. Flory, *Principles of Polymer Chemistry*, Cornell University Print, London, 1953.
31. M. J. Rosen, *Surfactant and Interfacial Phenomena*, John Wiley & Sons Inc, New York, 1978.
32. Z. Cao and Y. Sun, *ACS Appl Mater Interfaces*, 2009, **1**, 494-504.
33. Y. Y. Sun, T. Y. Chen, S. D. Worley and G. Sun, *J. Polym. Sci. Pol. Chem.*, 2001, **39**, 3073-3084.
34. E.-R. Kenawy, S. D. Worley and R. Broughton, *Biomacromolecules*, 2007, **8**, 1359-1384.
35. F. Siedenbiedel and J. C. Tiller, *Polymers*, 2012, **4**, 46-71.
36. M. Biesalski and J. Ruhe, *Macromolecules*, 1999, **32**, 2309-2316.
37. P. Thebault, E. T. de Givenchy, R. Levy, Y. Vandenberghe, F. Guittard and S. Geribaldi, *Eur. J. Med.*, 2009, **44**, 4227-4234.

38. C. J. Waschinski, J. Zimmermann, U. Salz, R. Hutzler, G. Sadowski and J. C. Tiller, *Adv. Mater.*, 2008, **20**, 104-108.
39. P. Thebault, E. T. de Givenchy, R. Levy, Y. Vandenberghe, F. Guittard and S. Geribaldi, *Eur. J. Med. Chem.*, 2009, **44**, 717-724.
40. A. Popa, C. M. Davidescu, R. Trif, G. Ilia, S. Iliescu and G. Dehelean, *React. Funct. Polym.*, 2003, **55**, 151-158.
41. R. Kugler, O. Bouloussa and F. Rondelez, *Microbiology-Sgm*, 2005, **151**, 1341-1348.
42. H. Murata, R. R. Koepsel, K. Matyjaszewski and A. J. Russell, *Biomaterials*, 2007, **28**, 4870-4879.
43. K. Lewis and A. M. Klibanov, *Trends Biotechnol.*, 2005, **23**, 343-348.
44. J. C. Tiller, C. J. Liao, K. Lewis and A. M. Klibanov, *Proc. Nat. Acad. Sci. USA.*, 2001, **98**, 5981-5985.
45. J. C. Tiller, S. B. Lee, K. Lewis and A. M. Klibanov, *Biotechnol. Bioeng.*, 2002, **79**, 465-471.
46. J. Lin, J. C. Tiller, S. B. Lee, K. Lewis and A. M. Klibanov, *Biotechnol. Lett.*, 2002, **24**, 801-805.
47. S. B. Lee, R. R. Koepsel, S. W. Morley, K. Matyjaszewski, Y. J. Sun and A. J. Russell, *Biomacromolecules*, 2004, **5**, 877-882.
48. J. Lin, S. Y. Qiu, K. Lewis and A. M. Klibanov, *Biotechnol. Bioeng.*, 2003, **83**, 168-172.
49. D. Park, J. Wang and A. M. Klibanov, *Biotechnol. Progr.*, 2006, **22**, 584-589.
50. Z. Li, D. Lee, X. X. Sheng, R. E. Cohen and M. F. Rubner, *Langmuir*, 2006, **22**, 9820-9823.
51. Y. F. Pan, H. N. Xiao, G. L. Zhao and B. H. He, *Polym. Bull.*, 2008, **61**, 541-551.
52. P. H. Chua, K. G. Neoh, Z. Shi and E. T. Kang, *J. Biomed. Mater. Res. A.*, 2008, **87A**, 1061-1074.
53. K. Yliniemi, M. Vahvaselka, Y. Van Ingelgem, K. Baert, B. P. Wilson, H. Terryn and K. Kontturi, *J. Mat. Chem.*, 2008, **18**, 199-206.
54. D. Lee, R. E. Cohen and M. F. Rubner, *Langmuir*, 2005, **21**, 9651-9659.
55. F. Boulmedais, B. Frisch, O. Etienne, P. Lavalley, C. Picart, J. Ogier, J. C. Voegel, P. Schaaf and C. Egles, *Biomaterials*, 2004, **25**, 2003-2011.

56. A. Guyomard, E. De, T. Jouenne, J.-J. Malandain, G. Muller and K. Glinel, *Adv. Funct. Mat.*, 2008, **18**, 758-765.
57. K. D. Park, Y. S. Kim, D. K. Han, Y. H. Kim, E. H. B. Lee, H. Suh and K. S. Choi, *Biomaterials*, 1998, **19**, 851-859.
58. A. Razatos, Y. L. Ong, F. Boulay, D. L. Elbert, J. A. Hubbell, M. M. Sharma and G. Georgiou, *Langmuir*, 2000, **16**, 9155-9158.
59. D. Cunliffe, C. A. Smart, C. Alexander and E. N. Vulfson, *Appl. Environ. Microbiol.*, 1999, **65**, 4995-5002.
60. J. A. Lichter and M. F. Rubner, *Langmuir*, 2009, **25**, 7686-7694.
61. J. A. Lichter, K. J. Van Vliet and M. F. Rubner, *Macromolecules*, 2009, **42**, 8573-8586.
62. W. Y. Yuan, J. Ji, J. H. Fu and J. C. Shen, *J. Biomed. Mater. Res., Part B*, 2008, **85B**, 556-563.
63. L. Jonosson, Holmberg, Kronberg, *Surfactants and Polymers in Aqueous Solution*, Wiley, New York, 1998.
64. T. Cosgrove. (Editor), *Colloid science - Principles, Methods and Applications*, Wiley, 2010.
65. J. H. Clint, *Trans. Faraday Soc. J. Chem. Soc.*, 1975, **71**, 1327-1334.
66. h. c. u. e. a. d. f. p. a. s. structures.svg.png. Accessed 11/02/13
67. J. Lyklema, *Fundamentals of Interface and Colloid Science: Soft Colloids*, 1st Edition, Elsevier Inc., London, UK, 2005.
68. T. Odijk, *Macromolecules*, 1979, **12**, 688-693.
69. G. S. Roberts, R. Sanchez, R. Kemp, T. Wood and P. Bartlett, *Langmuir*, 2008, **24**, 6530-6541.
70. E. D. Goddard, *Colloids Surf*, 1986, **19**, 255-300.
71. E. D. Goddard, *Colloids Surf*, 1986, **19**, 301-329.
72. R. G. Nause, D. A. Hoagland and H. H. Strey, *Abstr Pap Am Chem Soc*, 2002, **224**, U451.
73. M. N. Jones, *J. Colloid Interface Sci.*, 1967, **23**, 36-42.
74. H. Lange, *Colloid Polym. Sci.*, 1971, **243**, 101-109.
75. M. Y. Khan, A. Samanta, K. Ojha and A. Mandal, *Asia Pac. J. Chem. Eng.*, 2008, **3**, 579-585.
76. J. C. Brackman and J. Engberts, *Chem. Soc. Rev.*, 1993, **22**, 85-92.

77. L. Bromberg, M. Temchenko and R. H. Colby, *Langmuir*, 2000, **16**, 2609-2614.
78. R. H. Colby, N. Plucktaveesak and L. Bromberg, *Langmuir*, 2001, **17**, 2937-2941.
79. H. Comas-Rojas, E. Aluicio-Sarduy, S. Rodriguez-Calvo, A. Perez-Gramatges, S. J. Roser and K. J. Edler, *Soft Matter*, 2007, **3**, 747-753.
80. L. Piculell and B. Lindman, *Adv. Colloid Interface Sci.*, 1992, **41**, 148-178.
81. P. Hansson and B. Lindman, *Curr. Opin. Colloid Interface Sci.*, 1996, **1**, 604-613.
82. E. Kalwarczyk, M. Golos, R. Holyst and M. Fialkowski, *J. Colloid Interface Sci.*, 2010, **342**, 93-102.
83. S. Nilsson, A. M. Blokhuis and A. Saure, *Langmuir*, 1998, **14**, 6082-6085.
84. S. Nilsson, A. M. Blokhuis, S. Hellebust and W. R. Glomm, *Langmuir*, 2002, **18**, 6504-6506.
85. K. Thalberg, B. Lindman and G. Karlstrom, *J. Chem. Phys.*, 1991, **95**, 6004-60011.
86. K. Thalberg, B. Lindman and G. Karlstrom, *J. Chem. Phys.*, 1991, **95**, 3370-3376.
87. K. R. Wormuth, *Langmuir*, 1991, **7**, 2048-2053.
88. K. Thalberg and B. Lindman, *Colloids Surf. A*, 1993, **76**, 283-288.

Chapter 2 – Experimental

Experimental

This chapter aims to describe the experiments that have been carried out during the course of the research including reagents, general procedures and techniques.

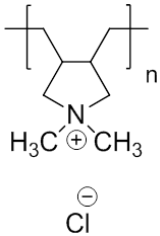
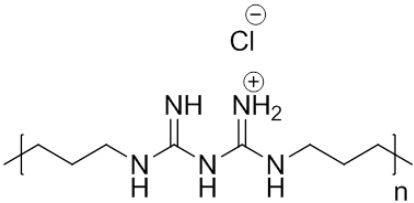
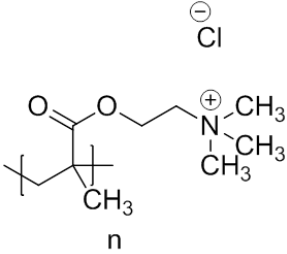
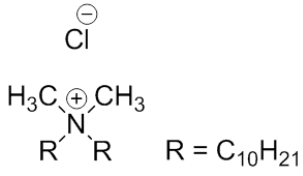
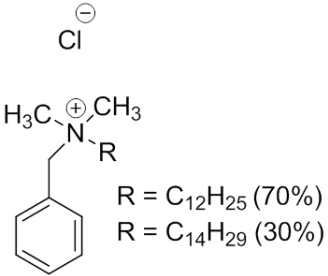
2.1 Reagents

Poly(diallyldimethyl ammonium chloride) (pDADMAC), $M_v = 8.5$ kDa was obtained from Poly Sciences Inc as a 28 wt% solution in water, and the $M_v = 21$ kDa and 140 kDa were obtained from Sigma Aldrich as 35 wt% and 20 wt% solutions respectively. Poly(hexamethylene biguanide chloride) (PHMB), $M_n = 3.3$ kDa was obtained from Arch Chemicals (Tradename - Vantocil IB) as a 20 wt% solution in water and Poly((2-dimethylamino ethyl methacrylate) methyl chloride) quaternary salt (PDMC) was obtained from Sigma Aldrich as a solid, $M_v = 3.4$ kDa

Didecyldimethyl ammonium chloride (DDQ) was obtained from Lonza (Tradename - Lonza Bardac 2240) and received as a 40 wt% solution in water. Alkyl (C_{12} , 70%; C_{14} 30%;) dimethyl benzyl ammonium chloride (BAC) was obtained from Thor (Tradename – Acticide BAC 50 M) and received as a 50 wt% solution in water. Chemical structures of these reagents can be viewed in Table 2.1 Both surfactants and polyelectrolyte were used as received without further purification unless otherwise stated.

The concentrations of the above stock solutions were verified by the removal of the water and the resulting residues weighed. The samples were placed into a vacuum oven at 80 °C until no further mass loss was recorded. If stated, the sodium chloride was obtained from Fisher Scientific, analytical grade.

Table 2.1 Chemical Structures of the principle polyelectrolytes and surfactants.

| Chemical Name | Structure |
|--|---|
| Poly(diallyldimethylammonium) chloride (pDADMAC) |  |
| Poly(hexamethylene biguanide) chloride (PHMB) |  |
| Poly(2-dimethylamino)ethyl methacrylate) methylchloride quaternary salt (PDMC) |  |
| Didecyldimethylammonium chloride (DDQ) |  |
| Alkyl (C ₁₂ 70%; C ₁₄ 30%) dimethyl benzyl ammonium chloride (BAC) |  |

When specifically stated, the pDADMAC 140 kDa was dialysed against Millipore filtered water for four days with the water changed twice every day. Benzoylated dialysis tubing (2 kDa molecular weight cut off, Sigma Aldrich, D7884-1FT) was used. The dialysis was finished when the conductivity of the water within the beaker returned to a level comparable with Millipore filtered water. The conductivity was measured on a Jenway 4010 Conductivity meter at 25 °C.

2.2 Standard Procedures

2.2.1 Formulating

Millipore filtered water was used for all solutions. Stock solutions were prepared in polypropylene bottles (Nalgene bottles, Style 200, 100 mL purchased from Sigma Aldrich). Individual samples were prepared in 10 mL polypropylene graduated sample tubes (VWR). Stock solution of 1, 5 and 10 wt% were made for the polyelectrolyte and surfactant samples when possible. While 0.1, 1.0, 2.0 and 5.0 M NaCl stock solutions were prepared in 100 mL volumetric flasks. Samples were measured via mass unless stated. Fresh solutions were used for all experiments. If required, the pH of the solutions was measured on a Jenway 3505 pH meter with a Jenway 924030 glass pH electrode and calibrated prior to use with pH 4, 7 & 9.2 buffer solutions (Fisher Scientific, buffer tablets). If required the solutions density was calculated with 1 mL of solution weighed onto a four decimal balance using a Gilson Pipetman P1000. An average from three measurements was used. The ambient temperature was recorded at the time of measurement.

2.2.2 Observations of Sample Phase Separation

Samples were stirred for one hour with a magnetic stirrer then inverted ten times by hand. Observations were taken 48 hours after last agitation to determine if phase separation had occurred.

2.2.3 Analysis of Sample Phases

A 30 g sample of an appropriate formulation was placed into a glass separating funnel. The sample was inverted by hand ten times and left to equilibrate for 24 hours. A number of aliquots were taken from the upper and lower phase and gravimetric analysis was conducted. ^1H NMR was conducted on each phases using the resulting residues. The residues were rehydrated with D_2O (Sigma Aldrich).

Gravimetric Analysis; Aliquots of each sample were placed into a metal pan and placed into a vacuum oven ($80\text{ }^\circ\text{C}$), three repeats per sample. The sample mass was weighed every 24 hours until the mass remained unchanged. An average of the three replicates was calculated to give an approximate concentration (wt%) of each phase.

2.2.4 Determination of Critical Phase Separating Concentration

A series of solutions (10 mL) were formulated at 100 mM surfactant concentration but differing electrolyte concentration. The lowest electrolyte concentration within the series observed to phase separate was the systems critical phase separating concentration. The polyelectrolyte systems were formulated via mass while the NaCl systems were formulated via volume using a Gilson pipetman P1000 and/or P10 mL.

The increment between each electrolyte concentration within the respective surfactant mixtures (BAC/DDQ) is show in Table 2.2.

Table 2.2 Electrolyte increments for the different surfactant BAC/DDQ series.

| Surfactant Ratio (BAC:DDQ) | Polyelectrolyte (wt%) | NaCl (M) |
|-------------------------------|--------------------------|----------|
| 1:0 | 0.5 | 0.1 |
| 8:2 | 0.5 | 0.1 |
| 6:4 | 0.5 | 0.05 |
| 4:6 | 0.1 | 0.01 |
| 2:8 | 0.1 | 0.01 |
| 0:1 | 0.1 | 0.01 |

2.2.5 Substrate Cleaning

Glass substrates (Fisher Scientific, Microscope slides) were cut into 2.5 cm² pieces using a diamond cutter. These were placed into a beaker of concentrated sulphuric acid (Fisher Chemicals, reagent grade) for 24 hours. The substrates were washed with Millipore filtered water and then placed into a sonication bath for 5 minutes. The substrates were then gently wiped (Kimberley Clark Professional, KIMCARE, Medical wipes) and washed with acetone (Sigma Aldrich) and placed into a beaker with acetone and put into the sonication bath for a further 5 minutes. The substrates were dried with compressed air and wrapped in foil until required.

2.2.6 Surface Treatment

The 2.5 cm² glass substrates were placed into a temperature controlled incubator (Stuart, Incubator S1600D) set at 30 °C. A temperature/ humidity meter was placed inside the chamber to monitor atmospheric conditions (Rotronic Hydropalm meter + Rotronic HC2-C04 probe). The substrate was left to equilibrate for 30 minutes inside the incubator prior to treatment. 20 µL of formulation was placed gently onto the substrate using a P20 Gilson pipetman. The single drop should closely resemble a

spherical cap like geometry on the substrate. The treated substrates were left for 24 hours within the incubator. The substrates were placed into a closed petri dish and stored out of direct sunlight prior to subsequent analyses. Drying conditions: Temperature $30\text{ }^{\circ}\text{C} \pm 0.5$, Relative Humidity 20 – 60 %. The incubator allowed the control of temperature but not relative humidity. The humidity values stated are the range of atmospheric conditions experienced during these experiments.

2.3 Techniques

2.3.1 Size Exclusion Chromotography

Size exclusion chromatography (SEC) was carried out using the TSK-GEL Filtration Columns (Supelco). Two different systems SEC systems were used: a low molecular weight and high molecular weight system. The particular column sets used in these systems are shown in Table 2.3.

Table 2.3 Summary of columns used for SEC, M_w range based on Poly(ethylene) oxide calibration.

| System | Columns | M_w Range |
|-----------------------|---------|---------------|
| Low Molecular Weight | G2000PW | <2000 |
| | G3000PW | <50,000 |
| High Molecular Weight | G4000PW | 2000-300,000 |
| | G5000PW | 4000-1000,000 |

All SEC systems used a Gilson 132 refractive index detector with a flow rate of 0.5 mL/min of a Citric acid 0.1 M buffer and 0.1 wt% azide at $25\text{ }^{\circ}\text{C}$, calibrated using polyethylene oxide standards. Solutions were filtered twice with a $0.22\text{ }\mu\text{m}$ polyethersulfone syringe filter before injection into column.

2.3.2 NMR

All experiments were run on a Bruker Ultrashield 400 MHz spectrometer. With the chemical shifts, δ , quoted in parts per million (ppm) down-field from tetramethylsilane.

2.3.3 IR

All samples were solids and run on a Thermo Scientific Nicolet is5, iD5 ATR spectrometer.

2.3.4 SI-MS

Electrospray ionisation mass spectroscopy (SI-MS) was conducted on a Micromass Platform 11. Solvent used was Millipore filtered water.

2.3.5 Viscometry

Dilute solution viscometry was carried out using an Ubbelohde (Rheotek -VIS3300) capillary viscometer. The viscometer was placed into a beaker containing DI water which was kept at 25 °C via a hotplate and temperature probe. Each solution was left for 30 minutes prior to measurement and an average of three measurements were taken.

When stated, the Anton Paar Micro Viscometer was preferred to the Ubbelohde Viscometer due to reduced sample required for measurement. Measurements were conducted at 25 °C with a 1.6 mm diameter glass capillary and a 1.5 mm steel ball (density 7.65 g/cm³).

Individual samples were formulated in a 1 M NaCl solvent. The original sample was formulated by mass with the addition of a pDADMAC stock, 2 M NaCl stock and Millipore filtered water. Subsequent dilution of each sample was made via the

addition of a 1 M NaCl solvent using a Gilson Pipetman P1000 and/or P10 mL. Huggins/Kraemer Plot produced for each polymer sample.

2.3.6 Tensiometry

Surface tension measurements were carried out using a Kibron Delta 8 Tensiometer which is based on the De-Nouy method with a platinum rod used as the probe. Serial dilutions of 0.5 from a concentrated stock solution were performed using a Epmotion 5075 Liquid Handler (Eppendorf) into a 12 x 8 well plate. Each well was filled with a total sample volume of 100 μ L. A total of 8 replicates were measured for each concentration. A purified distilled water control was present on each plate. For the polyelectrolyte plots a 5 wt% stock solution was used, while for the surfactants BAC, BAC/DDQ (2:3 mol:mol) and DDQ a 55, 25 and 22 mM stock solution was used respectively. Additional tensiometry plots were produced for the above surfactants which included the addition of a constant concentration of polyelectrolyte within each sample. An additional step was added during the dilution step on the liquid handler to include the addition of polyelectrolyte solution into the sample well.

Due to the unavailability of the Kibron Delta 8 Tensiometer, the surface tension plots of BAC, BAC/DDQ (2:3 mol:mol) and DDQ in the presence of 0.1 wt% pDADMAC (21 kDa) was performed on a torsion balance (Whit Electrical and industrial Company Ltd, Model OS torsion balance, Platinum ring). The torsion balance was calibrated against Millipore filtered water prior to use. The platinum ring was cleaned after each sample with a flame prior to use. Each sample was repeated at least three times or until the measurements were ± 0.1 mN/m. Samples were left to equilibrate for at least 30 minutes between replicate measurements. Any individual formulations which required surface tension to be measured were measured on the torsion balance.

2.3.7 Conductivity

A Jenway 4010 conductivity meter ($K= 0.96$) was used for the measurements. This was calibrated prior to use with 0.01 M HCl and Millipore filtered water. Samples

were placed into a water bath set a 25 °C for 1 hour prior to measurements. The probe was rinsed with copious amount of Millipore filtered water between samples.

2.3.8 Isothermal Titration Calorimetry (ITC)

A Microcal, ITC₂₀₀ was used for the measurements. Cell size 200 µL, maximum volume of syringe 38 µL, syringe end modified into a stirrer. Measurements taken at 25 °C, stirring at 1000 rpm within cell, 120 s delay between injections, initial injection of 0.5 µL followed by 37 x 1 µL injections. A concentrated surfactant solution was placed into the syringe while Millipore filtered water was placed into the sample cell. The surfactant stocks for BAC, BAC/DDQ (2:3 mol:mol) and DDQ surfactants were 70, 44 and 40 mM respectively. For the PHMB plot, a 1.5 wt% stock solution was used.

2.3.9 Photo-Luminescence (Pyrene)

Fluorescence measurements were performed on a Cary Eclipse. A quartz glass cell was used. The probe molecule was Pyrene (Sigma Aldrich).

Experimental parameters; $\lambda_{\text{excit}} = 320 \text{ nm}$, $\lambda_{\text{emission}} = 350\text{-}450 \text{ nm}$ and Slit size (excitation and emission) = 2.5 mm. All presented emission spectras were normalised. Formulations: A 2.5 µM stock solution of Pyrene was made in a 2 L volumetric flask with Millipore filtered water. All individual surfactant samples contained 2 µM of pryene. Solutions were left 24 hours before testing.

2.3.10 Photon Correlation Spectroscopy (PCS)

Photon correlation spectroscopy (PCS) particle sizing was performed using a Zetasizer-Nano from Malvern Instruments with a He-Ne laser having a wavelength of 632.8 nm and a back scattering detector set at 173°. Solutions were filtered twice with a 0.22 µm polyethersulfone syringe filter then placed into a Polystyrene 10 x 10

x 45 mm cuvette. The results are an average of four measurements taken at 25 °C. A CONTIN program was used to deconvoluted the size distribution.

To identify a suitable concentration of NaCl to be added into the surfactant solution, a series of solutions were formulated via volume for each surfactant type at constant surfactant concentration (100 mM). Surfactant cloud points were; BAC 1.1 M, DDQ 0.04 M and BAC/DDQ (2:3) 0.2 M NaCl. Consequently a NaCl concentration below the surfactant cloud points was chosen for the PCS experiment. For DDQ 5×10^{-3} M, BAC 0.3 M and BAC/DDQ (2:3) 0.05 M NaCl were used.

2.3.11 Equilibrium Contact Angle Measurements

Measurements were conducted on a Kruss DSA 100 with glass microscope slides used as the substrates (Fischer Scientific). A needle (Kruss, NE 41) with a 0.52 mm diameter was used with the manual dosing option selected. For each solution two substrates were used with six measurements on each substrate. The measurements were taken 10 seconds after drop impact.

2.3.12 Drying Drop Contact Angle Measurements

Measurements were conducted on a Kruss DSA 100 with glass microscope slides used as the substrates (Fisher Scientific). The glass substrate was placed in an environment chamber (Kruss, TC3010) enabling the control of temperature and humidity. A temperature controlled water bath pumped water through a ceramic plate at 30 °C enabling temperature control. While 6 mL of saturated Potassium Acetate (Fisher Scientific) solution (300 g in 100 g Millipore filtered water) was placed in a moat within the chamber to control humidity. The saturated salt solution was placed into a 30 °C water bath prior to use for 1 hour. The chamber was left to equilibrate for 3 hours.

A temperature/humidity meter was placed inside the chamber to monitor atmospheric conditions (Rotronic Hydropalm meter + Rotronic HC2-C04 probe). Before proceeding with measurements, the following atmospheric conditions were met;

temperature $30\text{ }^{\circ}\text{C} \pm 0.5$ and relative humidity of $24\% \pm 0.5$. 20 μL of the chosen solution was pumped (80 $\mu\text{L}/\text{min}$) onto the substrate through a needle (Kruss, NE 41, 0.52 mm diameter) using the automatic dosing option. The needle remained within the meniscus of the drop during dosing. The needle was slowly removed once all the solution had been deposited onto the substrate. A movie was then recorded of the drying drop at the following time frames; 1 minute 25 frames, 10 minutes 10 frames multiplied by three.

2.3.13 Optical Microscopy

Optical micrographs of treated surfaces were taken on a Leica Microsystems DM 2500 M microscope using objective lenses x10, x20 and x50. The images were taken with a Leica EC3 digital camera (x0.55 magnification). All images were taken in reflective mode.

Drying Drop Movies: Solutions were filtered twice with a 0.22 μm polyethersulfone syringe prior to use. A 20 μL single drop of the respective formulation was deposited onto the glass substrate using a Gilson P20 pipettman. The microscope was in reflective mode with images taken every minute during drying. Atmospheric temperature and humidity conditions were monitored using a Rotronic Hydropalm meter + Rotronic HC2-C04 probe).

2.3.14 Non-Contact Atomic Force Microscopy

Topography and phase contrast images were recorded using Atomic Force Microscopy (NC-AFM), (PSIA Inc, XE 100) in non-contact mode. A commercial silicon cantilever (PSIA Inc, 910M-NSC15) with a nominal spring constant of about 40 N/m was used. The glass substrates were secured to a metal disc using double sided tape and installed on the AFM scanner. Various sized scans were measured (25 and 60 μm^2).

2.3.15 Time of Flight Secondary Ion Mass Spectrometry (ToF-SIMS)

Substrate Treatment: Silicon wafer (Agar, G3391, 5 mm x 7 mm) treated with 2 μL of formulation with standard drying condition used for the incubator (30 $^{\circ}\text{C}$, 24 % Relative Humidity, 24 hours). The ToF-SIMS experiment was kindly conduct by Dr N. P. Lockyer. The measurements were conducted on a Bio-TOF SIMS instrument; the design of this has been fully explained previously within the literature.¹ This instrument is equipped with two ion beams columns: 20 kV C_{60}^{+} laser and a 20 kV gold/germanium liquid metal ion source. Analysis was performed using a 20 keV Au^{3+} using 20 ns pulses with DC beam currents of 300 pA. Spectral data was collected from a 1000 μm^2 area using a spectral fluence below 2×10^{10} ions/ cm^2 . Mass spectrometer set to detect +ve ions.

2.3.16 Inkjet Printing

Printing was conducted on a Dimatix Materials Printer (DMP-2800, Fujifilm Dimatix, Inc Santa Clara, USA) using a disposable piezo inkjet cartridge. Printhead nozzle plate consists of a single line of 16 nozzles separated by 254 μm with each nozzle having a diameter of 23 μm . The typical drop volume from these nozzles is 10 pL. This printer can create and define patterns over an area of 200 x 300 mm and handle substrates up to 25 mm thick. Additionally, both cartridge and substrate platen temperature can be varied from room temperature up to 100 $^{\circ}\text{C}$. For these experiments, the substrate platen was kept at 30 $^{\circ}\text{C}$. Glass substrates were placed onto the platen 30 minutes before printing. Inkjet printing was carried out with only one nozzle and a drop spacing of 150 μm was used. The cartridge printhead height from substrate was set at 1 mm. Cartridge temperature was kept at room temperature which varied between 18-22 $^{\circ}\text{C}$ during the course of these experiments. The atmospheric relative humidity was also monitored which varied within the range of 40 - 50 % during the course of the experiments. The formulations were jetted using a waveform with the following characteristics: 14.1 μs , 13 V and 5 kHz frequency. Upon printing, samples were kept on the platen for 30 minutes before being placed into a temperature controlled incubator (Stuart, Incubator S1600D) set at 30 $^{\circ}\text{C}$ for 24 hours.

2.4 Microbiology Procedures

2.4.1 MIC Testing of Polyelectrolytes (Conducted by Nishal Govindji)²

Bacteria tested; *Escherichia coli* K12 (a laboratory strain of XL1-blue, a K12 phage), and clinical isolates of *Escherichia coli*, *Klebsiella pneumoniae* and *Pseudomonas aeruginosa* obtained from urinary tract infections and characterised by Vitek[®] 2 (BioMérieux, Inc.) were used in this study. Characterisation of strains was kindly performed by the staff at the Central Manchester Foundation Trust (Clinical Sciences Building 2, Manchester, U.K.). The *E. coli* K12 laboratory strain was kindly supplied by Prof. Ian Douglas (University of Sheffield, School of Clinical Dentistry, Sheffield, U.K.). Stocks were stored at -80 °C in 80% glycerol (Fisher Scientific Ltd.). Stock bacteria were cultured for 18 hours on Luria-Bertani (LB) agar plates (Table 2.4) every two weeks. The working culture plates were stored at 4 °C. Overnight cultures were prepared by inoculating LB broth (Table 2.4) with several colonies from the working culture plates and incubating for 18 hours with shaking at 200 r. p. m. All cultures were incubated in an aerobic atmosphere at 37 °C.

MIC Determination; A stock concentration of antimicrobial was prepared in sterile distilled water with the pH adjusted to pH 7 (0.1 M NaOH, Fischer Scientific). This was used to prepare a range of dilutions at double the final concentration required in sterile distilled water. 100 µL of each concentration was transferred into 8 replicate wells of a flat bottomed untreated polystyrene 96 well microtitre plate (Greiner Bio-one Ltd, UK.) 1:50 dilution of each bacteria were prepared in LB broth from the overnight cultures, 100 µL of which were added to each well containing concentrations of the antimicrobial.

Positive growth controls were prepared by inoculating 8 wells with 100 µL 1:50 dilution of bacteria and 100 µL of sterile distilled water in which the antimicrobial was prepared. Negative controls, or media only controls were prepared in a further 8 wells by aliquoting 100 µL of LB broth without any organism and 100 µL sterile distilled water.

The microtitre plates were incubated under aerobic, static conditions 18 hours at 37 °C. After the incubation period, the optical density (OD_{595nm}) readings of planktonic growth were taken to determine the minimum inhibitory concentration (MIC) using spectrophotometer (BMG Labtech FLUstar OPTIMA). The MIC is determined as the lowest concentration of antimicrobial that completely inhibits visual bacterial growth.

Table 2.4 Details of Luria-Bertani (LB) broth and agar formulations.

| | Formulation | Suppliers |
|--------------------------|-------------------------------------|---------------------------|
| Luria-Bertani (LB) broth | 10 g tryptone | Becton, Dickenson Ltd. |
| | 5 g yeast extract | Becton, Dickenson Ltd. |
| | 10 g NaCl | Fisher Scientific Ltd. |
| | made up to 1 L with distilled water | |
| LB agar | 10 g tryptone | Becton, Dickenson Ltd. |
| | 5 g yeast extract | Becton, Dickenson Ltd. |
| | 10 g NaCl | Fisher Scientific Ltd. |
| | 15 g agar | Melford Laboratories Ltd. |
| | made up to 1 L with distilled water | |

2.4.2 Surface Testing (Conducted by Dr Chris Plummer)³

The bacterium used for this study was *Pseudomonas aeruginosa* ATCC 15442 100 µL of formulation was applied to dry stainless discs (n=5) in sterile petri dishes. Discs were previously sanitised with 70% isopropyl alcohol for 15 minutes. Stainless steel discs were 1.4301 (EN 10088-1), 2 cm in diameter with a Grade 2B finish on both sides in accordance with (EN 10088-2). Formulations were spread to cover the disc using a sterile inoculating loop. Formulation was allowed to dry on the disc overnight in an oven at 30 °C (16 hours). Once the formulation had completely dried, the disc was subjected to abrasive/contamination cycles.

An abrasive/contamination cycle involves the following action:

1. Fold a wipe (polypropylene, non-woven) in two and wrap around the lid-end of a plastic centrifuge tube (diameter = 3.5 cm). Centrifuge tube is weighted via inclusion of steel discs or other suitable dense material. Total weight including tube \approx 208 grams.
2. Hold the tube at arm's length (\approx 50 cm) and spray the wipe covering the tube-end and spray twice with standardised hard water solution from a trigger spray (make sure the trigger spray is set to a fine spray rather than a stream).
3. Wipe the disc with the wetted wipe, once forwards and once backwards = one wipe. Make sure that extra force is not applied to the disc, i.e. let the weighted tube take the strain only. (The disc is likely to move, so will need to be kept in place, this can be done by holding a pipette tip or tweezers to the side of the disc to prevent its movement). Re-spray the wipe in a different area for each disc to be sampled.
4. Allow the discs to dry in the oven at 30 °C. Once discs are dried, repeat step (3), using a non-wetted wipe.

The disc is then subjected to an artificial contamination of bacteria: Preparation of bacterial suspension (based on EN13697 methodology): For each challenge organism, a bacterial suspension is prepared from an 18 – 24 hours, 2nd passage culture on TSA, incubated at 37 °C. The bacterial suspension is prepared by suspending the bacterial growth from the 2nd passage subculture in tryptone-saline diluent. The concentration of the bacterial suspension is determined by spectrophotometry. The suspension is diluted as necessary, using tryptone-saline, to give a cell concentration of approximately 1.5 to 5.0×10^8 CFU/mL. For intermediate artificial contaminations, the 1.5 to 5.0×10^8 CFU/mL suspension needs to be diluted down 100-fold to ~ 1.5 to 5.0×10^6 CFU/mL challenge organism; just before using the inoculum, 1 mL of the 1.5 to 5.0×10^6 cell suspension is mixed with 1 mL of 0.6% bovine albumin solution and vortex mixed.

Bacteria Contamination Procedure;

1. 10 μ L of bacterial suspension prepared in tryptone-saline/bovine albumin solution is pipetted onto the disc and spread over its surface using a sterile plastic inoculation loop (Be sure that the bacterial suspension is not spread to the very edge of the disc, allow ~ 0.5 cm gap to the edge of the disc).
2. Allow the bacterial suspension to dry in the oven at 30 °C.
3. Once dry, repeat 3 wear cycles (Steps 3-4 in wearing cycle procedure). On the final (3rd) wear cycle, a final contaminating bacterial suspension is added to the discs. This is a fresh suspension prepared in tryptone at 1.5 to 5.0×10^8 CFU/mL. This is then mixed 1:1 with sterile 0.6% bovine albumin. This final artificial contamination is added to the discs (10 μ L) and spread over the surface. Bacteria are left in contact with the steel surface for 5 minutes. Following this time, the discs are picked up with tweezers and placed into tubes containing 10 mL of neutraliser solution.

4. Neutraliser tubes containing discs are then vortex mixed for 30 seconds.
5. Serial dilutions from the tube are prepared in suitable neutraliser solution. 1 mL samples from the undiluted or dilution tubes can be plated out using the pour plate methodology. Bacterial samples are plated with tryptone soya agar (TSA). Incubate TSA plates at 37 °C for 24 hours. Compare the countable colonies grown back on the test disc samples with those from water-treated control discs. Calculate average log reductions.

2.5 References

1. R. M. Braun, P. Blenkinsopp, S. J. Mullock, C. Corlett, K. F. Willey, J. C. Vickerman and N. Winograd, *Rapid Commun. Mass Spectrom.*, 1998, **12**, 1246-52.
2. N. Govindji, 'Inhibiting biofilms formed by gram-negative uropathogenic bacteria', PhD Thesis, The University of Manchester, 2013.
3. Unpublished Byotrol Standard Test Methodology.

Chapter 3 – Characterisation of Principal Materials

Characterisation of Principal Materials

This chapter aims to fully characterise the principal polyelectrolyte/surfactant materials used within this research. The aim is to confirm chemical structure, identify any impurities and establish polyelectrolyte molecular weight and degree of polydispersity.

3.1 Polyelectrolytes

3.1.1 Poly(diallyl dimethyl ammonium chloride) (pDADMAC)

Three different pDADMAC samples were studied of varying molecular weight and are denoted as viscosity average molecular weight (M_v). The concepts and determination of polyelectrolyte molecular weight will be described in a following section (3.2 Polyelectrolyte Molecular Weight Determination).

δ_H (400 MHz; D_2O); 0.90 – 1.70 (m), 2.25 (m), 2.50-2.80 (m), 3.00-3.50 (m), 3.60-3.90 (m)

Assignment of proton environments could not be achieved. The 1H NMR spectra for pDADMAC 8.5, 21 and 140 kDa can be viewed in Appendix 3-A, B and C. The 8.5 kDa sample did contain additional vinyl proton environments (δ 5.68, δ 6.01) indicating a small amount of the monomer diallyldimethyl ammonium chloride within the sample.

δ_C (400 MHz; D_2O); 26.43, 38.09, 38.67, 52.25, 53.95, 54.83, 70.3

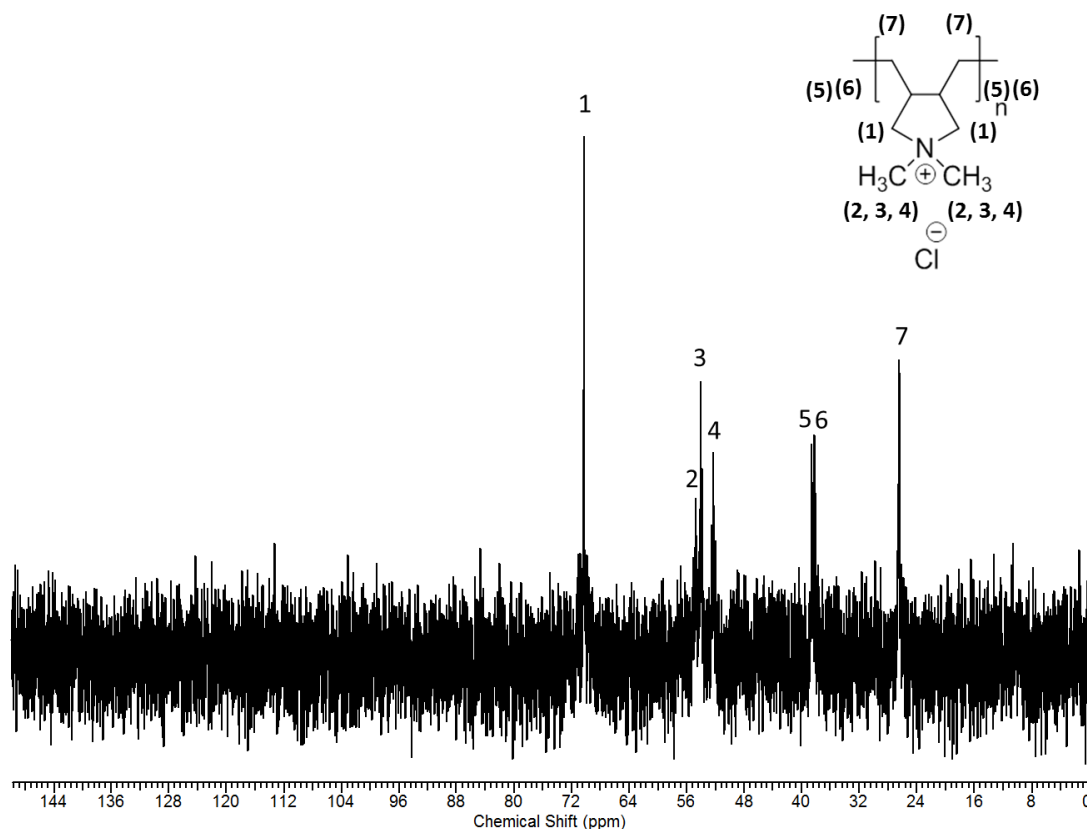


Figure 3.1 ^{13}C NMR Spectra of Poly(diallyl dimethyl ammonium chloride) 140 kDa (pDADMAC).

The carbon environments reported above are broadly in agreement with Lancaster *et al.*¹ who used ^{13}C NMR to confirm that pDADMAC existed as a 5 membered cyclic structure.

ν_{max} (ATR)/ cm^{-1} 3365 (b), 3017 (w) ($-\text{CH}_3$), 2961 (w), 2866 (w) and 1472 (s) (C-H)

3.1.2 Poly(hexamethylene biguanide) chloride (PHMB)

δ_H (400 MHz; D₂O); 1.26 (s), 1.47 (s), 1.57 (m) 2.89 (t) 3.10 (m)

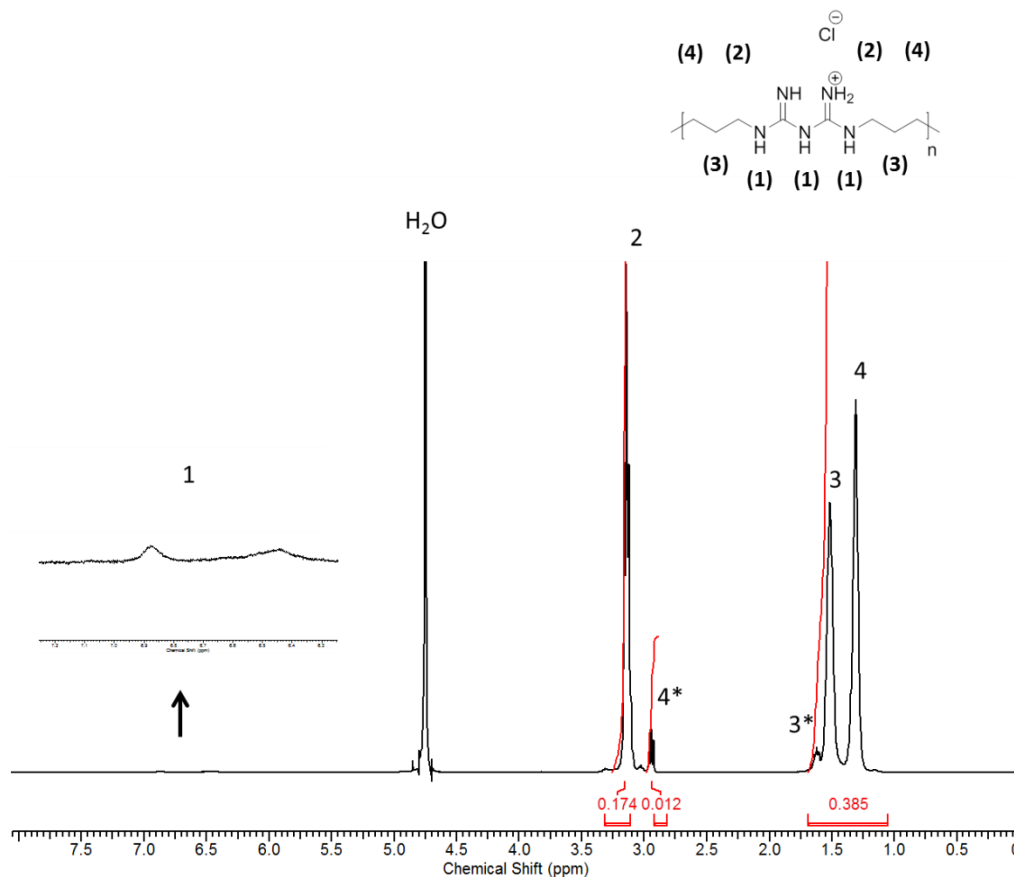


Figure 3.2 ^1H NMR Spectra of Poly(hexamethylene biguanide) chloride (PHMB).

The peaks annotated 4* and 3* are believed to be due to end groups (amine, guanide or cyanoguanide) and is fully discussed in Section 3.2.3.

ν_{max} (ATR)/ cm^{-1} 3303 (w) and 3181 (w) ($-\text{NH}-, =\text{NH}, =\text{NH}_2^+$), 2928 (w), 2854 (w), 1462 (s) and 719 (w) ($-\text{CH}_2-$, hexamethylene groups), 2174 (w) ($-\text{C}\equiv\text{N}$)

3.1.3 Poly(2-dimethylamino)ethyl methacrylate) methyl chloride quaternary salt (PDMC)

δ_{H} (400 MHz; D₂O); 0.80-1.22 (3H, m), 1.85-2.15 (1.5H, m), 3.25 (9H, d), 3.81 (2H, s), 4.35-4.57 (2H, m)

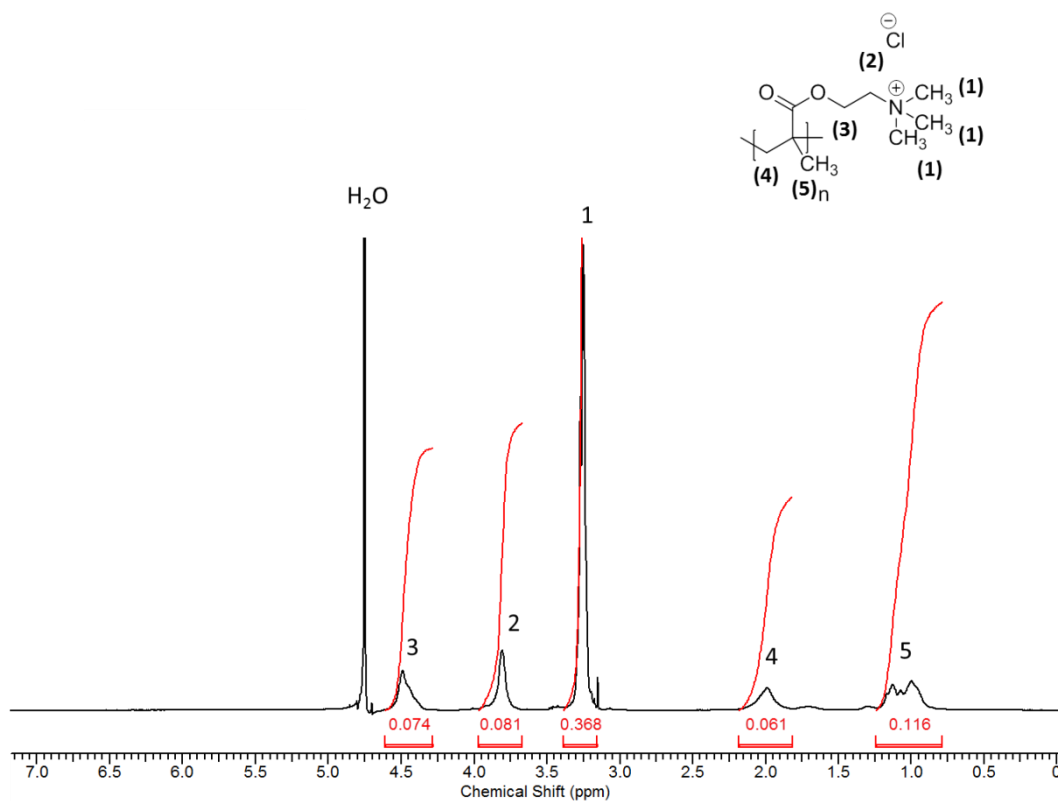


Figure 3.3 ¹H NMR Spectra of Poly(2-dimethylamino)ethyl methacrylate) methyl chloride quaternary salt (PDMC).

ν_{max} (ATR)/cm⁻¹ 3377 (b), 3017 (w) (-CH₃), 2961 (w) and 1478 (s) (C-H) 1721 (s) (C=O), 1148 (s) (-C-O-)

3.2 Polyelectrolyte Molecular Weight Determination

Polymers are polydisperse in nature, as such there are a range of molecular weights within a sample and the subsequent method in which these are averaged affects the value obtained. The weight average molecular mass (M_w), number average molecular mass (M_n) and viscosity average mass (M_v) have been reported within this work. The appropriate equations to calculate these terms have been described in Equations 3.1 - 3.3. If both the M_w and M_n are determined for a sample the so called polydispersity index (PDI) can be calculated (Equation 3.4). This gives a measure of the sample's polydispersity. The closer the value is to one, the more monodisperse the sample.²

$$M_w = \frac{\sum M_i^2 N_i}{\sum M_i N_i} \quad (3.1)$$

$$M_n = \frac{\sum M_i N_i}{\sum N_i} \quad (3.2)$$

$$M_v = \left[\frac{\sum M_i^{1+a} N_i}{\sum M_i N_i} \right]^{\frac{1}{a}} \quad (3.3)$$

$$PDI = \frac{M_w}{M_n} \quad (3.4)$$

where M_i = Concentration of the species, N_i = Number of molecules of the species and a = An exponent which represents the intrinsic viscosity- molecular weight relationship in each particular case.

The molecular weights of the studied polyelectrolytes were calculated using viscometry, size exclusion chromatography (SEC) and end group analysis using ^1H NMR.

3.2.1 Viscometry

The viscosity of a solution is defined as how resistant it is in an attempt to move through it. It has been well noted that polymer molecules increase the viscosity of liquids even at fairly low concentrations and the higher the molecular weight of the linear polymer the more viscous the solution will be.²

Intrinsic viscosity is defined as the capability of the polymer to enhance the viscosity of the solution and is calculated at infinite dilution. The intrinsic viscosity increases with increasing molecular weight for a linear polymer. The intrinsic viscosity can be related to the molecular weight by the Mark-Houwink relationship (Equation 3.5).²

$$[\eta] = KM^a \quad (3.5)$$

where $[\eta]$ = Intrinsic Viscosity, K and a = Constants, M = Molecular weight

To determine the intrinsic viscosity either an Ubbelohde capillary viscometer or a Anton Paar Microcapillary viscometer was used and a subsequent Huggins/ Kraemer plot produced. Equations 3.6 – 3.9 describes the various viscosity terms required for the plot.²

$$\eta_{rel} = \frac{\eta}{\eta_0} \quad (3.6)$$

$$\eta_{sp} = \frac{\eta - \eta_0}{\eta_0} = \eta_{rel} - 1 \quad (3.7)$$

$$\eta_{red} = \frac{\eta_{sp}}{c} \quad (3.8)$$

$$[\eta] = \lim_{c \rightarrow 0} \eta_{red} = \lim_{c \rightarrow 0} \frac{\ln \eta_{rel}}{c} \quad (3.9)$$

where η = Viscosity of solution, η_0 = Viscosity of pure solvent, η_{rel} = Relative viscosity, η_{sp} = Specific viscosity, η_{red} = Reduced viscosity

In the case of polyelectrolytes a solvent of 1 M NaCl is required for the determination of the molecular weight. The high electrolyte concentration suppress the electrostatic forces within the polyelectrolyte causing neutral polymer solution behaviour to occur.

The K and a constants in the Mark Houwink relationship (Equation 3.5) are readily available within the literature for the following polyelectrolytes. pDADMAC (average from a range of references); $K = 4.61 \times 10^{-3}$ (mL/g) and $a = 0.83$,³⁻⁵ PDMC; $K = 6.8 \times 10^{-3}$ (mL/g) and $a = 0.72$.^{6,7}

The pDADMAC samples were measured using a Ubbelohde capillary viscometer an example Huggin/Kraemer plot is shown in Figure 3.4 The PDMC sample was measured using the Anton Paar microcapillary viscometer due to restricted sample.

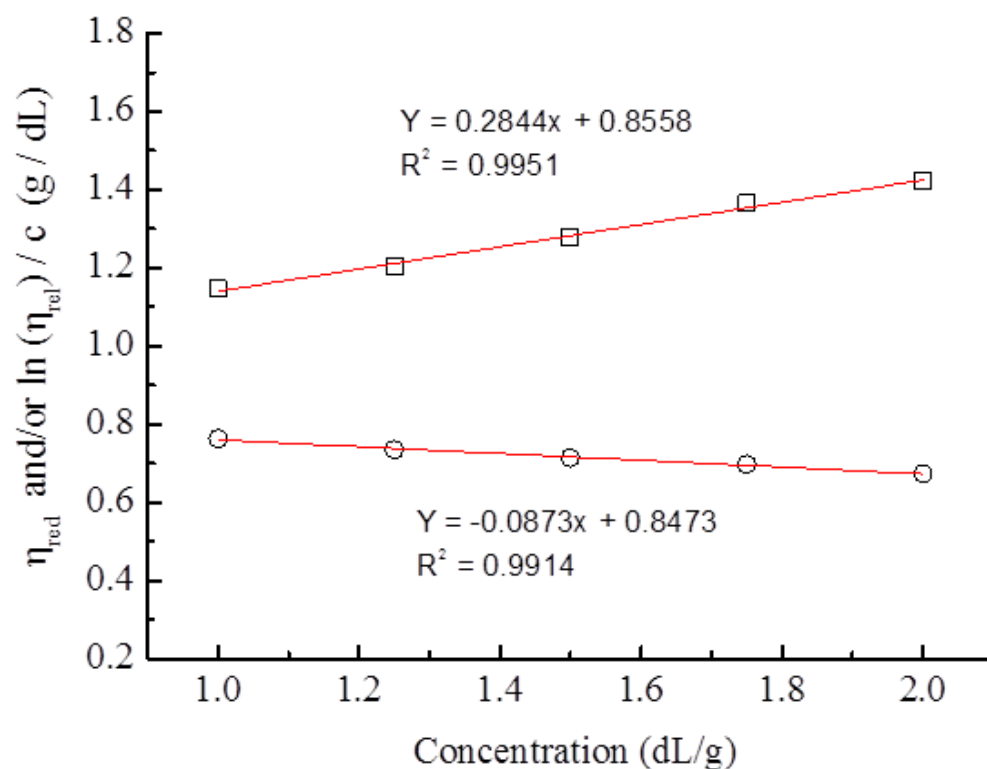


Figure 3.4 Example of a Huggins/Kraemer plot for a pDADMAC sample with extrapolation to $c = 0$ used to determine intrinsic viscosity $[\eta]$.

The Huggins/Kraemer plots of all the measured polyelectrolyte samples can be viewed in Appendix 2-G, H and I.

The determined intrinsic viscosities and molecular weights of the polyelectrolytes are shown in Table 3.1

Table 3.1 Intrinsic Viscosity of Polyelectrolytes in a 1 M NaCl solvent at 25 °C and Molecular weight (M_v).

| Polyelectrolyte | Supplier | Intrinsic Viscosity $[\eta]$ (dL/g) | Molecular Weight M_v (kDa) |
|-----------------|--------------------|--|---------------------------------|
| pDADMAC | Sigma Aldrich | 0.852 | 140 |
| pDADMAC | Sigma Aldrich | 0.177 | 21 |
| pDADMAC | Poly Sciences Inc. | 0.084 | 8.5 |
| PDMC | Sigma Aldrich | 0.024 | 3.4 |

Hereafter the pDADMAC and PDMC samples molecular weight will be denoted as M_v .

3.2.2 Size Exclusion Chromatography (SEC)

Size exclusion chromatography (SEC) was conducted on the pDADMAC and PDMC polyelectrolytes which enables the determination of the weight average molecular mass (M_w), number average molecular mass (M_n) and polydispersity index (PDI).

Figure 3.5 gives a graphical comparison of the different molecular weight distributions for the pDADMAC samples. These samples were measured on the high molecular weight system.

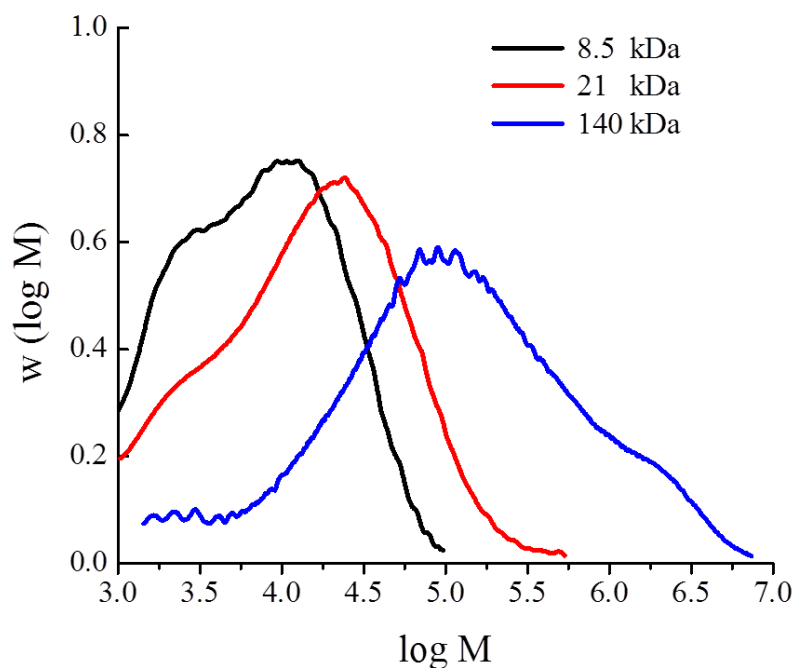


Figure 3.5 GPC trace of pDADMAC polyelectrolytes in the high column SEC system. M = Molecular mass, w = Weight fraction.

Molecular weights and PDIs of the various polyelectrolytes are reported in Table 3.2.

Table 3.2 M_w , M_n and PDI determined by SEC, Systems calibrated against Poly(ethylene) oxide.

| Polyelectrolyte | SEC System | M_w (kDa) | M_n (kDa) | PDI |
|-------------------|------------|-------------|-------------|-----|
| pDADMAC (8.5 kDa) | Low | 12 | 4.6 | 2.7 |
| pDADMAC (21 kDa) | Low | 38 | 4.1 | 9.3 |
| pDADMAC (140 kDa) | High | 400 | 19 | 21 |
| PDMC | Low | 8.2 | 6.1 | 1.4 |

3.2.3 End Group Analysis

For the polyelectrolyte Poly(hexamethylene biguanide) chloride (PHMB) appropriate SEC conditions could not be obtained. Also viscometry could not be used to determine the molecular weight as the Mark Houwink constants are not readily available within the literature so the number average mass (M_n) was calculated by end group analysis.

PHMB was first synthesised by Rose and Swain^{8,9} and commonly synthesised via the reaction of cyano groups with amine hydrochloride.^{10,11} The common methodology is melt polymerisation of hexamethylene diamine and bisdicyanodiamide. The end groups of the oligomeric material is reported to be a combination of amine, guanide and cyanoguanide end groups.¹² Although East *et al.*¹⁰ suggest the end groups are just cyanoguanide groups.

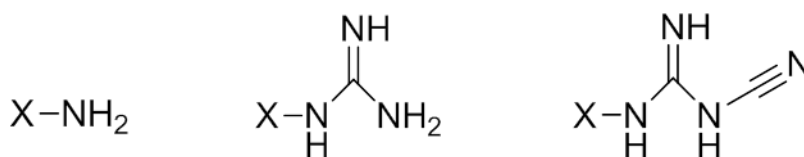


Figure 3.6 Chemical structures of the three possible PHMB end groups. Left to Right; Amine, Guanide, Cyanoguanide.

The presence of these end groups causes proton environment (2) within the 1H NMR spectra (Figure 3.7). This enables end group analysis to be conducted.

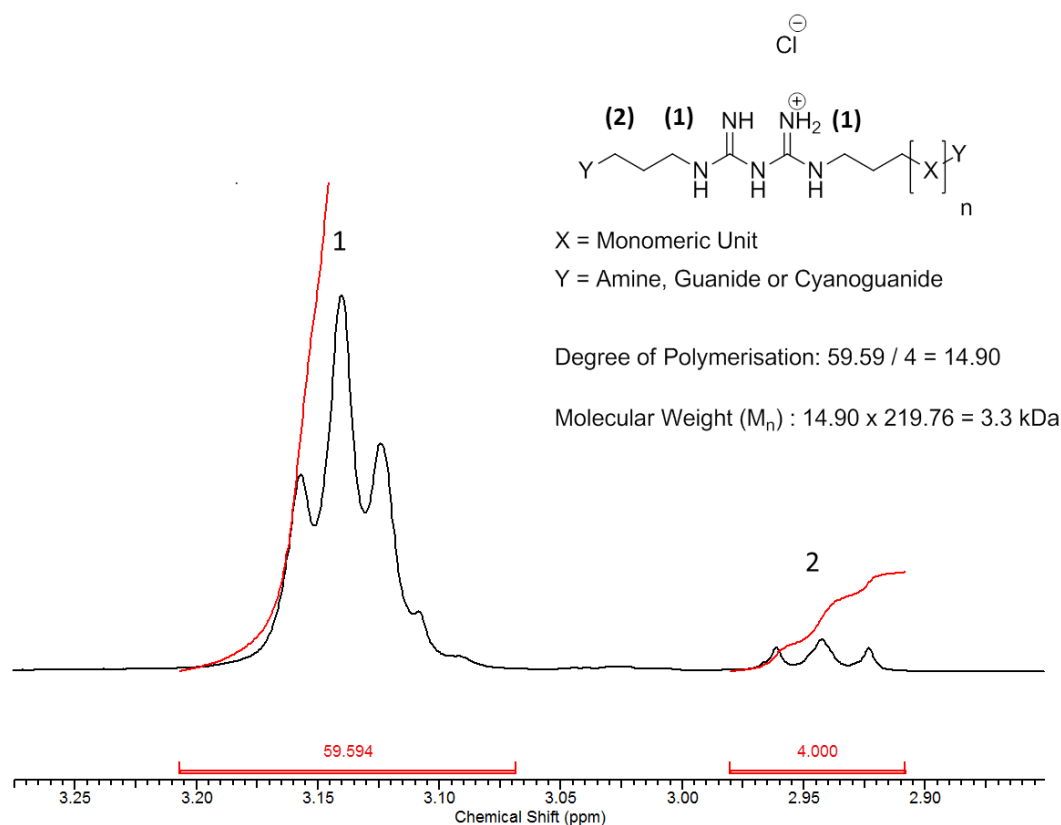


Figure 3.7 Magnified ^1H NMR spectra of Poly(hexamethylene biguanide) chloride (PHMB) required for end group analysis.

The integration of proton environment (2) was set to four as this peak corresponds to four hydrogens within the oligomer. This was compared to proton environment (1) which is contained within the monomeric unit. The integration of proton environment (1) was divided by four as it corresponds to 4 hydrogens within each monomeric unit. The resulting number ($n = 14.90$) indicates the degrees of polymerisation for PHMB and was multiplied via the monomeric molecular weight to determine the oligomers M_n (3.3 kDa).

3.2.4 Summary of Determined Molecular Weights

The molecular weights of the Polyelectrolytes are summarised in Table 3.3.

Table 3.3 Summary of the different determined molecular weights of the studied polyelectrolytes and the methodology used for their determination.

| Polyelectrolyte | SEC | | | Viscometry | ¹ H NMR |
|-----------------|----------------------|----------------------|---|----------------------|----------------------|
| | M _w (kDa) | M _n (kDa) | M _w /M _n (PDI) | M _v (kDa) | M _n (kDa) |
| pDADMAC | 12 | 4.6 | 2.7 | 8.5 | - |
| pDADMAC | 38 | 4.1 | 9.3 | 21 | - |
| pDADMAC | 400 | 19 | 21 | 140 | - |
| PDMC | 8.2 | 6.1 | 1.4 | 3.4 | - |
| PHMB | - | - | - | - | 3.3 |

Hereafter the pDADMAC and PDMC samples molecular weight will be denoted as M_v. The PHMB samples molecular weight will be denoted as M_n.

3.3 Characterisation of Surfactants

3.3.1 Alkyl (C₁₂ 70%; C₁₄ 30%) dimethyl benzyl ammonium chloride (BAC)

δ_H (400 MHz; D₂O); 0.81 (3H, m), 1.21 (19H, d), 1.73 (2H, m), 2.95 (6H, s), 3.05 (2H, m) 4.40 (2H, s), 7.39 (5H, m)

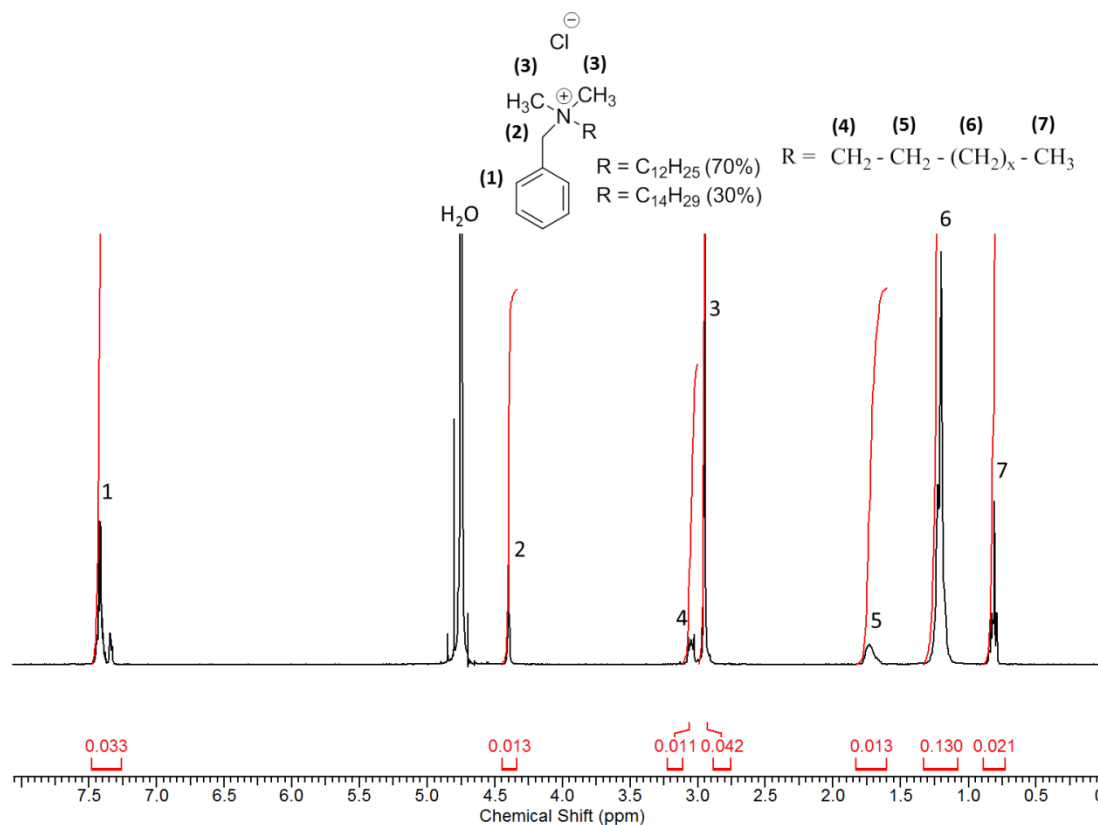


Figure 3.8 ¹H NMR Spectra of Alkyl (C₁₂ 70%; C₁₄ 30%) dimethyl benzyl ammonium chloride (BAC).

SI-MS m/z (ES+) [M-Cl]⁺ 304 attributed to C₁₂ BAC and [M-Cl]⁺ 332 attributed to C₁₄ BAC.

3.3.2 Didecyl dimethyl ammonium chloride (DDQ)

δ_H (400 MHz; D_2O); 0.78 (6H, t), 1.24 (28H, d), 1.57 (4H, m), 3.00 (6H,m), 3.16 (4H, m)

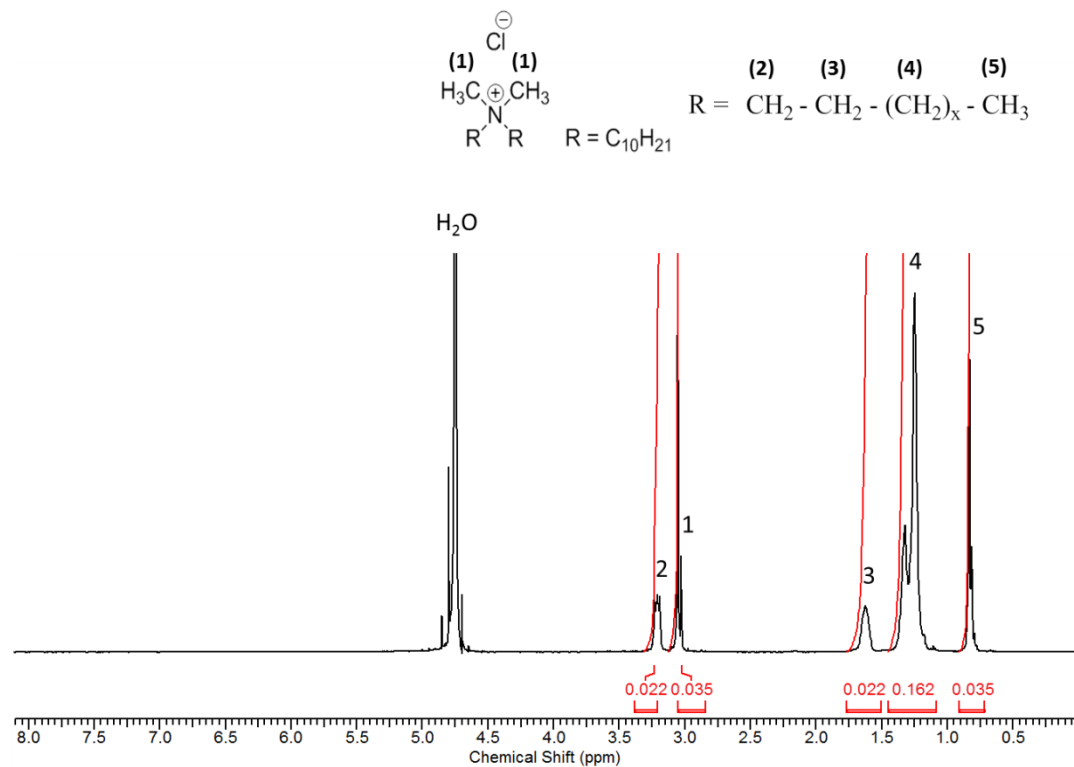


Figure 3.9 1H NMR Spectra of Didecyl dimethyl ammonium chloride (DDQ).

SI-MS m/z (ES+) $[M-Cl]^+$ 326 and slight impurity 298 attributed to a possible dinonyl dimethyl ammonium impurity.

3.4 References

1. J. E. Lancaster, L. Baccei and H. P. Panzer, *J. Polym. Sci., Part C: Polym. Lett.*, 1976, **14**, 549-554.
2. P. Flory, *Principles of Polymer Chemistry*, Cornell University Print, London, 1953.
3. H. Dautzenberg, E. Gornitz and W. Jaeger, *Macromol. Chem. Phys.*, 1998, **199**, 1561-1571.
4. G. J. Timofejeva, S. A. Pavlova, C. Wandrey, W. Jaeger, M. Hahn, K. J. Linow and E. Gornitz, *Acta Polym.*, 1990, **41**, 479-484.
5. C. W. Burkhardt, K. J. McCarthy and D. P. Parazak, *J. Polym. Sci., Part C: Polym. Lett.*, 1987, **25**, 209-213.
6. S. Manfred, *Angew. Makromol. Chem.*, 1984, **123**, 85-117.
7. T. Griebel, W. M. Kulicke and A. Hashemzadeh, *Colloid. Polym. Sci.*, 1991, **269**, 113-120.
8. Rose, FL Swain, G, *UK Pat.*, 702,268, 1954.
9. F. L. Rose and G. Swain, *J. Chem. Soc.*, 1956, 4422-4425.
10. G. C. East, J. E. McIntyre and J. Shao, *Polymer*, 1997, **38**, 3973-3984.
11. Y. M. Zhang, J. M. Jiang and Y. M. Chen, *Polymer*, 1999, **40**, 6189-6198.
12. L. P. O'Malley, A. N. Collins and G. F. White, *J. Ind Microbiol Biot*, 2006, **33**, 677-684.

Chapter 4 – Polyelectrolytes in Solution

Polyelectrolytes in Solution

This chapter aims to study the planktonic (solution) antimicrobial activity for a range of polyelectrolytes by the determination of their minimum inhibitory concentration (MIC) for a range of gram-negative bacteria. The solution properties of these structurally diverse range of polyelectrolytes in relation to the Manning parameter and chain conformation is considered. The MIC testing was kindly conducted by Nishal Govindji and subsequently reported in her PhD Thesis on Inhibiting biofilms formed by gram-negative uropathogenic bacteria.¹

4.1 Polyelectrolytes

Polyelectrolytes are polymers which have ionisable groups within them and when placed into a polar solvent (water) these groups dissociate. Upon dissociation charge is left on the polymer while the corresponding counter ion is released into the solution.²

This study will look at strong polyelectrolytes, These fully dissociate at most reasonable pHs (2-10). Two classes of polymer which will be studied are;

- i) A biguanide based polymer - Poly(hexamethylene biguanide) chloride (PHMB).
- ii) Two structurally diverse QACs polymers - Poly(diallyl dimethyl ammonium) chloride (pDADMAC) and Poly(2-dimethylamino)ethyl methacrylate) methyl chloride quaternary salt (PDMC).

4.2 Solution Properties

4.2.1 Manning Parameter

The counter ions of a polyelectrolyte are required to maintain electron neutrality within the solution. Consequently it could be favourable to have a number of counter ions close to or on the polyion surface to reduce this charge. This is termed Manning theory or the counter ion condensation phenomenon.³⁻⁵

To explore at what conditions this would occur the Manning parameter (Equation 4.1) can be employed.

$$\xi = \frac{l_B}{b} \quad (4.1)$$

$$b = \frac{L}{N} \quad (4.2)$$

Where ξ = Manning parameter, l_B = Bjerrum length (0.71 nm at 20 °C), b = distance between singly charged groups, L = Contour length and N = Number of charged groups.

The Bjerrum length (l_B) is defined as the characteristic distance that a stable dissociative state can form between a singly charged ion pair.⁶

$$l_B = \frac{e^2}{4\pi\epsilon_0\epsilon_r k_B T} \quad (4.3)$$

Where e = Elementary charge, ϵ_0 = Vacuum permittivity, ϵ_r = Dielectric constant, k_B = Boltzmann constant and T = Absolute temperature.

The Manning parameter is only valid at infinite dilution and where intermolecular polyion interactions are assumed to be absent.

The Manning parameter (ξ) predicts a maximum charge density for a monovalent system of $\xi \leq 1$ thus counter ion condensation occurs if the distance between the singly charged species (b) is smaller than the Bjerrum length(l_B). In this case, coulombic interactions dominate over the thermal interactions.

The fraction of condensed and uncondensed counter ions can be subsequently calculated (Equation 4.4 – 4.5).

$$\text{Condensed counter ions} = \left(1 - \frac{1}{\xi}\right) \quad (4.4)$$

$$\text{Uncondensed counter ions} = \left(\frac{1}{\xi}\right) \quad (4.5)$$

The condensed counter ions are assumed to be in equilibrium with the uncondensed counter ions present in the ionic atmosphere of the polyions.

The Manning parameter was calculated for the polyelectrolytes pDADMAC, PHMB and PDMC. Before calculating the Manning parameter some important factors must be accounted for due to their different structural properties. In Figure 4.1 schematic diagrams for the different polyelectrolytes are shown to illustrate how the Manning parameter was calculated.

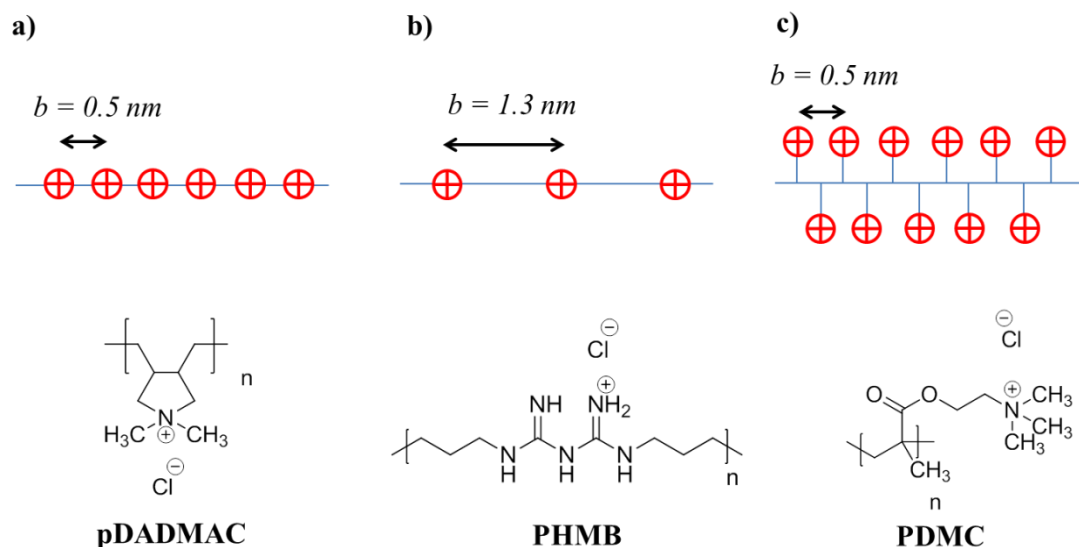


Figure 4.1 Schematic diagrams of polyelectrolytes relating chemical structures to assumptions required for Manning parameter calculation. b = distance between the singly charged groups.

The ionic charge on pDADMAC is contained on a 5 membered ring approximately two single carbon bonds from the backbone. For the purpose of the Manning parameter calculation, the point charge was assumed to be on the polymer backbone.

For the case of PHMB, the ionic charge is delocalised around its biguanide group but for the Manning parameter a point charge is required. The most stable tautomeric structure of PHMB at pH 7 was chosen (Figure 4.1).⁷

The chemical structure of PDMC presents its own problem because the ionic charge is located not on the polymer backbone but at the end of a pendant group. An assumption was made that within solution PDMC would form an almost “syndiotatic” like conformation as this would give the largest distance between the ionic charges of the pendant groups hence the most favourable conformation.

The chemical structures of the polyelectrolytes were drawn using Chem 3D Pro 12.0 and viewed in stick mode. The sizing freeware ImageJ was used to measure monomer length. The image was calibrated by using a single carbon bond (0.15 nm) within the structure. Monomer length (a) is equivalent to the distance between the singly charged species (b) except for PDMC when $b = 2a$. (In this case a = monomer length on the backbone of the polymer).

The Manning parameter for the polyelectrolytes PHMB, pDADMAC and PDMC are reported in Table 4.1.

Table 4.1 Manning parameter calculations for PHMB, pDADMAC and PDMC at 20 °C in water.

| Polyelectrolyte | Manning parameter (ξ) | Uncondensed counter-ions ($\frac{1}{\xi}$) | Condensed counter-ions ($1 - (\frac{1}{\xi})$) |
|-----------------|-----------------------------------|--|--|
| PHMB | 0.6 | n/a | n/a |
| pDADMAC | 1.4 | 0.7 | 0.3 |
| PDMC | 1.4 | 0.7 | 0.3 |

According to the Manning parameter, PHMB does not undergo counter ion condensation while pDADMAC and PDMC do undergo this phenomenon.

4.2.2 Surface Activity

The surface tension profile of the studied polyelectrolytes in Millipore filtered water was looked at in Figure 4.2a.

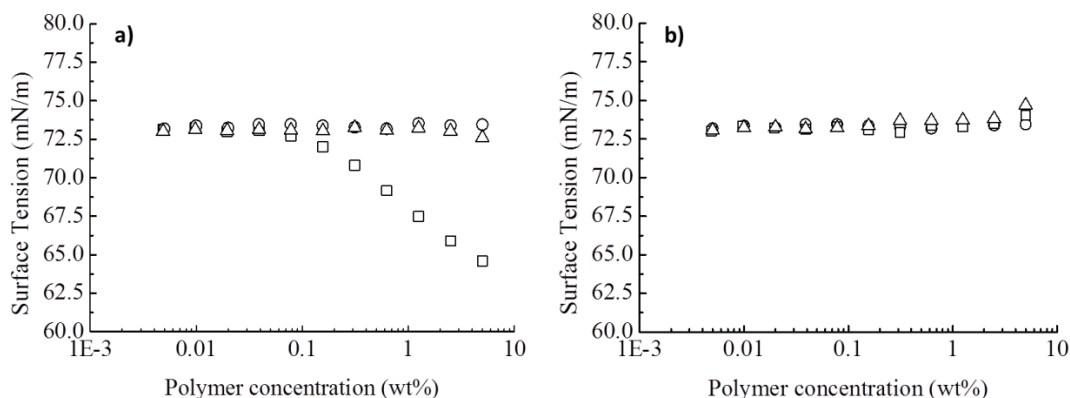


Figure 4.2 Surface tension profile in DI water at 25 °C of a) pDADMAC 8.5 kDa (○), PHMB (□) and PDMC (Δ). b) pDADMAC 8.5 kDa (○), 21 kDa (□), 140 kDa (Δ).

Water is known to have a high surface tension (72.0 mN/m) due to the large imbalance in the intermolecular hydrogen bonding between the water molecules at the interface compared to the bulk. Amphiphilic molecules contain distinct hydrophobic (water-hating) and hydrophilic (water-loving) regions. This amphiphilic property causes these types of molecules to adsorb onto the air-water interface so that the hydrophobic region of the molecule can remove itself from the polar solvent.⁸

Only PHMB was observed to be surface active over the concentration range studied (0.005 – 5 wt%). The pDADMAC and PDMC samples have the same surface tension as the solvent water. The effect of molecular weight (Figure 4.2b) was also looked at with the surface tension profiles of a range of pDADMAC samples observed to have almost no effect on surface activity however, at the higher concentrations a very slight increase in the surface tension was observed.

To gain further insight into PHMBs adsorption at the air-water interface, a thermodynamic profile (Figure 4.3) was produced using isothermal titration calorimetry (ITC). A concentrated solution of PHMB was injected into a vessel containing only the solvent water numerous times. After each injection the change in enthalpy (ΔH) was measured. ΔH is the net value of binding (endothermic) and dissociative (exothermic) events within the solution.

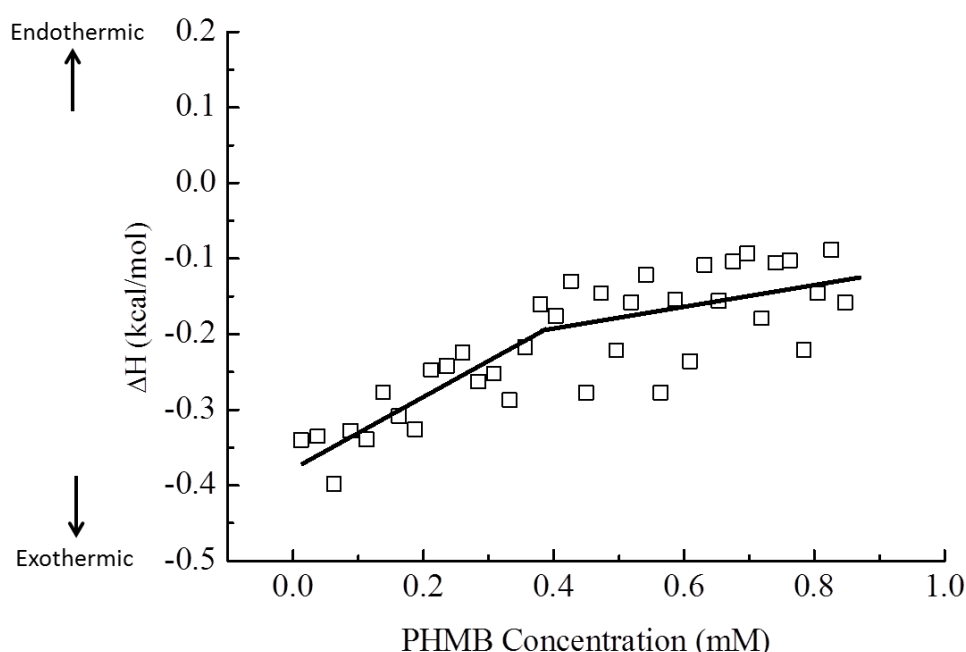


Figure 4.3 Isothermal Titration (ITC) profile of PHMB at 25 °C. Line to guide eye.

An inflection point was observed at 0.4 mM (0.1 wt%) which corresponds to the approximate concentration at which PHMB becomes surface active. An additional net exothermic effect was observed at this point. A study by Blackburn *et al.*⁷ suggested PHMB prefers to be in a kinked globular conformation driven by intramolecular hydrogen bonds between the biguanide groups. The uncoiling of this globular conformation upon absorption to the air-water interface could be a possible explanation but further investigation is required.

4.2.3 Relating Surface Activity/Image Charge /Manning Parameter

The surface activity behaviour of the polyelectrolytes we now be rationalised in relation to the image charge effect and the Manning parameter.

The image charge effect is defined as the repulsion of ions from the air-water interface. Ions can become strongly isotropically hydrated within water and as such they cannot approach the interface without losing some of this bound water which is an energetically unfavourable process. In addition the dielectric boundary of the air-water interface opposes the approach of these hydrated ions which induces image charge repulsion. The strength of repulsion is dependent on the square of the size of charge on the ions and inversely dependent on both the dielectric medium and the distance the ions are from the interface.⁹

The image charge effect has been suggested as the reason for the occurrence of non-surface active ionic (anionic and cationic) amphiphilic diblock copolymers which form micelles within solution. The large concentration of ionic species within the hydrophilic block creates enough image charge repulsion at the interface to prevent the hydrophobic block from absorbing onto the air-water interface even though these type molecules are amphiphilic in nature.^{10, 11}

If we now return back to the Manning parameter calculations; For the case of PHMB, the distance between the singly charged species (b) is greater than the Bjerrum length (l_B) thus in between the charged species the hydrophobic hexamethylene section of PHMB gives the chain amphiphilic character. A competition takes place between the image charge repulsion from the ions on the biguanide groups and the hydrophobic forces of the hexamethylene group. Adsorption to the air-water interface occurs due to the increasing chemical potential of PHMB within the bulk.

For the cases of pDADMAC and PDMC the distance between the singly charged species (b) is smaller than the Bjerrum length (l_B) and as such these polyelectrolytes have an over whelming ionic character with very limited amphiphilic property. These

polyelectrolytes do not have significant hydrophobic forces acting upon them and are inhibited from approaching the air-water interface due to the discussed image charge repulsion effect from the quaternary nitrogen ions.

4.2.4 Concentration Regimes

This section will look at the different chain conformation you would expect polyelectrolyte chains to be in within salt-free condition as a function of concentration. The aim of this section was to get an idea/estimation of what conformation the polyelectrolyte chain will be in around its corresponding MIC concentration.

By applying scaling concepts and considering an electrostatic contribution to the persistence length (L_p), Odijk divided salt-free polyelectrolyte concentrations into four distinct regimes.¹² The dilute regime, two semi-dilute transition regimes and an isotropic semi-dilute regime. The persistence length (L_p) is defined as the length over which correlations in the direction of the tangent are lost. The term is used to quantify the stiffness of a polymer chain.

Table 4.2 describes these four concentration regimes.

Table 4.2 Definition of the Odijk polyelectrolyte concentration regimes.

| Concentration Regime | Description of Regime | Polymer Concentration (C_p) |
|--------------------------|---|---------------------------------|
| Dilute | Nominal interaction between molecules. Rigid rod. | $C_p < C_R^*$ |
| Semi dilute – Transition | Molecules remain as a rigid rod but interact strongly with chain neighbours. Lattice structure. | $C_R^* < C_p < C_b^*$ |
| Semi dilute – Transition | Melting of lattice structure. Collapsing of molecule into a random coil conformation | $C_b^* < C_p < C_m^*$ |
| Semi dilute – Isotropic | Fully collapsed random coil conformation. | $C_m^* < C_p$ |

Odijk calculated three critical concentrations to determine the four concentration regimes; dilute to semi-dilute crossover (C_R^*), lattice to semi-dilute transition (C_b^*) and transition to isotropic crossover (C_m^*) (Equation 4.6 - 4.8).

$$C_R^* = (N_A L^2 a)^{-1} \quad (L_p \gg L) \quad (4.6)$$

$$C_b^* = (16\pi N_A L a b \xi)^{-1} \quad (L_p \approx L) \quad (4.7)$$

$$C_m^* = (32\pi^2 N_A a b^2 \xi^2)^{-1} \quad (L_p < L) \quad (4.8)$$

Where L = Contour length, a = Monomer length, b = Distance between the singly charged species, ξ = Manning parameter, L_p = Persistence length.

Using the Odijk theory the critical concentrations C_R^* , C_b^* and C_m^* were calculated for all the polyelectrolytes used within this study (Table 4.3). These critical concentrations have been previously calculated for a range of different molecular weight pDADMACs by Wandrey *et al.*¹³ The results reported in Table 4.3 are consistent with these values. The average viscosity molecular weight (M_v) was used for the Odijk calculations except for PHMB where the number average molecular weight (M_n) was used. The model does not account for polydispersity.

Table 4.3 Tabulated C_R^* , C_b^* and C_m^* data for the studied polyelectrolytes.

| Polyelectrolyte | Concentration ($\mu\text{g}/\text{mL}$) | | |
|-------------------|---|---------|---------|
| | Odijk Model | | |
| | C_R^* | C_b^* | C_m^* |
| pDADMAC (8.5 kDa) | 770 | 570 | 3300 |
| pDADMAC (21 kDa) | 130 | 230 | 3300 |
| pDADMAC (140 kDa) | 3.0 | 30 | 3300 |
| PHMB | 760 | 400 | 1800 |
| PDMC | 1900 | 740 | 2300 |

As reported in Table 4.3, the Odijk concentration regime model does not hold for the lower molecular weight polyelectrolytes with $C_b^* < C_m^*$. As described by Kaji *et al.*¹⁴ the existence/order of these transition regimes can be different for lower molecular weight samples.

4.3 Minimum Inhibitory Concentration (MIC)

The Minimum Inhibitory Concentration (MIC) was determined for the studied polyelectrolytes however due to the methodology used in testing the aqueous solvent contained 85 mM NaCl as well as some yeasts and peptides. A direct comparison between the previously reported solution properties and MICs cannot be directly related due to these solutes, however the reported MICs illustrates the antimicrobial properties of these polyelectrolytes within solution.

All the polyelectrolytes studied contain positively charged nitrogen moieties. These positively charged moieties are reported to have antimicrobial activity. The minimum inhibitory concentration (MIC) was determined for a range of gram-negative bacteria (*E.coli*, *Klebsiella Pneumonia* and *Pseudomas*). The MIC is defined as the lowest concentration that inhibits the visible growth of the bacteria after overnight incubation.¹⁵ The determined MICs for the polyelectrolyte studied are reported in

Table 4.4.

Table 4.4 Tabulated Minimum Inhibitory Concentration (MIC) of studied polyelectrolytes.

| Polyelectrolyte | MIC (µg/mL) | | | |
|-------------------|-----------------------|---------------------------------------|---|---|
| | <i>E. coli</i> K12 | <i>E. coli</i> Clinical isolate | <i>Klebsiella</i> <i>Pneumonia</i> Clinical isolate | <i>Pseudomonas</i> Clinical isolate |
| pDADMAC (8.5 kDa) | 15 | 15 | 30 | 30 |
| pDADMAC (21 kDa) | 20 | 30 | 60 | 200 |
| pDADMAC (140 kDa) | 20 | 100 | 100 | 400 |
| PHMB | 10 | 60 | 200 | 100 |
| PDMC | 10 | 50 | 1000 | 5000 |

A graphical comparison of MICs for different polyelectrolyte type (Figure 4.4a) and differing molecular weight pDADMACs (Figure 4.4b) is shown. It should be noted that for Figure 4.4a the MIC of PDMC for *Pseudomonas* was plotted as 1000 $\mu\text{g/mL}$ instead of 5000 $\mu\text{g/mL}$ as it allowed for a better graphical comparison of the other MICs within the graph.

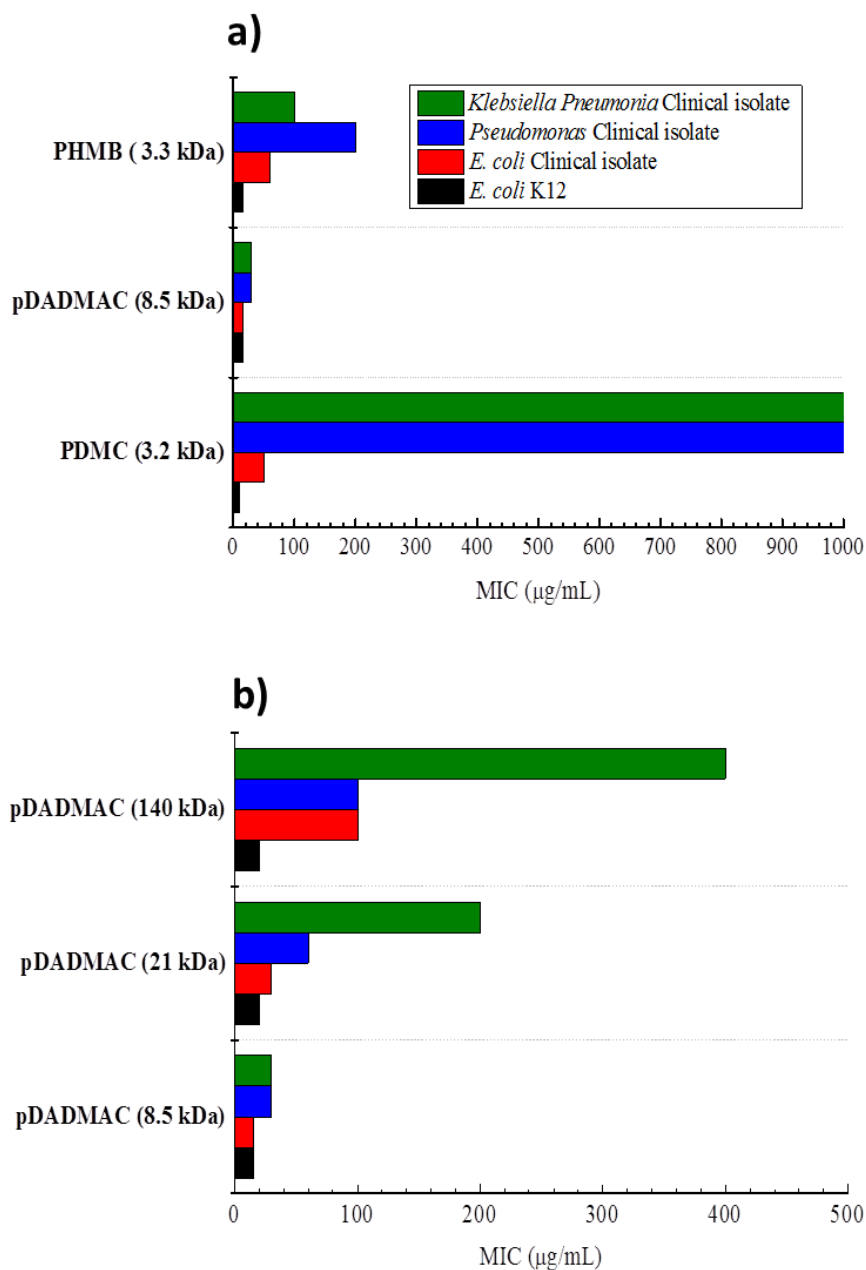


Figure 4.4 a) MICs for different polyelectrolyte types. b) MICs for a range of different molecular weight pDADMAC sample. Molecular weight denoted M_v , except PHMB denoted M_n .

The following general trends were observed with MICs ranked low to high:

(low = better biocide)

Figure 4.4a. pDADMAC (8.5 kDa) > PHMB > PDMC.

Figure 4.4b. pDADMAC 8.5kDa > 21 kDa > 140 kDa

To give the MIC values some context to different biocides the didecyl dimethyl ammonium chloride surfactant (DDQ) and silver acetate has been reported to have an MIC of 1.3 µg/ mL and 0.5-2.5 µg/mL against *E. coli*.^{16, 17}

4.4 Discussion of Polyelectrolyte MIC

It has been widely reported that a combination of factors influences a polymeric substance's antimicrobial activity. These include the hydrophilic/lipophilic balance (HLB), salinity of the solvent, counter ion type, molecular weight and polydispersity.¹⁸⁻²¹

4.4.1 Polyelectrolyte Type

We will first consider Figure 4.4a and the effect of polyelectrolyte type. For PHMB (3.3 kDa), pDADMAC (8.5 kDa) and PDMC (3.2 kDa) the molecular weights were all below 10 kDa.

The antimicrobial properties of PHMB have been well reported within the literature but for the two quaternary ammonium based polyelectrolytes (pDADMAC and PDMC) research is sparse as they are used commercially as hair conditioning agents (> 100 kDa) and not biocides.²¹⁻²⁴

All three polyelectrolytes (PHMB, pDADMAC and PDMC) have differing structural properties in respect to the linker spacing between polyions. The differences in this

spacing length can affect the conformation and charge density properties of the polyelectrolytes. This will consequently affect how the polyelectrolyte interacts with the bacteria. The only previous study which could be found looking at linker spacing was by Ikeda *et al.*²⁵ who looked at the effect of altering the spacer distance between the cationic moieties for a range of polymeric pyridinium salts. A range of gram-positive and gram-negative bacteria were tested but no conclusive relationship was observed.

No clear relationship was observed regarding the linker spacing between the polyions and their reported MICs. It was somewhat surprising to observe that pDADMAC (8.5 kDa) had the lowest MICs followed by PHMB and lastly PDMC. A potential reason for pDADMAC (8.5 kDa) reporting lower MICs than PHMB (3.3 kDa) was a molecular weight effect but further investigation is required. Beyond the general ranking of the three polyelectrolytes types studied it is difficult to justify the MIC behaviour in terms of the structural and conformational differences. A study with better control of polyelectrolyte molecular weight, polydispersity and solvent salinity would be required.

4.4.2 Molecular Weight

To further explore the use of pDADMAC as a potential biocidal agent a range of different molecular weights were tested (Figure 4.4b). The lower the molecular weight of pDADMAC, the lower the MICs.

Numerous studies have reported trends in antimicrobial activity as a function of molecular weight. The dependence on antimicrobial activity for a range of different polyphosphonium and biguanide based compounds on M_w was bell shaped. A critical region of optimal performance was identified, $M_w \approx 14\text{--}100$ kDa. These studies looked at the gram-positive bacteria *S. aureus*.^{26, 27} Chen *et al.*²⁸ observed a parabolic dependence on molecular weight for a range of quaternary ammonium functionalised poly(propyleneimine) dendrimers. This study looked at the gram-positive *S. aureus*

and the gram-negative *E. coli*. Broxton *et al.*²² looked at a range of oligomeric PHMB polymers ($n = 2, 6$ and ≥ 10) against *E. coli* and reported an increase in antimicrobial activity for the higher molecular weight oligomers.

It was surprising to observe that the lower molecular weight pDADMAC (8.5 kDa) had the better antimicrobial activity which was a different molecular weight trend compared to what has previously been observed for cationic polymer of various architectures and types.

4.5 Conclusion

The solution properties of a range of homo-polyelectrolytes were explored within Millipore filtered water. However a direct comparison of solution properties and antimicrobial activity could not be achieved as the antimicrobial methodology required the addition of NaCl, yeasts and peptides to the solvent. The antimicrobial testing did illustrate the potential use of cationic polyelectrolytes as biocides within solution. The only polymeric based biocide commercially available, PHMB, was studied and used as a benchmark. Two additional commercially available polyelectrolytes, pDADMAC and PDMC, were also tested. The polyelectrolyte pDADMAC was identified as a potential antimicrobial agent with the lowest molecular weight sample (8.5 kDa) observed to have the lowest MICs for all samples tested.

4.6 References

1. N. Govindji, 'Inhibiting biofilms formed by Gram negative uropathogenic bacteria', PhD Thesis, The University of Manchester, 2013.
2. H. Morawetz, *Macromolecules in Solution*, 2nd Edition, Robert E. Krieger Publishing Company, 1975.

3. G. S. Manning, *J. Chem. Phys.*, 1969, **51**, 924-933.
4. G. S. Manning, *Q. Rev. BioPhys.*, 1978, **11**, 179-246.
5. G. S. Manning, *Biophys. Chem.*, 1977, **7**, 95-102.
6. G. S. Roberts, R. Sanchez, R. Kemp, T. Wood and P. Bartlett, *Langmuir*, 2008, **24**, 6530-6541.
7. R. S. Blackburn, A. Harvey, L. L. Kettle, J. D. Payne and S. J. Russell, *Langmuir*, 2006, **22**, 5636-5644.
8. R. Hunter, *Foundation of Colloid Science*, 2nd Edition., Oxford University Press, 2001.
9. M. Chaplin, *Water*, 2009, **1**, 1-28.
10. A. Ghosh, S.-i. Yusa, H. Matsuoka and Y. Saruwatari, *Langmuir*, 2011, **27**, 9237-9244.
11. H. Matsuoka, H. Chen and K. Matsumoto, *Soft Matter*, 2012, **8**, 9140-9146.
12. T. Odijk, *Macromolecules*, 1979, **12**, 688-693.
13. C. Wandrey, J. Hernandez-Barajas and D. Hunkeler, *Adv. Polymer. Sci.*, 1999, **145**, 123-182.
14. K. Kaji, H. Urakawa, T. Kanaya and R. Kitamaru, *J. Phys.*, 1988, **49**, 993-1000.
15. J. M. Andrews, *J. Antimicrob. Chemother.*, 2001, **48**, 5-16.
16. T. Yoshimatsu and K.-I. Hiyama, *Biocontrol*, 2007, **12**, 93-99.
17. C. Greulich, D. Braun, A. Peetsch, J. Diendorf, B. Siebers, M. Eppel and M. Koeller, *RSC Adv*, 2012, **2**, 6981-6987.
18. E.-R. Kenawy, S. D. Worley and R. Broughton, *Biomacromolecules*, 2007, **8**, 1359-1384.
19. L. Timofeeva and N. Kleshcheva, *Appl. Microbiol. Biotechnol.*, 2011, **89**, 475-492.
20. L. M. Timofeeva, N. A. Kleshcheva, A. F. Moroz and L. V. Didenko, *Biomacromolecules*, 2009, **10**, 1416-1428.
21. J. J. Merianos, *Block, S. S. Disinfection, Sterilization, and Preservation, Fourth Edition. Williams and Wilkins: York, Pennsylvania, USA; Lea and Febiger: Malvern, Pennsylvania, USA; London, England, Uk. Illus*, 1991.
22. P. Broxton, P. M. Woodcock and P. Gilbert, *J. Appl. Bacteriol.*, 1983, **54**, 345-353.

23. P. Broxton, P. M. Woodcock, F. Heatley and P. Gilbert, *J. Appl. Bacteriol.*, 1984, **57**, 115-124.
24. T. Ikeda, A. Ledwith, C. H. Bamford and R. A. Hann, *Biochim. Biophys.*, 1984, **769**, 57-66.
25. T. Ikeda, H. Hirayama, K. Suzuki, H. Yamaguchi and S. Tazuke, *Makromolekulare Chemie.*, 1986, **187**, 333-340.
26. T. Ikeda, H. Hirayama, H. Yamaguchi, S. Tazuke and M. Watanabe, *Antimicrob Agents Chemother.*, 1986, **30**, 132-136.
27. T. Ikeda, H. Yamaguchi and S. Tazuke, *Antimicrob Agents Chemother.*, 1984, **26**, 132-144.
28. C. Z. S. Chen, N. C. Beck-Tan, P. Dhurjati, T. K. van Dyk, R. A. LaRossa and S. L. Cooper, *Biomacromolecules*, 2000, **1**, 473-480.

Chapter 5 – Surfactant/Polyelectrolytes of Similar Charge

Surfactant / Polyelectrolyte Mixtures of Similar Charge

This chapter investigates the phase separation phenomena which occur within concentrated polyelectrolytes/surfactant aqueous mixtures of similar charge. Various systems are investigated using the quaternary ammonium surfactants; Alkyl (C_{12} 70%; C_{14} 30%) dimethyl benzyl ammonium chloride (BAC), Didecyldimethylammonium chloride (DDQ) and the polyelectrolytes Poly(diallyldimethyl ammonium) chloride (pDADMAC) and Poly(hexamethylene biguanide) chloride (PHMB).

5.1 Cationic Surfactants

We first characterise and discuss the differing surfactant properties of BAC and DDQ.

Surfactants are amphiphilic molecules. Amphiphilic molecules contain a hydrophilic (water-loving) head group and a hydrophobic (water-hating) tail. In this case the surfactants of interest are cationic surfactants as they contain a quaternary ammonium nitrogen with a corresponding counter ion (chloride) as part of the headgroup. When a surfactant is placed in an aqueous environment, the surfactant adsorbs onto the air-water interface. At a critical concentration, the so called critical micelle concentration (CMC) becomes more thermodynamically favourable for the surfactant unimers to remain within the bulk solution and form dynamic aggregates, so called micelles. The hydrophobic tail is oriented towards the micelle interior while the polar headgroup is exposed to the water exterior.¹⁻³

The critical micelle concentration (CMC), head group size, dissociation constant, micelle size and geometry were investigated using a range of analytical techniques including surface tensiometry, conductivity, isothermal titration calorimetry (ITC) and photon correlation spectroscopy (PCS).

5.1.1 Surface Tensiometry

One of the most common techniques to study a surfactant is via surface tensiometry. This technique measures the surface tension of the solution as a function of surfactant concentration. The adsorption of the surfactant unimers on the air-water interface causes a decrease in the surface tension of the solution. Once the concentration is above the CMC the surface tension plateaus. The surface tension profiles of BAC, DDQ and a BAC/DDQ (2:3 mol:mol) mixture are shown in Figure 5.1.

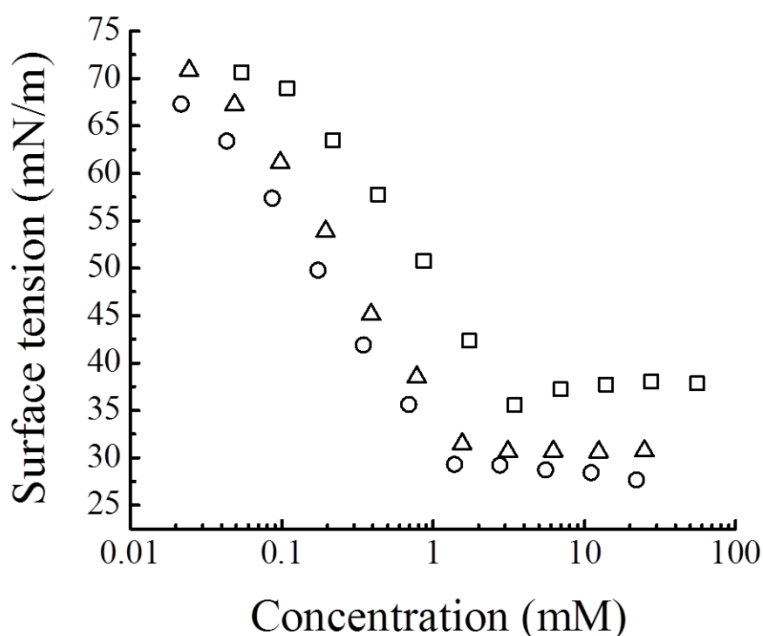


Figure 5.1 Surface tension profiles in water at 25 °C of (□) BAC, (O) DDQ, and (Δ) BAC/DDQ (2:3 mol:mol).

The CMC of a surfactant is determined by the intersection of the two linear fits before and after the inflection point on a surface tension profile. From the surface tension profile the Langmuir adsorption equation¹ (Equation 5.1-5.2) can be employed to determine the maximum area/headgroup at the micellar surface.¹

$$d\gamma = -2RT\Gamma_2 d \ln C_2 \quad (5.1)$$

$$A = \frac{10^{23}}{N_A \Gamma_2} \quad (5.2)$$

Where γ = Surface tension (N/m), Γ_2 = Surface excess concentration (moles/ 1000 m²), C_2 = Concentration (mol/L) and A = The maximum area/surfactant headgroup at the interface (Å²).

The CMCs and headgroup areas are reported in Table 5.1.

Table 5.1 Tabulated CMC and area of surfactant headgroup values. Results obtained by surface tensiometry.

| Surfactant | CMC (mM) | Area of Head group (Å ² ±1) |
|---------------|----------|--|
| BAC | 3.5 | 83 |
| DDQ | 1.4 | 79 |
| BAC/DDQ (2:3) | 1.9 | 78 |

5.1.2 Conductivity

The conductivity of a solution is defined as its ability to conduct an electrical current.⁴ It is widely reported that for a surfactant an inflection point is observed at the CMC. This inflection has been attributed to size and counter ion dissociation differences between the unimer and micelle form. The conductivity profiles of BAC, DDQ and a BAC/DDQ (2:3 mol:mol) mixture are shown in Figure 5.2.

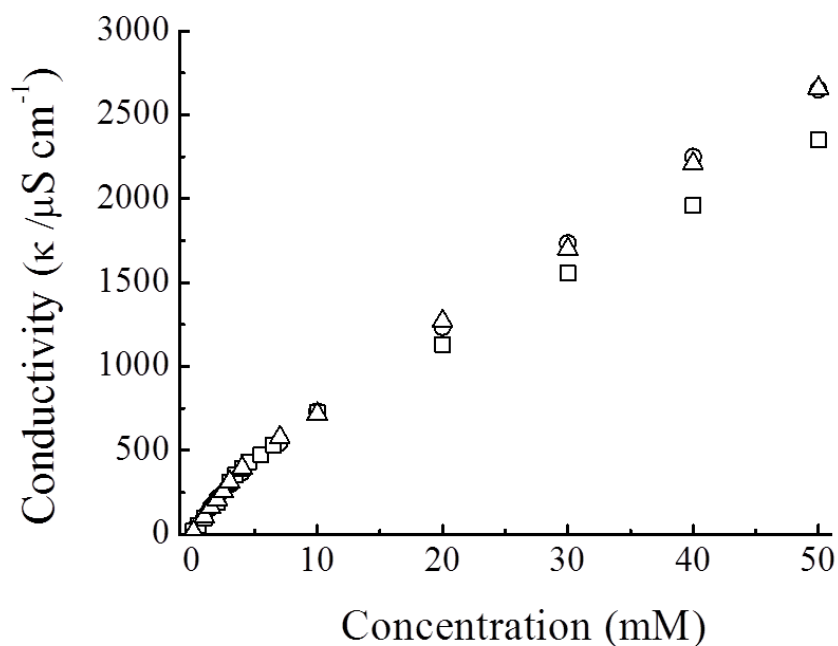


Figure 5.2 Conductivity profiles in water at 25 °C of (□) BAC, (O) DDQ, and (Δ) BAC/DDQ (2:3 mol:mol).

As well as enabling the determination of the CMC an estimation of the counter ion dissociation constant can be made using the so called Frahm model⁵ (Equation 5.3).

$$\alpha = \frac{S_2}{S_1} \quad (5.3)$$

Where α = Dissociation constant, S_1 = Slope before CMC and S_2 = Slope after CMC.

The counter ion dissociation constant (α) is defined as the fraction of counter ions not bound to the micelle surface. Frahm's model assumes that the inflection point within the conductivity profile is solely due to the counter ion dissociation difference between the unimer and micelle form. It is assumed that within the concentration

regime measured micelle size does not change significantly.⁵ The CMCs and dissociation constant are reported in Table 5.2.

Table 5.2 Determination of CMC and dissociation constant using Frahm's model. Results obtained via conductivity at 25 °C.

| Surfactant | CMC (mM) | Dissociation Constant |
|---------------|----------|-----------------------|
| BAC | 4.8 | 0.44 |
| DDQ | 3.0 | 0.50 |
| BAC/DDQ (2:3) | 3.9 | 0.48 |

5.1.3 Pyrene

Spectroscopic techniques used for investigating the CMC have been well reported within the literature. These techniques involve the emission of light from a probe molecule. The probe molecule should be sparingly soluble in the solvent and hydrophobic enough so it will solubilise within the micelle. The most common probe molecules are fluorescent. The advantage compared to optical based methods is the sensitivity which allows a lower concentration of a probe molecule to be used, thus reduces any effect of the additive on the CMC. Pyrene is the most common fluorescent probe molecule.³

As reported by Kalyanasundaram and Thomas⁶ the ratio between the I and III peak in the pyrene fluorescence emission spectra changes depending on its hydrophilic/hydrophobic environment. The larger the peak ratio (III/I), the more hydrophobic the environment in which pyrene resides. A sharp increase in the peak ratio (III/I) signifies the onset of micellisation. An example of a pyrene fluorescence spectra below and above a surfactant's CMC is illustrated in Figure 5.3.

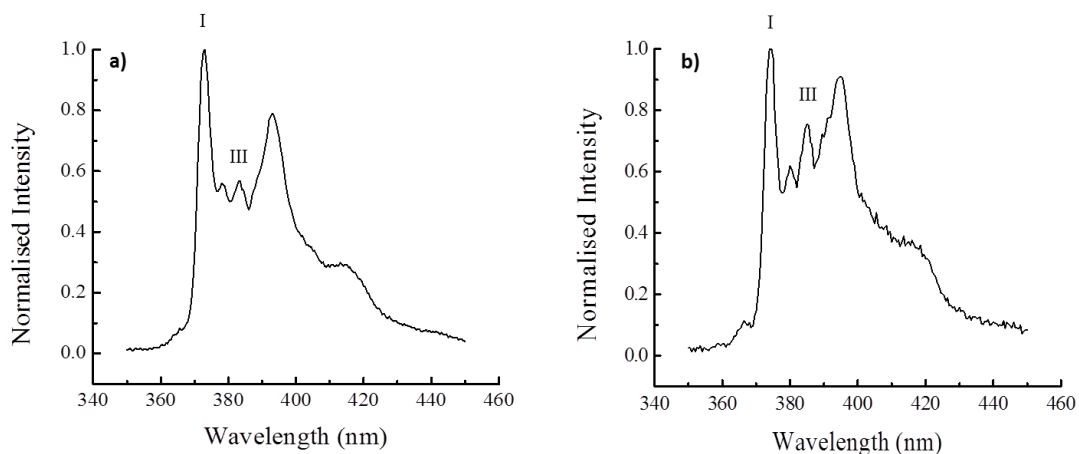


Figure 5.3 Pyrene monomer fluorescence spectra in aqueous BAC solutions, at BAC concentration a) below CMC, b) above CMC.

For the surfactants BAC, DDQ and BAC/DDQ (2:3 mol:mol), the peak ratios (III/I) were plotted as a function of surfactant concentration to determine the CMC (Figure 5.4). The midway point of the sharp increase in peak ratio was determined as the CMC for the surfactants.

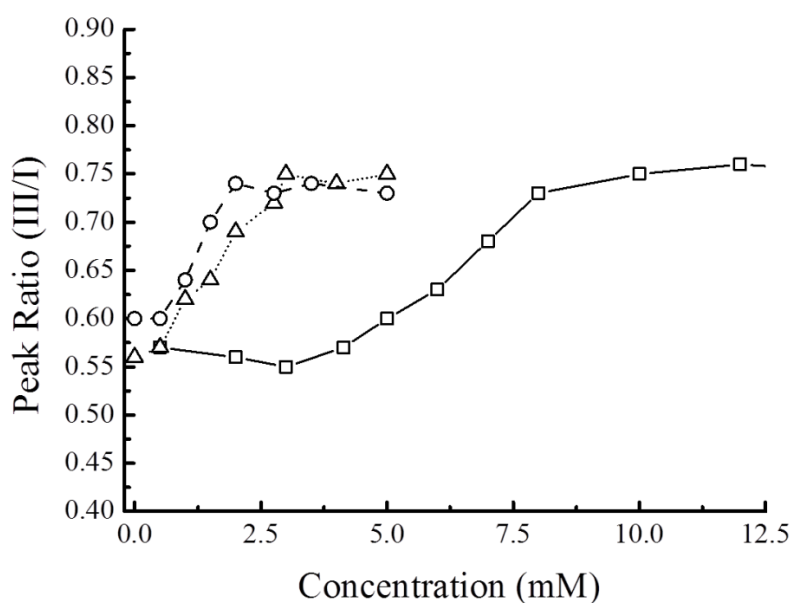


Figure 5.4 Variation in the ratio of peaks III and I as a function of surfactant concentration (\square) BAC, (O) DDQ, and (Δ) BAC/DDQ (2:3 mol:mol).

The CMC values for BAC, DDQ and the BAC/DDQ (2:3 mol:mol) mixture are reported in Table 5.3.

Table 5.3 Surfactant CMCs determined via pyrene method.

| Surfactant | CMC (mM) |
|---------------|----------|
| BAC | 6.6 |
| DDQ | 1.2 |
| BAC/DDQ (2:3) | 1.6 |

5.1.4 Isothermal Titration Calorimetry (ITC)

The final technique used to determine the surfactant CMCs was isothermal titration calorimetry (ITC). A concentrated solution of surfactant was injected into a vessel containing only the solvent water numerous times. After each injection the change in enthalpy (ΔH) was measured. ΔH is the net value of associative (endothermic) and dissociative (exothermic) events within the solution.⁷ A detailed explanation of the principles of ITC can be found in the instrumentation chapter (Section 2.2).

For the case of surfactants, when the vessel concentration is below the CMC, the concentrated surfactant solution containing micelles dissociates upon dilution, causing an overall exothermic response. When the vessel concentration reaches the CMC a dramatic endothermic response is observed which signifies the onset of micellisation as the surfactant unimers begin associating together.

Thermodynamic profiles of BAC, DDQ and BAC/DDQ (2:3 mol:mol) surfactants were measured and can be viewed in Figure 5.5.

The midway point of the sharp endothermic increase was taken as the CMC for the surfactants. For BAC, the start of the endothermic increase was more subtle so the midway point between 4 mM and 11 mM was identified as the CMC.

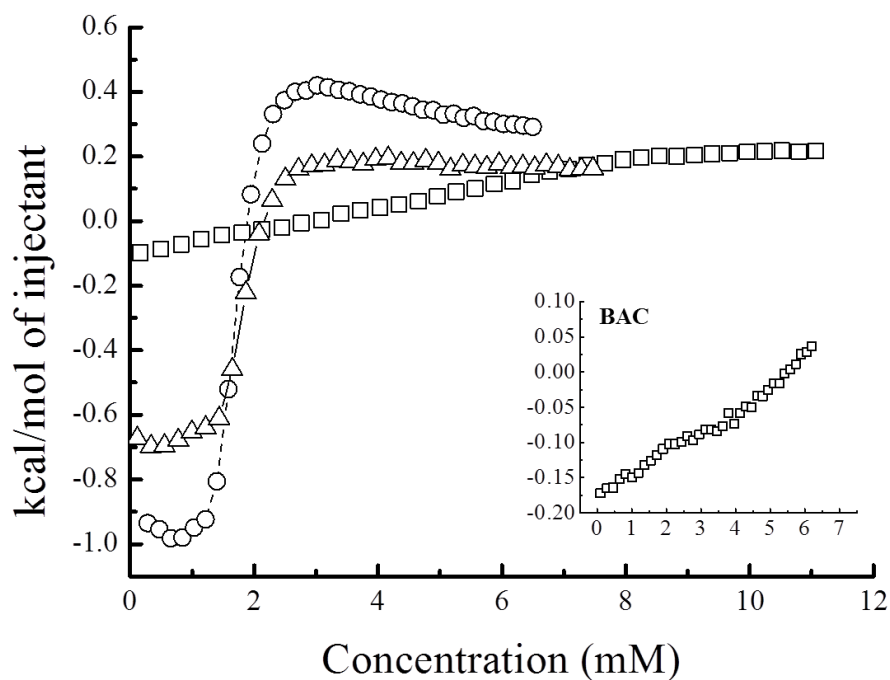


Figure 5.5 ITC Thermodynamic profile of aqueous surfactant solutions as a function of concentration (\square) BAC, (\circ) DDQ, and (Δ) BAC/DDQ (2:3 mol:mol) at 25 °C. Inset of BAC at low surfactant concentration.

The CMCs for all the surfactants determined via the ITC thermodynamic profiles are reported in Table 5.4.

Table 5.4 Surfactant CMCs determined via ITC.

| Surfactant | CMC (mM) |
|---------------|----------|
| BAC | 6.1 |
| DDQ | 1.6 |
| BAC/DDQ (2:3) | 1.9 |

5.1.5 Photon Correlation Spectroscopy (PCS)

The various analytical techniques described previously have identified the critical micelle concentration (CMC) of the respective surfactant as well as the area of the surfactant headgroup and dissociation constant of the micelles. The next analytical technique employed is photon correlation spectroscopy (PCS). PCS enables the determination of micelle size and an indication of geometry.

A detailed explanation of PCS can be viewed in the Instrumentation chapter (Section 8.3). For the purpose of this section, PCS calculates the diffusion coefficient then using the Einstein Stokes equation (Equation 5.4) the hydrodynamic radius of the micelle is determined.^{3, 8} To obtain the size distribution deconvolution of the autocorrelation function is conducted using a CONTIN program.⁹

$$R_H = \frac{kT}{6\pi\eta D} \quad (5.4)$$

Where; R_H =Hydrodynamic radius (m), k = Boltzmann constant (J/K), T = Absolute temperature, η =Viscosity of solution (N.s/m²), D = Diffusion coefficient. (m²/s).

The Einstein Stokes equation is only valid at infinite dilution. The equation does not account for interparticle interactions within the solution. The effect of interparticle interactions on the diffusion coefficient is illustrated in Figure 5.6. Figure 5.6 assumes that within the concentration regime studied micelle size does not change significantly.

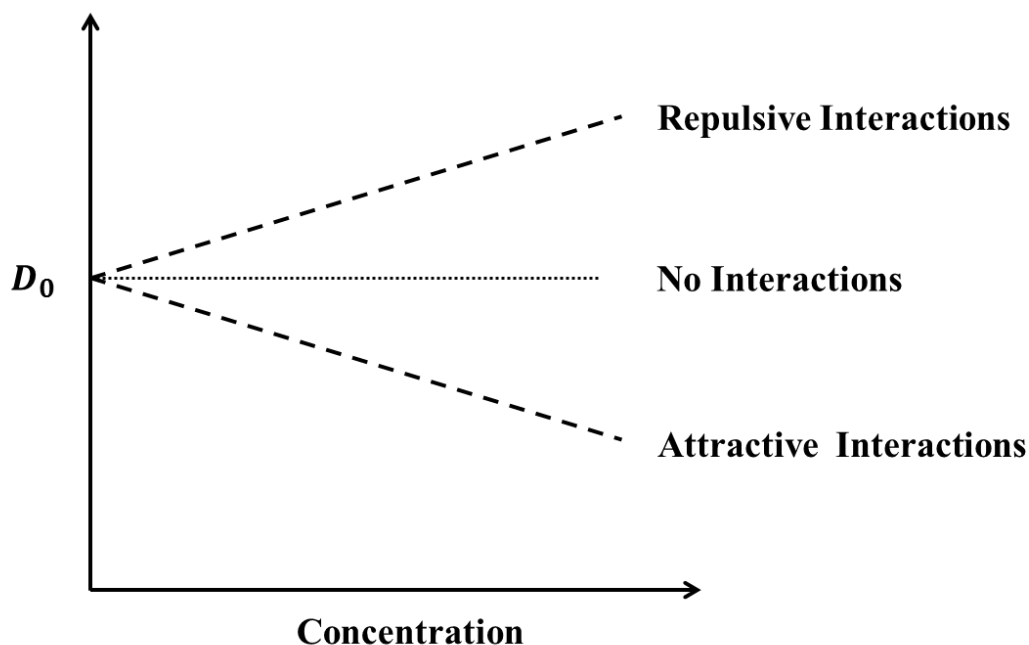


Figure 5.6 Schematic diagram illustrating the determination of the micellar diffusion coefficient at infinite dilution. D_0 = Diffusion coefficient at infinite dilution. Hydrodynamic effects excluded.

In the case of ionic micelles it is believed that the presence of the counter ion dissociating and associating with the micelles causes the increase in the measured diffusion coefficient not related to hydrodynamic size. To compensate, an appropriate amount of electrolyte can be added which suppresses this effect. In this case the chloride ion is more tightly held next to the cationic site thus reducing its ability to affect the diffusion coefficient.⁸

An initial experiment found the respective surfactant cloud points at 100 mM (Table 5.5). The cloud point is defined as the NaCl concentration which the solution becomes turbid and subsequently phase separates. It was observed that DDQ has a very low tolerance to NaCl compared to BAC.

Table 5.5 Cloud points of surfactants (100 mM) upon addition of NaCl.

| Surfactant | NaCl (M) |
|---------------|----------|
| BAC | 1.10 |
| DDQ | 0.04 |
| BAC/DDQ (2:3) | 0.20 |

Within the literature a standard method for determining micellar size is to measure the diffusion coefficient as a function of surfactant concentration but at a constant NaCl concentration. This is repeated until a NaCl concentration is found where the diffusion coefficient is independent of concentration (Figure 5.6).⁸ This has been previously determined for BAC micelles by J. Rodriguez *et al.*¹⁰ who determined the hydrodynamic diameters to be, $C_{12} = 3.6$ nm and $C_{14} = 4.2$ nm.

It was decided that this method was not suitable for this study because of DDQs low tolerance toward NaCl. Instead a NaCl concentration for each respective surfactant was chosen well below the determined cloud points. For the case of BAC and the BAC/DDQ mixture, a NaCl concentration of 0.3 and 0.05 M respectively was chosen approximately a factor of four below the cloud point. For DDQ, because of its low tolerance towards NaCl, a concentration of 5×10^{-3} M was chosen; a factor of eight below the cloud point. A range of concentrations above the CMC was studied up to 100 mM. The PCS intensity profiles can be viewed in Figure 5.7.

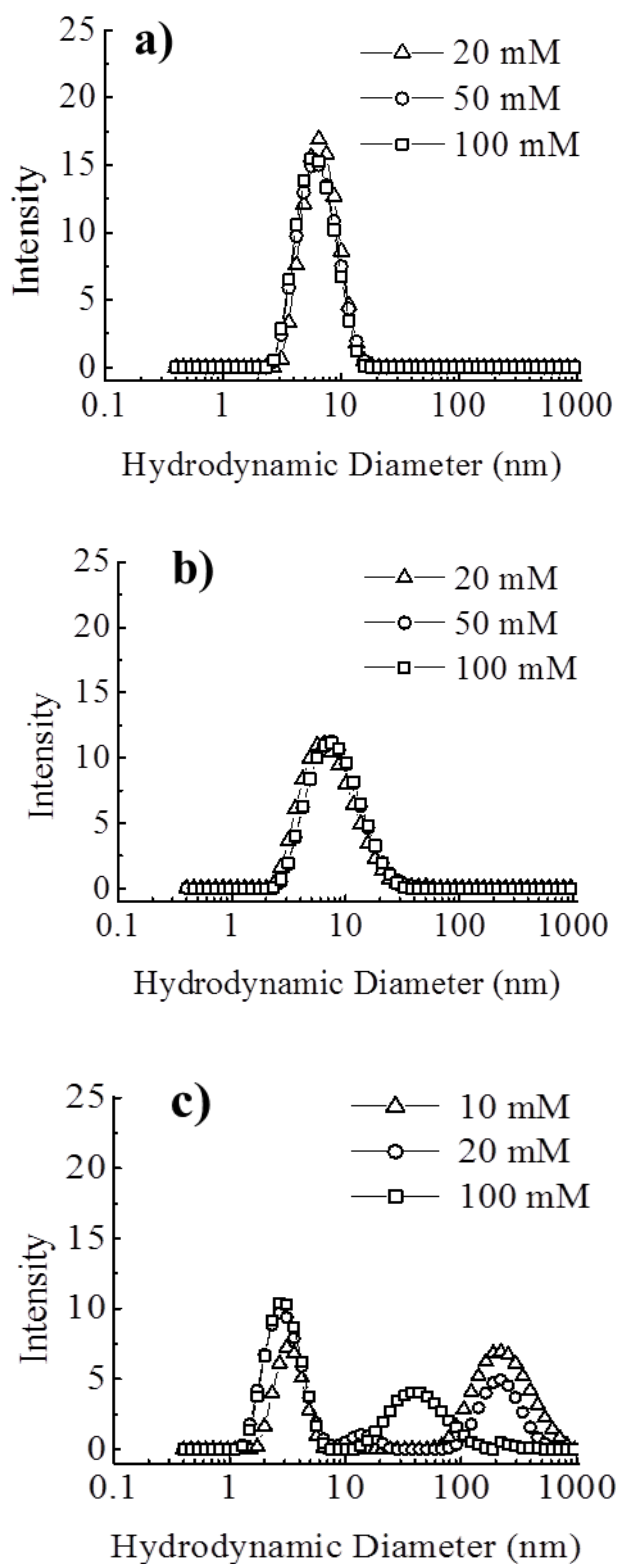


Figure 5.7 PCS intensity profiles at 25 °C as a function of concentration of (a) BAC (0.3 M NaCl) (b) BAC/DDQ 2:3 mol:mol (0.05 M NaCl) and (c) DDQ (5×10^{-3} M NaCl).

The tabulated hydrodynamic diameter for each of the respective surfactants is reported in Table 5.6.

Table 5.6 Tabulated PCS Hydrodynamic diameter of the respective surfactants

| Surfactant Concentration (mM) | Intensity – Hydrodynamic Diameter (nm) | | |
|----------------------------------|--|---------|-------------------------------|
| | BAC | BAC/DDQ | DDQ |
| 10 | N/A | N/A | (1) 3.3 (2) 235.0 |
| 20 | 7.8 | 8.0 | (1) 3.1 (2) 13.0 (3) 263.4 |
| 50 | 6.8 | 9.2 | N/A |
| 100 | 7.1 | 9.1 | (1) 3.1 (2) 48.1 |

For a spherical monodisperse system a monomodal distribution is normally observed hence the hydrodynamic diameter is determined.⁸

The PCS profiles of BAC (Figure 5.7a) show a monomodal distribution over the concentration range of interest. By calculating the length of the extended tail (C_{14}) and multiplying by two the maximum micelle diameter for a BAC spherical micelle was calculated to be 3.9 nm. The hydrodynamic diameter from PCS is approximately double this value suggesting an ellipsoidal geometry. The PCS profiles of BAC/DDQ 2:3 mol:mol (Figure 5.7b) also show a monomodal distribution but at a slighter higher hydrodynamic diameter, suggesting the presence of DDQ causes an elongation of the micelle to a more cylindrical like geometry.

The PCS profiles of DDQ (Figure 5.7c) shows multimodal distributions at 10, 20 and 100 mM. The PCS calculates the average diffusion coefficient hence for a spherical monodisperse system when the diffusion coefficient is deconvoluted to obtain a size distribution (CONTIN program) one peak should appear. The presence of multiple

peaks suggests either you have a very polydisperse mixture of different sizes or the shape of the particles/micelles divergences greatly from a spherical geometry such as a worm like geometry. Elongated geometries undergo translational and rotational diffusion motion. The fact that these multimodal distributions were observed for DDQ suggests one or both of these scenarios exist for this surfactant. Assignment of individual structures to specific peaks would be entirely speculative so will not be attempted.

To give context to our findings within the literature Rauwel *et al.*¹¹ conducted a Diffusion-Ordered Spectroscopy (DOSY) experiment in D₂O which observed a decrease in the diffusion coefficient between the concentrations 10-200 mM. Using the Einstein-Stokes equation an increase in the average hydrodynamic diameter of 3.4-6.0 nm was shown. The study suggested that the decrease in diffusion coefficient is due to the formation of vesicles in equilibrium with micelles. Additionally Lianos *et al.*¹² observed an increase in aggregation number of DDQ micelles from 20 to 86 when increasing concentration from 10 to 81 mM.

5.1.6 Discussion of Micelle Characteristics

The critical micelle concentration (CMC) of the respective surfactants have been determined via a wide range of analytical methods. The CMCs have been tabulated for comparison and an average value has been calculated (Table 5.7).

Table 5.7 Summary of determined CMCs.

| Surfactant | CMC (mM) | | | | |
|------------|-------------|--------------|--------|-----|-----------|
| | Tensiometry | Conductivity | Pyrene | ITC | Average |
| BAC | 3.5 | 4.8 | 6.6 | 6.1 | 5.3 ± 0.7 |
| DDQ | 1.4 | 3.0 | 1.2 | 1.6 | 1.8 ± 0.4 |
| BAC/DDQ | 1.9 | 3.9 | 1.6 | 1.9 | 2.3 ± 0.5 |

As reported in Table 5.7, a range of CMC values for the surfactants would be expected as they measure different physical properties.¹ For the case of the surfactant BAC the large difference in the CMCs can be attributed to a number of factors. Firstly in the case of the surface tensiometry (Figure 5.1) a characteristic minimum is observed around the inflection point. This is generally attributed to amphiphilic impurities within the sample such as long chain alcohols. This minimum makes accurate extrapolation in determination of the CMC more difficult. Secondly as observed in Pyrene (Figure 5.4) and ITC (Figure 5.5), profiles the micellisation of BAC occurs over a wide range of concentration especially when compared to DDQ.

The average experimental CMC values were compared against literature values in Table 5.8. For the case of the BAC/DDQ (2:3 mol:mol) the experimental values were compared with the Clint equation (Equation 5.5).²

$$\frac{1}{CMC} = \frac{X_1}{CMC_1} + \frac{1 - X_1}{CMC_2} \quad (5.5)$$

Where; CMC_1 = CMC of surfactant one, CMC_2 = CMC of surfactant two and X_1 = Mole fraction of surfactant one.

The Clint equation assumes that the CMC of the surfactant mixture will be an average of the single surfactants CMCs contained within the mixture. Any deviations indicate interactions are taking place between the different surfactant headgroups. As reported in Table 5.8 the calculated and experimentally obtained CMC values for the BAC/DDQ (2:3 mol:mol) mixture are within experimental error.

Table 5.8 Comparison of experimental CMC to literature values.

| Surfactant | Average CMC (mM) | Literature CMC (mM) |
|------------|------------------|--|
| BAC | 5.3 ± 0.7 | $C_{12} - 8.1,^{13} 8.8^{10}$ $C_{14} - 1.9,^{14} 2.0^{10}$ |
| DDQ | 1.8 ± 0.4 | $1.2,^{11} 1.9^{12}$ |
| BAC/DDQ | 2.3 ± 0.5 | 1.9 (Clint Eqn 5.5) |

Additional information regarding micelle characteristics including maximum headgroup area (Table 5.1) and dissociation constant (Table 5.2) were calculated. The maximum headgroup area was calculated from the tensiometry profiles (Figure 5.1) using the Langmuir adsorption equation (Equation 5.1). A significant contribution to this area would be the ionic repulsion between the headgroups. Structural factors can also contribute to the headgroup size. In the case of BAC the phenyl orientates itself next to the quaternary ammonium head group instead of inside the micellar interior thus creating a more bulky head group,^{15, 16} A schematic diagram of the BAC micelle structure is shown in Figure 5.8.

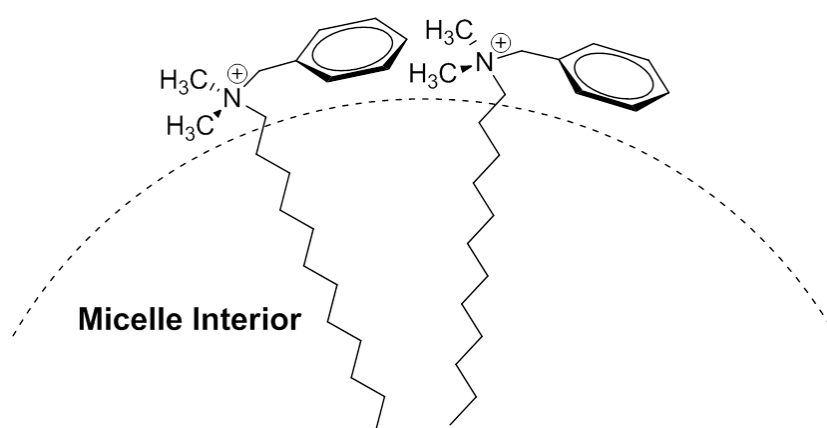


Figure 5.8 Schematic diagram of the proposed micellar headgroup structure of BAC with the phenyl group close to the quaternary ammonium headgroup.

For DDQ the two decyl tails of the surfactant cause greater tail packing,¹⁷ constraining the surfactants ability to adsorb efficiently at the air-water interface or its micellar structure. BAC was reported (Table 5.1) to have a slightly bigger headgroup size compared to DDQ.

Using the conductivity profile, Frahms model (Equation 5.3) was employed to calculate an estimate of the surfactants dissociation constant. It was determined that DDQ has a larger dissociation constant compared to BAC. This result was unexpected as you would have expected the surfactant with the larger headgroup size (BAC) to have a larger dissociation constant due to less ionic repulsion between the headgroups.

As a consequence this was fully investigated. Firstly a comparison was made with the surfactant cloud point experiment (Table 5.5) where the concentration of surfactant was kept constant and different concentrations of NaCl were added until the solution became turbid and subsequently phase separates. Upon the addition of NaCl the aggregation number of the micelles would be expected to increase due to the ionic atmosphere around the headgroup decreasing in size. At a critical NaCl concentration the surfactant solution phase separates. It would be expected that the surfactant with the lowest initial dissociation constant (BAC) would phase separate at a lower concentration compared to a surfactant with a higher initial dissociation constant (DDQ), this was not the case.

The PCS intensity profile (Figure 5.7) for DDQ was reported to show a multimodal distribution at concentration 10-100 mM indicating either a cylindrical geometry or a mixture of micelles and vesicles. We account for DDQ favouring a cylindrical or vesicle geometry due to the fact that DDQ has a lipid like structure which has a strong desire for its twin tails to inter digitate. In comparison BACs intensity profile was reported to show a monomodal distribution with the hydrodynamic diameter suggesting an ellipsoidal geometry. The BAC/DDQ (2:3) mixture also showed a

monomodal distribution but at a slightly larger hydrodynamic diameter suggesting a more elongated geometry compared to BAC.

It has been noted previously within the literature that the degree of counter ion dissociation within a micellar structure is smaller for cylindrical micelles compared to spherical micelles. The reasoning behind this is that the distance between the surfactant head groups is larger within a spherical geometry compared to a cylindrical geometry.¹⁷⁻¹⁹

Using the learnings from PCS the validity of the dissociation constant calculated from Frahm's model can be questioned. The Frahm model presumes that the inflection point within the conductivity profile is solely due to the difference in dissociation constant between the unimer and micellar form. For the case of DDQ a significant change in either micelle geometry and/or size is likely for the concentration range used in the conductivity profile. These changes in the micellar properties are not accounted for in the model.

To conclude, the surfactant headgroup size, cloud point and PCS results all suggest that the DDQ micelles should have a lower dissociation constant compared to BAC. This is in contrary to the reported dissociation constant calculated via Frahm's model.

5.2 Concentrated Polyelectrolyte-Surfactant Mixtures

Due to their commercial importance in cosmetics, detergents, pharmaceutical and biotechnological applications²⁰⁻²⁴, many aqueous polymer/surfactant solutions, at fixed temperature, have been shown to undergo phase separation at a given concentration.

Phase separation can be categorised into two general types; segregative and associative. Segregative phase separation is when the solute composition is extremely asymmetric between the two phases. In the case when two polymers are

present within the solution it is referred to as polymer incompatibility. This type of phase separation is driven when the interactions between the two solutes are repulsive and/or the solutes differ in solubility towards the solvent. The second type of phase separation is referred to as associative phase separation and is when one phase is concentrated in both solutes/polymers while the other phase essentially contains only solvent. For the case of polymer mixtures this is referred to as complex coacervation.²⁵

The area of like charged polyelectrolyte – surfactant mixtures has only been scantily reviewed.²⁵⁻³³ A number of studies have reported segregative phase separation within these systems (anionic and cationic) with a polyelectrolyte rich bottom phase and a surfactant rich top phase.^{25, 30-33} It was observed by Thalberg and Lindman³³ that for the system sodium hyaluronate/sodium dodecyl sulfate the water did not distribute evenly between the two phases. This was also observed by Kalwarczyk *et al.*³⁰ who studied the systems; Poly(sodium-4-styrenesulfonate)/sodium dodecyl sulfate and pDADMAC/cetyltrimethylammonium bromide. The distribution of water between the phases was explained by the need to maintain chemical potential neutrality of water between the two phases. However while this explains the final equilibrium state it fails to explain what initially triggers the phase separation within these mixtures.

A number of studies observed that the addition of NaCl to these types of systems decreases compatibility between the solutes with phase separation occurring at much lower concentrations.^{25, 32, 33}

Nilsson *et al.*^{31, 32} looked at the effect of hydrophobic cosolutes and observed that the addition of octane increases the compatibility of these types of mixtures whilst in comparison, octanol decreases the compatibility. This behavior was justified as a micelle aggregation number effect. In a mixture of two macromolecular molecules, if the molecular weight is increased the concentration range in which they are miscible reduces hence promoting phase separation. In this specific case a change to the micelle aggregation number/molecular weight was believed to occur upon the addition of these hydrophobic cosolutes. Long chain alcohols are known to induce

micellar growth thus promoting rod like aggregates while alkanes are known to reduce the micelle aggregation number and promote a rod to spherical transformation, although the reason behind these micellar transformations do not seem to be fully understood yet.^{31, 32, 34-36}

This study will consider in detail systems containing surfactants and polyelectrolytes of similar charge, particularly formulations of quaternary ammonium chloride polyelectrolytes and surfactants.

5.2.1 pDADMAC Systems

5.2.1.1 pDADMAC (8.5 kDa)/DDQ/Water Mixture

This system was observed to phase separate so a phase diagram was constructed to identify the phase boundary between non-phase separating and phase separating mixtures (Figure 5.9a).

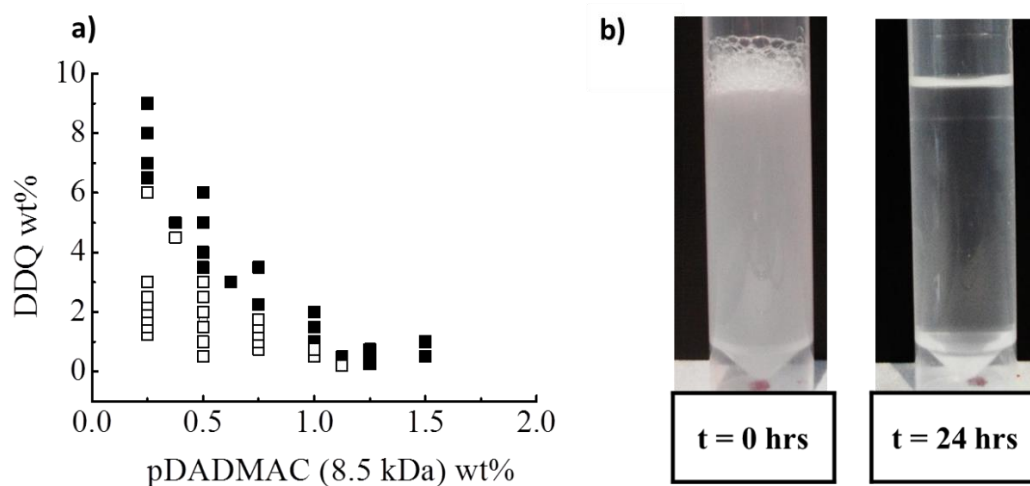


Figure 5.9 (a) Phase Separation boundary for pDADMAC (8.5 kDa)/DDQ/water at 25 °C; (□) one phase, (■) two phase. (b) Phase separation image for sample pDADMAC (3 wt%)/DDQ (3 wt%)/water (t = time since last agitation).

^1H NMR of both phases confirmed that segregative phase separation takes place with a top surfactant phase and a bottom polyelectrolyte phase. The overlapped spectra of both phases can be viewed in Figure 5.10.

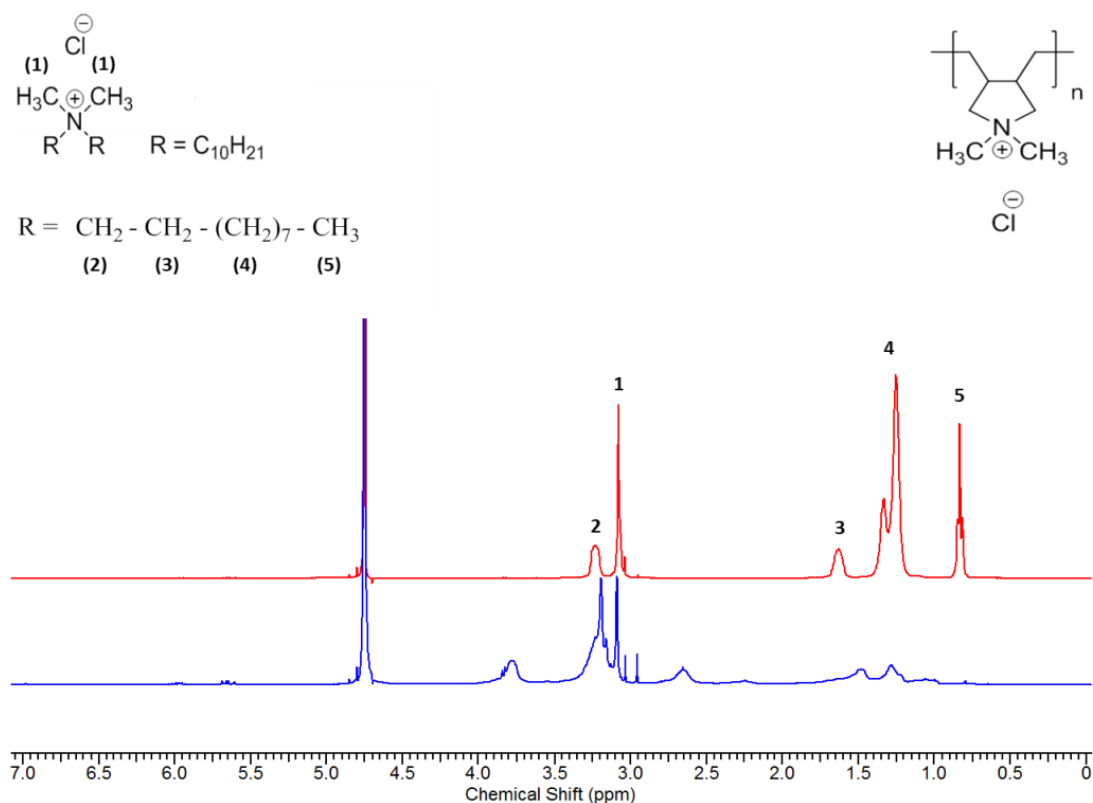


Figure 5.10 ^1H NMR of the top phase and the bottom phase for the sample pDADMAC 8.5 kDa (3 wt%)/DDQ (3 wt%)/water sample, 24 hours since last agitation. (red) top phase (DDQ), (Blue) bottom phase (pDADMAC).

Aliquots from the top (DDQ) and bottom (pDADMAC) phases were taken from a pDADMAC 3 wt%/DDQ 3 wt%/water sample (Figure 5.9b) which was placed into a separating funnel. Aliquots were taken 24 hours from last agitation. Gravimetric analysis of both phases (Table 5.9) indicated a concentrated top phase and a more dilute bottom phase. The volume of each phase was measured prior to gravimetric analysis so that a predicted wt% could be calculated which assumed complete phase separation occurred between the two phases.

Table 5.9 Gravimetric analysis of top and bottom layer of pDADMAC 8.5 kDa (3 wt%)/DDQ (3 wt%)/water, 24 hours after last agitation.

| Layer | Volume (mL) (± 0.05) | Predicted (wt%) | Actual (wt%) |
|--------|-------------------------------|-----------------|----------------|
| Top | 0.60 | 24.0 ± 2.0 | 22.7 ± 0.1 |
| Bottom | 4.40 | 3.3 ± 0.1 | 4.4 ± 0.1 |

The actual wt% of each phase obtained from gravimetric analysis was compared to the predicted wt%. The predicted and actual wt% is in close agreement although not statistically comparable. As such the terms surfactant rich and polyelectrolyte rich layers will be used to describe different phases.

5.2.1.2 A Range of pDADMAC / Surfactant/Water Mixtures

To explore a range of different pDADMAC systems the concentration where the phase separation boundary occurs was determined. To illustrate where this two phase region occurs Figure 5.11 plots only the single phase samples closest to the phase boundary hence indicating where the two phase region begins. Samples at a higher concentration than those plotted phase separate into two phases.

The effect of pDADMAC molecular weight (Figure 5.11a) and surfactant type (Figure 5.11b) were studied. The pDADMAC/BAC/water system was confirmed as a segregative phase separation process via ^1H NMR and can be viewed in Appendix 5A.

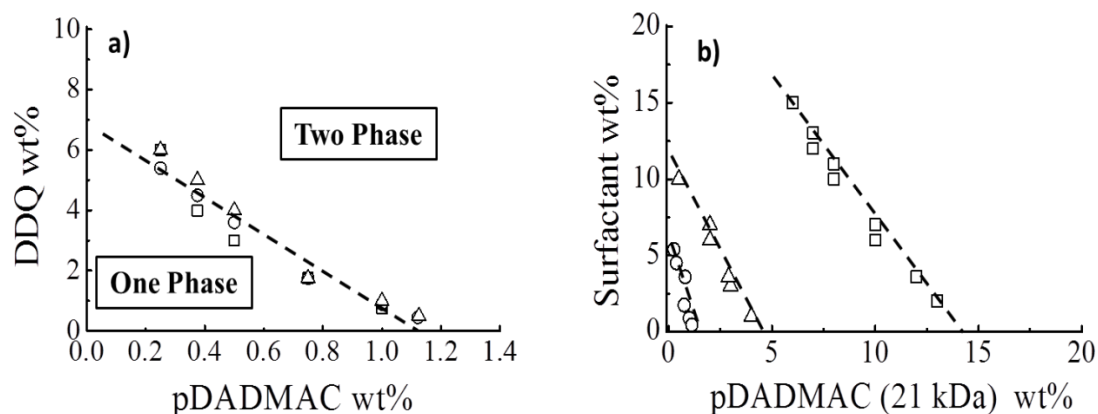


Figure 5.11 Phase separation boundary (a) pDADMAC/DDQ/water as a function of pDADMAC molecular weight; (□) 8.5 kDa, (○) 21 kDa and (Δ) 140 kDa (b) Phase boundary for pDADMAC (21 kDa)/surfactant/water for (○) DDQ, (□) BAC and (Δ) BAC/DDQ (2:3 mass:mass). Dashed line indicates approximate location of phase boundary.

The main conclusions from the phase boundary studies (Figure 5.11);

- The molecular weight of the pDADMAC only has a nominal effect on the phase boundary position (Figure 5.11a).
- Changing surfactant type from DDQ to BAC has a dramatic effect with the phase boundary moving to a region greater than a factor of 10 more concentrated (Figure 5.11b).
- A mixture of BAC/DDQ (2:3 mass:mass) established that the phase separation boundary can be manipulated via changing the BAC/DDQ ratio (Figure 5.11b).

To fully investigate the effect of the surfactant ratio BAC/DDQ on the phase boundary a series of solution were formulated at constant surfactant concentration (100 mM / \approx 3.6 wt%) but differing pDADMAC (21 kDa) concentration. The first

sample within the series to phase separate was identified as the phase separation concentration for that system (Figure 5.12). For comparison the experiment was compared against surfactant/NaCl/water mixtures. These were observed to phase separate and appeared analogous to the phase separation within the surfactant/polyelectrolyte/water systems.

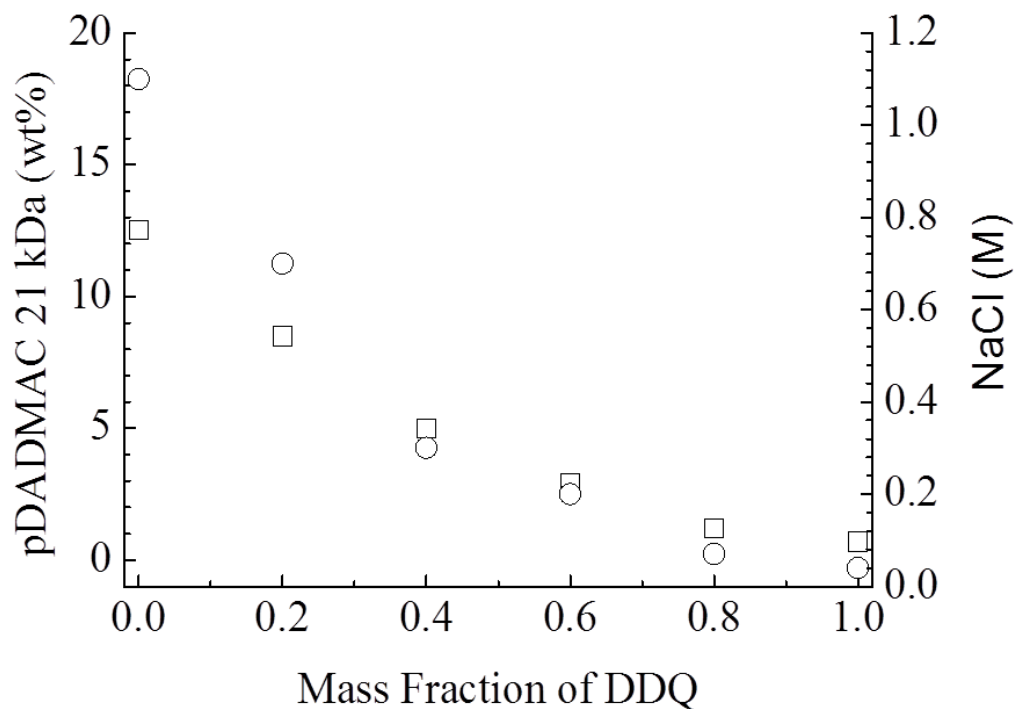


Figure 5.12. Critical phase separation concentration as a function of BAC/DDQ mass ratio. Surfactant (BAC/DDQ) concentration was kept constant (100 mM/ \approx 3.6 wt%), (○) NaCl and (□) pDADMAC (21 kDa).

Figure 5.12 illustrates that the phase boundary can be manipulated quite dramatically by altering the ratio of BAC/DDQ for both the pDADMAC (21 kDa) and NaCl systems.

So a direct comparison could take place between the critical pDADMAC and NaCl phase separating concentrations the number of moles of electrolyte and consequently the number of chloride ions ($N_{CL-Phase\ Separation}$) required for phase separation was

calculated. Figure 5.13 compared the $N_{CL-Phase\ Separation}$ for the pDADMAC and NaCl systems as a function of BAC/DDQ ratio.

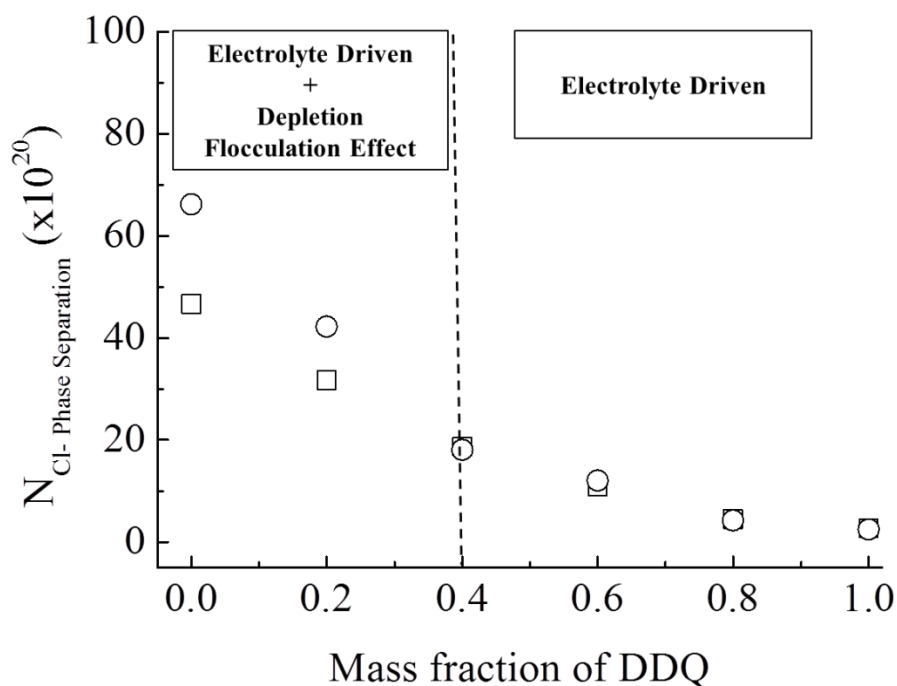


Figure 5.13 Number of chloride ions from electrolyte to induce phase separation ($N_{CL-Phase\ Separation}$) as a function of BAC/DDQ ratio. Surfactant (BAC/DDQ) concentration was kept constant (100 mM/ \approx 3.6 wt%). Electrolyte Type; (\circ) NaCl and (\square) pDADMAC (21 kDa).

We see that for a surfactant or surfactant mixture where the mass fraction of DDQ is greater than 0.4 the ionic strength of the solution reaches a critical concentration, irrespective of whether it is in the form of NaCl or polyelectrolyte, phase separation will occur. This suggests an electrolyte driven mechanism.

We ascribe this electrolyte driving force to the ionic atmosphere around the surfactants quaternary ammonium head group reducing in size resulting in condensing of the counter ion. Upon phase separation the surfactant becomes insoluble in water forming immiscible oil which due to its lower density will cream to the top of the solution and coalesce to form a surfactant rich phase. The surfactant

molecules become soluble within this surfactant rich phase due to the absence/reduction in polyelectrolyte concentration.

From the data presented it is not possible to determine whether the reduced ionic atmosphere around the quaternary nitrogen was enough to induce phase separation on its own or if an actual intimate ion pair is formed. An intimate ion pair is when the charged moiety, in this case the quaternary ammonium group, is in direct contact with its corresponding counter ion subsequently neutralizing the ionic charge. Further investigation is required on this aspect of the mechanism with an ion-selective electrode based method which continuously measures the chloride solution concentration a possible method in determining ion pair formation.

The mixtures containing a larger mass fraction of DDQ require a lower ionic strength to induce phase separation. The different micellar properties of the surfactants DDQ and BAC is believed to be a major factor. It has been noted previously within the literature that the degree of counter ion dissociation within a micellar structure is smaller for cylindrical micelles compared to spherical micelles. The reasoning behind this is that the distance between the surfactant head groups is larger within a spherical geometry compared to a cylindrical geometry.¹⁷⁻¹⁹ PCS results suggest that over the concentration regime and salt concentration studied BAC micelles are ellipsoidal in shape with nominal change in micelle size compared to DDQ which undergoes either spherical to cylindrical or spherical to vesicle geometry transformations. A difference in the micelle counter ion dissociation constant of the two surfactants seems likely to be a major factor in the differing critical ionic strengths required to induce phase separation within the above mixtures.

When the mass fraction of DDQ is less than 0.4 a deviation is observed between NaCl and polyelectrolyte systems, with the polyelectrolyte system inducing phase separation at a lower ionic strength. To further explore this additional effect a range of different molecular weight pDADMAC molecules were studied at certain BAC/DDQ ratios. The critical phase separation concentration was identified and subsequently the $N_{CL-Phase\ Separation}$ was calculated (Table 5.10).

Table 5.10 The number of chloride ions (N_{Cl-}) added into the mixtures from the electrolyte to induce phase separation. Surfactants were studied at constant concentration (100 mM / \approx 3.6 wt%). BAC/DDQ ratio = (2:3 mass:mass).

| Surfactant Type | Electrolyte Type | Wt% of polyelectrolyte | $N_{Cl-Phase Separation}$ ($\times 10^{20}$) |
|-----------------|--------------------------------|------------------------|--|
| DDQ | NaCl | 0.04 M | 2.4 |
| DDQ | pDADMAC (8.5 kDa) | 0.7 | 2.6 |
| DDQ | pDADMAC (21 kDa) | 0.7 | 2.6 |
| DDQ | pDADMAC (140 kDa) | 0.6 | 2.2 |
| BAC/DDQ | NaCl | 0.20 M | 12 |
| BAC/DDQ | pDADMAC (8.5 kDa) | 3 | 11 |
| BAC/DDQ | pDADMAC (21 kDa) | 2.9 | 11 |
| BAC/DDQ | pDADMAC (140 kDa) | 2.2 | 8 |
| BAC/DDQ | pDADMAC (140 kDa) ^a | 2.5 | 9 |
| BAC | NaCl | 1.1 M | 66 |
| BAC | pDADMAC (21 kDa) | 12.5 | 47 |
| BAC | pDADMAC (140 kDa) | 10 | 37 |

^a Dialysed against water to remove low molecular weight impurities.

As reported in Table 5.10 the higher the molecular weight of pDADMAC the lower $N_{CL-Phase Separation}$ for each respective surfactant mixture. This effect is more pronounced the lower the DDQ mass fraction within the mixture. We speculate this trend is explained as an additional depletion flocculation effect.

In the case of non-absorbing colloid mixtures entropic depletion interactions have been known to induce phase separation. Entropic depletion interactions results from changes in the conformational entropy of the polymer chains which prevents polymers from getting too close to a micelle. Geometric constraints prevent the centre mass of the polymer coil from getting closer than a certain distance to the micelle. This distance is approximately;

$$2(\alpha + R_G) \quad (5.6)$$

Where; α = radius of the micelle and R_G = radius of gyration of the polymer.

As a result of this, when two micelles are close enough together to prevent the polyelectrolyte from separating them the region between the micelles is said to be depleted of polymer. The polyelectrolyte outside the depletion zone between micelles induces an osmotic pressure pushing micelles together and encouraging phase separation within the solution mixture.^{3, 30, 37} A schematic illustrating of depletion flocculation is shown in Figure 5.14.

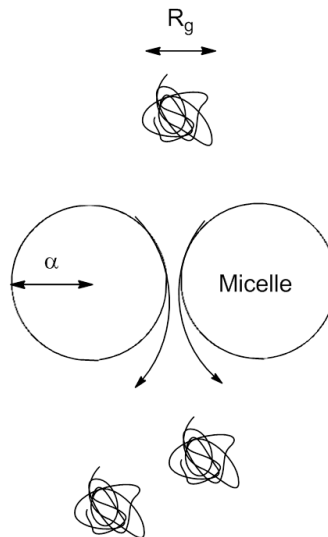


Figure 5.14 Schematic diagram illustrating entropic depletion flocculation.

A number of studies have shown that in colloid-polymer mixtures of like charge and low salinity an enhanced depletion interaction was observed at much lower concentrations compared to neutral systems. Long-range repulsive electrostatic forces were found to be behind this enhanced depletion interaction, with the Debye length of the solvent reported to be a major factor. It was also noted that at higher electrolyte concentrations the radius of gyration of the polymer became an important factor increasing the range of the depletion force.³⁸⁻⁴¹

For the pDADMAC mixtures studied here the proposed depletion effect is more significant for the mixtures containing a lower mass fraction of DDQ as observed in Figure 5.13. We speculate this is because these mixtures are more concentrated. In more concentrated mixtures a smaller Debye length would be expected but also entropic interactions will become more dominant, increased depletion interactions would be expected. The depletion effect is also more pronounced for the higher molecular weight pDADMACs. This result was further investigated with the pDADMAC 140 kDa dialysed against water to remove any possible low molecular weight impurities and gave comparable results for the BAC/DDQ (2:3 mass:mass) surfactant mixture (Table 5.10). The molecular weight dependence is likely to do with the increase in the radius of gyration (R_G) of the polyelectrolyte which has been proposed to increase the range of the depletion interactions.

5.2.2 PHMB Systems

The polyelectrolyte Poly(hexamethylene biguanide) chloride (PHMB) was studied to see how the proposed mechanisms can be generalised across polyelectrolyte types. The critical phase separation concentration was identified and subsequently the $N_{CL-Phase\ Separation}$ was calculated (Table 5.11).

Table 5.11 Tabulated results showing the number of chloride ions (N_{Cl-}) added into the (PHMB) mixtures by the electrolyte to induce phase separation. DDQ, BAC and a BAC/DDQ (2:3 mass:mass) surfactant were studied. (100 mM / \approx 3.6 wt%).

| Surfactant Type | Electrolyte Type | Wt% of polyelectrolyte | $N_{Cl-Phase Separation}$ ($\times 10^{20}$) |
|-----------------|------------------|------------------------|--|
| DDQ | NaCl | 0.04 M | 2.4 |
| DDQ | PHMB | 0.9 | 2.4 |
| BAC/DDQ | NaCl | 0.2 M | 12 |
| BAC/DDQ | PHMB | N/A | > 47 |
| BAC | NaCl | 1.1 M | 66 |
| BAC | PHMB | N/A | > 47 |

The DDQ/PHMB/water mixtures phase separate at the expected $N_{CL-Phase Separation}$ suggesting that the counter ion condensing mechanism is valid for this system. For the systems containing the surfactant mixtures BAC/DDQ (2:3 mass:mass) and BAC phase separation was not observed. The highest PHMB concentration formulated was 18 wt%.

PHMB is structurally a very different polyelectrolyte compared to pDADMAC as explained in detail in Chapter 4. In summary the ionic charges of PHMB are delocalised around the biguanide groups and are at a distance greater than the Bjerrum length of the solvent (water). This gives PHMB amphiphilic character as between these ionic charges is hydrophobic hexamethylene groups. In comparison the ionic charges within pDADMAC are at a distance less than the Bjerrum length of the solution (water) thus pDADMAC has an overwhelming ionic hydrophilic character, not amphiphilic. In these types of mixtures the Bjerrum length of the solvent would be much lower than DI water but this would be expected to further enhance PHMBs amphiphilic character.

We speculate that BAC which has a phenyl group around the quaternary ammonium headgroup (Figure 5.8) may interact with the hydrophobic regions of PHMB inhibiting the phase separation process. Further work is required to confirm this hypothesis.

5.3 Conclusion

Within this chapter we propose a segregative phase separation mechanism for like charged quaternary ammonium polyelectrolyte/surfactant/water mixtures. This type of segregative phase separation is induced by a reduction in the thickness of the ionic atmosphere around the quaternary nitrogen and chloride counter ion of the ionic surfactant. The nature of surfactant type is dominant in determining the onset of phase separation. By tuning the BAC/DDQ ratio the phase separation point can be controlled. An additional depletion flocculation effect was identified for surfactant mixtures containing a lower mass fraction of DDQ. This effect was more pronounced for higher molecular weight pDADMACs. Finally a comparison between pDADMAC and PHMB mixtures was made. While DDQ/PHMB/Water mixtures appeared to follow the same counter ion condensing mechanism the BAC containing mixtures failed to phase separate. We speculate a BAC/PHMB hydrophobic/hydrophobic interaction inhibits phase separation in these mixtures.

5.4 References

1. M. J. Rosen, *Surfactants and Interfacial Phenomena*, John Wiley & Sons Inc, New York, 1978.
2. L. Jonosson, Holmberg, Kronberg, *Surfactants and Polymers in Aqueous Solution*, Wiley, New York, 1998.

3. R. Hunter, *Foundations in Colloid Science*, 2nd Edition, Oxford University Press, 2001.
4. P. Atkins and J. Paulo, *Elements of Physical Chemistry*, 4th Edition, Oxford University Press, Oxford, 2005.
5. J. Frahm, S. Diekmann and A. Haase, *Ber Bunsen Phys Chem*, 1980, **84**, 566-571.
6. K. Kalyanasundaram and J. K. Thomas, *JACS*, 1977, **99**, 2039-2044.
7. R. Ghai, R. J. Falconer and B. M. Collins, *J. Mol. Recogn.*, 2012, **25**, 32-52.
8. R. Finsy, *Adv. Colloid Interface Sci*, 1994, **52**, 79-143.
9. S. W. Provencher, *Comput. Phys. Commun*, 1982, **27**, 229-242.
10. J. R. Rodriguez and J. Czapkiewicz, *Colloids Surf. A*, 1995, **101**, 107-111.
11. G. Rauwel, L. Leclercq, J. Criquelion, J.-M. Aubry and V. Nardello-Rataj, *J. Colloid Interface Sci.*, 2012, **374**, 176-186.
12. P. Lianos, J. Lang and R. Zana, *J. Colloid Interface Sci.*, 1983, **91**, 276-279.
13. J. A. Cella, D. N. Eggenberger, D. R. Noel, L. A. Harriman and H. J. Harwood, *JACS*, 1952, **74**, 2061-2062.
14. L. P. Panicheva, A. E. Boldeskul, Z. N. Markina and I. E. Boldeskul, *Colloid. J. USSR.*, 1982, **44**, 448-453.
15. L. T. Okano, O. A. ElSeoud and T. K. Halstead, *Colloid Polym. Sci.*, 1997, **275**, 138-145.
16. R. McNeil and J. K. Thomas, *J. Colloid Interface Sci.*, 1981, **83**, 57-65.
17. R. Nagarajan, *Langmuir*, 2002, **18**, 31-38.
18. J. N. Israelachvili, D. J. Mitchell and B. W. Ninham, *J. Chem. Soc., Faraday Trans*, 1976, **72**, 1525-1568.
19. E. Ruckenstein and J. A. Beunen, *Langmuir*, 1988, **4**, 77-90.
20. C. P. Oliveira, M. Ribeiro, N. Ricardo, T. V. D. Souza, C. L. Moura, C. Chaibundit, S. G. Yeates, K. Nixon and D. Attwood, *Int. J. Pharm.*, 2011, **421**, 252-257.
21. N. Ricardo, F. Costa, F. W. A. Bezerra, C. Chaibundit, D. Hermida-Merino, B. W. Greenland, S. Burattini, I. W. Hamley, S. K. Nixon and S. G. Yeates, *J. Colloid Interface Sci.*, 2012, **368**, 336-341.
22. E. D. Goddard, *Colloids Surf*, 1986, **19**, 255-300.
23. E. D. Goddard, *Colloids Surf*, 1986, **19**, 301-329.

24. P. Hansson and B. Lindman, *Curr. Opin. Colloid Interface Sci.*, 1996, **1**, 604-613.
25. L. Piculell and B. Lindman, *Adv. Colloid Interface Sci.*, 1992, **41**, 149-178.
26. H. Comas-Rojas, E. Aluicio-Sarduy, S. Rodriguez-Calvo, A. Perez-Gramatges, S. J. Roser and K. J. Edler, *Soft Matter*, 2007, **3**, 747-753.
27. L. Bromberg, M. Temchenko and R. H. Colby, *Langmuir*, 2000, **16**, 2609-2614.
28. R. H. Colby, N. Plucktaveesak and L. Bromberg, *Langmuir*, 2001, **17**, 2937-2941.
29. E. M. Kosacheva, D. B. Kudryavtsev, R. F. Bakeeva, A. I. Kuklin, A. K. Islamov, L. A. Kudryavtseva, V. F. Sopin and A. I. Konovalov, *Colloid J*, 2006, **68**, 713-720.
30. E. Kalwarczyk, M. Golos, R. Holyst and M. Fialkowski, *J. Colloid Interface Sci.*, 2010, **342**, 93-102.
31. S. Nilsson, A. M. Blokhus, S. Hellebust and W. R. Glomm, *Langmuir*, 2002, **18**, 6504-6506.
32. S. Nilsson, A. M. Blokhus and A. Saure, *Langmuir*, 1998, **14**, 6082-6085.
33. K. Thalberg and B. Lindman, *Colloids Surf. A*, 1993, **76**, 283-288.
34. P. Flory, *Principles of Polymer Chemistry*, Cornell University Print, London, 1953.
35. O. Bayer, H. Hoffmann, W. Ulbricht and H. Thurn, *Adv. Colloid Interface Sci.*, 1986, **26**, 177-203.
36. H. Hoffmann and W. Ulbricht, *J. Colloid Interface Sci.*, 1989, **129**, 388-405.
37. S. Asakura and F. Oosawa, *J. Chem. Phys.*, 1954, **22**, 1255-1256.
38. M. Pelaez-Fernandez, A. Moncho-Jorda and J. Callejas-Fernandez, *J. Chem. Phys.*, 2011, **134**, 054905-1-054905-9.
39. L. Belloni and P. G. Ferreira, *Trans. R. Soc. Lond. Ser. A Math. Phys. Eng. Sci*, 2001, **359**, 867-877.
40. S. Buzzaccaro, R. Piazza, J. Colombo and A. Parola, *J. Chem. Phys.*, 2010, **132**, 124902-1-124902-15.
41. J. Y. Walz and A. Sharma, *J. Colloid Interface Sci.*, 1994, **168**, 485-496.

Chapter 6 – Surface Patterning

Surface Patterning

This chapter aims to describe how different film topographies can be formed using aqueous mixtures of surfactant and polyelectrolytes of similar charge. A single sessile drop will be left to evaporate on a substrate.

6.1 Introduction

The previous chapter on polymer/surfactant mixtures (Chapter 5) described the segregative phase separation behaviour of both pDADMAC and PHMB systems in combination with QAC surfactants at a given concentration. Figure 6.1 illustrates how the phase separation boundary can be manipulated in the pDADMAC + QAC surfactant system depending on surfactant mixture.

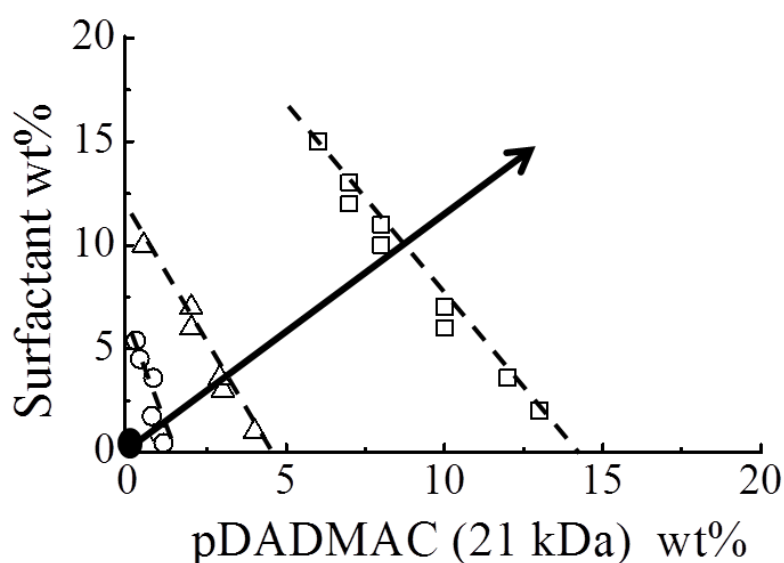


Figure 6.1 Phase boundary between one and two phase solutions, pDADMAC (21 kDa)/surfactant/water, (o) DDQ, (\square) BAC and (Δ) BAC/DDQ (2:3 mass:mass). Dashed line indicates approximate location of phase boundary.

Antimicrobial formulations typically consist of < 0.2 wt% active (QACs) therefore it is interesting to consider the drying behaviour of such solutions onto a surface in context of Figure 6.1.

A single drop of a dilute formulation represented as a black circle in Figure 6.1 was placed onto a glass substrate and left to evaporate in controlled environmental conditions. At some point during drying depending on formulation the critical phase separation concentration will be reached. The resulting films were subsequently analysed using optical microscopy and Non-Contact Atomic Force Microscopy (NC-AFM).

6.1.1 Evaporation of a Sessile Drop

It is important to understand the processes occurring within a drying sessile drop. The drop shape is controlled by the bond number (Equation 6.1) which accounts for the balance between surface tension and gravitational forces on the drop surface.¹

$$B_o = \frac{\rho g R h_0}{\sigma} \quad (6.1)$$

Where B_o = Bond number, ρ = Density of solvent (g/L), g = Gravitational Constant (m/s), R = Drop base radius (m), h_0 = Height of drop (m) and σ = Surface tension (N/m).

A bond number (B_o) < 1 indicates the drop shape is dependent on surface tension forces thus adopts a spherical cap geometry.

The physical properties of a sessile drop such as drop base diameter, three phase contact angle and drop volume all change during drop evaporation.

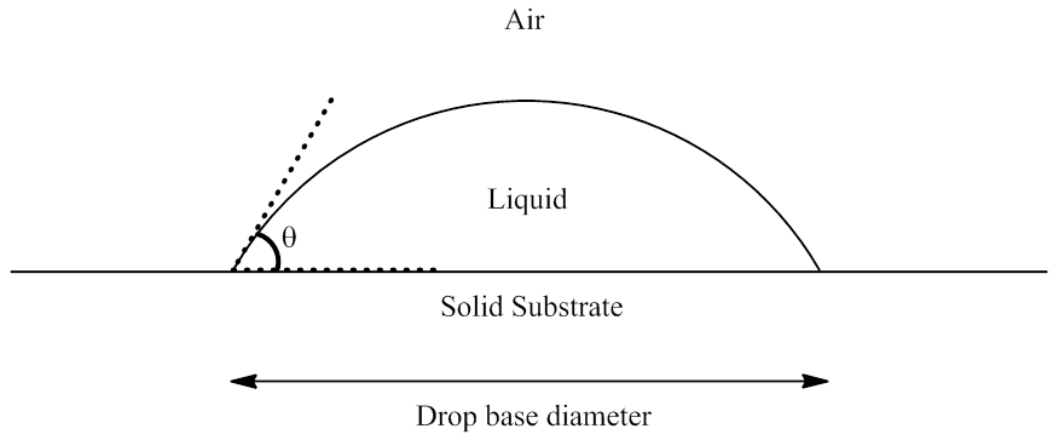


Figure 6.2 Schematic diagram of a Sessile drop. θ = Three phase contact angle.

Evaporation of sessile drops normally goes through two stages when $\theta < 90^\circ$.¹⁻⁴

1. Pinning of three phase contact line - the diameter of the drop base remains constant while the contact angle of the drop reduces
2. De-pinning of three phase contact line - the drop base diameter reduces until complete evaporation

The duration of each stage is dependent on the physio-chemical properties of the drop and the surface. For the case of water drops on clean glass, it was reported that the pinning mode accounted for 90-95% of drop volume.¹

6.1.2 Coffee Staining

When a sessile drop dries, a so called coffee ring effect is observed with a build-up of material dispersed toward the edge of the drying drop. This behaviour is due to capillary flow within the drying drop which was first explained by Deegan *et al.*⁵

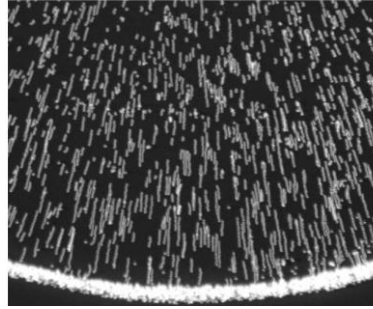


Figure 6.3 Coffee stain effect - Spheres within an evaporating drop.⁵

When a drop dries instead of shrinking in size straight away the contact line of the drop is pinned. Evaporation occurs preferentially at the three phase contact line compared to the drop centre due to differences in the evaporation flux along the drop surface. Evaporation flux is the comparison of the rate of evaporation in one area of a drop compared to an alternative area. The water which has evaporated away from the edge of the drop is replaced by water from the interior of the drop.⁵ The preferential evaporation at the drop edge is also believed to induce Marangoni flows. Marangoni effects are induced by a surface tension gradient along the air-water interface. If these flows are strong enough within the drop they can cause a redistribution of the material towards the centre of the drop.⁶ The Marangoni flows within a drying drop are illustrated in Figure 6.4, the direction/strength of the flows are system specific.

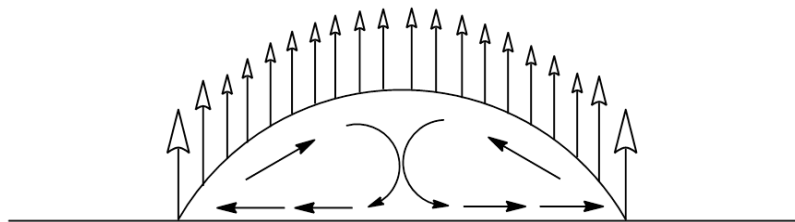


Figure 6.4 Schematic Diagram of a pinned sessile drying drop, Open arrows illustrates evaporation flux, Closed arrows indicates Marangoni flows within drop.

Eventually when there is not enough water left within the interior the drop base diameter begins to shrink until all the water evaporates away.

In an attempt to distort/manipulate the coffee ring effect the following factors have been studied within a range of colloidal dispersions; particle shape, addition of a surfactant, differing solvent combinations and altering of the ionic strength. All of these factors have been observed to alter the coffee ring staining effect in some way.⁷⁻¹²

This chapter will be the first to explore the effect of phase separation between like charged species within a sessile drop and its resulting film topography.

6.2 Dilute Polymer/Surfactant/Water Sessile Drops

The evaporation of a 20 μL sessile drop at constant temperature (30 $^{\circ}\text{C}$) and humidity (24 %) was conducted for a range of different pDADMAC (21 kDa)/surfactant/water formulations. The temperature and humidity were kept constant so drying conditions could be tightly controlled. A clean glass substrate was used. A 20 μL volume was chosen so that a larger surface area would be covered by the drop and subsequent analysis of film structure would be more pronounced and easier to analyse. Details of the formulations studied are presented in Table 6.1.

Table 6.1 Concentration and surface tension of formulations.
All solutions pH 5-6. BAC/DDQ ratio = 2:3 mass:mass.

| Surfactant Type | Surfactant (wt%) | pDADMAC (21 kDa) (wt%) | Surface Tension (mN/m \pm 0.1) |
|-----------------|---------------------|---------------------------|-------------------------------------|
| BAC | 0.1 | 0.1 | 35.6 |
| BAC/DDQ | 0.1 | 0.1 | 29.6 |
| DDQ | 0.1 | 0.1 | 28.4 |
| None | 0.0 | 0.1 | 72.3 |

The CMCs of the surfactants in the presence of 0.1 wt% pDADMAC was determined via tensiometry (Appendix 6-A) and reported in Table 6.2.

Table 6.2 CMC determination in the presence of 0.1 wt% pDADMAC (21 kDa) via surface tensiometry. RT = 25 °C.

| Surfactant Type | CMC (mM) | CMC (wt%) |
|-----------------|----------|-----------|
| BAC | 2.5 | 0.09 |
| BAC/DDQ (2:3) | 1.5 | 0.05 |
| DDQ | 1.3 | 0.05 |

All the surfactant containing formulations reported in Table 6.1 were found to be above their respective CMC. The CMC values were observed to be lower than the corresponding CMC values calculated in Millipore filtered water (Table 5.1). We believe that the increased electrolyte concentration within the solution due to the presence of pDADMAC (21 kDa) reduces the ionic atmosphere around the surfactant headgroup hence reducing headgroup repulsion which promotes micellisation.

6.2.1 Drying Drop Studies

Using the different formulations reported in Table 6.1 the three phase contact angle and drop base diameter of each sessile drop were measured as a function of time until camera resolution prevented the measurements from being recorded accurately. Each formulation was measured multiple times, however the DDQ containing formulation proved experimentally difficult to measure due to the lower initial contact angle making it harder for the camera to detect the sessile drop.

The formulations were slowly pumped onto the substrate then the needle was pulled out of the drop and through the air-water interface. For the first 50 seconds the drops underwent equilibration until the thermodynamically favoured geometry for the drop was achieved. During this process the drop base diameter increased while the three

phase contact angle decreased sharply. Figure 6.5 shows just one repeat of each formulation of which is best representative of the observed drying behaviours. The 0.1 wt% pDADMAC and water only solutions could not be appropriately measured as the initial contact angle was $< 15^\circ$ and subsequently the camera had insufficient resolution to accurately record the evaporating drop.

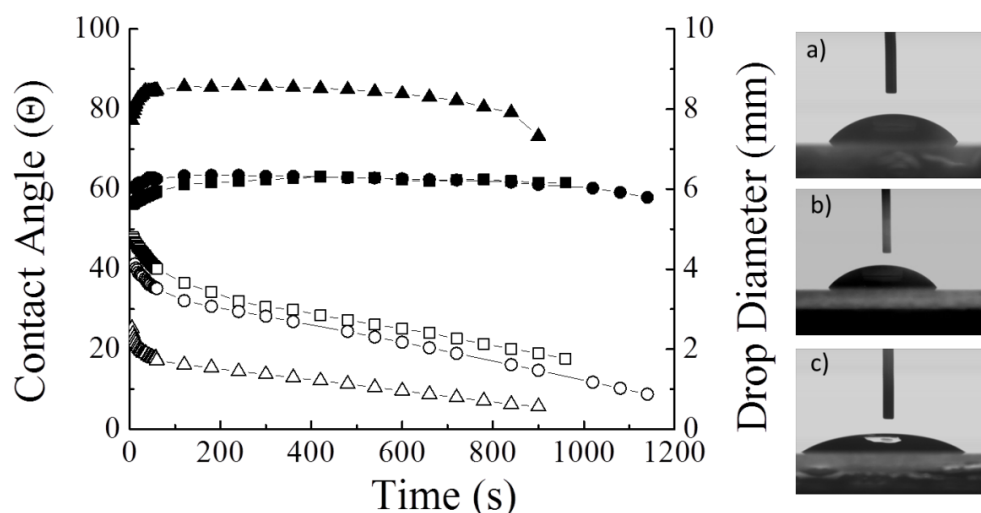


Figure 6.5 Contact angle and diameter of a drying drop as a function of time. 20 μL drop of a 0.1 wt% Surfactant + 0.1 wt% pDADMAC (21 kDa) formulation were placed onto a glass substrate. Drying conditions; $30^\circ\text{C} \pm 0.5$, $24\% \pm 0.5$ relative humidity. BAC (\square), BAC/DDQ (2:3) (\circ) and DDQ (\triangle), Open symbols = Contact angle, Closed Symbols = Drop diameter. Photographs of drop $t = 50\text{ s}$ a) BAC, b) BAC/DDQ (2:3), c) DDQ.

Upon equilibration, the three phase contact line became pinned and the contact angle of the drop decreased in a linear fashion for all formulations. The vast majority of the recorded data was in the time region when the three phase contact line was pinned however, the last few data points of each series does indicate a slight decrease in the drop base diameter indicating the three phase contact line unpinning and the drop entering the final stage of drying. The unpinning of the contact line is more pronounced in the DDQ containing mixture data. The initial contact angle of the respective formulations closely correlates with the solutions surface tension (Table 6.1). The lower the surface tension of the solution the lower the subsequent contact angle on glass.

The bond number (Equation 6.1) of the previously measured drops (after 50 seconds) was between 0.98-1.15 indicating that the drops were at the boundary of when gravitational forces affect drop geometry, which can cause a flattening of the spherical cap geometry. For the purpose of this experiment however, spherical cap geometry was assumed and using the determined contact angle and drop base diameter. Equation 6.2 can be used to determine the drop volume of the sessile drop.

$$V_s = \frac{1}{6} \pi \cdot a^3 \tan \frac{\theta}{2} \left(3 + \tan^2 \frac{\theta}{2} \right) \quad (6.2)$$

Where; V_s = Drop Volume, θ = Contact angle and a = Drop base radius

In Figure 6.6 the volume of the evaporating sessile drops were plotted as a function of time.

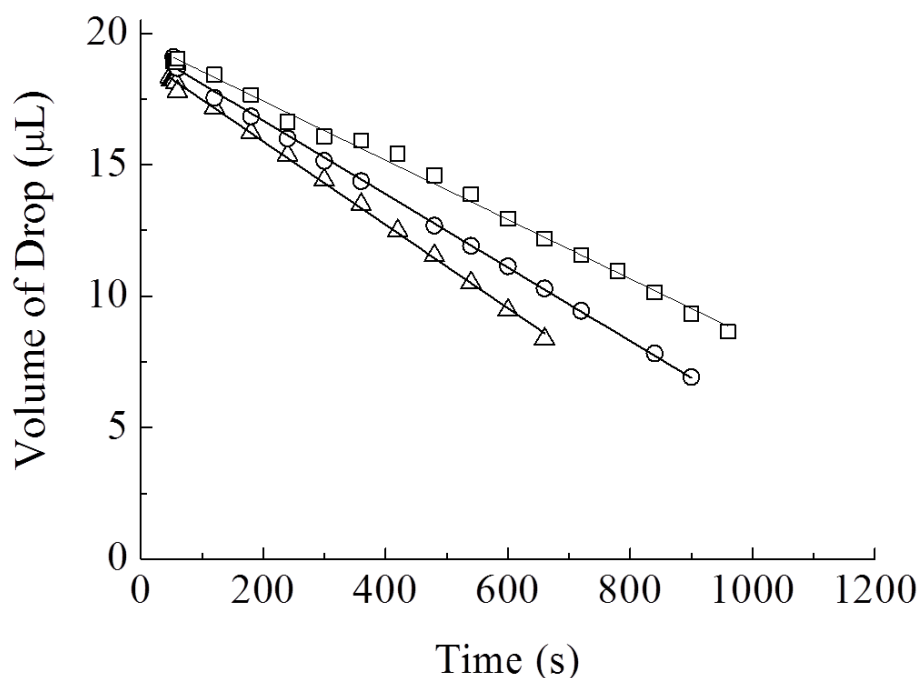


Figure 6.6 Volume of a drying drop as a function of time. 20 μ L drop of a 0.1 wt% surfactant + 0.1 wt% pDADMAC (21 kDa) formulation was placed onto a glass substrate. Drying conditions; 30 $^{\circ}$ C \pm 0.5, 24 % \pm 0.5 relative humidity. BAC (\square), BAC/DDQ (2:3) (\circ) and DDQ (Δ),

For each data series, only the data points where the drop diameter was pinned were plotted. In Figure 6.6 a linear relationship was observed and the subsequent gradient of this trend was calculated and reported in Table 6.3. The gradient of each line gives an estimation of the sessile drops rate of evaporation.

Table 6.3 Rate of evaporation of a 20 μL drop of 0.1 wt% surfactant + 0.1 wt% pDADMAC (21 kDa) formulation placed onto a glass substrate. Drying conditions; 30 $^{\circ}\text{C} \pm 0.5$, 24 % ± 0.5 relative humidity.

| Formulation | Rate of Evaporation ($\mu\text{L/s}$) $\times 10^{-2}$ |
|---------------|---|
| BAC | 1.13 |
| BAC/DDQ (2:3) | 1.40 |
| DDQ | 1.59 |

Since evaporation rate is proportional to the drops surface area, the larger the drop surface area the faster the rate of evaporation. As expected the DDQ containing mixture with its lower contact angle and larger drop base diameter had the fastest rate of evaporation followed by the BAC/DDQ mixture and lastly the pure BAC.

It should be noted that the calculated rate of evaporation is only an estimate and is calculated when the three phase contact line was pinned thus the drop surface area was approximately constant. Extrapolation past the data points would give an over estimation of the rate of evaporation because the three phase contact becomes unpinned hence the surface area of the drop would begin decreasing.

The important observations that can be taken from these drying drop studies are;

- A significant difference in the three phase contact angle between the pDADMAC (21 kDa)/surfactant/water mixtures with DDQ having the lowest contact angle followed by BAC/DDQ and lastly the BAC containing mixture.
- Due to the differences in the contact angle and drop base diameter the DDQ containing sessile drop evaporates faster followed by the BAC/DDQ mixture and finally the BAC sessile drops.

6.2.2 Direct Visualisation of Phase Separation

The previous section looked at the contact angle and drop base diameter of a drying sessile drop. This section aims to view a drying sessile drop using an optical microscope so that the phase separation process of the surfactant and polyelectrolyte can be directly viewed. It should be noted that the drying conditions could not be controlled for this experiment although the ambient temperature and relative humidity was recorded for each experiment. For each sample an image was taken every minute during drying.

A set of surfactant only and pDADMAC (21 kDa) only controls were conducted to confirm that phase separation does not occur within these formulations. A test system is shown below for the BAC system.

The selected optical micrographs for a 0.1 wt% BAC solution is shown in Figure 6.7.

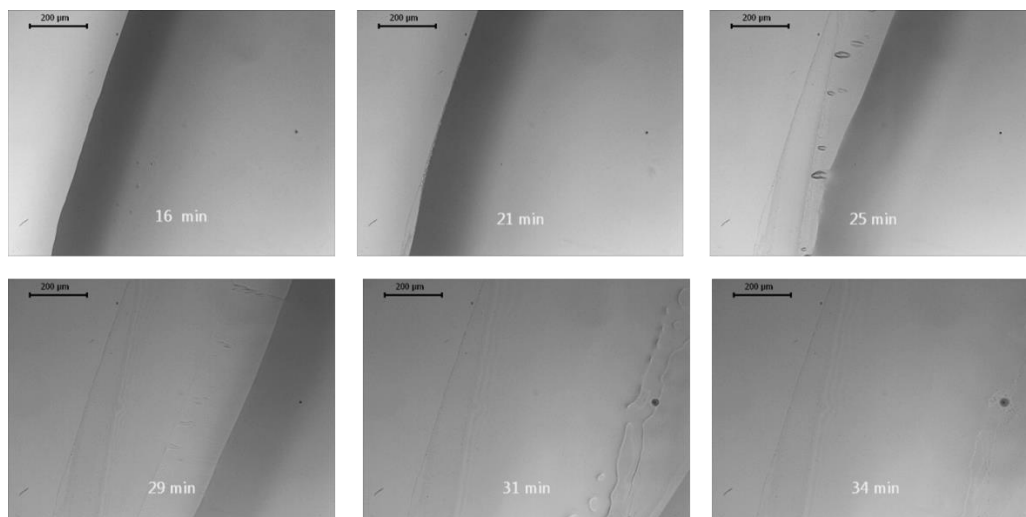


Figure 6.7 Optical micrographs of a drying sessile drop (20 μL) on a glass substrate, 0.1 wt% BAC only, Scale bars = 200 μm , Room Temperature = 22 $^{\circ}\text{C}$. Relative Humidity 20-30%.

The selected optical micrographs for a 0.1 wt% pDADMAC (21 kDa) solution is shown in Figure 6.8.

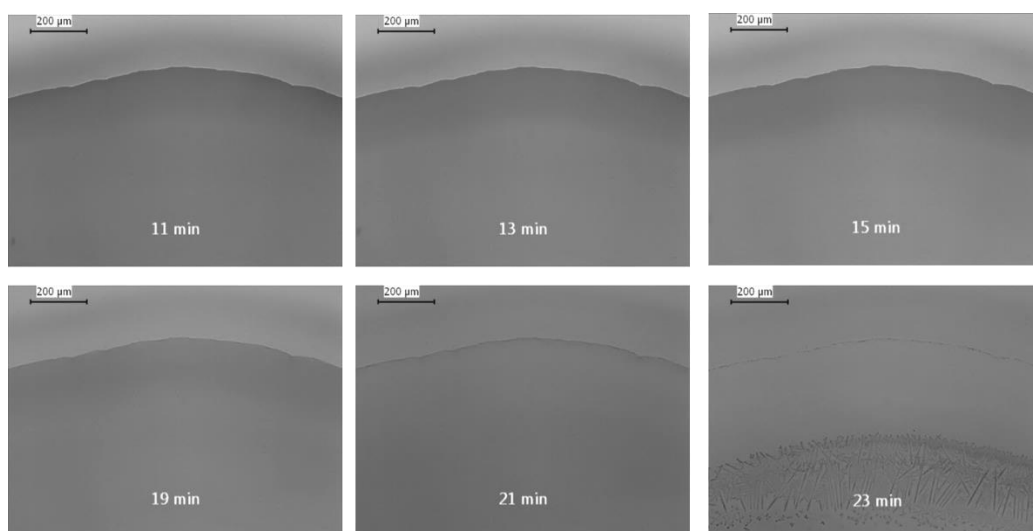


Figure 6.8 Optical micrographs of a drying sessile drop (20 μL) on a glass substrate, 0.1 wt% pDADMAC (21 kDa) only, Scale bars = 200 μm , Room Temperature = 28 $^{\circ}\text{C}$. Relative Humidity 20-30%.

The optical micrographs of both the surfactant only and pDADMAC only solutions were observed not to phase separate during drying. Selected optical micrograph images for the 0.1 wt% BAC/DDQ (2:3 mass:mass) and DDQ surfactant controls can be viewed in Appendix 6-B and 6-C. The BAC/DDQ solution was not observed to phase separate while the DDQ solution did show an indication of phase separation once the three phase contact line had de-pinned and was contracting towards the drop centre (29 minutes). The concentration of the drop would be expected to be very high and the formation of a liquid crystal lamellar phase is a possible cause for this observation.

As described previously in Chapter 5 (Polymer/Surfactant Mixtures) at a critical concentration phase separation occurs within QAC surfactants (BAC, DDQ) and pDADMAC mixtures. This process involves the surfactant removing itself from the polyelectrolyte phase and creaming to the top of the solution and forming its own surfactant rich phase. If phase separation is observed within a sessile drop it is likely that the creation of this surfactant rich phase will be observed.

Selected optical micrographs for the 0.1 wt% BAC + 0.1 wt% pDADMAC mixture is shown in Figure 6.9.

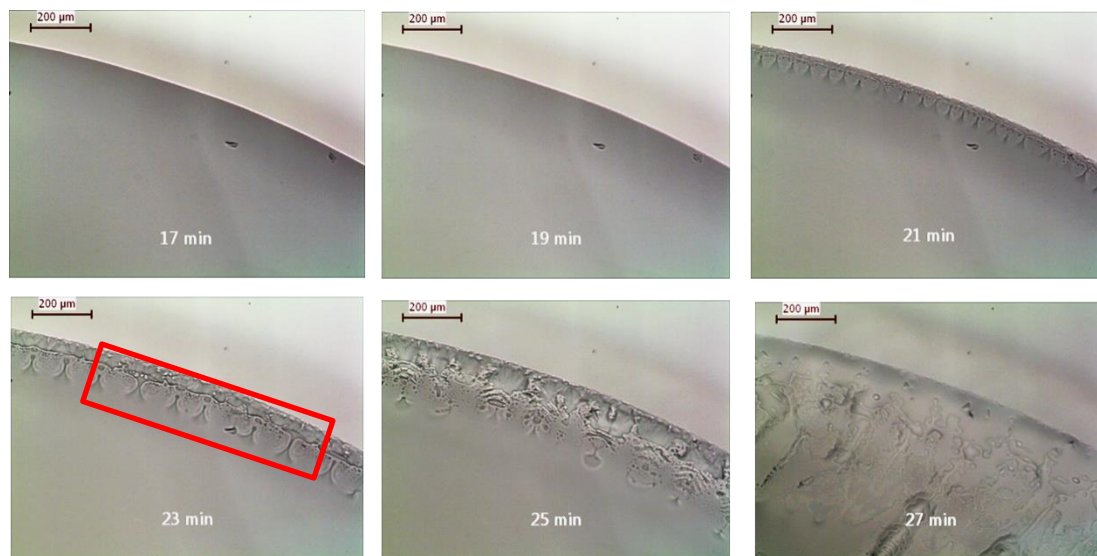


Figure 6.9 Optical micrographs of a drying sessile drop (20 μL) on a glass substrate, 0.1 wt% BAC + 0.1 wt% pDADMAC (21 kDa) , Scale bars = 200 μm , Room Temperature = 28 $^{\circ}\text{C}$. Relative Humidity 20-30%. Red box illustrates phase separation region.

For the BAC containing formulation (Figure 6.9) the phase separating process was observed from 21 minutes onwards. The three phase contact line was still pinned and the phase separation process was observed next to the three phase contact line. The BAC system illustrated that the phase separation process is taking place within the drying drop for QAC pDADMAC/surfactant/water systems.

Next the BAC/DDQ (2:3) and DDQ containing mixtures were studied. The selected optical micrographs for the BAC/DDQ mixture are shown in Figure 6.10.

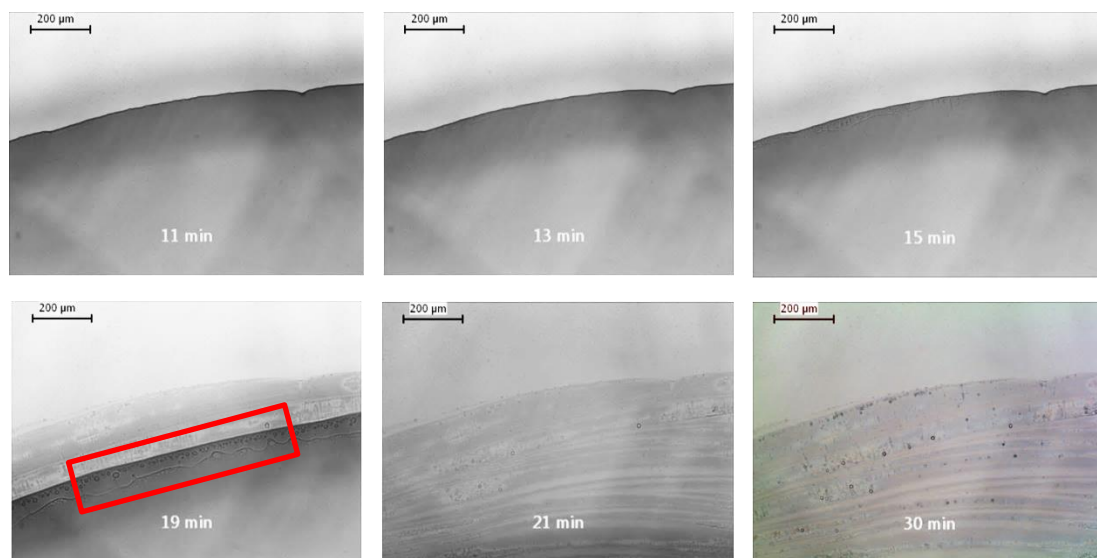


Figure 6.10 Optical micrographs of a drying sessile drop (20 μ L) on a glass substrate, 0.1 wt% BAC/DDQ (2:3) + 0.1 wt% pDADMAC (21 kDa), Scale bars = 200 μ m. Room temperature = 30 $^{\circ}$ C. Relative Humidity 20-30%. Red box illustrates phase separation region.

For the BAC/DDQ containing mixture (Figure 6.10) the phase separating process was observed from 15 minutes onwards and began before the three phase contact line became de-pinned. Phase separation appears to be focused at the three phase contact line. When the three phase contact line de-pinned and contracted inwards the resulting surfactant/polyelectrolyte film appears almost featureless however nodule like structures began appearing within the film from 21 minutes onwards.

The selected optical micrographs for the DDQ containing mixture are shown in Figure 6.11.

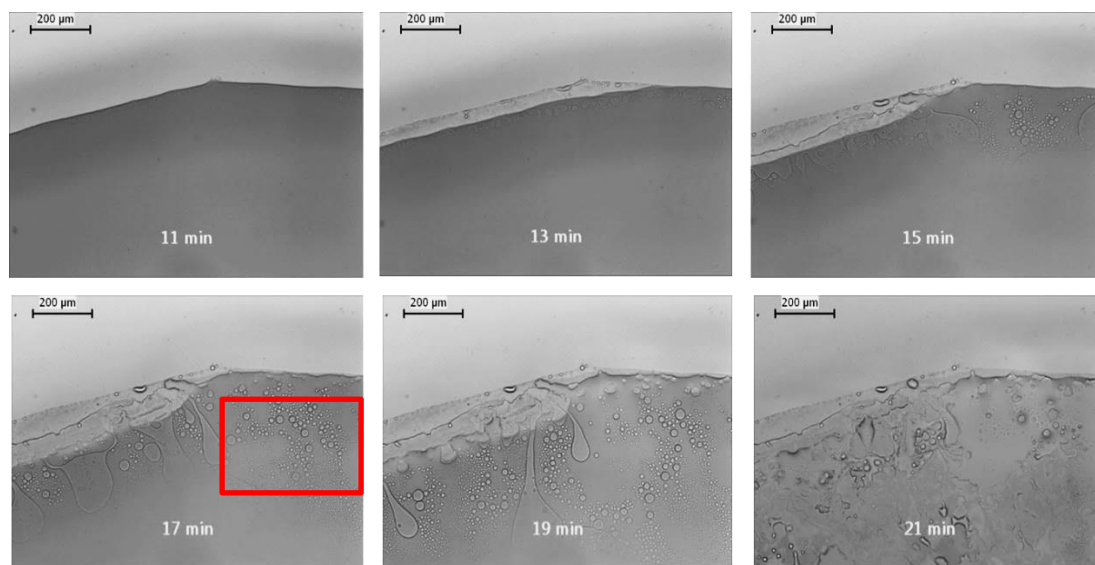


Figure 6.11 Optical micrographs of a drying sessile drop (20 μ L) on a glass substrate, 0.1 wt% DDQ + 0.1 wt% pDADMAC (21 kDa), Scale bars = 200 μ m, Room Temperature = 28 $^{\circ}$ C. Relative Humidity 20-30%. Red box illustrates phase separation region.

For the DDQ containing mixture (Figure 6.11) the phase separation process was observed to occur from 11 minutes onwards. As the phase separating process was observed the three phase contact line also de-pinned. Distinct droplets due to phase separation could be observed over most of the sessile drops surface area which was distinctly different from the BAC and BAC/DDQ containing mixtures.

6.2.3 Calculation of the Critical Phase Separation Concentration

An attempt was made to quantify the approximate concentration phase separation was observed in a drying drop, in relation to its corresponding solution phase separation concentration (Figure 6.1). This is only an approximate value because the environmental conditions were not controlled for the optical micrograph movies. The calculation assumes an even concentration across the whole drop.

Table 6.4 Phase separation concentration within a evaporating drop (20 μ L). Formulations contain; 0.1 wt% surfactant + 0.1 wt% pDADMAC (21 kDa)

| | Drop | Time of | Drop Conc. at | Solution Conc. |
|------------|-------------------|-----------------|---------------|----------------|
| Surfactant | Evaporation | observed Phase | Phase Sep. | at Phase Sep. |
| | Rate (μ L/s) | Separation (s). | (wt%) | (wt%) |
| BAC | 0.0114 | 1260 | 0.35 + 0.35 | 10.0 + 10.0 |
| BAC/DDQ | 0.0140 | 900 | 0.27 + 0.27 | 4.0 + 4.0 |
| DDQ | 0.0159 | 660 | 0.21 + 0.21 | 1.5 + 1.5 |

The active concentrations at phase separation within the drops are a lot lower than the corresponding solution concentrations (Figure 6.1). A build-up of material near the three phase contact line would give a higher localised concentration in this area compared to the drop centre and explains why phase separation was observed in this region for the BAC and BAC/DDQ (2:3) mixtures.

The DDQ mixture was observed to phase separate more evenly across the droplet. It seems likely this is due to the lower solution phase separation concentration and contact angle hence smaller changes in the localised concentration are enough to induce phase separation across the drop.

6.2.4 Summary

The following conclusions can be drawn from these dilute pDADMAC (21 kDa)/surfactant/water sessile drops;

- All solutions were observed to begin phase separating while the three phase contact line was pinned.
- Even though environmental condition were not tightly controlled the DDQ, BAC/DDQ (2:3) and lastly BAC containing mixtures phase separated in the expected order (DDQ > BAC/DDQ > BAC). However the calculated phase

separation concentration within the drop was a lot lower than the corresponding solution concentration. This was believed to be due to localised concentration effects.

- For the BAC and BAC/DDQ (2:3) containing mixtures the phase separation phase (surfactant phase) accumulated near the three phase contact line. In comparison for the DDQ containing mixture distinct droplets (surfactant phase) were observed fairly evenly distributed over the drop surface.

Due to the drying condition not being tightly controlled and the possibility of localised heating from the light source required for imaging, the resulting film structures from this study were not analysed.

6.3 Film Structures of pDADMAC/Surfactant/Water Systems

6.3.1 Controls

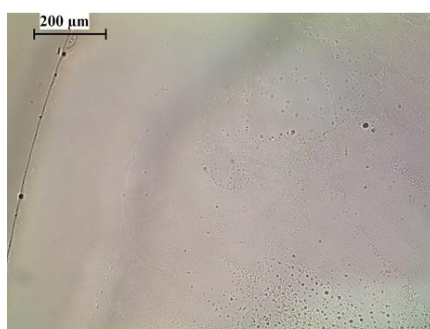
Before looking at more complex mixtures, a set of control surfaces were prepared looking at the film topography of surfactant only (BAC and DDQ) and pDADMAC (21 kDa) only formulations at a concentration of 0.1 wt%. The DDQ (1.4 mM / 0.05 wt%) and BAC/DDQ mixture (1.9 mM / 0.07 wt%) surfactants are above the surfactants CMC while the BAC (3.5 mM/ 0.13 wt%) solution is below its CMC (CMC values determined previously via tensiometry Table 5.1).

The solution properties for these control formulations are reported in Table 6.5.

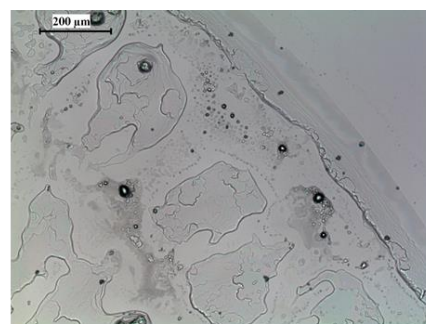
Table 6.5 Solution properties of control formulations. pH of solutions 5 -6, RT= 22-25 °C. Glass Substrate.

| Formulation (0.1 wt%) | Surface Tension (mN/m) ± 0.1 | Equilibrium Contact Angle (θ) ± 1 |
|-----------------------|-------------------------------------|---|
| BAC | 36.4 | 35 |
| BAC/DDQ (2:3) | 29.9 | 34 |
| DDQ | 28.6 | 29 |
| pDADMAC (21kDa) | 72.3 | 15 |

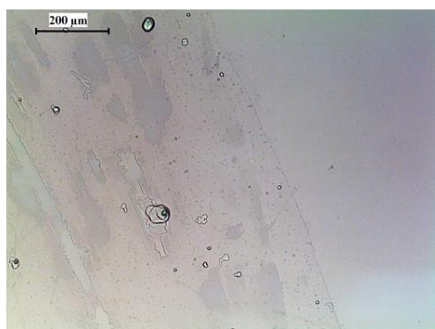
Optical micrographs of the treated glass substrate with the above control formulations are reported in Figure 6.12.



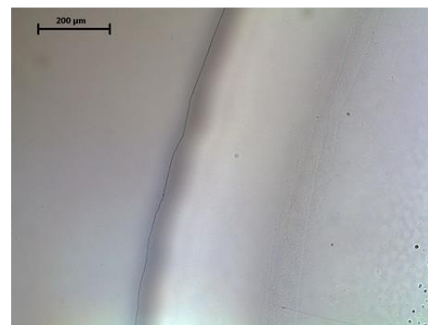
BAC



DDQ



BAC/DDQ (2:3 mass:mass)



pDADMAC (21 kDa)

Figure 6.12 Optical micrographs of glass substrates treated with 20 μ L of 0.1 wt% surfactant or pDADMAC (21 kDa) solution. Scale bars = 200 μ m. Drying conditions; 30 °C, 20-30 % relative humidity, 24 hours drying time.

The surfactant controls were observed to be a film like topography with the occasional spherical structures contained within the film. The pDADMAC control was observed to form an almost featureless film except for some coffee staining effect within the structure.

6.3.2 pDADMAC (21 kDa)/Surfactant/Water Systems

As illustrated in Table 6.4 the phase separation boundary of each formulation is dependent on this surfactant ratio. 20 μ L of each formulation was placed onto a clean glass substrate and left to dry in an incubator chamber enabling the control of temperature (30 $^{\circ}$ C). Relative Humidity could not be controlled but was measured and found to be between 20-30 %.

The initial study looked at three mixture containing 0.1 wt% BAC, BAC/DDQ (2:3 mass:mass) or DDQ surfactant in the presence of 0.1 wt% pDADMAC (21 kDa). The resulting film topographies are shown in Figure 6.13.

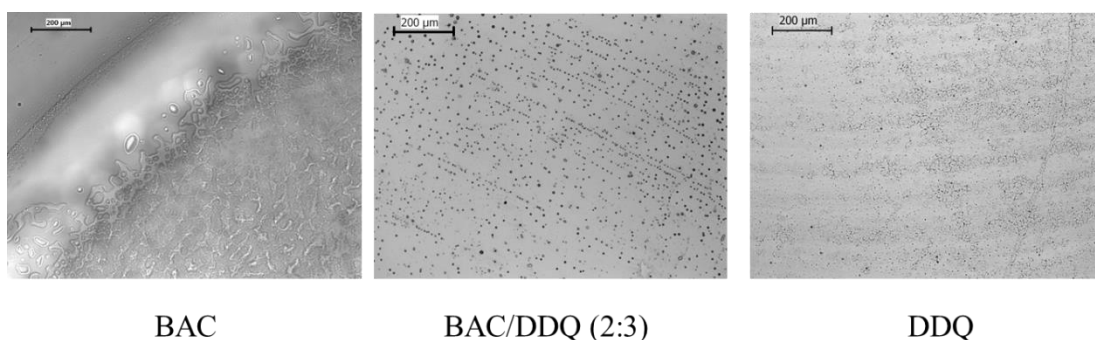


Figure 6.13 Optical micrographs of glass substrates treated with 20 μ L of 0.1 wt% surfactant + 0.1 wt% pDADMAC (21 kDa) solution. Scale bars = 200 μ m. Drying conditions; 30 $^{\circ}$ C, 20-30 % relative humidity, 24 hours drying time.

The film topographies of the three mixtures were observed to be very different with the BAC and DDQ mixtures resembling a film like topography while the BAC/DDQ was observed to have a nodular like structure. As a result of these observations a more comprehensive study was conducted. The concentrations and the ratio between

the polyelectrolyte and surfactant were kept constant but the surfactant mass ratio between the BAC and DDQ surfactants was altered. The solution properties for these solutions are reported in Table 6.6.

Table 6.6 Solution properties of 0.1 wt% BAC/DDQ + 0.1 wt% pDADMAC (21 kDa) formulations, pH of solution 5-6, RT= 22-24 °C. Glass Substrate.

| DDQ Mass Fraction | Surface Tension (mN/m \pm 0.1) | Equilibrium Contact Angle ($\theta \pm 1$) |
|-------------------|--------------------------------------|---|
| 0 | 35.6 | 36 |
| 0.1 | 34.4 | 33 |
| 0.2 | 32.7 | 32 |
| 0.3 | 31.5 | 33 |
| 0.4 | 30.3 | 33 |
| 0.5 | 30.0 | 32 |
| 0.6 | 29.6 | 31 |
| 0.7 | 29.2 | 32 |
| 0.8 | 28.3 | 31 |
| 0.9 | 28.4 | 31 |
| 1.0 | 28.2 | 29 |

The surface tension and contact angle of the solutions are observed to decrease as the mass fraction of DDQ increases within the formulation. Based on the CMC determination of BAC, BAC/DDQ (2:3) and DDQ in the presence of 0.1 wt% pDADMAC (Table 6.2) it is reasonable to assume all formulation reported in Table 6.6 are above their respective CMC.

The resulting film structures were analysed using an optical microscope and selected images are shown in Figure 6.14 (Top). To quantify this observed behaviour the nodule diameter was plotted as a function of DDQ mass fraction and is shown in Figure 6.14 (Bottom).

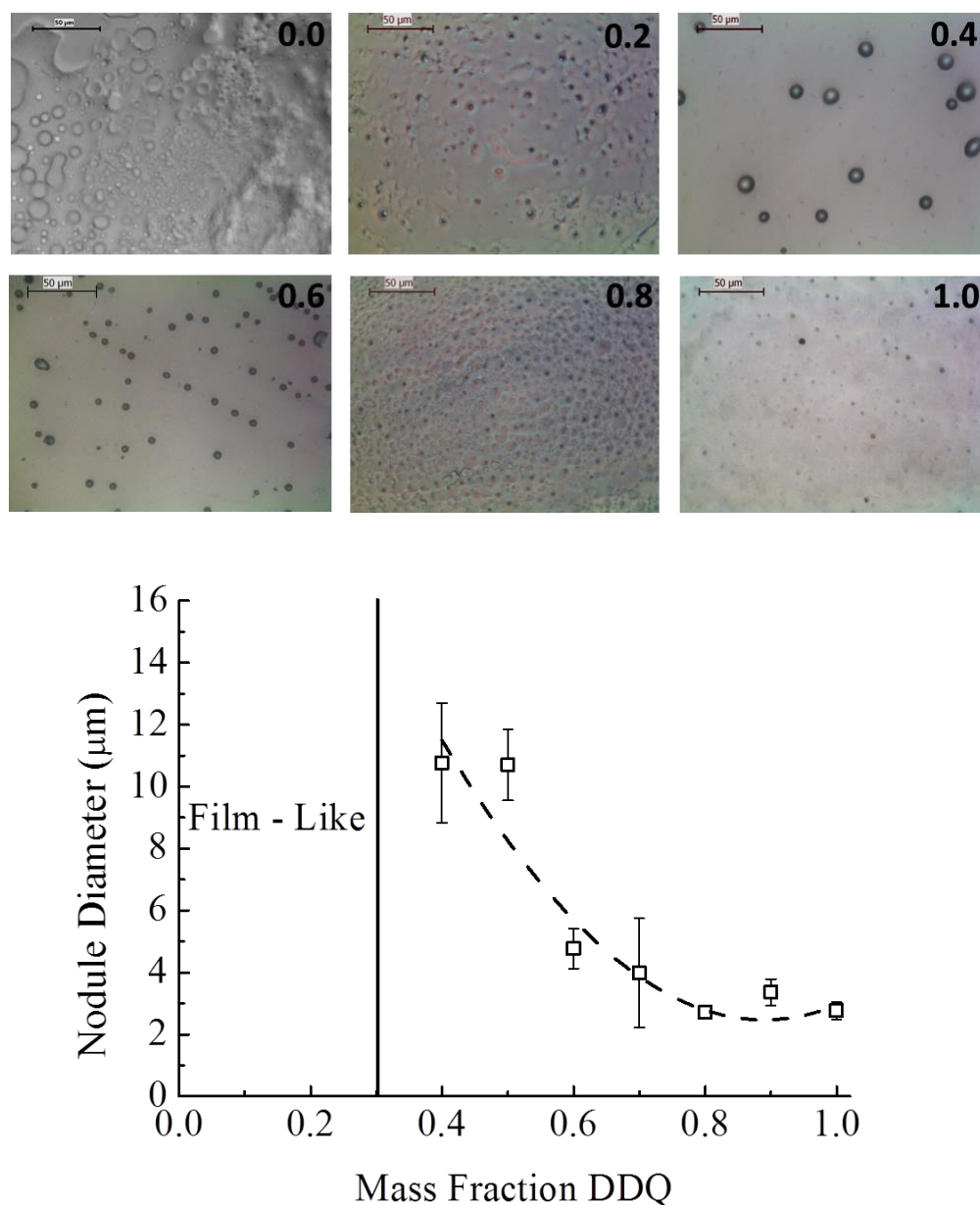


Figure 6.14. (Top) Optical micrographs of glass substrates treated with 20 μL of 0.1 wt% BAC/DDQ + 0.1 wt% pDADMAC (21 kDa) formulations. (Bottom) Average Nodule diameter, nodule size plotted as a function of DDQ mass fraction. Drying conditions; 30 °C, 20-30 % relative humidity, 24 hours drying time. 30 - 80 nodules were counted per substrate. Dashed line to guide eye.

It was observed that when the mass fraction of DDQ was between 1.0-0.8, small spherical nodule like structures could be observed within the film. When the mass fraction of DDQ was reduced from 0.8 – 0.4 these nodules increased in size quite

dramatically. Finally when the DDQ mass fraction was reduced < 0.4 the nodule like structures almost disappear leaving just a film like topography.

To gain further information about film topography, Non-Contact Atomic Force Microscopy (NC-AFM) was conducted on selected substrates. A detailed explanation of NC-AFM is given in Section 8.7. Two types of measurement were taken, firstly a topography image which gives information about surface roughness and structure height and secondly a phase image which gives information about a materials mechanical property. The NC-AFM topography and phase images for the selected substrates are shown in Figure 6.15.

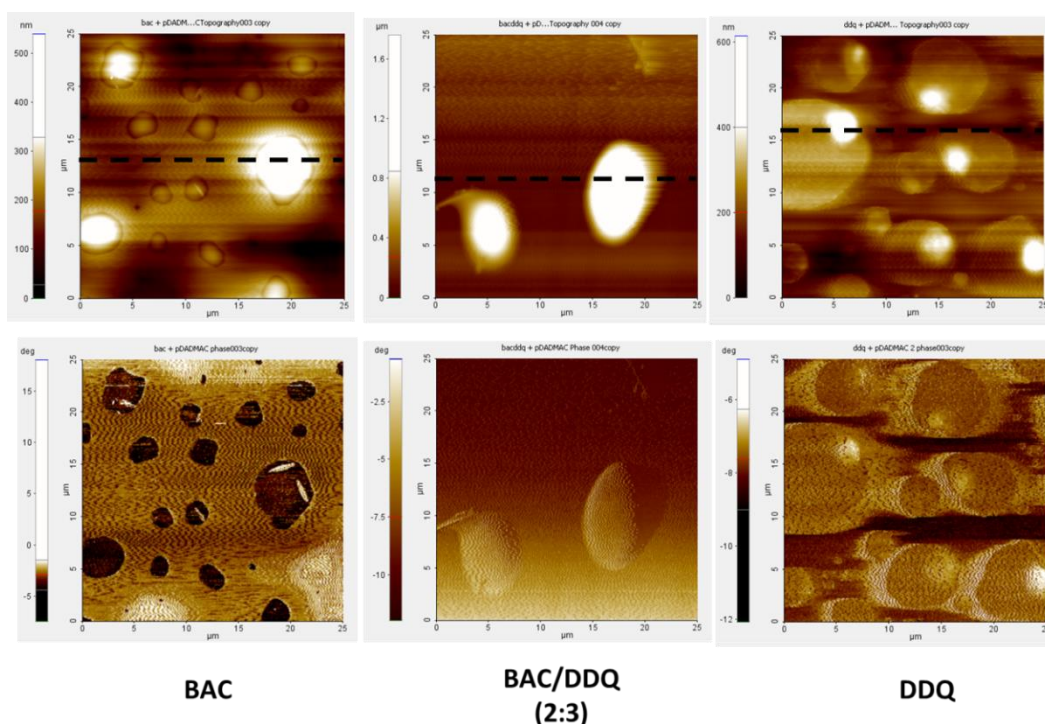


Figure 6.15 NC-AFM of glass substrates treated with a 20 µL 0.1 wt% surfactant + 0.1 wt% pDADMAC (21 kDa) formulation. Drying conditions; 30 °C, 20-30 % Relative humidity, 24 hours. Images 25 µm², Top = Topography, Bottom = Phase.

In Figure 6.15 within the topography images (Top) is a dashed line. This line indicates the height profiles of each sample shown in Figure 6.16.

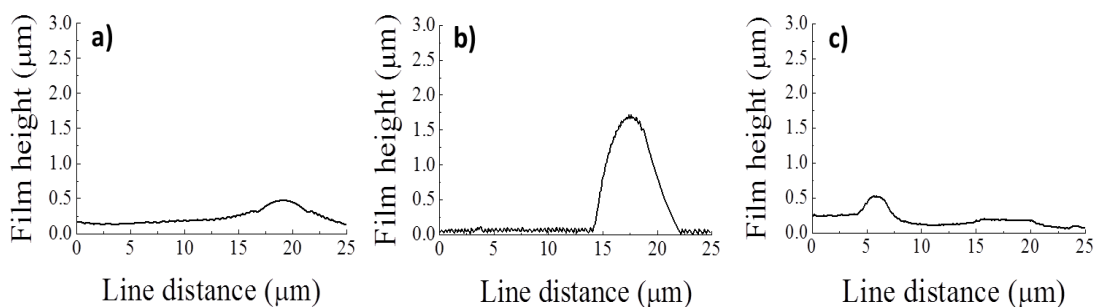


Figure 6.16 Height profile from NC-AFM topography images (Figure 6.15). Dashed line within topography images indicates where profile was taken. a) BAC, b) BAC/DDQ (2:3) c) DDQ.

From Figure 6.15 and Figure 6.16 the following conclusions can be drawn;

- The nodules observed when the DDQ mass fraction was between 0.8-0.4 give the film topography extra height/surface roughness compared to the mass fractions 1.0-0.8 and < 0.4 . The height of the measured nodule on the 0.6 mass fraction sample was $\approx 1.75 \mu\text{m}$.
- The phase image of the BAC sample shows three distinct regions with two distinct phases within the film. A primary lighter region and secondary darker regions. The different mechanical properties of these phases indicate they are possibly made up of different materials (surfactant/polymer). Within the secondary darker region cylindrical crystals also appear to be present. The origins of these crystals are unknown but could be an electrolyte based impurity from the pDADMAC sample.
- The BAC/DDQ (2:3) and the DDQ phase images do not show such a distinct contrast in phase regions however the DDQ phase regions have a slighter darker region in between the lighter circular regions.

6.3.3 Film Analysis (ToF-SIMS)

ToF-SIMS is an analytical technique with enables the determination and mapping of molecular species present on a surface. ToF-SIMS was conducted on a 0.1 wt% BAC/DDQ (2:3) + 0.1 wt% pDADMAC (21 kDa) treated silicon wafer substrate. The aim of the experiment was to determine the location of the surfactants and polyelectrolyte within this nodular film topography.

Before the mixture was analysed, three control samples (BAC, DDQ and pDADMAC (21 kDa) were analysed to identify the distinguishing species between the three compounds (Mass spectrums for controls can be viewed in Appendix 6-D, 6-E and 6-F). The distinguishing ions for each control are reported in Table 6.7.

Table 6.7 Principal Positive Secondary Ions Species within Controls.

| Control | Secondary Ions (m/z) |
|------------------|--|
| BAC | $[\text{Me}_2\text{HSi}^+] = 57$ |
| | $\text{C}_{12} [\text{M}^+-\text{Cl}^-] = 303$ |
| | $\text{C}_{14} [\text{M}^+-\text{Cl}^-] = 332$ |
| | $[\text{C}_6\text{H}_5 - \text{CH}_2^+] = 90$ |
| DDQ | $[\text{Me}_2\text{HSi}^+] = 57$ |
| | $[\text{M}^+-\text{Cl}^-] = 326$ |
| pDADMAC (21 kDa) | $[\text{Me}_2\text{HSi}^+] = 57$ |
| | $[(\text{CH}_3)_3\text{-Si}^+] = 73$ |
| | $[\text{Me}_3\text{SiOSiMe}_2^+] = 146$ |

Siloxane contaminants were identified in all the samples however clear distinguishing species were identified for the BAC and DDQ surfactants. For the

pDADMAC sample, the principal species appear to be from siloxane contaminants not the polymer. A peak at 162 m/z was expected to correspond to its monomeric unit however this was not observed.

The distinguishing species of the surfactants were mapped across the substrate in an attempt to identify how the surfactants and polymer are structured on the surface (Figure 6.17). There is surface damage on the left hand side of the ion mapping images from previous attempts at imaging species.

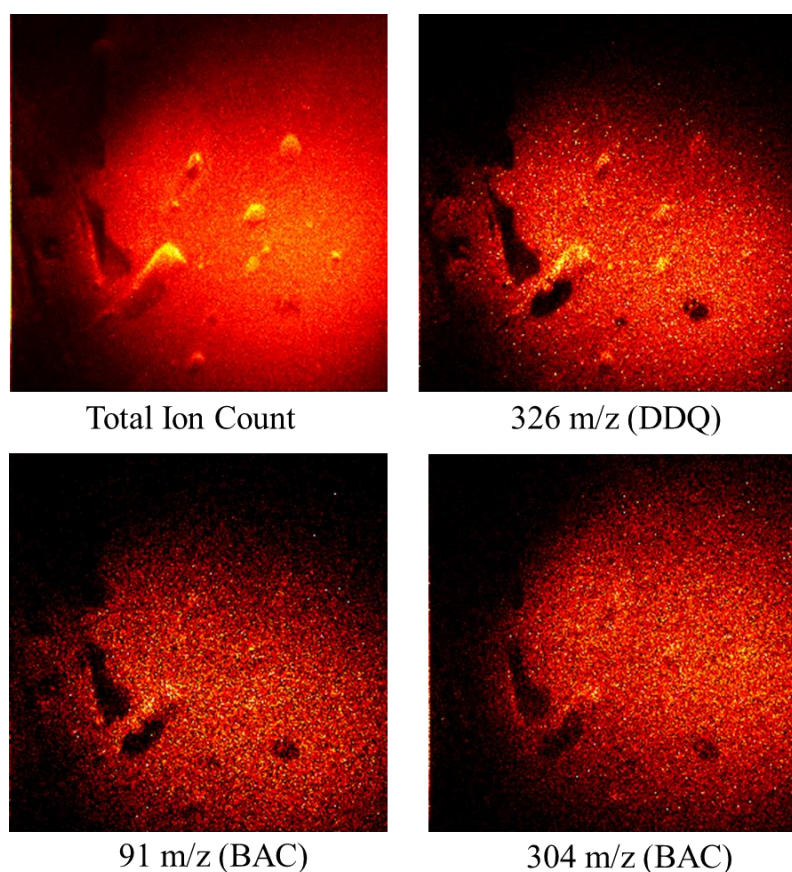


Figure 6.17 ToF-SIMS Ion mapping, 1000 μm^2 , Silicon wafer substrate treated with a 2 μL drop of a 0.1 wt% BAC/DDQ (2:3) + 0.1 wt% pDADMAC (21 kDa) formulation, Drying conditions; 30 $^{\circ}\text{C}$, 25 % Relative Humidity. Brighter colours = higher ion concentration.

The total ion image illustrates where the highest concentration of ions were located on the surface. From the image, definite nodule like structures can be observed with a high concentration of ions coming from the nodule areas.

Additional ion mapping was conducted on the most prominent distinguishing species found for the respective surfactants (BAC, DDQ). The ion mapping of all the species (91, 304 and 326 m/z) illustrates the same general trend. The species were detected over the whole sample however higher concentration of ions comes from the nodule area. However the ToF-SIMS ion mapping analysis does not identify the location of the pDADMAC within the film structure. Based on these observations two possible surface structures are proposed with the surfactant concentrating at the top of the film and the polyelectrolyte concentration towards the bottom of the film next to the substrate.

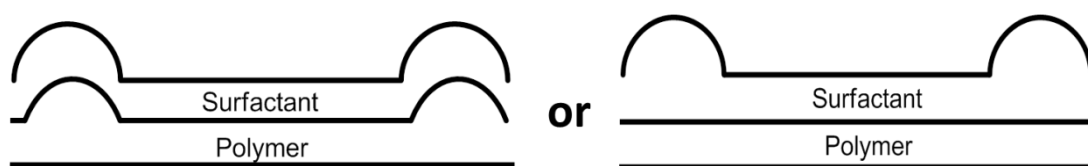


Figure 6.18. Possible surface structures in respect of surfactant and polymer location.

The layer of surfactant observed in the ion mapping is consistent with the NC-AFM phase image (Figure 6.15) which illustrated a lack of phase contrast between the nodule and the surrounding film. To identify where the pDADMAC is located within the film structure a more subtle experiment would be required involving etching away the upper most layer of the film.

6.3.4 Overview

Figure 6.19 shows the combined analyses (Optical microscopy and NC-AFM) for the 0.1 wt% surfactant (BAC, BAC/DDQ (2:3) and DDQ) + 0.1 wt% pDADMAC (21 kDa) mixtures.

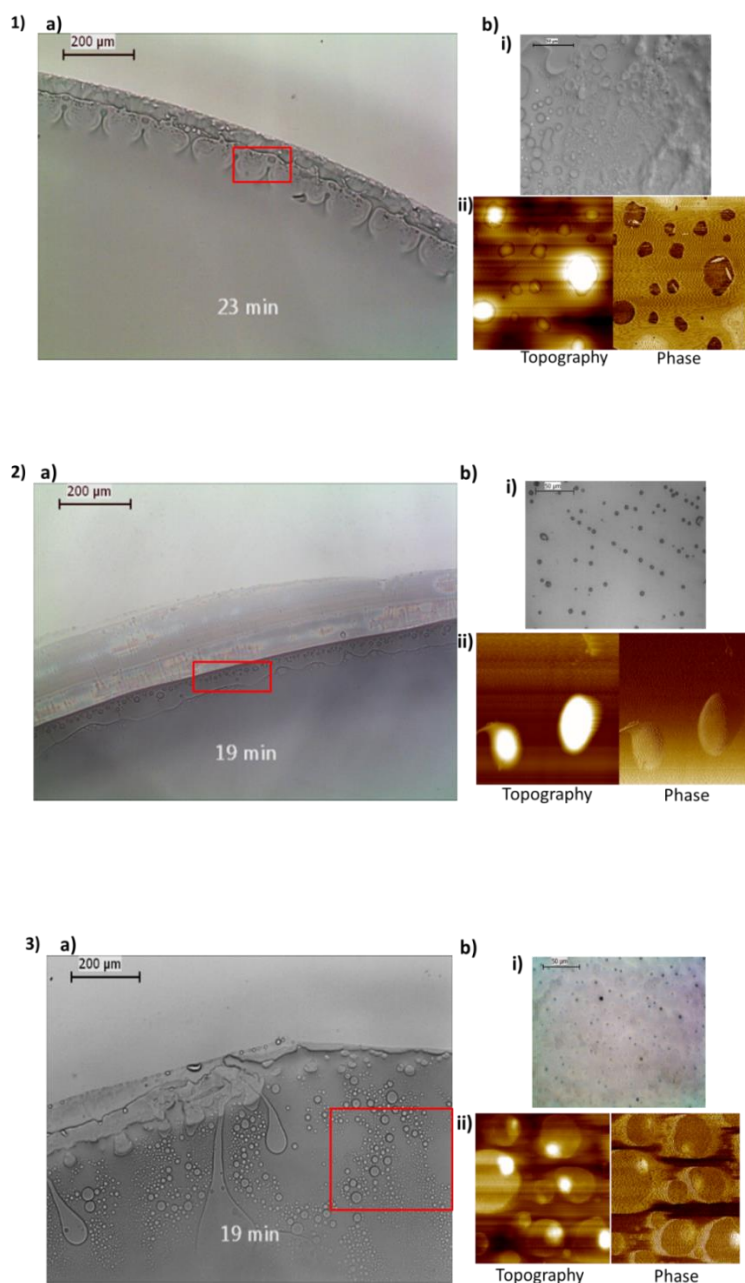


Figure 6.19 Combined analysis 1) BAC 2) BAC/DDQ (2:3) 3) DDQ, a) Optical micrograph of drying drop, Scale bar = 200 μm b) i) optical micrograph of dried film, Scale bar = 50 μm ii) NC-AFM Topography and phase images (25 μm^2).

Within these complex mixtures phase separation begins to occur while the drop remains pinned to the substrate. The solution phase separation concentration and equilibrium contact angle seem to be important in determining the concentration and location of phase separation within a drying drop.

6.3.5 Effect of pDADMAC Molecular Weight

Three different molecular weight pDADMACs were tested these were 8.5, 21 and 140 kDa (molecular weight denoted as M_v). These were formulated into 0.1 wt% BAC/DDQ (2:3) + 0.1 wt% pDADMAC formulations. Optical micrographs of the treated substrates can be viewed in Figure 6.20.

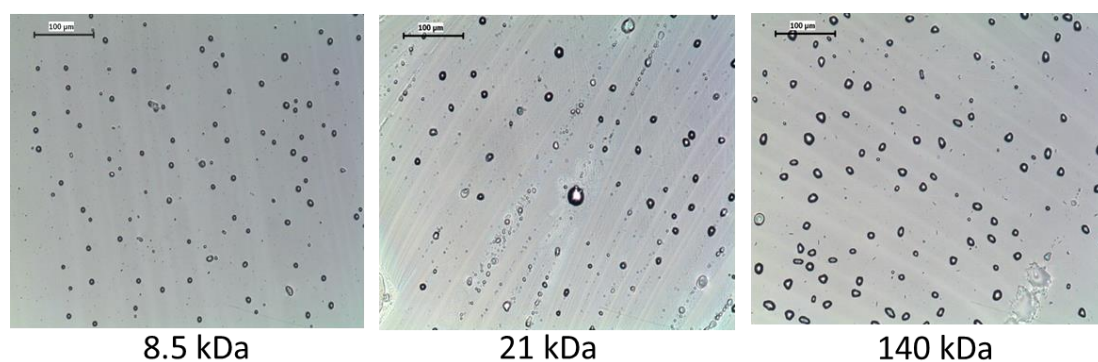


Figure 6.20 Optical micrographs of glass substrates treated with 20 μ L of 0.1 wt% BAC/DDQ (2:3) + 0.1 wt% pDADMAC. Samples denoted as a function of pDADMAC M_v . Drying conditions; 30 $^{\circ}$ C, 37 % relative humidity, 24 hours. Scale bar length = 100 μ m.

For all the treated substrates nodule like behaviour was observed. The nodule diameter for each substrate was measured and reported in Table 6.8.

Table 6.8 Average nodule size of glass substrates treated with 20 μL of 0.1 wt% BAC/DDQ (2:3) + 0.1 wt% pDADMAC. Drying conditions; 30 $^{\circ}\text{C}$, 37 % relative humidity, 24 hours. 50 nodules were counted per substrate.

| pDADMAC (M_v) | Average Nodule diameter (μm) | Standard Deviation (μm) |
|-------------------|---|--------------------------------------|
| 8.5 | 6.9 | 2.2 |
| 21 | 7.1 | 3.2 |
| 140 | 9.6 | 3.7 |

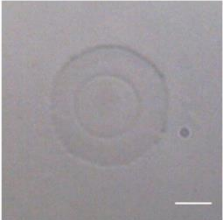
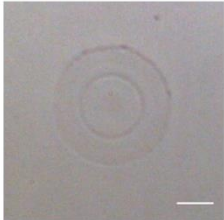
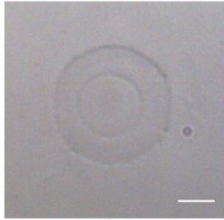
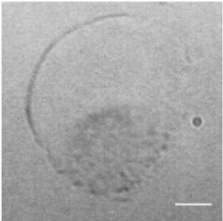
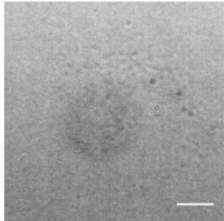
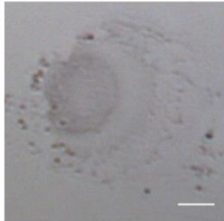
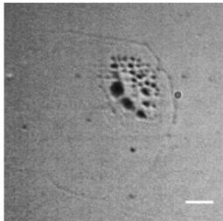
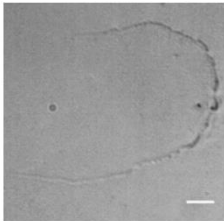
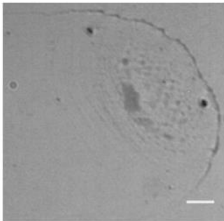
The nodule diameter size for each formulation reported in Table 6.8 indicates a possible trend with the nodule size increasing with increasing pDADMAC molecular weight.

6.3.6 Inkjet Printing

The previous sections looked at macro drops of 20 μL placed onto a glass substrate. In this section a piezo-drop on demand (Piezo-DOD) inkjet printer was used to apply drops of ≈ 10 pL to glass substrates. A detailed explanation of how a drop on demand inkjet printer works is given in Section 8.9. A volume this small enables the analysis of the whole drop by taking optical micrographs and NC-AFM topography and phase images. The pDADMAC (21 kDa)/surfactant/water system was used for this study.

The initial study looked at surfactant only formulations and the optical micrographs are reported in Table 6.9.

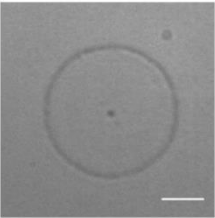
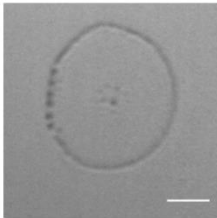
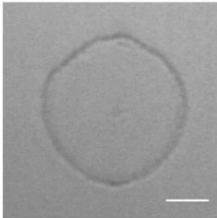
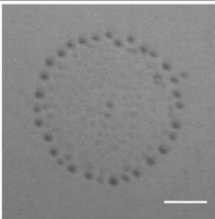
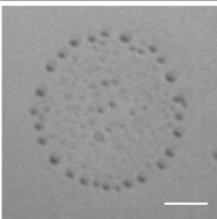
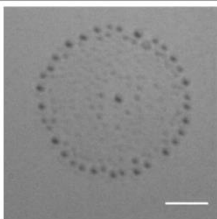
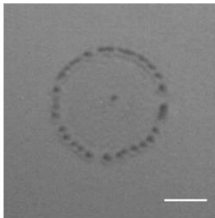
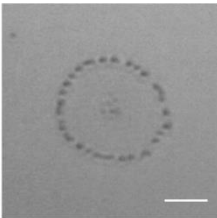
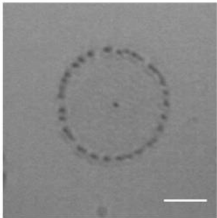
Table 6.9 Optical micrographs – Inkjet drops of ≈ 10 pL printed onto a glass substrate. Formulation of 0.1 wt% Surfactant only, Substrate temperature set at 30 °C and atmospheric relative humidity was between 40- 50 %. Scale bar = 10 μ m.

| Formulation | Drop 1 | Drop 2 | Drop 3 |
|------------------|--|---|--|
| BAC |  |  |  |
| BAC/DDQ (2:3) |  |  |  |
| DDQ |  |  |  |

The BAC drops were observed to be quite consistent and reproducible with a characteristic coffee staining effect within the surfactant film. The BAC/DDQ and DDQ drops were not as reproducible and formed irregular residues on the substrate.

The inkjet drops for the surfactant/pDADMAC (21 kDa)/water system is reported in Table 6.10.

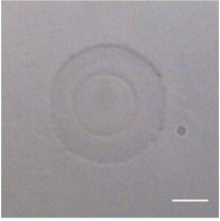
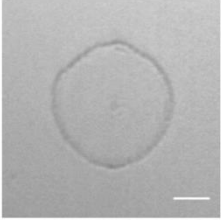
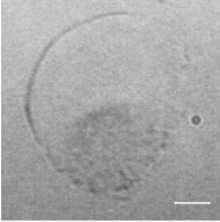
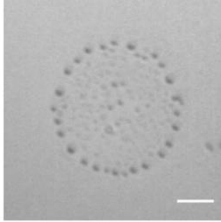
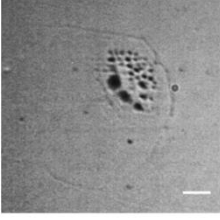
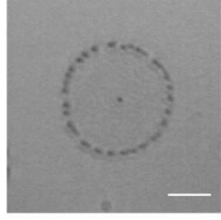
Table 6.10 Optical micrographs - Inkjet drops of ≈ 10 pL printed onto a glass substrate. Formulations of 0.1 wt% surfactant and 0.1 wt% pDADMAC (21 kDa), Substrate temperature set at 30 °C and atmospheric relative humidity was between 40- 50 %. Scale bar = 10 μ m.

| Formulation | Drop 1 | Drop 2 | Drop 3 |
|------------------|--|---|--|
| BAC |  |  |  |
| BAC/DDQ (2:3) |  |  |  |
| DDQ |  |  |  |

From the optical micrographs in Table 6.10 it was observed that the BAC containing drops resembles almost a featureless film except for a slight coffee staining effect. In contrast the BAC/DDQ containing mixture was observed to resemble a nodular like structure. Finally for the DDQ containing mixture a smaller residue corona was observed with some slight nodule like texture.

In Table 6.11 a comparison was made between the surfactant only formulations and the pDADMAC (21 kDa)/surfactant formulations with distinct differences observed.

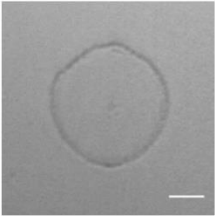
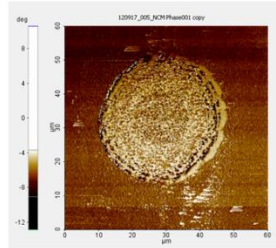
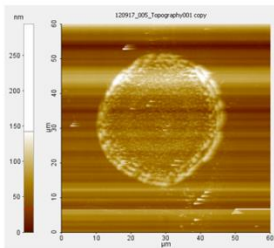
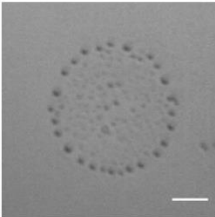
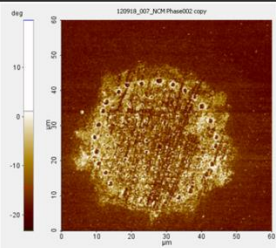
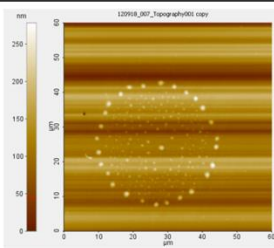
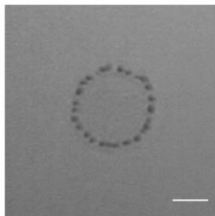
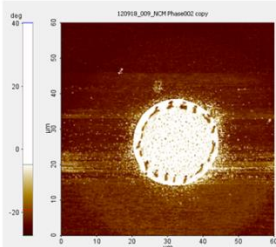
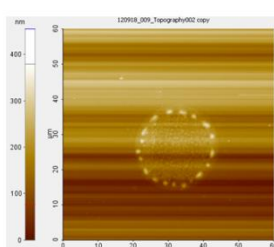
Table 6.11. Optical micrographs - Inkjet drops of ≈ 10 pL printed onto a glass substrate. Comparison of 0.1 wt% surfactant + 0.1 wt% pDADMAC (21 kDa) formulations and 0.1 wt% surfactant only solutions, Substrate temperature set at 30 °C and atmospheric relative humidity was between 40- 50 %. Scale bar = 10 μ m.

| Formulation | Surfactant only | Mixture |
|------------------|--|---|
| BAC |  |  |
| BAC/DDQ (2:3) |  |  |
| DDQ |  |  |

The BAC only containing mixture has minimal effect on the surface structure compared to the surfactant only formulation. However large differences were observed between the DDQ containing mixtures and the surfactant only formulations.

To gain further information about surface structure, NC-AFM topography and phase images were taken and are shown in Table 6.12.

Table 6.12 Optical micrographs / NC-AFM Phase and Topography - Inkjet drops of ≈ 10 pL printed onto a glass substrate. Formulations of 0.1 wt% Surfactant + 0.1 wt% pDADMAC (21 kDa), Substrate temperature set at 30 °C and atmospheric relative humidity was between 40- 50 %. Scale bar = 10 μ m.

| Formulation | Optical Image | NC-AFM Phase | NC-AFM Topography |
|------------------|--|---|--|
| BAC |  |  |  |
| BAC/DDQ (2:3) |  |  |  |
| DDQ |  |  |  |

The NC-AFM phase images show that the BAC only containing surface structure is as previously concluded; a featureless film except for some minor coffee staining effect.

For the BAC/DDQ mixture the phase image indicates nodular structures with a film layer in between these structures. The NC-AFM topography image indicates that the nodules observed in the BAC/DDQ mixtures surface structure protrude above this film.

Lastly, the DDQ only containing mixture phase image indicates an outer halo not observed on the optical micrographs with a concentrated central corona of residue which was observed in the micrographs.

From the NC-AFM phase images and the optical micrographs it is observed that the BAC and BAC/DDQ drops appeared to have pinned and dried with similar drop base diameters. In comparison the DDQ mixture had a much larger initial drop base diameter. There is a possibility that the three phase contact line for the DDQ mixture did not pin to the substrate after the initial impact onto the substrate hence the drop base diameter began receding straight away resulting in a concentrated corona of material at the centre of the drop.

The inkjet drop behaviour in general appears to be analogues to the macro drops studied in Figure 6.14.

6.4 PHMB/Surfactant/Water Systems

The previous sections have looked at pDADMAC based systems. This section will look at Poly(hexamethylene biguanide) chloride (PHMB) based systems using macro drops (20 μL). The substrates were treated in the same manner as the previously reported pDADMAC containing systems.

In Section 5.2.2 a phase separation study of these PHMB containing mixtures was conducted which reported that while the DDQ containing mixture phase separated at the same approximate concentration as the pDADMAC containing mixtures, the BAC and BAC/DDQ (2:3) surfactant mixtures was not observed to phase separate. These observations should have consequences on the resulting surface structure. The solution properties of these solutions are reported in Table 6.13.

Table 6.13 Solution properties for 0.1 wt% surfactant + 0.1 wt% PHMB mixtures, pH of solution 5 -6, RT= 20-22 °C. Glass substrate.

| Surfactant | Surface Tension (mN/m \pm 0.1) | Equilibrium Contact Angle ($\theta \pm 1$) |
|---------------|--------------------------------------|---|
| BAC | 37.3 | 30 |
| BAC/DDQ (2:3) | 29.8 | 25 |
| DDQ | 27.8 | 19 |

The CMCs of the surfactants in the presence of 0.1 wt% PHMB were determined via tensiometry (Appendix 6-G) and are reported in Table 6.14.

Table 6.14 CMC determination in the presence of 0.1 wt% PHMB via surface tensiometry. RT = 25 °C.

| Surfactant Type | CMC (mM) | CMC (wt%) |
|-----------------|----------|-----------|
| BAC | 1.3 | 0.05 |
| BAC/DDQ (2:3) | 1.0 | 0.04 |
| DDQ | 1.0 | 0.04 |

All the formulations reported in Table 6.13 are above their respective CMC. Similar to the pDADMAC system, the CMC values were observed to be lower than the corresponding CMC values calculated in Millipore filtered water (Table 5.1) and believed to be due to an increase in electrolyte concentration within the solution due to the presence of PHMB.

6.4.1 Direct Visualisation of Phase Separation

Sessile drops of 0.1 wt% surfactant (BAC, BAC/DDQ (2:3 mass:mass) or DDQ) + 0.1 wt% PHMB were studied using the optical microscope to see if phase separation was observed. Selected optical micrographs for the BAC and BAC/DDQ containing mixture can be viewed in Appendix 6-H and 6-I. They were not observed to phase

separate during drop evaporation. Selected optical micrographs for the DDQ containing mixture are shown in Figure 6.21.

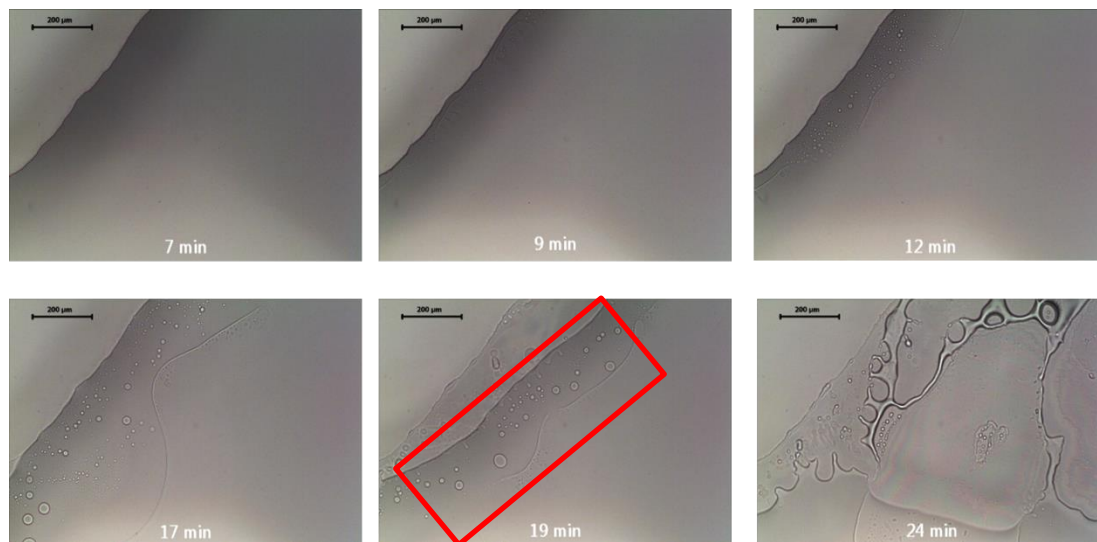



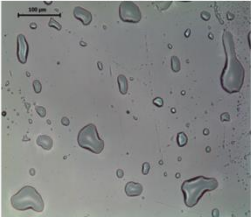
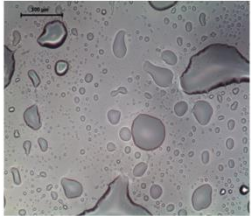
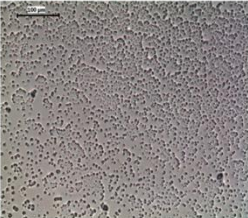

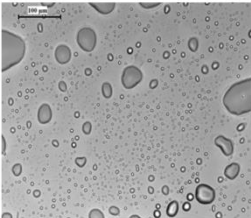
Figure 6.21 Optical micrographs of a drying sessile drop (20 μ L) on a glass substrate. 0.1 wt% DDQ + 0.1 wt% PHMB, Scale bars = 200 μ m, Room Temperature = 22 $^{\circ}$ C. Relative Humidity 50-60%. Red box illustrates phase separation region.

The DDQ containing mixture was observed to phase separate from 17 minutes onwards. The phase separation behaviour within the evaporating sessile drop appears analogous to the solution phase separation behaviour observed in Chapter 5 (5.2.2).

6.4.2 Film structure

Optical micrographs were taken of these mixtures 24 and 120 hours after treatment and can be viewed in Table 6.15. The substrates were left in an environmental chamber at 30 $^{\circ}$ C for 24 hours then transferred into a closed petri dish and stored at ambient temperature.

Table 6.15 Optical micrographs of glass substrates treated with 20 μL of 0.1 wt% surfactant + 0.1 wt% PHMB solution. Samples denoted as surfactant type. Drying conditions; 30 $^{\circ}\text{C}$, 32% relative humidity, 24 hours. Scale bar length = 100 μm .

| Since Application (Hrs) | BAC | BAC/DDQ | DDQ |
|-------------------------|--|---|--|
| 24 |  |  |  |
| 120 |  |  |  |

The first sets of images were taken 24 hours after application with the BAC mixture resembling almost a complete featureless film. The BAC/DDQ and DDQ images illustrated homogeneous sized nodules/residues likely formed due to a de-wetting process during drying. A second set of images were taken of the substrates 120 hours after application and were strikingly different compared to the 24 hour images. The featureless BAC film transformed into a nodule like film. Within the nodule/residues of the BAC/DDQ film distinct secondary micro domains were observed. The DDQ containing mixture remained unchanged.

To gain further insight into the film structures NC-AFM topography and phase images were taken for the PHMB containing films and is shown in Figure 6.22.

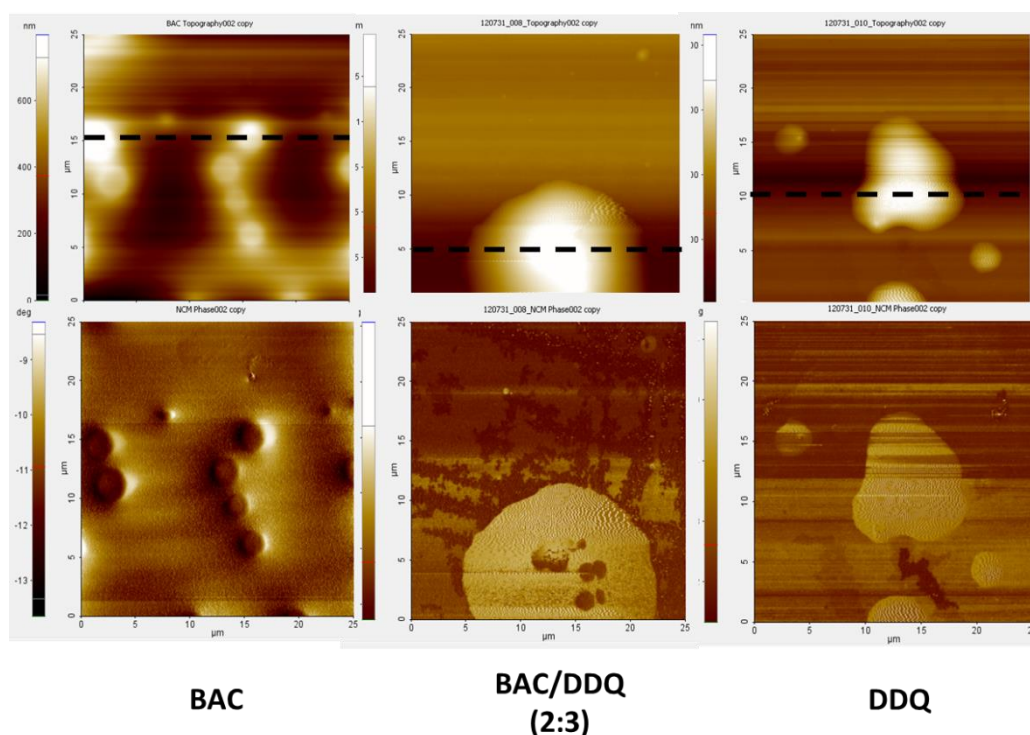


Figure 6.22 NC-AFM of glass substrates treated with 20 μL of 0.1 wt% surfactant + 0.1 wt% PHMB Drying conditions; 30 $^{\circ}\text{C}$, 41 % relative humidity, 120 hours. Images 25 μm^2 , Top = Topography, Bottom = Phase.

Figure 6.23 illustrates the depth profile of the PHMB containing films taken from the NC-AFM topography images (Dashed Line).

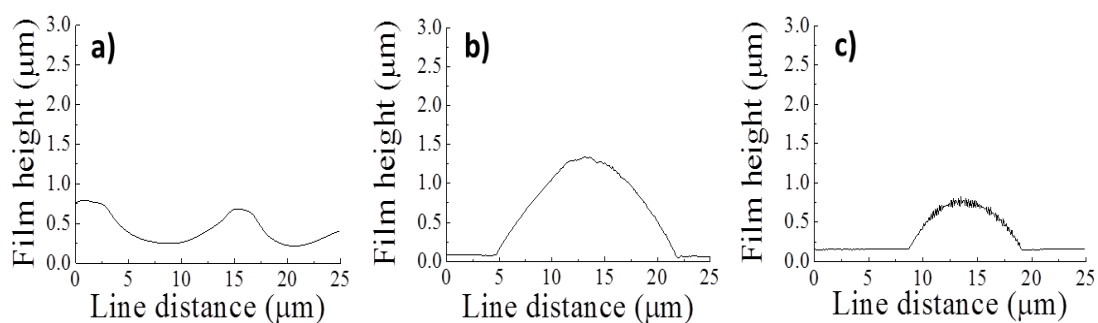


Figure 6.23 Height profile from NC-AFM topography images (Figure 6.22). Dashed line within topography images indicates where profile was taken. a) BAC, b) BAC/DDQ (3:2) c) DDQ.

The NC-AFM phase images do suggest different chemical domains within the BAC and BAC/DDQ treated substrates. We propose that the BAC/PHMB does not phase separate during the drying of the drop as seen previously for the pDADMAC containing mixtures but within the residual film left after drop evaporation. This reasoning would explain the differences between the 24 and 120 hours images shown in the optical micrographs shown in Table 6.15 and the NC-AFM images shown in Figure 6.22.

The DDQ only mixture was observed to phase separate during drop evaporation and the film topography was not observed to change between 24 -120 hours after application.

6.5 Potential Antimicrobial Surface Application

A potential application for cationic surfactant and polyelectrolyte composite films is in creating antimicrobial surfaces. To illustrate the potential of these formulations antimicrobial surface testing was conducted. The surface microbiology testing was performed by Byotrol Plc and is confidential. The testing methodology is a standard industrial test which uses a steel surface. The surface structuring work reported previously cannot be directly related to these microbiology results due to the change in substrate type but does illustrate the potential use of these formulations in creating antimicrobial resistant surfaces.

A steel surface was treated with the formulation and three abrasive wear cycles were used against the treated surface to remove any active not suitably adhered to the surface. Once the abrasive wear cycles were complete the gram-negative bacteria, *P. aeruginosa*, of known concentration was applied to the surface for a set period of time. The bacteria was then removed and counted to see how many survived the antibacterial coating. Surfactant and polymer controls (0.1 wt%) and a mixture

containing 0.1 wt% Surfactant + 0.1 wt% polymer were tested. The results of this screening test are reported in Table 6.16.

Table 6.16 Residual antibacterial efficacy of formulations against *P. aeruginosa* on a stainless steel surface following 3 abrasive wear cycles. Surfactant and Polymer concentrations = 0.1 wt%.

| Sample | Average log Reduction in <i>P. aeruginosa</i> | Standard Deviation |
|-------------------------------------|---|--------------------|
| pDADMAC (8.5 kDa) | 0.04 | 0.04 |
| pDADMAC (21 kDa) | 0.12 | 0.02 |
| pDADMAC (140 kDa) | 0.16 | 0.03 |
| PHMB | 3.95 | 0.12 |
| BAC | 1.92 | 0.37 |
| BAC/DDQ (2:3) | 1.30 | 0.17 |
| DDQ | 1.42 | 0.26 |
| BAC + pDADMAC (21 kDa) | 1.28 | 0.25 |
| BAC/DDQ (2:3) + pDADMAC (21 kDa) | 2.31 | 0.24 |
| DDQ + pDADMAC (21 kDa) | 0.96 | 0.06 |
| BAC + PHMB | > 4.92 | 0 |
| BAC/DDQ (2:3) + PHMB | > 4.92 | 0 |
| DDQ + PHMB | > 4.92 | 0 |

From Table 6.16 the following conclusions can be made;

- pDADMAC (8.5, 21 and 140 kDa) provided negligible antibacterial property to the surface without QAC surfactants. PHMB gave good antibacterial properties without QAC surfactants far superior to pDADMAC.

- QAC surfactants gave antibacterial properties superior to pDADMAC but less effective than PHMB.
- The combination of BAC or DDQ + pDADMAC (21 kDa) saw inferior/comparable antibacterial properties compared to QAC surfactant only samples.
- In combination the BAC/DDQ + pDADMAC (21 kDa) surfactant mixture saw a log 1 increase in antibacterial performance compared to the surfactant mixture only sample.
- For QAC surfactant + PHMB samples all measurable bacteria were killed when placed on the surface, results superior to both polyelectrolyte and surfactant only samples.

The best formulations were the QAC surfactants + PHMB samples which showed almost complete bacterial kill. The disadvantage of PHMB containing formulations is that there is currently regulatory concern about the environment impact of PHMB particularly its impact on aquatic ecosystems. No such concerns exists for pDADMAC containing formulations thus any potential strategy to improving antibacterial performance via manipulation of surface structure would be of significant commercial interest.

6.6 Conclusion

We have demonstrated the ability to manipulate film structures after the evaporation of a sessile drop containing a surfactant mixture of BAC/DDQ and the

polyelectrolyte pDADMAC on a glass substrate. The film structures varied from an amorphous film to a nodular like topography. The mechanism into how these structures are formed was investigated in respect to the previously reported solution phase separation behaviour. A number of factors have been identified as integral to structure formation these include; formulation surface tension, contact angle and critical phase separation concentration. An attempt was made to identify the location of the surfactant and polyelectrolyte within a nodular film structure via ToF-SIMS. The results were somewhat inconclusive. A top layer of surfactant was identified across the whole substrate. Further work is required on the mapping of the polyelectrolyte/surfactant location. A PHMB system was also investigated with the BAC containing mixtures observed to phase separate within the resulting film not during drop evaporation.

6.7 Reference

1. H. Hu and R. G. Larson, *J. Phys. Chem. B*, 2002, **106**, 1334-1344.
2. C. Bourgesmonnier and M. E. R. Shanahan, *Langmuir*, 1995, **11**, 2820-2829.
3. H. Y. Erbil, G. McHale and M. I. Newton, *Langmuir*, 2002, **18**, 2636-2641.
4. K. S. Birdi, D. T. Vu and A. Winter, *J. Phys. Chem.*, 1989, **93**, 3702-3703.
5. R. D. Deegan, O. Bakajin, T. F. Dupont, G. Huber, S. R. Nagel and T. A. Witten, *Nature*, 1997, **389**, 827-829.
6. H. Hu and R. G. Larson, *J. Phys. Chem. B*, 2006, **110**, 7090-7094.
7. R. D. Deegan, *Phys. Rev.*, 2000, **61**, 756-765.
8. P. J. Yunker, T. Still, M. A. Lohr and A. G. Yodh, *Nature*, 2011, **476**, 308-311.
9. J. Park and J. Moon, *Langmuir*, 2006, **22**, 3506-3513.
10. V. X. Nguyen and K. J. Stebe, *Phys. Rev. Lett.*, 2002, **88**, 164501.
11. V. Truskett and K. J. Stebe, *Langmuir*, 2003, **19**, 8271-8279.
12. T. Still, P. J. Yunker and A. G. Yodh, *Langmuir*, 2012, **28**, 4984-4988.

Chapter 7 – Conclusions and Further Work

Conclusions and Further Work

This chapter aims to summarise the major findings from each result chapter followed by a detailed plan of future work which can be used to build on the major findings of this research.

7.1 Conclusions

7.1.1 Polyelectrolytes in Solution

The solution properties and antimicrobial activities for a range of cationic polyelectrolytes types (pDADMAC, PDMC and PHMB) and molecular weights were investigated. The structural differences between PHMB and the two QAC polyelectrolytes (pDADMAC and PDMC) were studied in respect of the Manning parameter and surface activity. pDADMAC and PDMC were determined to undergo counter ion condensation and were subsequently observed not to be surface active. In comparison, PHMB was not expected to undergo counter ion condensation and was found to be surface active at concentrations > 0.1 wt%. Chain conformation as a function of concentration was theoretically estimated in salt free conditions using the Odijk model.

The antimicrobial activities of these polyelectrolytes were identified for a range of gram-negative bacteria via the determination of their respective minimum inhibitory concentration (MIC). All polyelectrolytes were observed to have some level of antimicrobial activity. The lowest range of MICs was observed for the lower molecular weight pDADMAC (8.5 kDa) which was even superior then PHMB. Relationships between polyelectrolyte solution properties and MIC could not be made due to differences in solution salinity.

7.1.2 Polyelectrolyte/Surfactant Mixtures of Similar Charge

The solution interactions between cationic polyelectrolytes (pDADMAC and PHMB) and QAC surfactants (BAC and DDQ) which are commonly used within antimicrobial formulations were investigated. At a critical concentration these mixtures segregatively phase separate into a surfactant rich upper phase and polyelectrolyte rich lower phase.

The pDADMAC containing mixtures were studied first. The phase separation phenomenon was investigated in respect of surfactant type as well as polyelectrolyte molecular weight. Surfactant type was observed to be the dominant factor in determining the onset of phase separation and by mixing different ratios of surfactants (BAC/DDQ) the ability to tune this phase separation concentration was shown. A counter ion condensing mechanism was inferred to initiate phase separation as well as an additional depletion flocculation effect at lower DDQ mass fractions which was more prominent for higher molecular weight pDADMACs. The effect of polyelectrolyte type was investigated with a comparison made between pDADMAC and PHMB mixtures. While DDQ/PHMB/water mixtures followed the same counter ion condensing mechanism the BAC containing mixtures failed to phase separate. A potential hydrophobic/hydrophobic interaction between PHMB/BAC was hypothesised.

An article based on results from this chapter has recently been accepted in the peer reviewed journal Langmuir (P W. Wills et al., Segregation in like charged polyelectrolyte - surfactant mixtures can be precisely tuned via manipulation of surfactant mass ratio, DOI: 10.1021/la400130x).

7.1.3 Surface Patterning

Dilute solutions of these surfactant/polyelectrolyte/water mixtures well below their respective phase separation concentration were deposited onto glass substrates via a drop cast or inkjet printer method. It was observed that pDADMAC mixtures phase

separate within the drop as the water evaporates and the solute concentration increases. The surfactant/polyelectrolyte film composites left after drop evaporation were investigated to see if this phase separation process can be used to manipulate surface structure. It was observed that changing the BAC/DDQ ratio of the formulation results in different film topographies ranging from an amorphous film to nodular like structures. The ToF-SIMS chemical mapping results were inconclusive so the location of the surfactant and polyelectrolyte within these films and needs to be further investigated. The PHMB containing mixtures which contained the surfactant BAC were observed not to phase separate during drop drying but within the resulting film composite.

The ability to order/structure onto a surface as observed here could alter the active adhesion and surface roughness properties of the film. This change in surface property could consequently effect antimicrobial performance but needs to be fully investigated via a carefully thought out microbiology based investigation.

7.2 Further Work

To build on the principal findings of this research the following work program is proposed which aims to test some of the theories and hypotheses presented within this thesis. The section has been divided into three sections; phase separation mechanism, inkjet printing and film analysis.

7.2.1 Phase separation mechanism

In chapter 5 a segregative phase separation mechanism was proposed for surfactant/polyelectrolyte mixtures of similar charge. The addition of an electrolyte (inorganic or polyelectrolyte) was believed to cause a reduction in the thickness of

the ionic atmosphere around the quaternary nitrogen and chloride ion of the surfactant headgroup, resulting in phase separation.

To further explore the effect of ionic strength on the critical phase separation concentration, the addition of different inorganic electrolytes into these systems is proposed. Sodium bromide would illustrate the effect of changing the anion within the electrolyte, while calcium chloride would look at the effect of a divalent electrolyte.

Additionally, at the critical electrolyte concentration which induces phase separation, it is unclear if an intimate ion pair forms between the quaternary nitrogen and counter ion of the surfactant. An intimate ion pair is when both ions are in direct contact with each other. The formation of this intimate ion pair could be the point in which phase separation is triggered. To test this hypothesis, an ion selective (chloride) electrode experiment is proposed which would measure the concentration of free chloride ions within the solution as the electrolyte is added. This may give an indication of intimate ion pair formation.

7.2.2 Inkjet Printing

The inkjet printing study (chapter 6) of the pDADMAC systems illustrated nodule to film like topographies. This topography change was also observed in the macro drop studies which looked at a number of BAC/DDQ ratios. To provide further evidence that the macro drop study and inkjet printing studied are analogues, an inkjet printing study is proposed with formulations at these same BAC/DDQ ratios. This will confirm if the inkjet surface topographies are completely analogues to the macro drop studies reported in Figure 6.14.

7.2.3 Film Analysis

In the surface patterning chapter (chapter 6), the location of the pDADMAC within the composite films could not be confirmed. However, the hypothesis presented was that the polymer was at the bottom of the composite film, hence absorbed directly onto the substrate surface. To determine whether this hypothesis is correct the following experiments are proposed;

A ToF-SIMS study involving the etching away of the uppermost layer in an attempt to analysis the lower layers would be an appropriate first experiment. Alternatively, a fluorescent probe molecule either covalently attached or solubilised within the micelles could be used to differentiate between the actives within the film and a fluorescent microscope would be used to analyse the film. The addition of a fluorescent probe molecule could change the solutions phase separation properties and would need to be investigated prior to use.

Chapter 8 – Instrumentation

Instrumentation

This chapter aims to describe the underlying principals involved in some of the main analytical instrumentation used within this research.

8.1 Surface Tensiometry

Surface tension measurements were performed on either a Kibron Delta-8 tensiometer or a Torsion balance (Whit Electrical and industrial Company Ltd). Both tensiometers are based on the De-Nouy method with a platinum rod or ring used as the probe.

De-Nouy Theory: A platinum ring or rod is submerged into the solution and the maximum force required to pull the ring off the air-water interface corresponds to the solutions surface tension (mN/M).¹

8.2 Isothermal Titration Calorimetry (ITC)

Isothermal Titration Calorimetry (ITC) enables the quantitative measurement of binding events taking place within a solution.²

Theory: The temperature difference between the sample cell and the reference cell is kept constant during the experiment using a cell feedback system (CFS). This is called the baseline. The sample cell is filled with either the solvent or solute of choice depending on experimental design. A small amount of the chosen titrate is added multiple times into the sample cell. The end of the pipette is modified so that stirring can take place within the cell (max 1000 rpm).

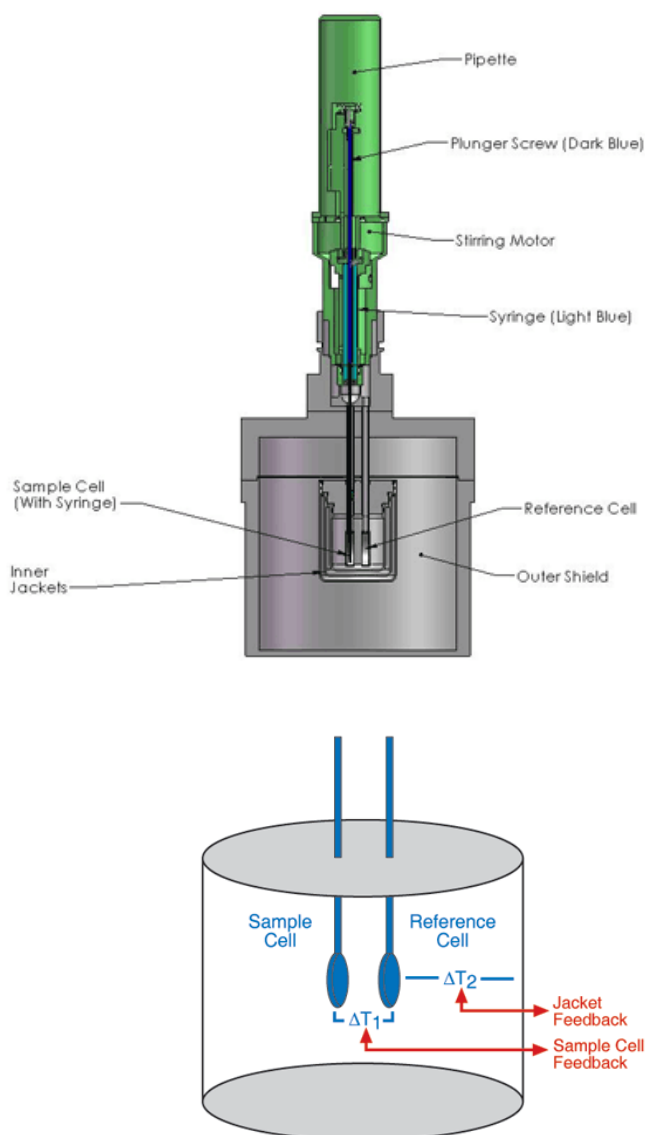


Figure 8.1 Schematic diagram of the Isothermal Titration Calorimetry equipment.²

When binding occurs within the sample cell, a small change in temperature is detected and the appropriate amount of heat is added or removed so that the sample cell returns to the previously established baseline temperature. The integral of the power required to re-establish baseline is proportional to the resulting heat given off due to the binding event. The computer software Oracle plots the difference in rates of heat production or absorption between the reference and sample.²

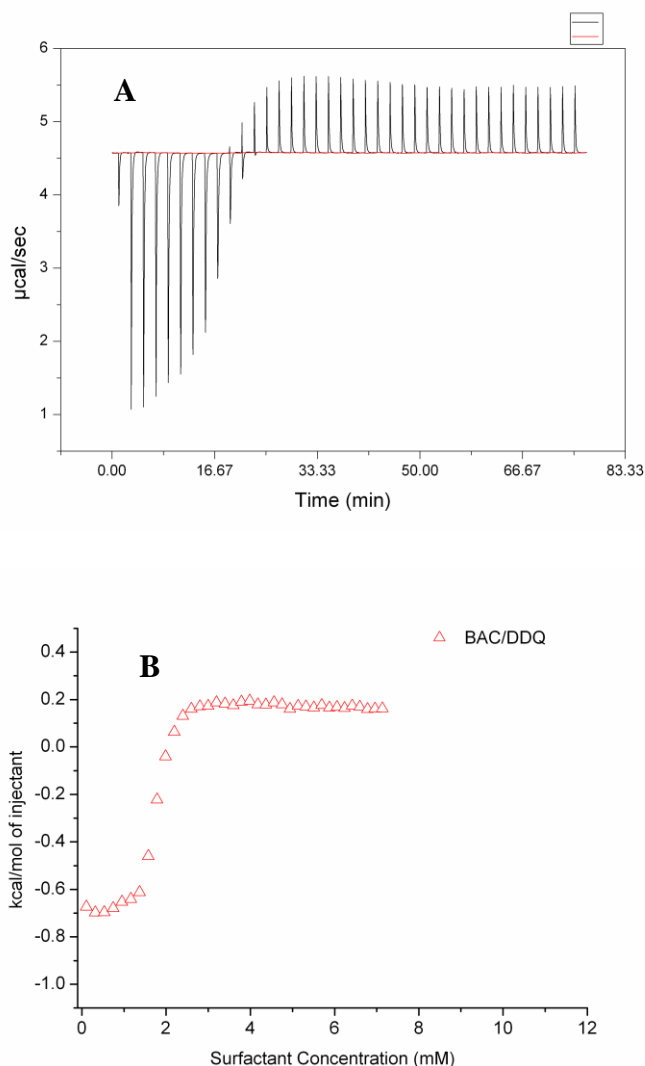


Figure 8.2 ITC thermodynamic profile. A = Raw ITC data, B = Integral of the power needed to return to the baseline.

A simple example of a thermodynamic profile is the micellisation of a surfactant (Figure 8.2). A surfactant which has a concentration is above its CMC is titrated into a cell containing water. Firstly an exothermic response is observed as the micelles dissociate upon their addition into the cell. When the concentration within the cell reaches the CMC instead of dissociating the surfactant unimers will aggregate into micelles thus inducing an endothermic (bond making) response. As more surfactant is injected into the cell a plateau is observed as a constant rate of micellisation is achieved.

8.3 Photon Correlation Spectroscopy (PCS)

Photon correlation Spectroscopy (also known as Quasi-elastic light scattering) is a particle sizing technique used to characterise nanometer – micrometer diameter particles.¹

When a particle is dispersed within a liquid medium the particle moves due to Brownian motion. Brownian motion of the particle is due to collisions with the much smaller solvent molecules. The solvent molecules are in random thermal motion.

When a light photon hits a moving particle it re-radiates the light at a slightly different frequency compared to a stationary particle. The re-radiated frequency increases and decreases depending on if the particle is moving away or towards the detector. This effect is termed “Doppler Broadening” and if it can be measured accurately the average diffusion coefficient of the particles can be determined.¹

To be able to accurately determine the diffusion coefficient, the refractive index of the dispersing medium and the scattering angle of the detector need to be known. The PCS instrument used within this study was the Malvern Zetasizer Nanoseries which has a back scattering photon detector set at 173° . This information can then be used to calculate the scattering vector of the solution

The Malvern Zetasizer Nanoseries calculates the autocorrelation function of the scattered light which enables the determination of the average diffusion coefficient of the particles. Particles move around in solution at lots of different velocities as most samples contain some degree of polydispersity. The scattered light from these particles all moving at different velocities in reasonably concentrated samples causes interference between the neighbouring particles. The autocorrelation function attempts to track the position of the particles from this interference element in the scattered light.

If the particles were stationary, the correlation function would be unity. However, due to the Brownian motion of the particles, the intensity of scattered light fluctuates within small areas of the solution due to the interference of neighbouring particles discussed previously. The faster the motion of the particles the faster any correlation between the scattering pattern. From this, the autocorrelation function can be determined. The autocorrelation function enables the determination of the diffusion coefficient and is most suitable for monodispersed spherical systems.^{1, 3}

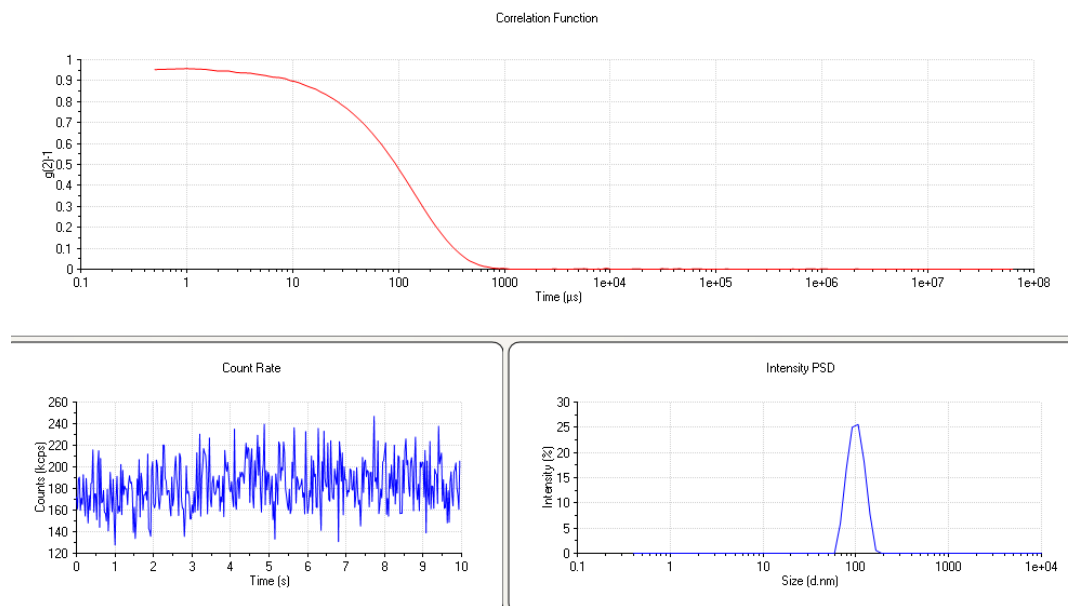


Figure 8.3 Data from a Malvern Zetasizer Nanoseries. (Sigma Aldrich 0.1 μm diameter standard latex particles).

Once the average diffusion coefficient of the particles has been determined the Einstein Stokes equation (Equation 8.1) can be used to determine the hydrodynamic radius of the particle.

$$D = \frac{KT}{6\pi\eta r} \quad (8.1)$$

Where D = diffusion coefficient (m^2/s), K = Boltzmann Constant (J/K), T = Absolute Temperature (K), η = Viscosity of solution (N.s/m^2) and r = radius of particle (m).

To obtain the size distribution of the particles present within the solution deconvolution of the autocorrelation function is required using a non-negatively constrained least squares algorithm. The Malvern Zetasizer Nano series used within this study used a CONTIN algorithm.⁴

8.4 Size exclusion chromatography (SEC)

Size exclusion chromatography (SEC) is a chromatographic technique which separates molecules in solution by hydrodynamic size. The separation of polymer molecules via SEC is also referred to as Gel Permentation Chromatography (GPC).

The analyte, in this case the polymer, is solubilised within a solvent and acts as the mobile phase. The separation of the polymer molecules is based on their hydrodynamic volume within the chosen solvent. The stationary phase is a column packed with porous beads. The elution time of the polymer from the column depends on its hydrodynamic volume with the larger volumes eluting first followed by the smaller volumes.⁵

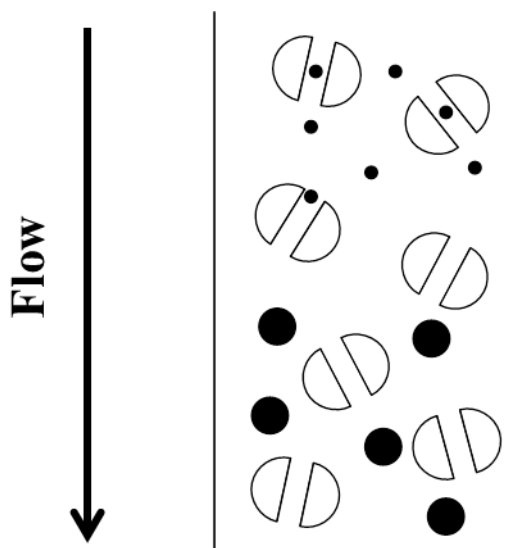


Figure 8.4 Schematic diagram of a SEC column illustrating the separation process.

The molecules with a larger hydrodynamic diameter cannot penetrate into the pores of the beads and instead travel between the beads. In comparison, the molecules with a smaller hydrodynamic diameter can penetrate into the beads increasing its respective elution time. The analyte must not interact with the stationary phase.

A wide range of detectors are available to analyse the eluent. These include refractive index, UV and light scattering detectors.

In chemistry the elution time of the polymer is used to calculate the polymer molecular weight (M_w , M_n) and its degree of polydispersity (M_w/M_n). The elution time is compared to a calibrated graph produced using well defined low polydisperse polymer samples. In aqueous SEC systems this is commonly polyethylene oxides.⁵

8.5 Anton Paar Viscometer

The viscosity of the solutions was based on a falling ball viscometer. A sphere of known diameter and density descends through the medium. The spheres terminal velocity is measured by timing the ball speed between two set points. By knowing the spheres diameter, density and its terminal velocity Stokes law can be used to calculate the solutions viscosity.¹

$$V_s = \frac{2}{9} \frac{r^2(\rho_s - \rho_f)}{\mu} \quad (8.2)$$

Where V_s = Terminal velocity of Sphere (m/s), r =radius of sphere (m), ρ_s =density of sphere (g/L), ρ_f =density of solution (g/L), μ = dynamic viscosity (N.s/m²).

8.6 Ubbelohde Viscometer

The Ubbelohde viscometer is a capillary based viscometer. It is a U-shaped piece of glassware with a solvent reservoir on one side and a capillary on the other. The solvent is sucked up into the capillary from the reservoir and the time the solvent takes to travel back down the capillary between two calibrated marks gives a measure for viscosity.

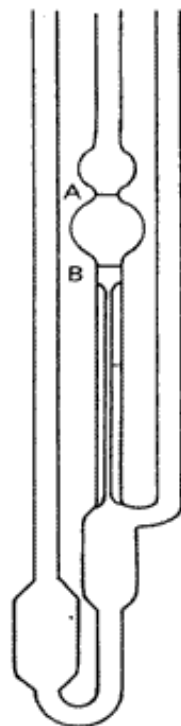


Figure 8.5 Schematic Diagram of a Ubbelohde Viscometer. A and B indicates the calibrated lines between which the solution viscosity is measured.

The viscometer is normally placed into a carefully thermostated water bath so temperature can be tightly controlled. The solvent run time should be greater than 100 seconds so that kinetic contributions can be ignored.^{6,7}

8.7 Non-Contact Atomic Force Microscopy (NC-AFM)

A cantilever is attached to a sharp tip. When the tip approaches a surface it detects forces between the tip and the surface leading to a deflection of the cantilever. The deflection of the cantilever is measured using an optical lever system which involves a laser being beamed onto the tip. From the tip, the laser is deflected onto a position sensitive photodiode (PSPD) thus when the cantilever undergoes a deflection, the

lasers position on the PSDS changes thus calculating the degree of cantilever deflection.^{8,9}

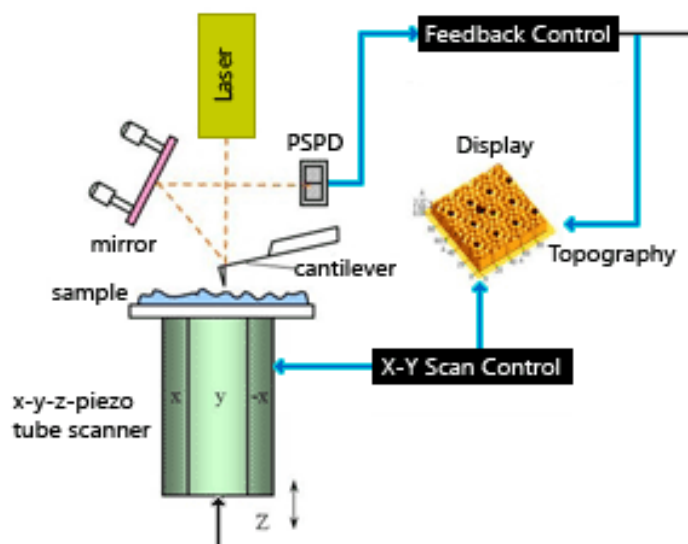


Figure 8.6 Schematic diagram of a Park XE-100-AFM Setup.⁸

Non-contact mode: In this mode the tip does not touch the surface. The cantilever is oscillated just above its resonance frequency. Any Van der Waals forces or electrostatic force which extends above the surface causes a decrease in the resonance frequency of the cantilever. The decrease in frequency is detected and so that the resonance frequency remains constant the distance between the tip and surface is adjusted appropriately. By measuring the tip to surface distance at each X-Y data point the surface topography can be obtained.⁹

As well as topographic information of the substrate, a phase image can be obtained at the same time. The phase imaging is as a result of a phase shift/delay in the oscillation of the cantilever which is dependent on the mechanical properties of the substrate such as viscoelastic and adhesion forces. Although it is worth noting that the phase image does contain some small topographic contributions so careful analysis is required for these images.^{8,9}

8.8 Time of Flight Secondary Ion Mass Spectrometry (ToF-SIMS)

ToF-SIMS is an analytical technique used to identify the molecular constituents of a surface. A primary ion beam (Cs^+ , O^{2+} , Ar^+ , Au^{3+}) is aimed and pulsed at the surface causing secondary ions to fly off the surface. These secondary ions are collected by the mass spectrometer and identified by their mass and charge.¹

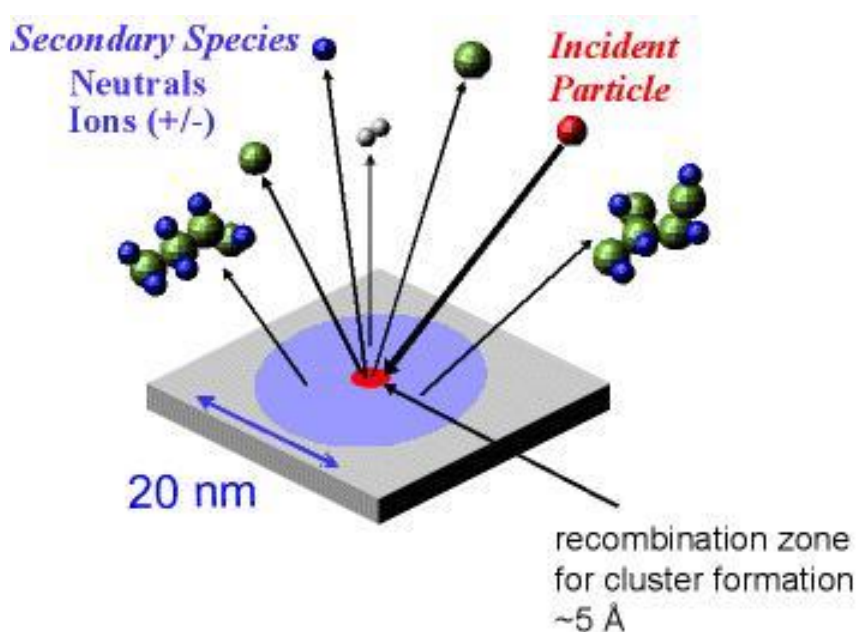


Figure 8.7 Schematic diagram illustrating the ToF-SIMS process.¹⁰

The primary ion beam can be focused to a diameter of 1 μm and can reach an approximate depth of 10 nm into the surface. The ion beam can be scanned across the surface to obtain microanalysis of the surface structure.

8.9 Dimatix Printer (Piezo-DOD)

Piezo Drop on Demand inkjet printers use a piezoelectric material behind the printer nozzle to force the formulation out of the cartridge. When a voltage is placed across the material an accumulation of charge occurs resulting in changes to its shape and size. The change in size/shape of the material causes a pressure build-up forcing the formulation out of the nozzle. Typical inkjet volumes are in the range of 2-200 pL. The pressure required to generate a drop is dependent on the solution properties of the formulation. The two most important factors are solution viscosity and surface tension. The printing of a drop involves three stages: drop generation, drop flight and drop impact. The timescale of all three stages is typically 5-250 μs .¹¹

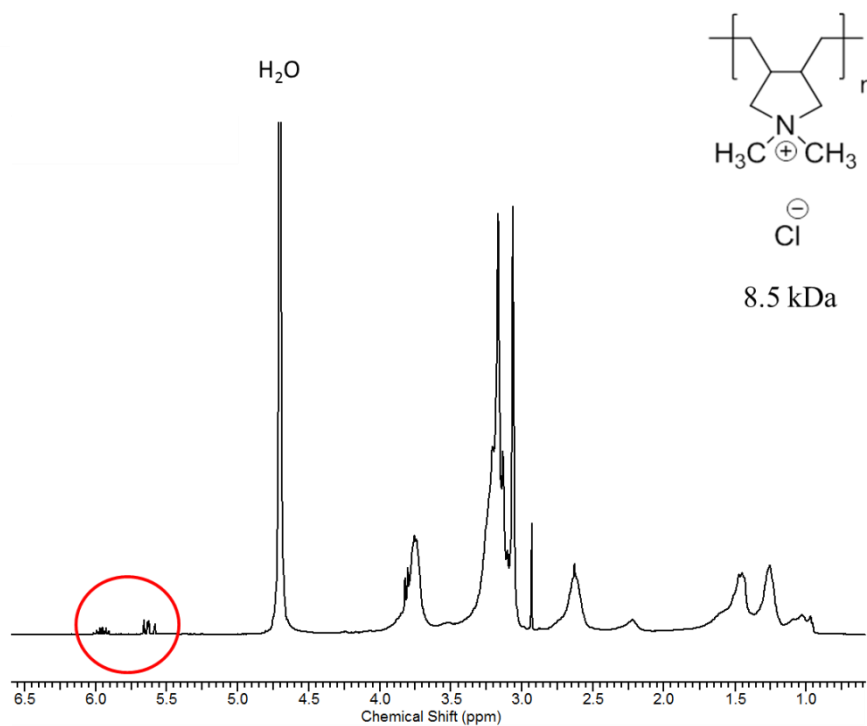
8.10 References

1. R. Hunter, *Foundations of Colloid Science*, 2nd Edition, Oxford University Press, Oxford, 2001.
2. <http://www.microcal.com/technology/itc.asp>, Accessed 22/02/13.
3. *Zetasizer Nano Series User Manual, Issue 2.1*, Accessed 29/01/13.
4. S. W. Provencher, *Comput Phys Commun*, 1982, **27**, 229-242.
5. M. Potschka and P.L. Dubin (Editors), *Strategies in Size Exclusion Chromatography*, ACS, Washington, 1996.
6. P. Flory, *Principles of Polymer Chemistry*, Cornell University Press, London, 1953.
7. P. Atkins and J. De Paulo, *Atkins Physical Chemistry*, 8th Edition., Oxford University Press, Oxford, 2006.
8. http://www.parkafm.com/AFM_guide/true_non_contact_mode_1.php, Accessed 29/02/13.
9. P. Eaton and P. West, *Atomic Force Microscopy*, Oxford University Press, Oxford, 2010.
10. http://serc.carleton.edu/research_education/geochemsheets/techniques/ToFMSI.html, Accessed 31/01/2013.

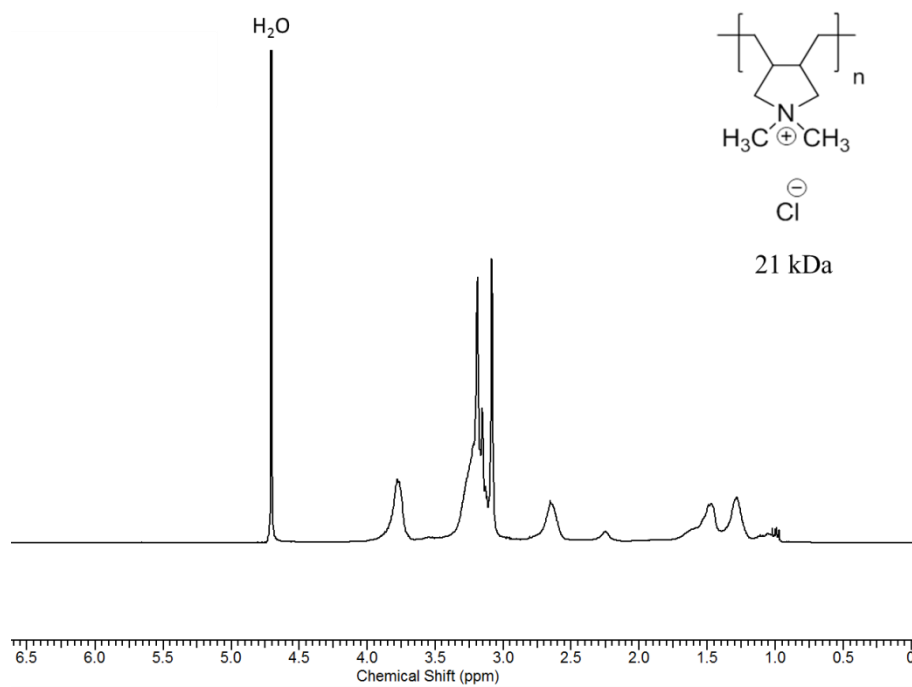
11. S. Magdassi (Editor), *The Chemistry of Inkjet Inks*, World Scientific, 2010.

Appendices

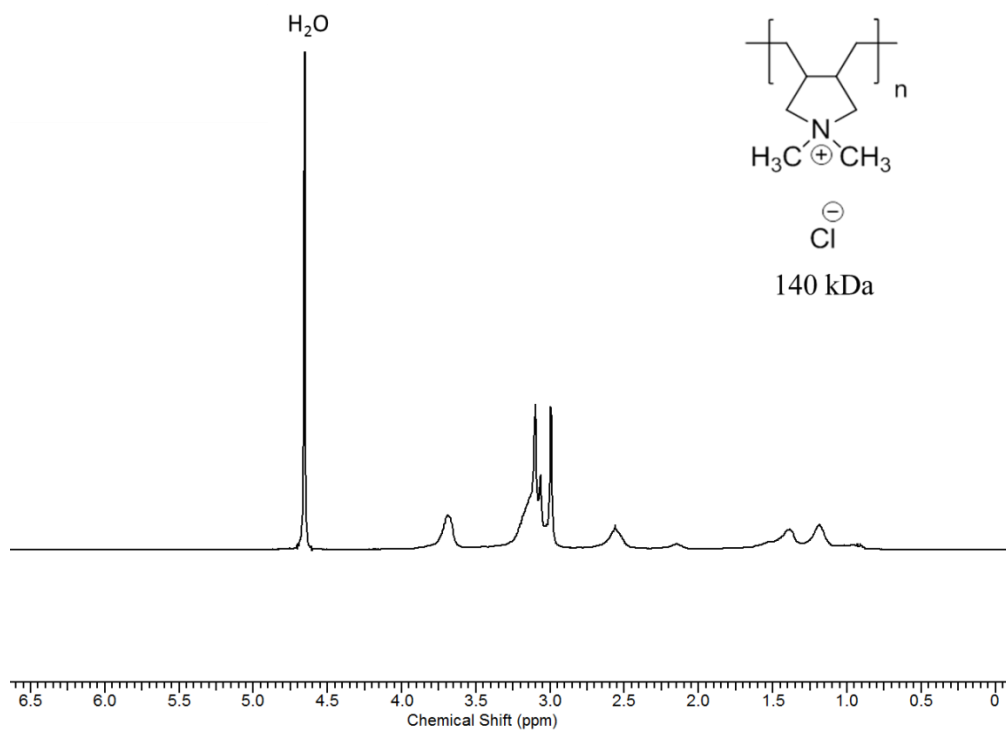
Appendices



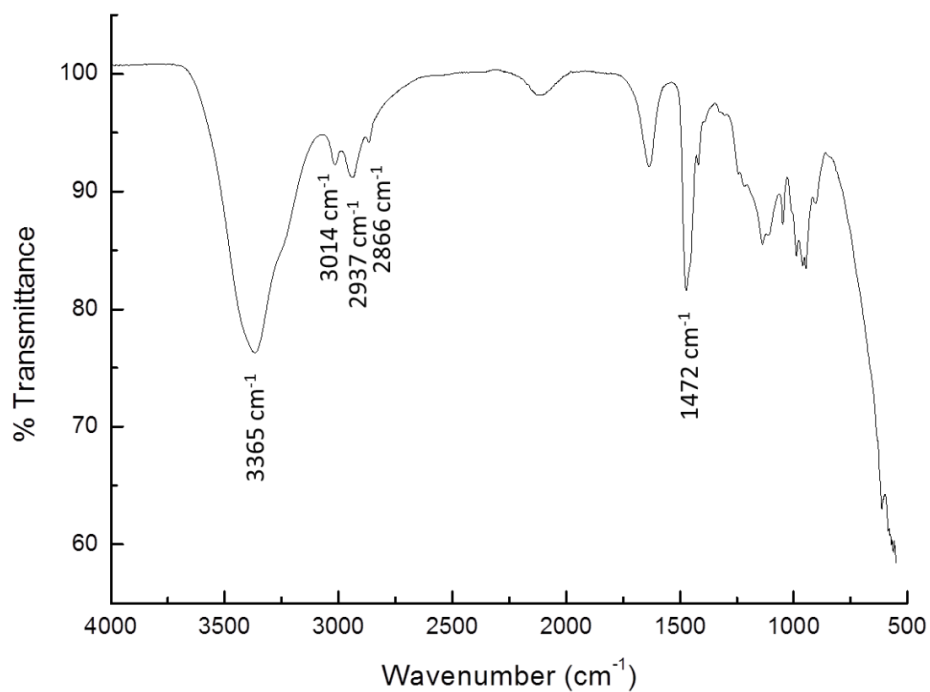
Appendix 3-A ^1H NMR of pDADMAC 8.5 kDa.



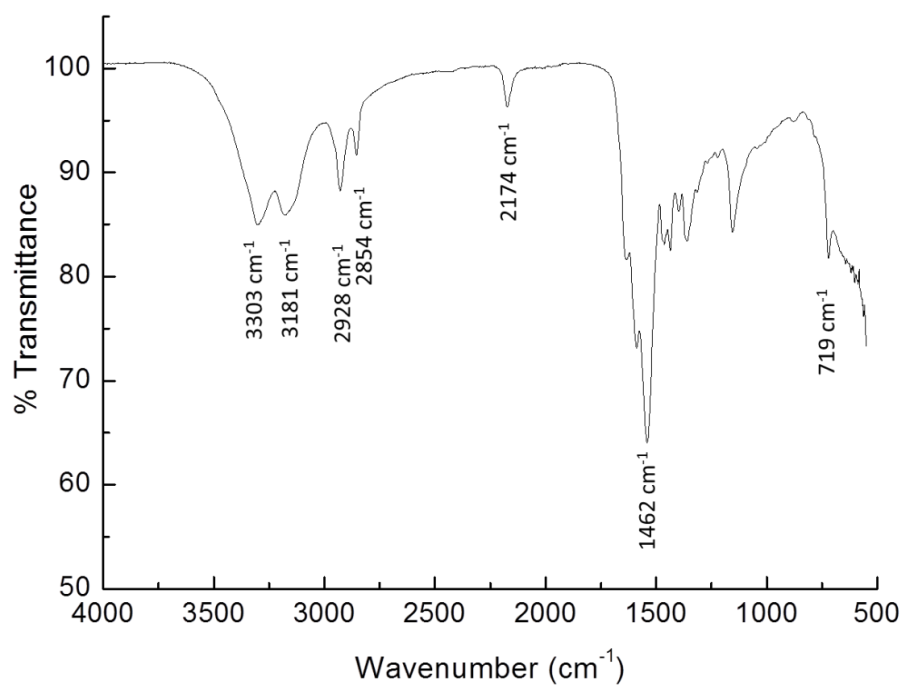
Appendix 3-B ^1H NMR of pDADMAC 21 kDa.



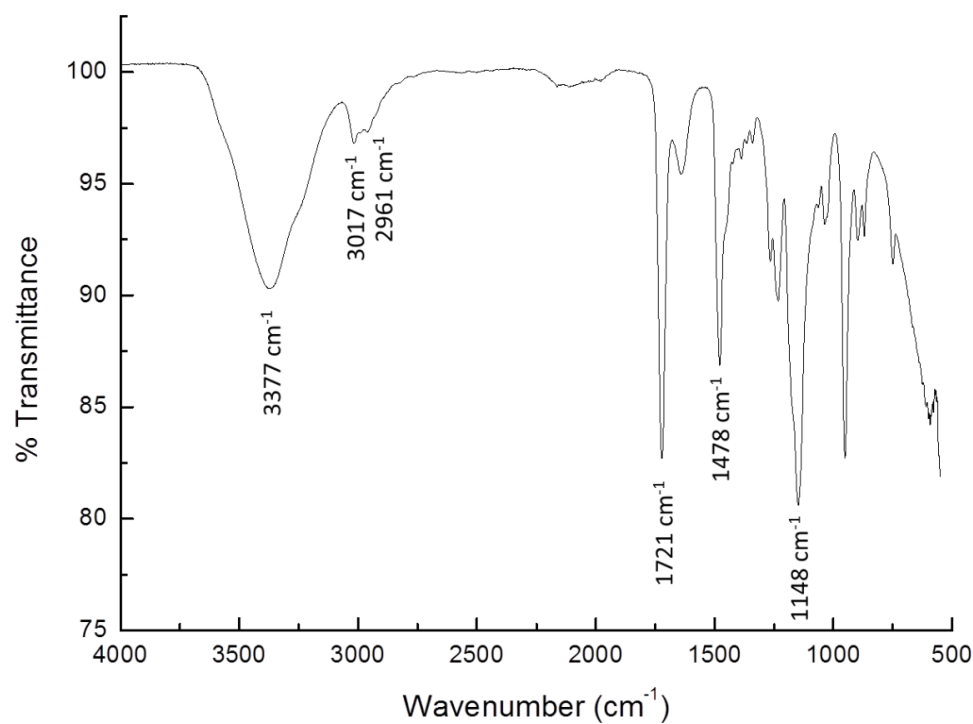
Appendix 3-C ^1H NMR of pDADMAC 140 kDa.



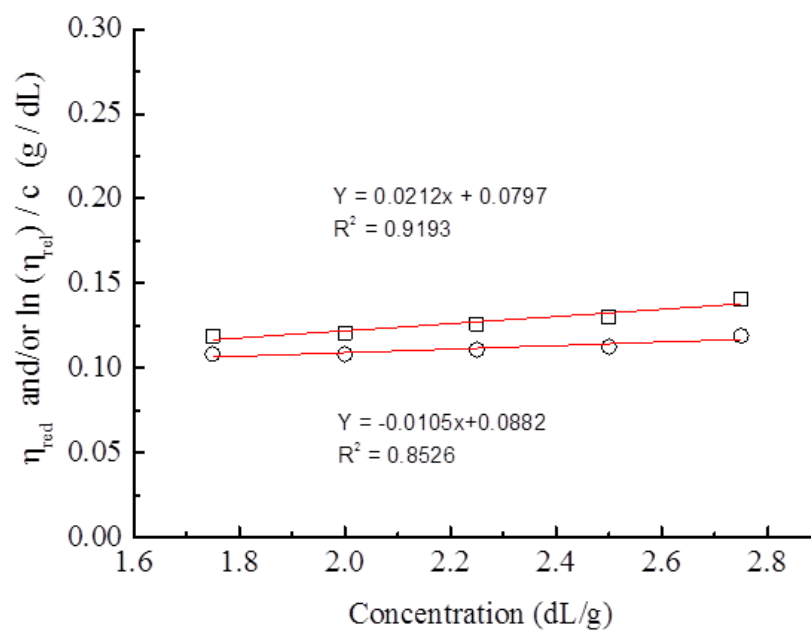
Appendix 3-D ATR-IR of pDADMAC 21 kDa.



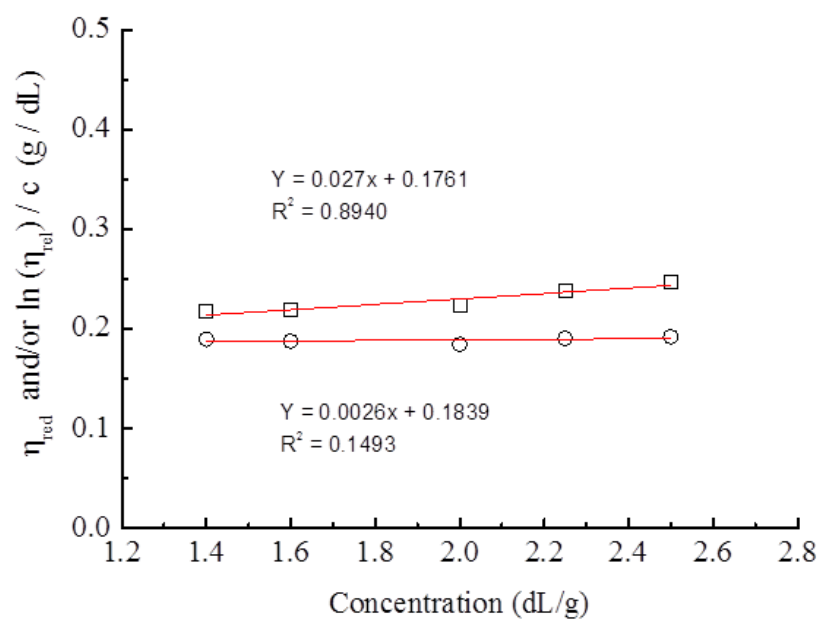
Appendix 3-E ATR-IR of PHMB.



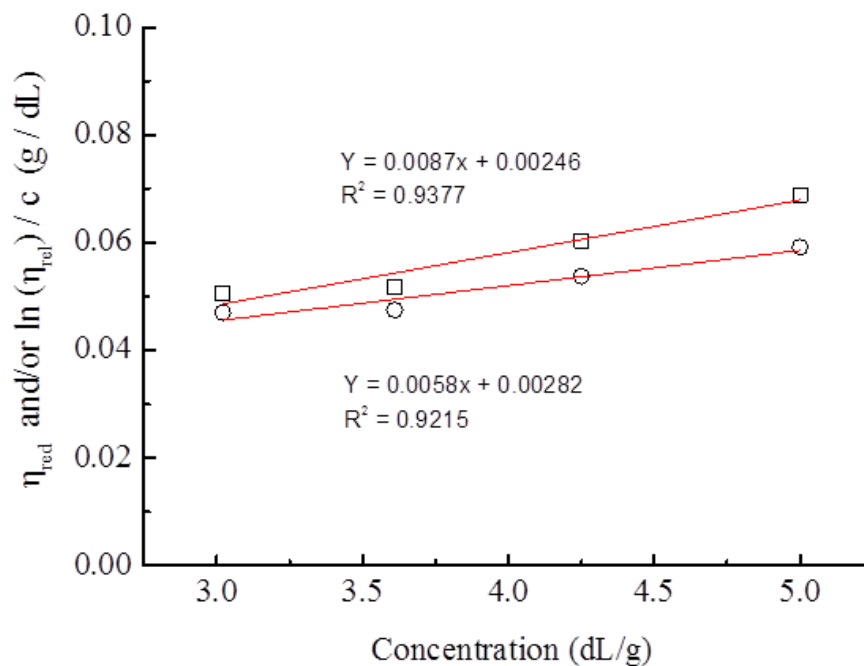
Appendix 3-F ATR-IR of PDMC.



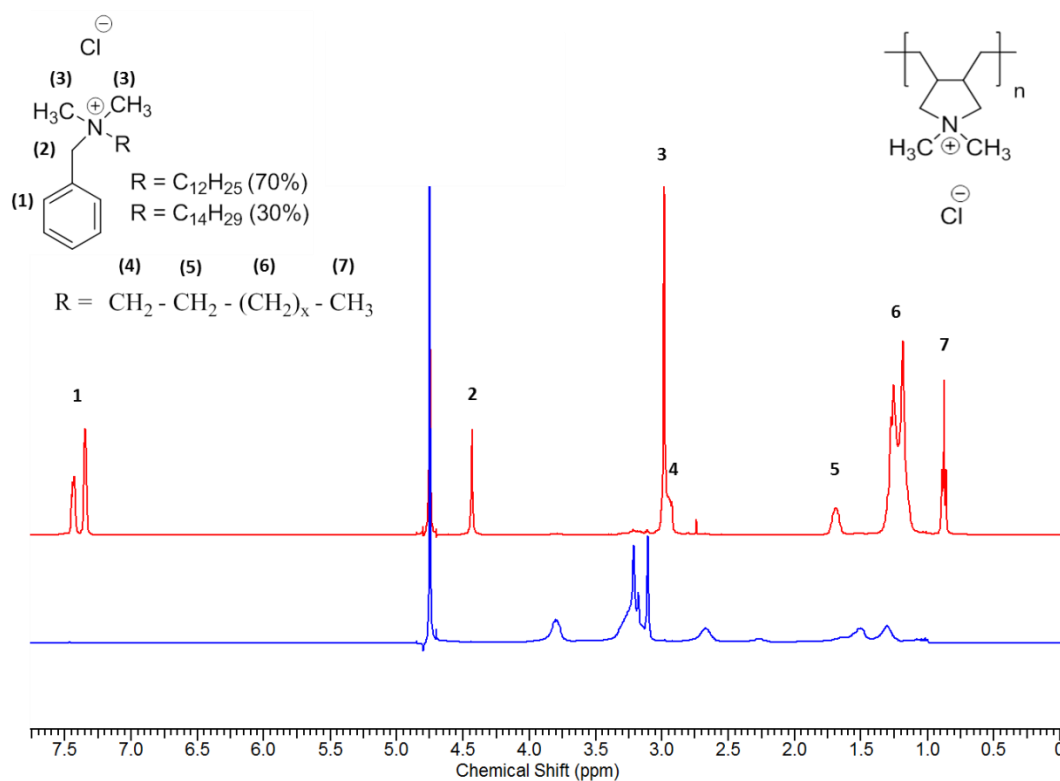
Appendix 3-G Huggins/Kraemer plot for pDADMAC (8.5 kDa) at 25 °C in 1 M NaCl.



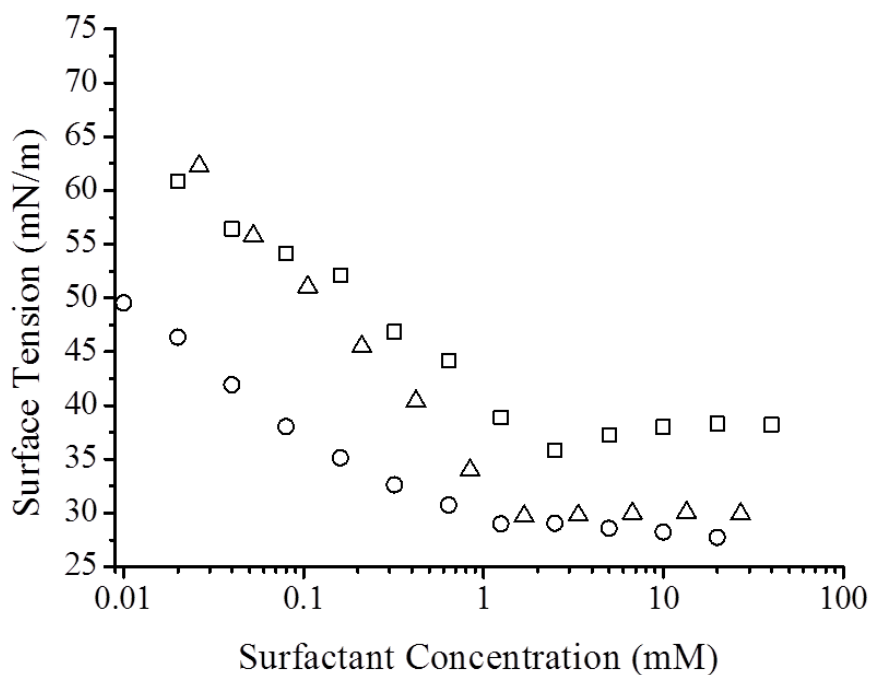
Appendix 3-H Huggins/Kraemer plot for pDADMAC (21 kDa) at 25 °C in 1 M NaCl.



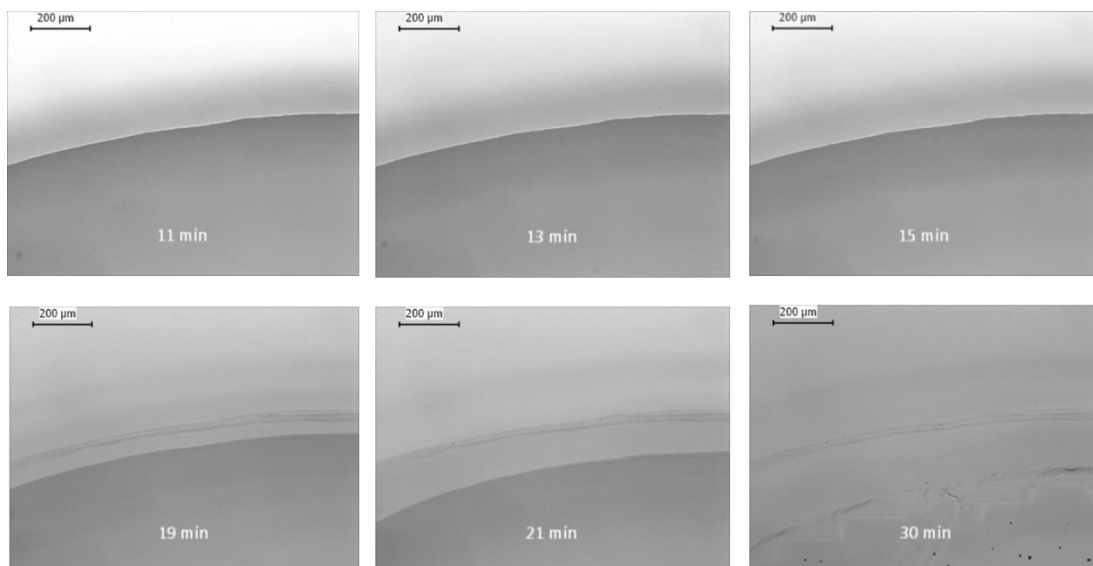
Appendix 3-I Huggins/Kraemer plot for PDMC at 25 °C in 1 M NaCl.



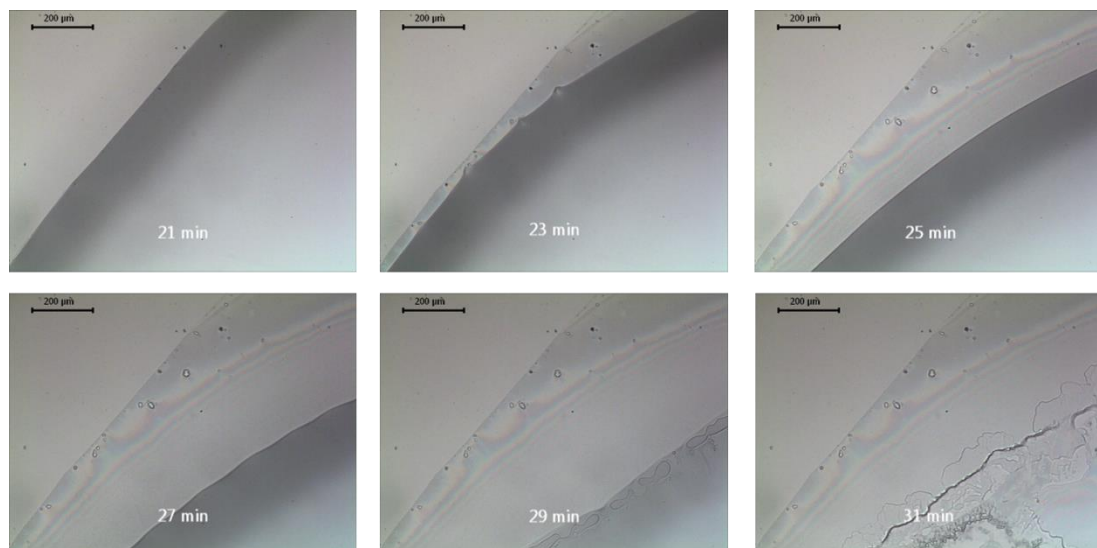
Appendix 5-A ¹H NMR of the top phase and the bottom phase for the sample pDADMAC 21 kDa (14 wt%)/BAC (14 wt%)/water sample, 24 hrs since last agitation. (red) top phase (DDQ), (Blue) bottom phase (pDADMAC).



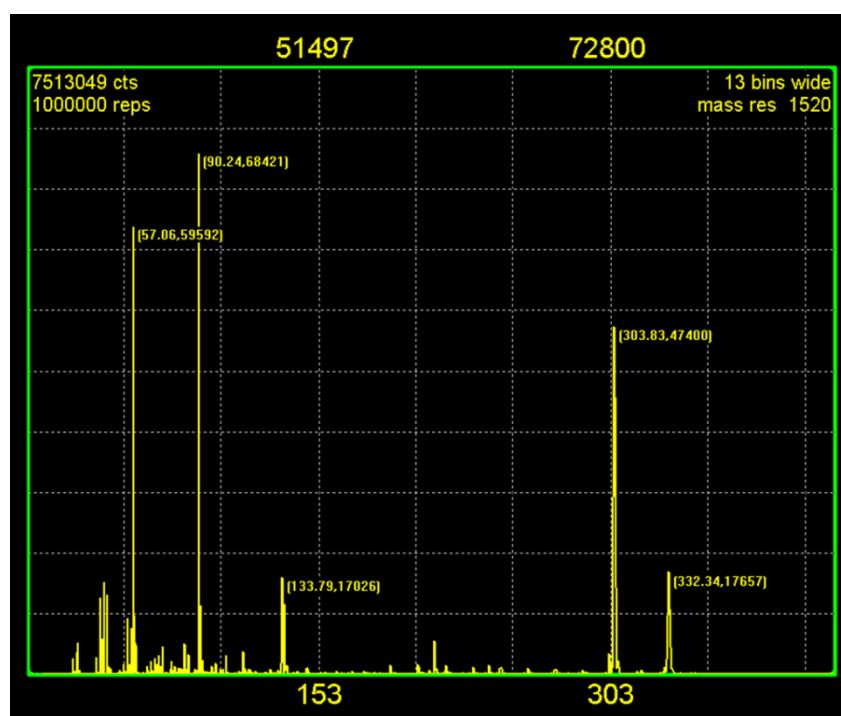
Appendix 6-A Surface tension profiles in the presence of 0.1 wt% pDADMAC (21 kDa) at 25 °C of (□) BAC, (O) DDQ, and (Δ) BAC/DDQ (2:3 mol:mol). Conversion of BAC/DDQ ratio from mol/mol to mass/mass gives comparable ratio of 2:3.



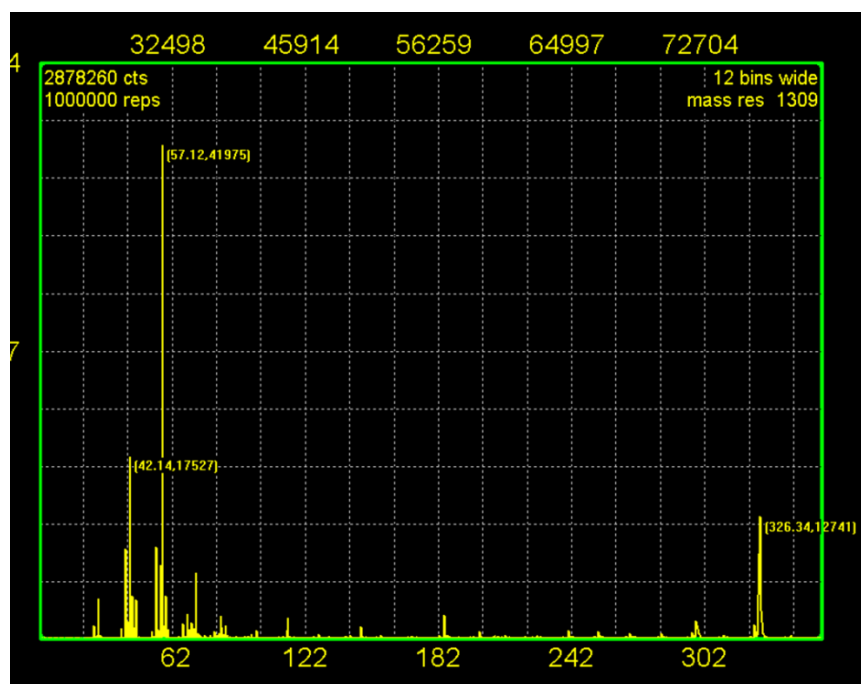
Appendix 6-B Optical micrographs of a drying sessile drop (20 μL) on a glass substrate, 0.1 wt% BAC/DDQ (2:3) only, Scale bars = 200 μm, Room Temperature = 28 °C. Relative Humidity 20-30%.



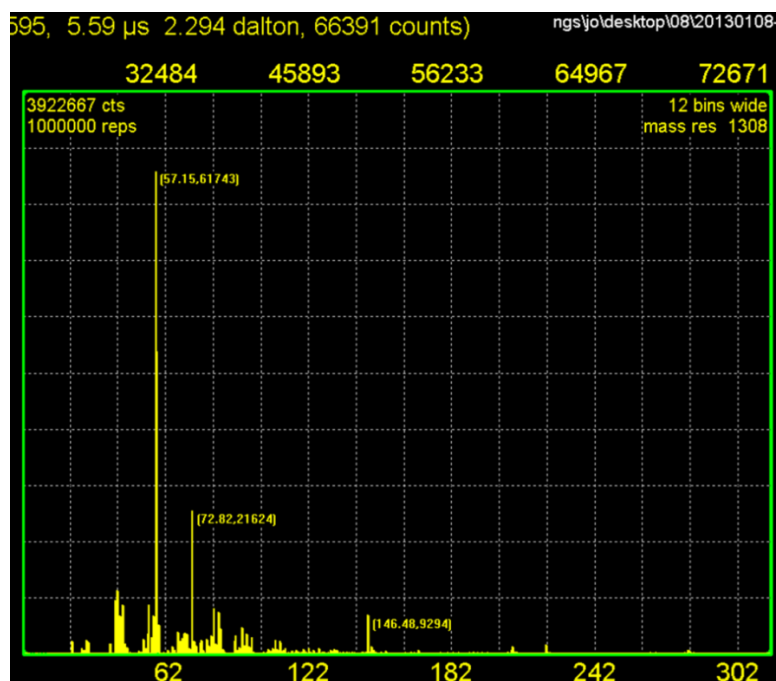
Appendix 6-C Optical micrographs of a drying sessile drop (20 μL) on a glass substrate, 0.1 wt% DDQ only, Scale bars = 200 μm , Room Temperature = 22 $^{\circ}\text{C}$. Relative Humidity 20-30%.



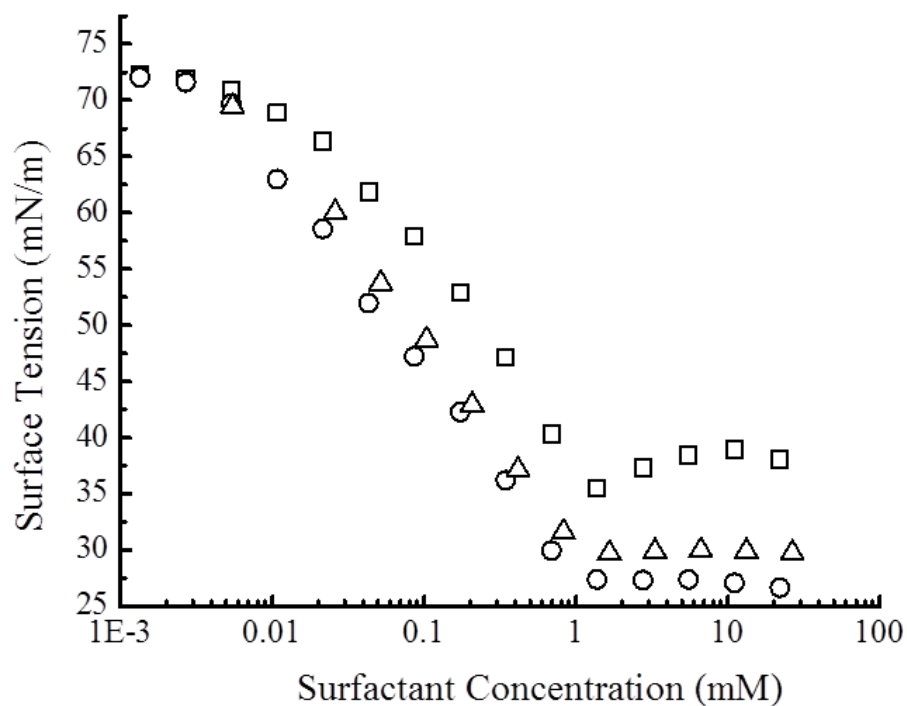
Appendix 6-D ToF-SIMS Mass spectrum of a silicon wafer treated with 2 μL 0.1 wt% BAC formulation. X-axis = mass/charge (m/z).



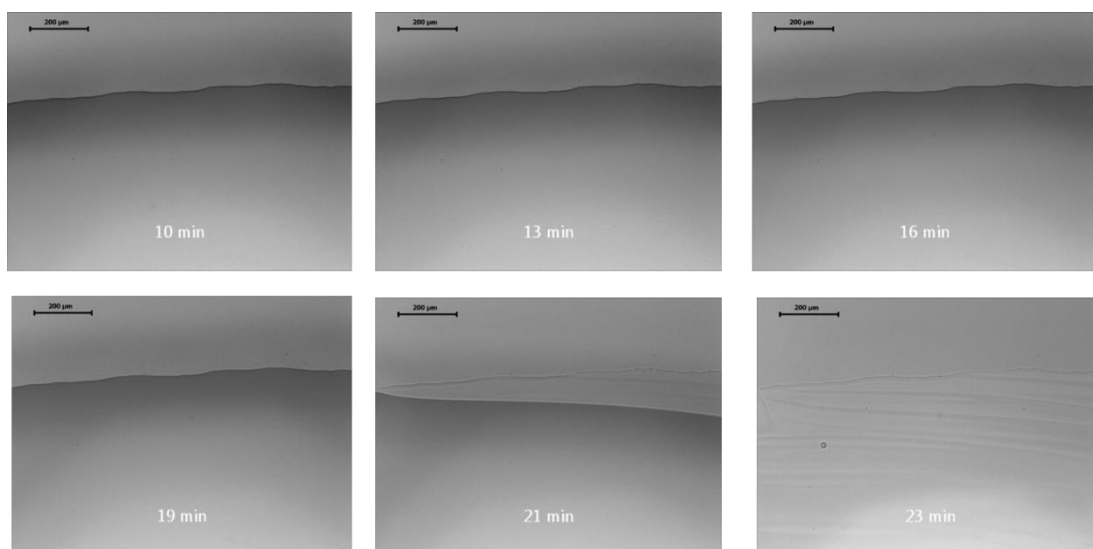
Appendix 6-E ToF-SIMS Mass spectrum of a silicon wafer treated with 2 μ L 0.1 wt% DDQ formulation. X-axis = mass/charge (m/z).



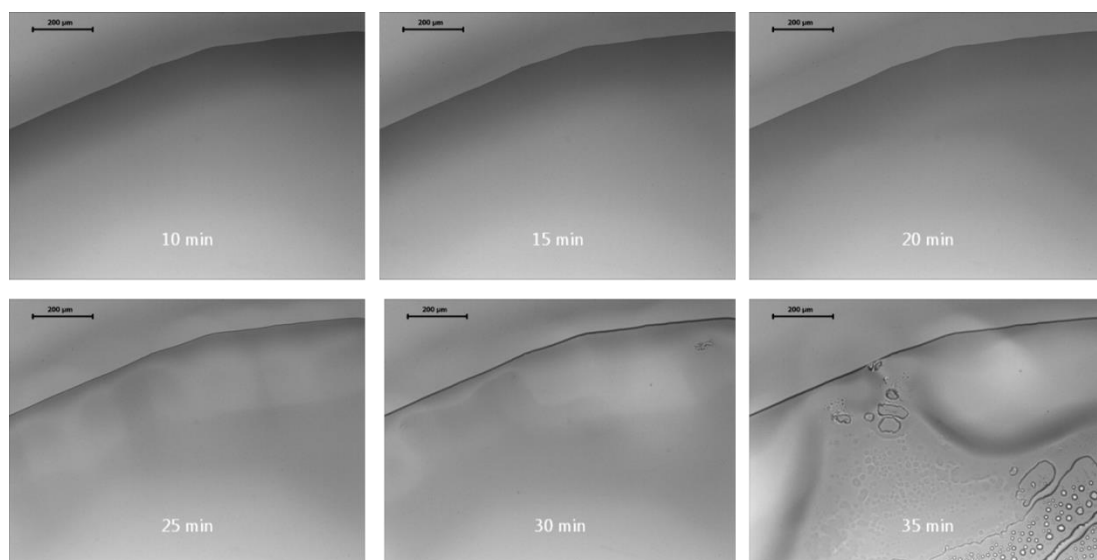
Appendix 6-F ToF-SIMS Mass spectrum of a silicon wafer treated with 2 μ L 0.1 wt% pDADMAC formulation. X-axis = mass/charge (m/z).



Appendix 6-G Surface tension profiles in the presence of 0.1 wt% PHMB (21 kDa) at 25 °C of (□) BAC, (O) DDQ, and (Δ) BAC/DDQ (2:3 mol:mol). Conversion of BAC/DDQ ratio from mol/mol to mass/mass gives comparable ratio of 2:3.



Appendix 6-H Optical micrographs of a drying sessile drop (20 μL) on a glass substrate, 0.1 wt% BAC + 0.1 wt% PHMB, Scale bars = 200 μm, Room Temperature = 22 °C. Relative Humidity 50-60%.



Appendix 6-I Optical micrographs of a drying sessile drop (20 µL) on a glass substrate, 0.1 wt% BAC/DDQ (2:3) + 0.1 wt% PHMB, Scale bars = 200 µm, Room Temperature = 22 °C. Relative Humidity 50-60%.